

Thesis submitted for the degree of  
**Doctor of philosophy**  
at the University of Leicester

By

**Ioanna Maria Pateli**

Department of Chemistry

University of Leicester

October 2020



# **Metal oxides processing using deep eutectic solvents**

**Ioanna Maria Pateli**

**University of Leicester 2020**

## **Abstract**

Metal oxides are the form from which most metals are extracted. They are found in natural ores and many industrial residues and end-of-life products, which makes their efficient processing an important topic. The state-of-the-art processes for the extraction of metal oxides include either the pyrometallurgy or hydrometallurgy, which both have a significant environmental footprint. The investigation of more efficient alternatives for their extraction is crucial, in order to develop sustainable flowsheets for recycling materials like cathodes from lithium ion batteries.

The understanding of the dissolution mechanism of selected metal oxides was attempted using deep eutectic solvents. In general, Pourbaix diagrams have shown that metal oxides can be digested either through protonation, complexation or by redox processes. The two former methods were investigated to determine their effect on solubility, and it was shown that the surface complexation had a greater impact on their solubility compared to the proton activity of the solvent.

Speciation is known to be the key to designing selective processes, so the ability to tune the deep eutectic solvents to selectively dissolve some metals over others is a great asset. The selective extraction of Co and Mn over Ni from cathode materials of lithium ion batteries and Y and Eu from spent fluorescent lamp phosphors was demonstrated.

Apart from the chemical dissolution, the electrochemical oxidation of metal oxides was also investigated as this was previously shown to be efficient for the dissolution of metal sulfides, tellurides and selenides. It was found that a significant enhancement of the metal oxide dissolution rate could be obtained in solvents that are neither acidic nor consist of complexing agents. Indeed, the rate of dissolution, which was dependent upon the band gap of the metal oxides, was strongly enhanced, sometimes even more than 10000 times.

## Publications and Dissemination

Parts of this work have already been published:

- Pateli I.M, Thompson D., Alabdullah S.S.M, Abbott A.P, Jenkin G.R.T and Hartley J.M, “The effect of pH and hydrogen bond donor on the dissolution of metal oxides in deep eutectic solvents”, 2020, *Green Chemistry*, 22, 5476-5486
- Pateli I.M, Abbott A.P, Binnemans K. and Rodriguez, N.R. “Recovery of yttrium and europium from spent fluorescent lamps using pure levulinic acid and the deep eutectic solvent levulinic acid-choline chloride”, 2020, *RSC Advances*, 10, 28879-28890

Parts of this work have been presented in oral and poster form at the following events:

- 3-Minutes Thesis (3MT) (oral presentation) 31/05/2017, University of Leicester, UK
- Electrochemical processing of metal oxides using deep eutectic solvents. (oral presentation) 24/07/2018, *Midlands Electrochemistry Group (MEG)*, University of Birmingham, UK
- Metal Oxides processing using Deep Eutectic Solvents (DESs), (poster presentation) 30-31/08/2018, Early Career Symposium-Royal Society of Chemistry, ACC Liverpool, UK
- Processing of metal oxides using deep eutectic solvents, (oral presentation) 24-27/06/2019, *1<sup>st</sup> International Meeting on Deep Eutectic Systems*, Universidade of Lisboa, Lisbon, Portugal
- Recycling of REEs from spent fluorescent lamp phosphors using deep eutectic solvents. (oral presentation) 5-6/10/2019, *International Process Metallurgy Symposium*, Aalto University, Espoo, Finland
- Recycling of REEs from fluorescent lamp residues using levulinic acid (poster presentation) 24/02/2020, College of Life Sciences Poster Fair, University of Leicester, UK

## Statement of Originality

The work presented in this thesis for the degree of Doctor of Philosophy (Ph.D.) with the title “Processing of metal oxides using deep eutectic solvents” was carried out by the author in the Materials Centre, Department of Chemistry at the University of Leicester between January 2017 and May 2020.

In this thesis, the work recorded is original except where acknowledged or referenced. None of the work has been submitted, and is not presently submitted, for another degree at this or any other university.

Signed *Ioanna Maria Pateli*  Date ....01/10/2020....

Ioanna Maria Pateli  
Materials Centre, Department of Chemistry,  
University of Leicester, University Road,  
LE1 7RH

## Acknowledgements

Primarily and most importantly, I would like to thank my supervisor Professor Andy Abbott for his guidance throughout the project. I always admired his passion for science and research, and I feel very lucky to have been his student. I also always enjoyed our talks about general things, like photography, history and art.

I want also to express my deep gratitude to Dr Jennifer Hartley, since she assisted me in many aspects of my thesis. She was always ready and happy to answer my questions and to pass on her knowledge. She made also my workdays much more fun with our everyday talks, lunches together and occasionally swimming in the pool of the university. In the same way, I would like to thank Dr Nerea Rodriguez Rodriguez, as she was my mentor during my secondment at KU Leuven in Belgium. She has taught me so many things about how to be a good researcher, how to analyse data and write manuscripts. I will never forget my days in KU Leuven.

In addition, I would like to thank Dr Adam Cox for all the ICP-MS analyses that he provided me, and Dr Robert Harris, Dr Iain Aldous, Dr Igor Efimov, Dr Chris Zaleski and Dr Chunhong Lei for their guidance throughout my thesis. Furthermore, I would like to express my deep gratitude to Dr Ahmed Al Bassam, Dr Sahar Alabdullah, Dr Francesca Bevan and Dr Shannon Stodd for all our talks about the experiments and other everyday life things during their Ph.D. studies at Materials Centre. All my appreciation and love also goes to my colleagues, Dana, Jason, Jack, Chloe, Farrah, Sean, Maryam, Steve, Hannah and Jasmine at Materials Centre that made my life much more interesting and fun. A special thanks also goes to Stelios, my colleague and housemate for three years. Thanks for all your help in every aspect of my life.

I feel obliged also to thank the European Commission that funded my studies and the people of SOCRATES. It was an amazing experience and I had the opportunity to meet so many people, make friends and travel. A special thanks also goes to Dr Mathias Christinne for being my mentor during my secondment at Metallo Belgium.

Last but definitely not least, I would like to express my deep love and appreciation to my family, dad, mum and my brother for always supporting me, believing in me and making me smile and my friends for listening all my problems and helping me release my anxiety. Also, Alex my partner and best friend for life, I don't know if I could finish these studies without your daily encouragement, daily effort to make me happy and your endless love.

## **Dedication**

*I would like to dedicate this thesis to:*

*All of my family, dad, mum and my brother. I will always love you and thank you for believing in me and supporting me.*

*Also, to all the other people I love, you know who you are. Thanks for everything. Without you, life would be empty.*

Ioanna Maria Pateli

Leicester 2020

# Contents

<b>Abstract</b> .....	ii
<b>Publications and Dissemination</b> .....	iii
<b>Statement of Originality</b> .....	iv
<b>Acknowledgements</b> .....	v
<b>Dedication</b> .....	vi
<b>1 Chapter</b> .....	12
1.1 Overview .....	12
1.1.1 Transition metal oxides .....	13
1.2 Minerals processing .....	17
1.2.1 Pyrometallurgy .....	18
1.3 Hydrometallurgy .....	24
1.3.1 Brief comparison of pyrometallurgical and hydrometallurgical method .....	31
1.4 Ionometallurgy .....	33
1.4.1 Ionic Liquids.....	34
1.4.2 Deep eutectic solvents .....	42
Metal processing in deep eutectic solvents .....	46
1.5 Thesis aims.....	47
1.6 References .....	48
<b>2 Experimental Procedures</b> .....	59
2.1 Materials.....	59
2.1.1 Chemicals .....	59
2.1.2 Preparation of deep eutectic solvents .....	61
2.2 Leaching experiments .....	62
2.2.1 Ultrasound assisted chemical dissolution.....	63
2.3 Analytical techniques for the characterisation of metal content .....	64
2.3.1 Inductively Coupled Plasma Mass Spectrometry ICP-MS .....	64
2.3.2 Inductively Coupled Plasma Optical Emission Spectroscopy ICP-OES .....	68
2.3.3 X-ray Fluorescence.....	68
2.4 UV-Vis Spectroscopy.....	69
2.5 Nuclear Magnetic Resonance spectroscopy (NMR).....	70
2.6 Electrochemical processes .....	71
2.6.1 Cyclic Voltammetry .....	71

2.6.2 Paint Casting.....	73
2.6.3 Chronopotentiometry.....	73
2.6.4 Chronocoulometry.....	74
2.7 Bulk electrochemical dissolution.....	74
2.8 Scanning Electron Microscopy – Energy Dispersive X-rays spectroscopy.....	76
2.9 References.....	78
3 Chapter.....	81
3.1 Introduction.....	81
3.1.1 Metallurgical processing of metal oxides.....	81
3.1.2 Aims.....	84
3.2 Chemical dissolution of metal oxides in DESs.....	85
3.2.1 Dissolution of metal oxides in ethylene glycol: choline chloride.....	86
3.2.2 Effect of pH on dissolution in ethylene glycol: choline chloride.....	91
3.2.3 Ligand effect on dissolution.....	96
3.3 Dissolution kinetics.....	105
3.4 Dissolution of cathode materials of LIBs.....	107
3.4.1 Importance of LIBs recycling.....	107
3.4.2 Characterisation of cathode materials.....	110
3.4.3 Dissolution of the cathode materials in OxA:ChCl.....	112
3.5 Conclusions.....	121
3.6 References.....	124
4 Chapter.....	135
4.1 Introduction.....	135
4.1.1 Oxidative dissolution of metal oxides.....	135
4.1.2 Aims.....	138
4.2 Electrochemical studies of metal oxides.....	138
4.2.1 Paint casting of MOs.....	138
4.2.2 Chronopotentiometry.....	149
4.2.3 Chronocoulometry.....	150
4.3 Bulk anodic dissolution of MOs.....	154
4.4 Bulk anodic deposition.....	161
4.5 Conclusions.....	163
4.6 References.....	165
5 Chapter.....	172

5.1 Introduction .....	172
5.1.1 Rare earth elements and the importance of their recycling .....	172
5.1.2 Fluorescent lamps and their recycling .....	175
5.1.3 Aims .....	180
5.2 Extraction of REEs from spent fluorescent lamps using solvometallurgy .....	181
5.2.1 Selection of deep eutectic solvent for the extraction of REEs from phosphors .....	181
5.2.2 Optimization of dissolution parameters.....	185
5.2.3 Dissolution of synthetic mixture of phosphors.....	188
5.2.4 Dissolution of real lamp phosphor waste .....	189
5.2.5 Comparison with other hydrometallurgical and solvometallurgical processes .....	192
5.3 Recovery of REEs from lamp phosphor .....	194
5.3.1 Recovery using precipitation with oxalic acid .....	194
5.3.2 Recovery using solvent extraction.....	197
5.4 Conclusions .....	198
5.5 References .....	200
6 Chapter.....	206
6.1 Conclusions .....	206
6.2 Suggestions for future work .....	210
7 Chapter.....	213
7.1 Supplementary Information for Chapter 3 .....	213
7.2 Supplementary information for Chapter 4 .....	224
7.3 Supplementary information for Chapter 5 .....	227

## List of Abbreviations

MO	– Metal oxide
DES	– Deep eutectic solvent
HBD	– Hydrogen bond donor
ChCl	– Choline chloride
OxA	– Oxalic acid
LacA	– Lactic acid
LevA	– Levulinic acid
AceA	– Acetic acid
EG	– Ethylene glycol
Gly	– Glycerol
TFSA	– trifluoromethanesulfonic acid
DEHPA	– di-(2-ethylhexyl)phosphoric acid
IL	– Ionic Liquid
RTIL	– Room temperature ionic liquid
EoL	– End-of-life
LIB	– Lithium ion battery
PLS	– pregnant leach solution
L:S	– liquid to solid ratio
REE	– Rare earth elements
HREEs	– Heavy rare earth elements
LREEs	– Light rare earth elements
CV	– Cyclic voltammogram
WE	– Working electrode
OCP	– Open circuit potential
SEM/ED(A)X	– Scanning Electron Microscopy/Energy Dispersive (Analysis) by X-ray
ICP-MS/OES	– Inductively Couple Plasma-Mass Spectrometry/Optical Emission Spectroscopy
NMR	- Nuclear magnetic resonance
EXAFS	- Extended X-ray absorption fine structure
EPR	– electron paramagnetic resonance
XRF	– X-ray fluorescence

# Chapter 1: Introduction

1.1 Overview .....	12
1.1.1 Transition metal oxides .....	13
1.2 Minerals processing .....	17
1.2.1 Pyrometallurgy .....	18
1.3 Hydrometallurgy .....	24
1.3.1 Brief comparison of pyrometallurgical and hydrometallurgical method .....	31
1.4 Ionometallurgy .....	33
1.4.1 Ionic Liquids.....	34
1.4.2 Deep eutectic solvents .....	42
Metal processing in deep eutectic solvents .....	46
1.5 Thesis aims.....	47
1.6 References .....	48

# 1 Chapter

## 1.1 Overview

Metals play a vital role in everyday life. A modern lifestyle depends on a variety of metals, predominantly iron and base metals (Al, Pb, Cu, Co, Ni, Zn, Sn) which are used in construction and manufacturing.<sup>1</sup> However, other less common metals also play an increasingly important role. For example, rare earth elements (REEs - Y, Eu, Ce, La, Nd, Dy, Tb, Sm, Sc) increasingly contribute to green and low carbon technologies (NiMH batteries, fuel cells, plasma screens, medical imaging)<sup>2</sup> and platinum group metals (PGMs - Au, Ag, Pt, Rh, Ru, Pd) have applications in autocatalysis, electronics, fuel cells, medicines and jewellery.<sup>3</sup> In general, metals comprise 25% of the Earth's crust and appear in different forms with the main forms being oxides, chlorides, sulfides, sulfates, silicates and carbonates. Some of these elements are rather abundant in the Earth's crust such as Al - 8.0% and Fe - 5%<sup>4</sup>, whereas other elements are scarce such as Pt- 0.0030 ppm, Au- 0.0011 ppm and Rh- 0.0002 ppm.<sup>5</sup> The abundance of metals in the Earth's upper crust is given in **Figure 1.1**, where it is apparent that metals with higher atomic number tend to be scarcer.<sup>6</sup>

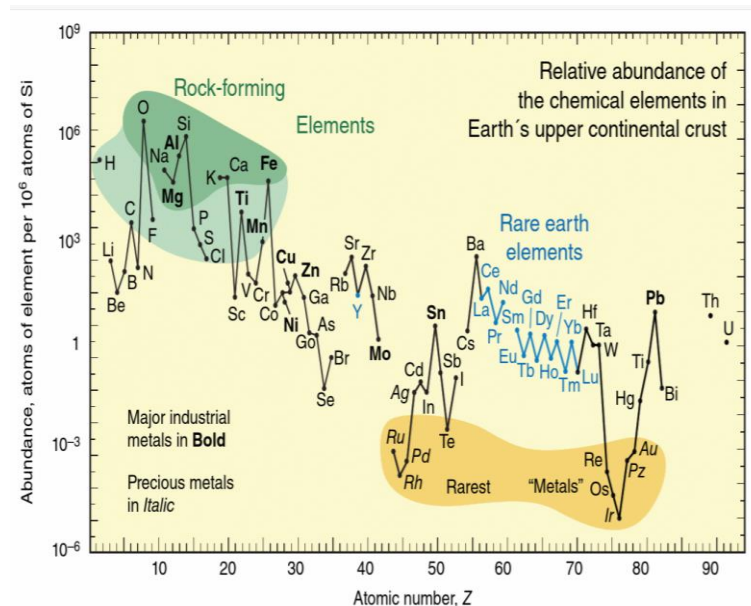


Figure 1.1: Abundance of chemical elements in Earth's upper crust as function of atomic number<sup>6</sup>

The continental crust is mainly covered with andesite, a group of minerals consisting of  $\text{SiO}_2$ , which also contains the mineral phases of plagioclase feldspar with the formula

$\text{NaAlSi}_3\text{O}_8 - \text{CaAl}_2\text{Si}_2\text{O}_8$ , which explains the reason for Al high abundance in the Earth's crust.<sup>7</sup>

Most metals found on Earth are in the form of oxides making metal oxides (MOs) a very important group of chemical compounds. In most cases, the bond between the metal and the oxygen is very stable and strong and in order to break it and extract the metals, conditions of extremely high temperatures or very acidic / basic solvents are required. Both pyrometallurgy and hydrometallurgy have been employed for the processing of MOs, but due to their high environmental footprint and energy consumption the need for novel approaches is more relevant than ever.

In addition, the current situation in Europe with an increased need of technological metals, alternative sources of metals like end-of-life (EoL) products (batteries, magnets, fluorescent lamps etc.) are needed. The processing of these materials needs to be designed in an economically feasible way while also being environmentally friendly.

In this thesis, extraction of metals from MOs is investigated employing deep eutectic solvents (DESs) both with chemical and electrochemical processes. The choice of these MOs is taken due to their existence in industrial wastes and in spent EoL products. Furthermore, the recycling of Co, Ni and Mn from the cathodes of spent lithium ion batteries (LIBs) and Y and Eu from spent fluorescent lamps is examined.

### **1.1.1 Transition metal oxides**

MOs are chemical compounds consisting of an oxygen anion in the form of oxide ( $\text{O}^{2-}$ ) and a metal cation. Oxygen is the third most abundant element in the universe following  $\text{H}_2$  and He, it is the most abundant element in the Earth's crust and is the second most abundant species in the Earth's atmosphere (21%). This explains the reason that most metals are found in the form of oxides. Most metals, except from the noble ones (Au, Pt etc.) when left in open air or in water, react with oxygen to form MOs or with water to form metal hydroxides. This natural reaction is called corrosion and can be defined as the process when metals are oxidised to more stable forms e.g. oxides, sulfides, sulfates etc.<sup>8</sup> via the influence of their surroundings. Due to the high electronegativity of oxygen (Pauling electronegativity: 3.44), MOs tend to be very chemically stable compounds.

Transition metals are defined as metals that possess partially filled *d* or *f* subshells in their elemental state. Another definition may be the metals that possess partly filled *d* or *f*

subshells in their most common compounds including their ions. The latter definition is more appropriate, because it includes Cu, Ag and Au. Even though these elements possess a  $d^{10}$  filled electron configuration, their ions form partly filled  $d$  or  $f$  subshells.<sup>9, 10</sup> There are 40  $d$ -block elements and 28  $f$ -block elements. In terms of their occurrence, Fe is the most abundant of all the transition metals.

The  $f$ -block elements comprise of the lanthanides and the actinides and include the rarest transition elements, which is why together with Sc and Y they are called rare earth elements.

This thesis examines the processing of metals from the first row of  $d$ -block elements along with Pb. These metals, all show very good potential as engineering and technological materials and they show very high melting and boiling points. They have the  $3d$  electron shell partially filled and their configurations are presented in **Table 1.1**.

Oxygen, due to its high electronegativity, can bring out the highest oxidation states of these elements. For instance, Mn has its highest oxidation state in the ion of permanganate ( $\text{MnO}_4^-$ ). Compounds of MOs, in which the metal exists in its lowest oxidation state, form ionic bonds with the oxygen such as NiO and CoO, whereas when the metal exists in its higher oxidation states then covalency and polarisation of the compound increase. In addition, the acidity of the oxide grows when the oxidation state of the metal and the charge increases, while basicity increases in the opposite way. For instance, CrO is a basic oxide,  $\text{Cr}_2\text{O}_3$  is amphoteric (can behave both as an acid or base) and  $\text{CrO}_3$  is an acidic oxide. Depending on the acidity of the oxide, there are different approaches for its dissolution, which will be analysed in later chapters.

MOs show a wide range of electric conductivities, which are also highly affected by other metal contaminants in their structure and by deviations from stoichiometry.<sup>11</sup> As for their magnetic properties, there are oxides that are diamagnetic (TiO), antiferromagnetic (MnO, CoO, NiO and  $\text{Cr}_2\text{O}_3$ ), ferrimagnetic ( $\text{Fe}_3\text{O}_4$  and  $\text{Mn}_3\text{O}_4$ ) and ferromagnetic ( $\text{CrO}_2$ ).

MOs take on a variety of crystal structures. Some adopt a simple rock salt type of NaCl (MnO, CoO, and NiO), while others have the corundum structure ( $\text{Ti}_2\text{O}_3$ ,  $\text{Cr}_2\text{O}_3$ , and  $\text{Fe}_2\text{O}_3$ ), the spinel form ( $\text{Mn}_3\text{O}_4$ ,  $\text{Fe}_3\text{O}_4$ ) and the wurtzite structure (ZnO).<sup>12</sup> Some of these structures are shown in **Figure 1.2**. Depending on the crystal structure of each oxide,

different amount of energy for dissolution is required, because there are differences in the lattice energy.

*Table 1.1: Abundance in Earth's crust, electronic configuration and known oxidation states of elements of the first row of d-block and Pb*

Metal	Abundance (ppm)	Configuration	Oxidation states
Sc	16	$3d^1 4s^2$	3
Ti	5600	$3d^2 4s^2$	2, 3, 4
V	160	$3d^3 4s^2$	2, 3, 4, 5
Cr	100	$3d^5 4s^1$	2, 3, 4, 5, 6
Mn	950	$3d^5 4s^2$	2, 3, 4, 5, 6, 7
Fe	41000	$3d^6 4s^2$	2, 3, 4, 5, 6
Co	20	$3d^7 4s^2$	2, 3, 4, 5
Ni	80	$3d^8 4s^2$	2, 3, 4
Cu	50	$3d^{10} 4s^1$	1, 2, 3
Zn	75	$3d^{10} 4s^2$	2
Pb	14	$4f^{14} 5d^{10} 6s^2 6p^2$	-4, 2, 4

It is not easy to generalise data for crystal structure of oxides even in the same row of the periodic table and it is common for some oxides to have more than one crystal structures under the same conditions.<sup>13</sup>

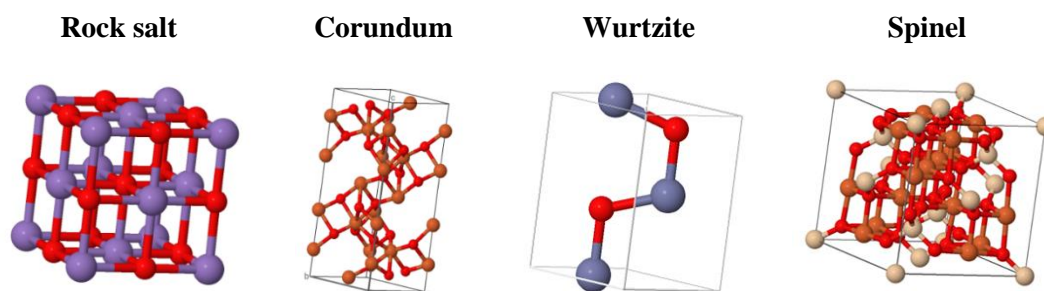


*Figure 1.2: Common crystal structures of transition metal oxides<sup>14, 15</sup>*

One widespread fact for *d*-block metals is that their ionic radii is smaller than that of  $O^{2-}$ , thus the oxygen anions are usually closed packed with the metal smaller cations situated in octahedral and tetrahedral holes.

Transition MOs have a variety of properties, which are useful for advanced materials, like their piezoelectric, electronic, photonic, magnetic properties and superconductivity,

ferromagnetism, ferroelectricity, half-metallicity etc.<sup>16</sup> One of their most widely developed applications is in the field of catalysis. They have also been employed in energy storage materials as LIBs, in hydrogen fuel cells, in electronics industry, in gas sensors, in green technological materials such as fluorescent lamps and solar panels and they are widely used in paints.<sup>17</sup> More information about the importance of them in industry will be given in Chapter 3.

The wide scale abundance and use of MOs makes facile processing of these compounds important so that closed loop cycling of material from different sources can be carried out. Recycling of EoL products has a continuously developing need for two reasons; a) the environmental and social consequences the wastes bring, and b) for the recycling and recovery of metals. In **Figure 1.3**, an example of a closed loop flowsheet for the recycling of spent lithium ion batteries (LIBs) is given. In order to produce a LIB, first the raw materials need to be mined, the metals to be extracted and recovered from their minerals and then all the materials together need to be processed in such a way that the batteries are working efficiently and in a safe way.

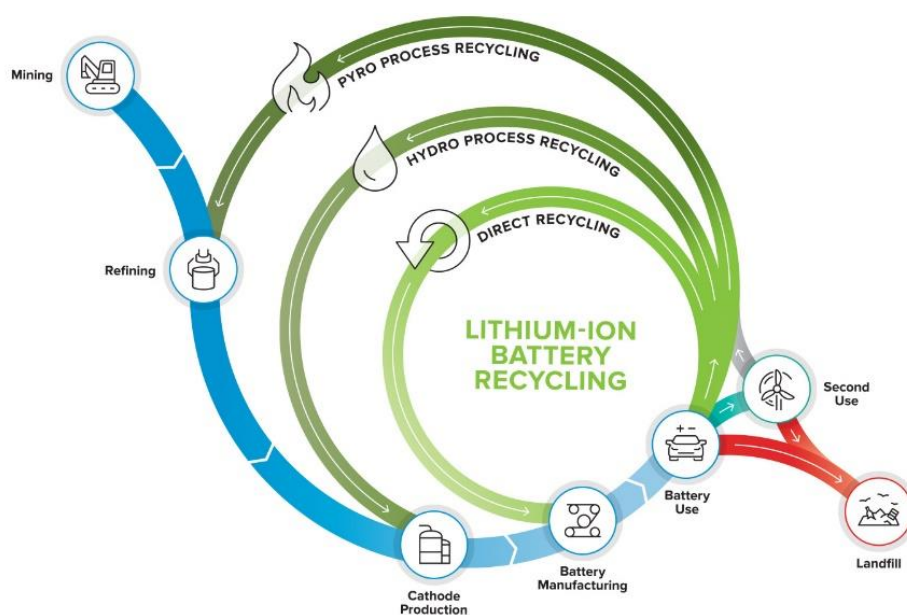


*Figure 1.3: Schematic presentation of the paths for closed-loop recycling of lithium ion batteries<sup>18</sup>*

When their functioning life ends, these materials are either discarded or recycled. The disposal becomes a problem due to the toxicity and high flammability of the components, which raises the manufacturing cost of batteries industry even more. Therefore, the recycling is the most profitable path, since it reduces the production cost by 10 – 30%, it eliminates the cost of disposal and it brings metals back in to the metal loop.<sup>18</sup> As seen in

**Figure 1.3**, currently there are three approaches for the recycling of LIBs, the recycling of the separated components of LIBs in new batteries and the extraction and recovery of metals with the employment of pyrometallurgical and hydrometallurgical methods. These two methods are going to be described in the next sections, as they are the state-of-the art approaches for the extraction of metals from MOs and for the recycling of EoL products that contain MOs.

## **1.2 Minerals processing**

An economic extraction of metals from natural resources requires the existence of sufficiently rich minerals or metal ores. Due to thousands of years of metal processing, many metals and especially the rarest ones cannot be found in rich ores any more increasing the cost of the resource. For this reason, metallurgy is constantly under development, in order to access poorer resources including previously discarded tailings in an economically way. There is a plethora of metal extraction techniques and the choice of the most economically feasible taken is mainly dependent on the matrix, the composition of the deposit, the value of the metals and their current need.

The flowsheet of a metal extraction process consists of multiple steps, starting from the discovery of the ore, and its mining and transportation to the metallurgical plant. The metallurgical part of the processes starts with the size reduction of the deposit followed by the separation of individual minerals or elements using a variety of physicochemical methods, finishing with the extraction and recovery of the targeted metals, for which different methods of low or high temperature conditions are employed, as seen in **Figure 1.4**.<sup>19</sup> The overall goal of such a flowsheet is the production of highly pure metal or metal alloys in a profitable process complying with the environmental regulations of the respective countries.

**Figure 1.4** presents the base of metallurgical flowsheets, whose steps may be different depending on the starting material, the desired product, the cost of each process etc. For example, the extraction of gold (Au) from low - grade ores is accomplished by the method of heap leaching because the cost of grinding, crushing and transportation of the ore is restrictedly significant.<sup>20</sup>

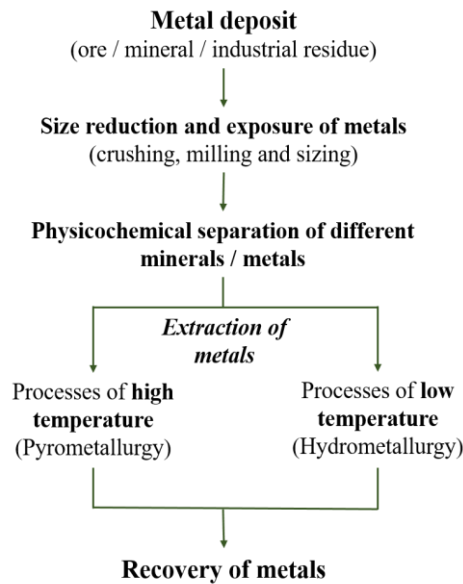


*Figure 1.4: General flowsheet of minerals processing*

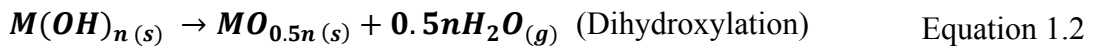
Pyrometallurgy and hydrometallurgy are the most common and well-studied extractive techniques and their distinguishing differences are the presence or absence of water in the process and the temperature conditions under which the extraction of metals takes place. The two processes are described and compared below.

### 1.2.1 Pyrometallurgy

Pyrometallurgy encloses two Greek words, “πυρά” and “μεταλλουργία” meaning fire and metallurgy. It is the oldest group of metal extraction techniques and includes the thermal treatment of high-grade ores, minerals, concentrates and scraps to enable the extraction of the targeted metals.<sup>21</sup> The elevated temperature contributes to the easier extraction of metals from very stable compounds like MOs using reducing agents such as CO or electricity ( $\text{Fe}_2\text{O}_3$  – melting point 1565 °C,  $\text{Al}_2\text{O}_3$  – melting point 2072 °C). In addition, high temperature conditions increase the mass transport and the chemical reactivity of the different compounds taking place in the process. Pyrometallurgy occurs under controlled levels of oxygen, so that the efficiency and the desired purity of the product can be achieved. At the end of the process, the product and the impurities are in a molten state and they can be easily separated due to their different densities.

Depending on the composition of the ore, there are different sub methods of pyrometallurgy, more specifically calcination, roasting and smelting. Prior to the main pyrometallurgical steps, the drying of the materials to be processed is essential, because the presence of moisture could cause accidents especially in electric arc furnaces.<sup>22</sup>

Drying of water happens under controlled thermal conditions and most of the times the thermal energy is derived from heat generated from other parts of the plant. Water can be found in two different forms, the crystallized water and the bulk one that is chemically attached to the different compounds in form of hydroxyl groups. Thus, the two different chemical processes of water removal are expressed by the general reactions (**Equation 1.1** and **Equation 1.2**) below.



Calcination is the stage where volatile species and impurities are removed by thermal decomposition under limited oxygen conditions. Its name derives from the Latin word *calcinare*, which means burning of lime, due to its most common application in the heating of limestone above 900 °C for the production of lime and the generation of CO<sub>2</sub>, by the general **Equation 1.3** below.



In particular, calcination may refer to any operation during which the volatile organics, chemically bound water and similar compounds are removed from the material.<sup>23</sup> Usually it takes place in shaft furnaces, rotary kilns and fluidized bed reactors. The general expression describing this stage for carbonate compounds is the **Equation 1.4**.



Roasting is one of the most essential steps in pyrometallurgy and is a thermal process that contributes to the transformation of sulfides to more amenable compounds, oxides, for the upcoming treatments. It occurs under controlled thermal and air conditions, during which hot and highly pressurized oxygen acts as an oxidising agent, as shown in **Equation 1.5**.



During roasting, solid-gas reactions take place and since the ore particles are not in the liquid state, the oxygen gas is in contact with the solid surface of the particle. According to the core-shrinking model, the oxidising gas is reacting with the outer shell of the particle, as presented in **Figure 1.5**, and depending on the thickness of the particles, it is either easier or more difficult to reach the core and to fully convert the sulfide into an

oxide.<sup>24</sup> Therefore, grinding of the particles before this stage is essential as it enhances the reactivity and exposes more surface to the gas.

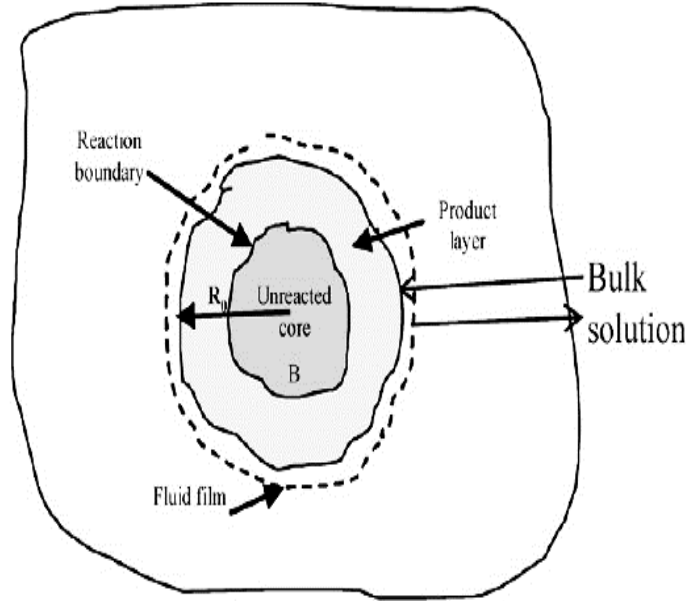
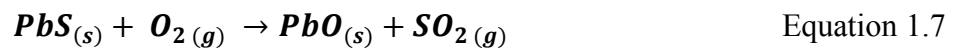
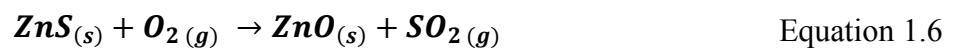


Figure 1.5: Schematic presentation of core-shrinking model<sup>25</sup>

Usually, roasting zinc and lead sulfides leads to their complete transformation into MOs according to the **Equation 1.6** and **Equation 1.7**, whereas roasting of copper sulfides results in partial conversion to MOs. The  $\text{SO}_2$  that is a by-product of these reactions can contribute to acid rain, so it needs to be extracted most usually to form sulfuric acid.



There are also other types of roasting such as the magnetic one, where a compound is transformed to a magnetic oxide that can be easily separated by magnetic methods (for example  $\text{Fe}_2\text{O}_3$  converts to magnetic  $\text{Fe}_3\text{O}_4$ ). Roasting takes place at temperatures below the melting point of the sulfides and their respective oxides (900 – 1000 °C) so every compound is in a solid form. There are different types of roasters such as the hearth roaster, the flash roaster and the fluidized bed roaster.

After all these pre-treatment steps, the most important step of pyrometallurgy where the smelting occurs. Smelting includes the process of carbothermic reduction of MOs into metallic species or metal rich products called matte, with the use of reducing agents such as carbon and carbon monoxide. During smelting, the temperature increases to a level where all materials melt, and the final products form two immiscible phases, the liquid

matte and the liquid slag. All the impurities gather in the slag phase with the use of additives, which can be separated easily due to the difference in densities with the molten metal phase.

Smelting relies on the Boudouard reaction, which is described by the **Equation 1.8**. This reaction is reversible and endothermic ( $171 \text{ kJ mol}^{-1}$  at  $25 \text{ }^\circ\text{C}$ ) and so the production of  $\text{CO}_2$  prevails at temperatures below  $700 \text{ }^\circ\text{C}$ .<sup>26</sup> After this temperature, the reversible reaction for the production of gaseous CO is favourable, due to the positive entropic term ( $T \times \Delta S$ ), which leads to a negative Gibbs energy and so to a spontaneous production of CO.<sup>26</sup> This fact contributes to the profitable function of the smelting process, which requires the production of CO that acts as a reducing agent for MOs according to **Equation 1.9**. In principle, CO acts as a good reducing agent due to its high affinity for oxygen, as presented in the Ellingham diagram of oxides, **Figure 1.6**.



Ellingham diagrams firstly developed by Harold Ellingham in 1944,<sup>27</sup> demonstrate the Gibbs energy of formation of MOs or other metal compounds at a given temperature, providing information about their stability. The most important knowledge that can be drawn from Ellingham diagrams of MOs is the ease of their reduction to a metallic state. Reactive metals are presented at the bottom of the diagram whose oxides are very stable and difficult to be reduced, such as CaO, MgO and  $\text{LiO}_2$ . At the top of the diagram, nobler metals are shown, whose oxides are rather unstable and a lot easier to be reduced. Carbon is a good reducing agent because its line, described by **Equation 1.10**, is downward and cuts across the lines of many metals. Carbon can reduce MOs at temperatures where the line of metals are above its line, for example, CO can only reduce MnO when the temperature is higher than  $1400 \text{ }^\circ\text{C}$ .



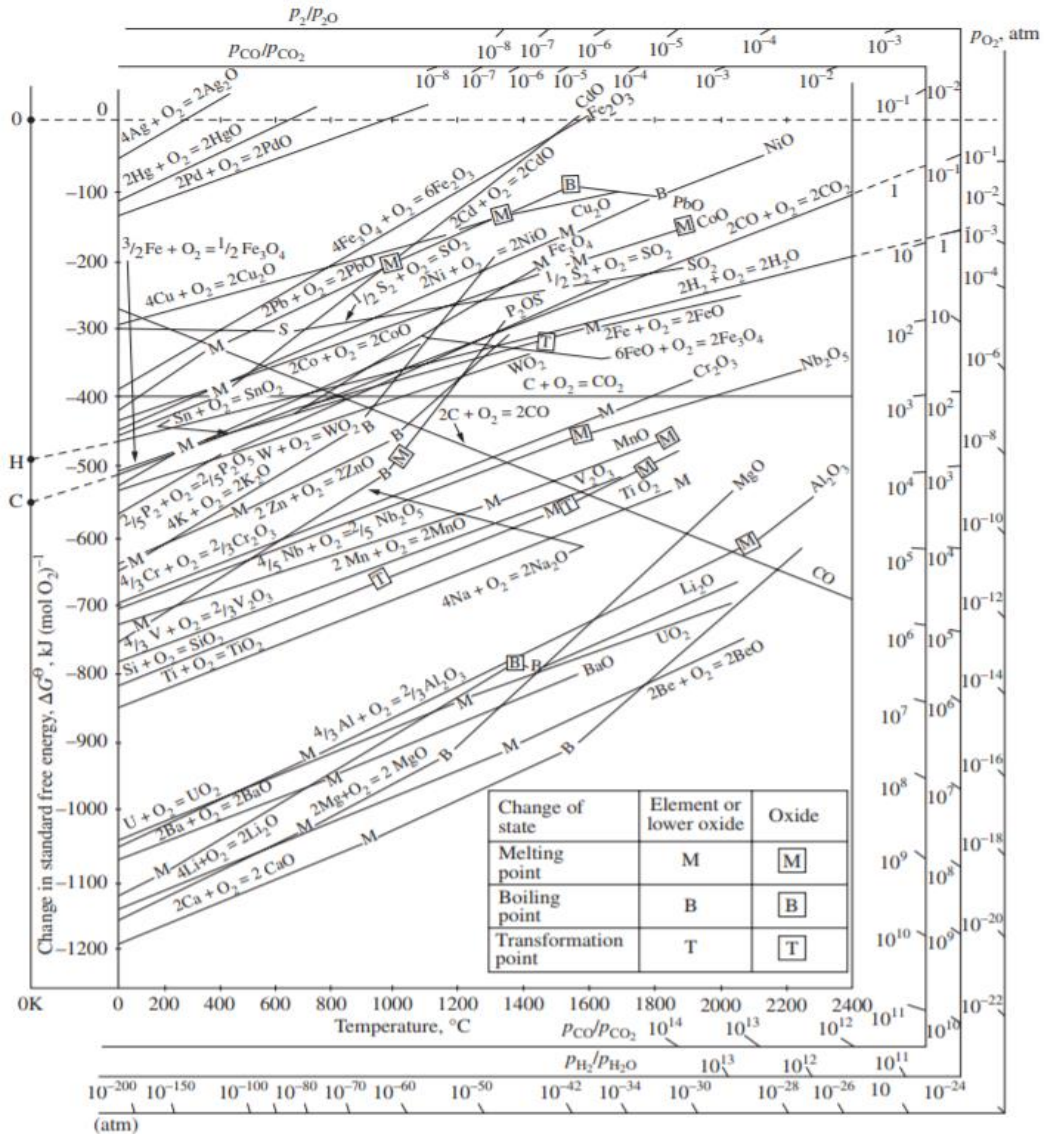
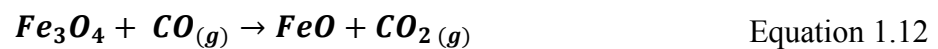
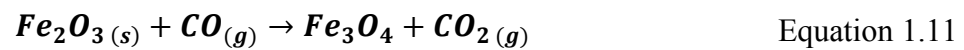


Figure 1.6: Ellingham diagram of metal oxides<sup>28</sup>

During smelting, additives called fluxes or slag formers enable easier melting of the impurities, in order to make a proper slag that stays on top of the molten metal. Most common fluxes are limestone (CaCO<sub>3</sub>) and dolomite (Ca, MgCO<sub>3</sub>), with dolomite is often favoured as it is less expensive and more readily available.<sup>29</sup>

The most common type of smelter is the blast furnace that can accommodate both the stages of roasting and smelting. It is employed mainly in the production of pig Fe, Cu and Pb and a schematic of the process is shown in **Figure 1.7**. It consists of different thermal zones where in each one a different chemical reaction occurs. For instance, for the reduction of hematite (Fe<sub>2</sub>O<sub>3</sub>) the furnace is fed with a mixture of roasted Fe<sub>2</sub>O<sub>3</sub>, in which Fe exists in its highest oxidation state, along with C and CaCO<sub>3</sub>. Elemental Fe is produced by the reduction of Fe<sub>2</sub>O<sub>3</sub> with the aid of CO in three stages depending on the temperature

of the different parts of the furnace. The reduction of  $\text{Fe}_2\text{O}_3$  to magnetite ( $\text{Fe}_3\text{O}_4$ ) occurs at a range of temperatures between 200 – 700 °C (**Equation 1.11**), the reduction of  $\text{Fe}_3\text{O}_4$  to  $\text{FeO}$  takes place at temperatures above 850 °C (**Equation 1.12**) and the final reduction of  $\text{FeO}$  to  $\text{Fe}$  occurs approximately at 1200 °C (**Equation 1.13**). Finally,  $\text{Fe}$  melts at the temperature of 2000 °C. The constant production of  $\text{CO}$  from the reaction of  $\text{C}$  and  $\text{CO}_2$  (**Equation 1.10**) facilitates the reduction. The product of liquid matte gathers at the bottom of the furnace below the molten slag and then both are tapped out from different holes.



Pyrometallurgy is the main method of  $\text{Fe}$  production because its main ores are MOs namely  $\text{Fe}_2\text{O}_3$ ,  $\text{Fe}_3\text{O}_4$  and goethite -  $\text{FeO} (\text{OH})$ . In addition, the ores of most base metals such as  $\text{Zn}$ ,  $\text{Co}$ ,  $\text{Sn}$  and  $\text{Pb}$  as well as the majority of  $\text{Cu}$  and  $\text{Ni}$  ores are treated thermally. Thus, it is apparent that pyrometallurgy is a well-established science of metal extraction and is widely used in MOs processing.

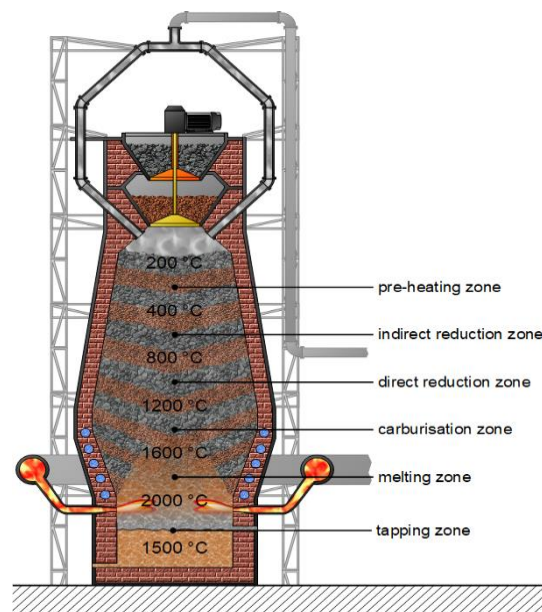


Figure 1.7: Schematic diagram of different zones in a blast furnace<sup>30</sup>

### 1.3 Hydrometallurgy

Hydrometallurgy derives from two Greek words “ὕδωρ” and “μεταλλουργία”, which mean water and metallurgy respectively. This group of techniques include methods of mainly low and rarely high temperatures conditions that employ aqueous solvents for the dissolution and recovery of metals.<sup>31</sup> It is well established since the 19th century and one of the most remarkable examples is the extraction of Au and Ag by cyanidation.<sup>20</sup> Cyanidation is one of the oldest industrially implemented hydrometallurgical processes and dates back to 1887, when a chemical metallurgist named John Stewart MacArthur was granted a patent related to the “Process of obtaining Gold and Silver from Ores”.<sup>33</sup> In this process, sodium cyanide (NaCN) was employed to dissolve Au and Ag by complexing with the targeted metals to form soluble  $[\text{Au}(\text{CN})_2]^-$  and  $[\text{Ag}(\text{CN})_2]^-$  species, as described in **Equation 1.14**.



As previously discussed, most of the base metals are extracted via thermal routes but even so hydrometallurgy is an essential approach for the processing of rare earth elements (REEs), and Al, Zn, Ni, and Mo.<sup>29</sup> It is very important for the processing of low-grade ores and for recycling of low metal containing residues, as it does not require extreme energy consumption like pyrometallurgical approaches. Sometimes, both pyrometallurgy and hydrometallurgy are employed, as in the case of the processing of sphalerite (ZnS), where the mineral first is calcined and roasted to its respective oxide (ZnO), then is leached in sulfuric acid (H<sub>2</sub>SO<sub>4</sub>) and finally Zn is recovered by electrowinning.<sup>34</sup>

In hydrometallurgy, aqueous solutions act as the solvents and/or electrolytes. Before the development of any industrial flowsheet, sufficient water supply near the unit operations needs to be confirmed. Contingent upon the starting material, its composition, its value and the desired product there are physical and chemical methods that may aid the extraction of metals. Physical separation methods include processes such as flotation, distillation and filtration, whereas chemical methods consist of the processes of leaching, solvent extraction, ion exchange, cementation and precipitation, as seen schematically in **Figure 1.8**. There is also the category of electrochemical methods that incorporates the processes of electro-dissolution and electro-winning both constituting the general science of electrometallurgy, which most of the times considered as a subcategory of hydrometallurgy.<sup>19</sup>

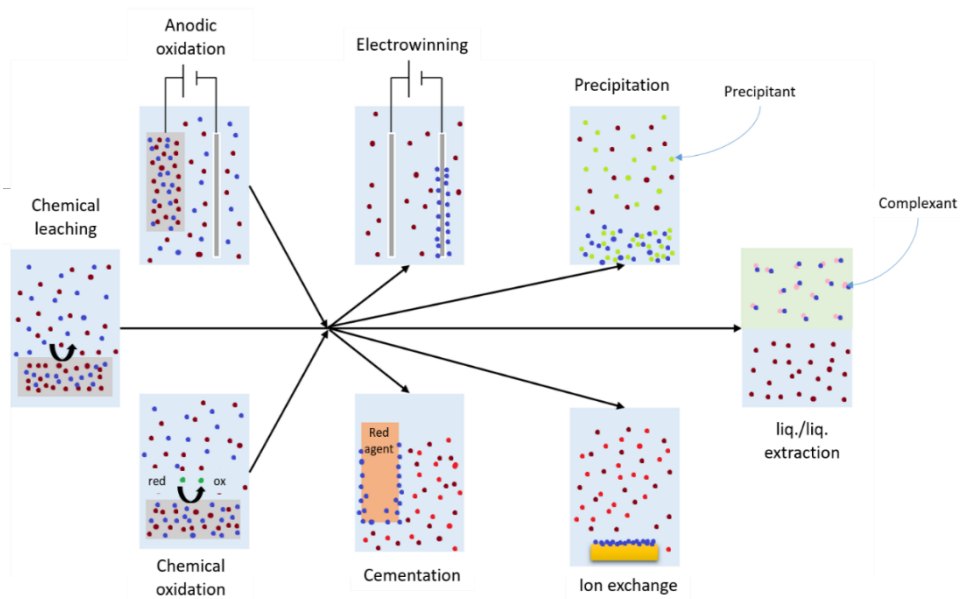
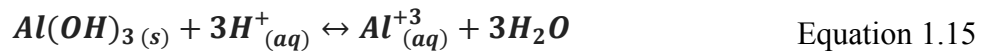


Figure 1.8: Schematic representation of the different stages and processes of metal extraction and recovery (adapted from<sup>35</sup>)

The first step of any hydrometallurgical approach is the beneficiation of the mineral, during which the mineral is ground to fine particles or roasted, as in case of metal sulfides. Next, leaching occurs where high- or low- grade ores or minerals, industrial residues and in general any metal containing material is dissolved in an aqueous or non-aqueous solvent, until the selective extraction of targeted metals is accomplished.<sup>36</sup> For a successful extraction, the liberation of metals from their compounds and their transformation in metal ions, by breakage of the bonds from their ligands are required. Compounds like metal chlorides and nitrates are more soluble in water than their corresponding oxides or sulfates.

For metal compounds that are covalent and thus insoluble in water as MOs, sulfides, silicates and phosphates the extraction requires the presence of another ion that facilitates the dissolution. For that reason, since most of metals are found in the compounds of oxides and sulfides, most of the hydrometallurgical routes include the employment of acidic or basic solutions.<sup>37</sup> For example, the dissolution of aluminium hydroxide, which is insoluble in water, requires the presence of protons that will form water molecules with the hydroxide group (**Equation 1.15**). These protons are coming from the dissociation of an acid in water and apparently the stronger the acid (lower  $pK_a$ ) the stronger the proton activity in the solution.



The **Equation 1.15** does not include any complexation reaction, which in some cases is required for metal extraction from insoluble compounds. For example, the dissolution of Fe<sub>2</sub>O<sub>3</sub> in water may occur via protonation, complexation and reduction.<sup>38</sup> An example of a complexation reaction for Fe<sub>2</sub>O<sub>3</sub> is given with **Equation 1.16**, where chloride acts as ligand and complexes Fe, resulting in the formation of soluble [FeCl<sub>3</sub>]<sup>-</sup> species.<sup>39</sup>



Another example of a successful leaching agent for the dissolution of iron oxides in water is oxalic acid. This agent is appropriate, since it is one of the best reducing organic acids and it has good complexation properties, rendering the easy recovery of iron by its precipitation in the form of iron oxalates. These oxalates then may be transformed to pure iron oxides by calcination.<sup>40</sup> The dissolution of iron is happening through a complex photo-electrochemical reduction process that encloses the mechanism of charge transfer between the oxalate ligand and the iron on the iron surface and between the oxalate species [Fe(C<sub>2</sub>O<sub>4</sub>)<sub>3</sub>]<sup>3-</sup> and [Fe(C<sub>2</sub>O<sub>4</sub>)<sub>2</sub>]<sup>2-</sup>.<sup>41</sup>

In general, the choice of the leaching agent is made depending on its physicochemical properties, cost, selectivity and possibility to regenerate. It is essential that the selected leaching agent has relatively low cost, selectivity towards the metal and its surrounding gangue material, low toxicity, can be easily produced in large amounts and can bring about rapid extraction.<sup>29</sup> In most hydrometallurgical flowsheets, aqueous solvents of acids or bases are employed due to their ability for efficient extraction of metals. Acidic solutions of sulphuric acid (H<sub>2</sub>SO<sub>4</sub>), nitric acid (HNO<sub>3</sub>), hydrochloric acid (HCl) or aqua regia (3:1HCl/HNO<sub>3</sub>) are some of the most common leaching agents because they are cheap and show excellent solvation properties. An example of acidic leaching is the extraction of Zn from ZnO existing in electric arc furnace dust using sulphuric acid.<sup>42</sup> Basic solvents are also used for metal extraction with one of the most established and industrially implemented examples to be the alumina (Al<sub>2</sub>O<sub>3</sub>) dissolution in sodium hydroxide (NaOH).<sup>43</sup> In most industrial processes, the solvents are recirculated in the process for both economic and environmental reasons.

To sum up, the generic mechanisms for metal solubilisation of a metal are:

- Protonation using acidic or basic media
- Formation of soluble complexes using strong ligands

- Electron transfer by using oxidising / reducing agents
- Electron transfer by electrochemical approaches

The first two mechanisms have been discussed before with examples. The electron transfer (ET) occurs when an oxidising or reducing agent is added to the solution, often in the form of an oxidising acid.<sup>44</sup>

As for the fourth method, a reactive substance contributed to the breakage of the metal and non-metal bond. This reactive substance either forms a soluble complex with the metal or makes a bond with the non-metal part so the metal is free in the solvent as an ion.

After the successful and selective leaching of the targeted metals, impurities, suspended particles and solid undissolved material are removed, so that the concentration of the desired metal to be increased, aiding the operation requirements of the next stage, the recovery. Different techniques developed for the recovery of metals such as cementation, electrowinning, solvent extraction, ion exchange, precipitation and liquid-liquid extraction, which are schematically shown in **Figure 1.8**.

Cementation is an electrochemical process during which the desired metal is reduced to the metallic state at a solid sacrificial metallic interface and these two metals need to have different electrode potentials. In **Table 1.2** the electrode potentials of some metals are presented.<sup>45</sup> The sacrificial metal, usually in the form of a powder or sheet is introduced to the solution containing the leached metal ions and these exchange with the sacrificial metal. Cementation shows a similar redox process as electrowinning, with the distinguishing feature to be the absence of external voltage. The force that drives the targeted metal to be precipitated and the cementing metal to dissolve, is the difference in electrode potentials. The process of cementation is thermodynamically possible when the sacrificial metal has a more negative potential. For example, the cementation of metallic Cu with the use of metallic Fe is common practice for more than 600 years now and recovery of Cu is successful due to the different standard reduction potentials of Cu and Fe,<sup>46, 47</sup> shown in **Table 1.2**. The process is accomplished by the spontaneous simultaneous reduction of Cu on the Fe surface and the oxidation of Fe into the solution. The electrode potentials of Cu and Fe are given by the Nernst equation that describes the whole cell of the reaction (**Equation 1.17**).

$$E = E_{Cu}^0 - E_{Fe}^0 - \frac{RT}{2F} \ln \frac{a_{Fe^{2+}}}{a_{Cu^{2+}}} \quad \text{Equation 1.17}$$

It is apparent that the overall potential of the **Equation 1.17** is positive thus the enthalpy is negative, and the reaction is spontaneous without the need of an applied voltage. Cementation is relatively simple and cheap process, so it can be used for the recovery of metals that have low value. Sometimes, it is used prior to the metal recovery to remove hazardous metals from the solutions, like Pb or Cd.

*Table 1.2: Standard reduction potentials for selected metals and reactions<sup>48</sup>*

Metal	Half-cell reduction reaction	E° (V)
Mg	$Mg^{+2} + 2e^{-} \rightarrow Mg$	-2.37
Al	$Al^{+3} + 3e^{-} \rightarrow Al$	-1.66
Mn	$Mn^{+2} + 2e^{-} \rightarrow Mn$	-1.63
Zn	$Zn^{+2} + 2e^{-} \rightarrow Zn$	-0.76
Fe	$Fe^{+2} + 2e^{-} \rightarrow Fe$	-0.44
Ni	$Ni^{+2} + 2e^{-} \rightarrow Ni$	-0.25
H <sub>2</sub>	$2H^{+} + 2e^{-} \rightarrow H_2$	0.00
Cu	$Cu^{+2} + 2e^{-} \rightarrow Cu$	+0.34
Ag	$Ag^{+} + e^{-} \rightarrow Ag$	+0.80
Au	$Au^{+3} + 3e^{-} \rightarrow Au$	+1.50

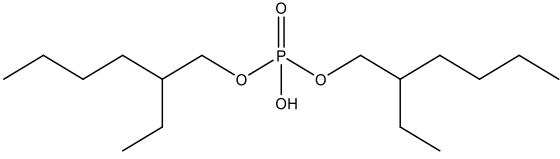
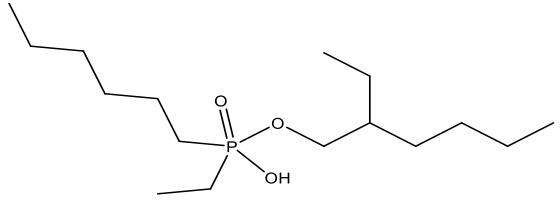
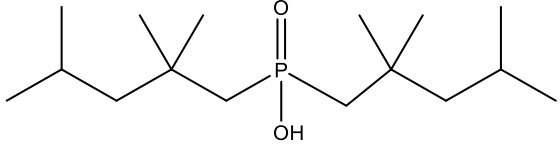
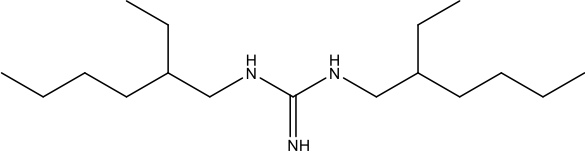
Precipitation is a method of metal separation from its leachates and occurs mainly with the manipulation of temperature and pH, which highly affect the solubility of metals, or with the addition of a chemical substance functioning as a precipitant. In addition, it may take place by evaporating the solvent or with a process of reduction / oxidation. It is a very common industrial approach for the removal of heavy metals from waste waters, the precipitates of which can then be filtered and the water can be reused or discarded.<sup>49</sup> The introduction of chemical substances like antisolvents, precipitants, coagulants and flocculants contribute to precipitation of metals by reducing the solubility of metals with the formation of insoluble complexes. An example of a common precipitant is oxalic acid that has been used in many applications for the recovery of metals from their leachates, especially for processes of rare earth elements (REEs).<sup>50-52</sup> The distinctive difference between precipitation and crystallization is that the former is faster.<sup>53</sup> Metal precipitation takes place when the concentration of the metal in a solvent exceeds its solubility, forcing the system towards the formation of solid metal particles, so that equilibrium is achieved

between the metal ions in the solution and the metal salts precipitated.<sup>54</sup> The difference between the solubility product ( $K_{sp}$ ) and the ionic product ( $K_{ss}$ ) is the driving force of the precipitation. Supersaturated solutions show a very fast precipitation because the equilibrium is already shifted and a very small increase in the concentration of the metal leads to the formation of a precipitate. To sum up, during precipitation three different steps take place, the super saturation, nucleation and crystal growth.

Electrowinning uses electrodeposition to reduce the leached metal onto another metallic surface by passing current through the system.<sup>55</sup> The most commonly and industrially electrowon metals are Al, Cu, Au, Ag, Zn, Co and Ni. A significant issue of aqueous solutions is that electrowinning is hindered by hydrogen evolution on the cathode for metals that are more negative than hydrogen, like Ni, Mn, Fe, Zn, Al etc., as shown in **Table 1.2**. For these metals different electrolytes are required, like molten salts or ionic liquids<sup>56</sup>, otherwise the hydrogen evolution will sharply decrease the efficiency of the process and will bring on the embrittlement of the deposit. Prior to electrowinning, the removal of any impurities in the leachate is crucial, due to the possible contamination of the deposited metal from other metals that have less negative or positive electrode potentials.

Another method of recovery is the solvent extraction (also called liquid-liquid extraction), which is a technique taking advantage of the different solubilities of metals in different solvents. It is widely used in hydrometallurgy for the recovery of a broad range of metals like Co, Ni, Zn, U, Mo, W, V, Zr, Nb, Ta, Ga, Ge, PGMs and REEs. It is advantageous because it can support selective processes under mild conditions, in a rapid and non-complicated way and requires simple equipment. Usually a polar aqueous and a non-polar organic solvent are employed, which are immiscible. The organic phase consists of an extractant dissolved in a diluent and in some cases, a modifier and a synergistic agent are also present. The modifier enhances the properties of the solvent, by increasing the solubility of the employed extractant, reducing adsorption losses etc. and the synergistic agent increases the activity of the extractant.<sup>57</sup> During the extraction process, the desired metal undergoes a change in ligation to make it more soluble in the organic phase. Currently, there are approximately 40 extractants that are used for separation of metals with the most common to be presented in **Table 1.3**.

Table 1.3: Common extractants employed for separation of metals<sup>58</sup>

Extractant	Application
 <p data-bbox="411 517 847 546">di-(2-ethylhexyl)phosphoric acid (DE2HPA)</p>	<p data-bbox="994 566 1369 595">Separation of Co / Ni and REEs</p>
 <p data-bbox="343 808 914 837">ethyl hexyl hydrogen 2-ethyl hexyl phosphonate (PC-88A)</p>	
 <p data-bbox="352 1055 903 1084">bis(2,2,4 trimethyl pentyl)phosphinic acid (Cyanex 272)</p>	<p data-bbox="1007 943 1358 1003">Separation of Co / Ni, Zn / Fe and REEs</p>
 <p data-bbox="427 1301 829 1330">1,3-Bis(2-ethylhexyl)guanidine (LIX-79)</p>	<p data-bbox="1026 1189 1337 1249">Au recovery from cyanide solutions</p>

The driving force of the distribution of the desired metal between the two solvents is the chemical potential, since when the process of solvent extraction is finished the overall system reaches the lower free energy of the stable configuration. The distribution coefficient  $K_d$  of the metal is affected by its solubility in each one of them and is equal to the ratio of the solubilities of the metal in the aqueous and in the organic phase, as seen in Equation 1.18.<sup>59</sup>

$$K_d = \frac{\text{Concentration of metal in organic phase}}{\text{Concentration of metal in aqueous phase}} \quad \text{Equation 1.18}$$

A final method for metal recovery is ion exchange, a reversible process where ions are exchanged between the leachate and a solid phase and is widely used for the recovery of Au, U, Mo, Ni, Cu and other metals. The ion-exchange resin has a styrene or acrylic

backbone with an ionic functionality and is insoluble in the leach liquor media.<sup>60</sup> There are two typical categories of resin, the functionalized macroporous and the gel polymer. It is possible to tailor the properties of the resin and the selectivity of the process by introducing different functional groups during its synthesis.<sup>61</sup> Other type of ion-exchangers are the zeolites, montmorillonite and clays. In general, the ion-exchangers are subdivided into two: cation and anion ones, which exchange positive charged ions or negative ones, respectively. During the process of ion exchange, electroneutrality is always preserved by the exchange of same amounts of counter ions.<sup>62</sup>

### **1.3.1 Brief comparison of pyrometallurgical and hydrometallurgical method**

The advantages and disadvantages, of pyrometallurgy and hydrometallurgy are summarized in **Table 1.4**. Often the factors which decide the type of processing of an ore are the logistics of transportation e.g. if coke is not locally available the hydrometallurgy may be more suitable.

Table 1.4: Advantages and disadvantages of the two main metallurgical methods; pyrometallurgy and hydrometallurgy

	<b>Advantages</b>	<b>Disadvantages</b>
<b>Pyrometallurgy</b>	<p>Rapid reaction rates</p> <p>High temperature conditions allow not thermodynamically possible reactions to occur</p> <p>Limited chemical consumption</p> <p>Easy separation of melted metal and gangue material due to difference in densities</p> <p>Stable solid residues</p>	<p>Economically viable only for high-grade ores</p> <p>Not selective and appropriate only for simple ores or minerals</p> <p>High capital investment and inability of testing the process in small pilot scale</p> <p>Extreme temperature conditions and significant energy consumption</p> <p>Emission of greenhouse gases and dust</p>
<b>Hydrometallurgy</b>	<p>Possibility in employment in processing of low metal containing deposits</p> <p>Flexibility in operation</p> <p>Simple equipment and possibility of continuous and automated process</p> <p>Low capital investment</p> <p>Processes under mild conditions</p> <p>Tailored to be selective towards different metals</p> <p>Ability in separation of similar metals (Co/Ni, PGMS and REEs)</p> <p>Clean operating environment</p>	<p>Slower reaction rates</p> <p>Large chemical consumption</p> <p>Toxic reagents (e.g. <math>CN^-</math>)</p> <p>Strong acidic / basic solutions required for the processing of stable compounds</p> <p>Less stable solid residues</p> <p>Vast amounts of aqueous wastes either corrosive, poisonous or rich in heavy metals that need purification before disposal</p>

Pyrometallurgical and hydrometallurgical processes are extremes of the temperature and ligand scale and the current study is to investigate whether low temperature molten salts (ionic liquids) can offer a hybrid of the two approaches.

## 1.4 Ionometallurgy

Ionometallurgy is a sub category of solvometallurgy, which uses ionic rather than molecular non-aqueous solvents.<sup>63</sup> Ionometallurgy, in principal, involves the processing of metals using ionic liquids and deep eutectic solvents.<sup>64</sup> These solvents have proven to be good candidates for substituting aqueous solutions making use of properties such as wide potential windows.<sup>56</sup> It gives flexibility, in the sense that both ionic liquids and deep eutectic solvents can be tailor made for specific processes and therefore, the selectivity of the extraction process can be improved by the appropriate choice of anion species, preventing also the use of hazardous additives common in hydrometallurgy.

The first ionic solvents applied and still employed in metallurgical processes are the molten salts (also known as fused salts). Molten salts are solvents that are composed solely from ions, they are solid at ambient temperatures, while liquefying at higher ones.<sup>65</sup> They have been known for a very long time, with the first experiments in the field of electrolysis held by Davy in 1807.<sup>66</sup> They have found applications in the field of metallurgy, electrochemistry, nuclear chemistry and energy storage devices due to their favourable properties of chemical, electrochemical and thermal stability that enables them to be employed at very high temperatures. These properties include non-volatility, low viscosity, wide potential window and high conductivity.<sup>67, 68</sup> The large concentration of ions in the solutions also enhances their properties as electrolytes and due to high temperatures used it increases the reaction rates. Inorganic molten salts may also be produced in bulk quantities in an economic process since the components are derived from naturally occurring minerals. In addition, they are very useful in applications where aqueous solutions are hindered. The electrowinning of Al that is more negative than hydrogen is not possible in molecular aqueous solvents, but it is can be successful in high temperature molten salts (cryolite -  $\text{NaAlF}_6$ ).<sup>69</sup>

In this work, emphasis will be given only in ionic solvents that are liquid at ambient temperatures, as room temperature ionic liquids (RTILs) and deep eutectic solvents (DESSs).

### 1.4.1 Ionic Liquids

Nowadays, the term ionic liquids (ILs) is used to define solvents composed solely from ions, which are liquid at temperatures below 100 °C.<sup>56</sup> This definition is very important for drawing a line between them and molten salts, since both consist of oppositely charged ions but have very different melting points. IL research started with eutectic mixtures of AlCl<sub>3</sub> with NaCl and KCl etc.<sup>67</sup> The melting point of AlCl<sub>3</sub> is 192 °C and the melting points of NaCl and KCl are 803 and 772°C respectively. The melting point of the binary mixtures AlCl<sub>3</sub>:NaCl and AlCl<sub>3</sub>:KCl are much lower, 151 °C and 256 °C respectively.<sup>70</sup> So, by mixing these components, ionic solvents with lower melting point than the ones of molten salts were achieved.

**Figure 1.9**, shows some of the main developments in ILs but more comprehensive reviews of ILs together with their, applications, properties and limitations are given in the literature.<sup>71-73</sup>

In 1888 Gabriel found the IL ethanolanmonium nitrate, with a melting point of 52-55 °C but his contribution never received much attention.<sup>74</sup> In most reviews ethylammonium nitrate [EtNH<sub>3</sub>] [NO<sub>3</sub>], synthesized by Paul Walden in 1914 by neutralising ethylamine (CH<sub>3</sub>CH<sub>2</sub>NH<sub>2</sub>) with concentrated nitric acid (HNO<sub>3</sub>), is reported to be the first room temperature ionic liquid (RTIL) with a melting point of 13-14 °C.<sup>75</sup> After Walden's invention, 40 years passed until ILs come to the spotlight again with the synthesis of 1-ethylpyridinium bromide - aluminium chloride [C<sub>2</sub>py]Br AlCl<sub>3</sub> in 1951 by Hurley and Weir. This type of IL took the name chloroaluminate liquids / eutectics and was tested first for the electroplating of Al and then of other metals.<sup>76</sup> Chloroaluminate liquids are mixture of alkyl halides with AlCl<sub>3</sub> with very low melting points compared to other inorganic eutectic salts. The mole fraction of AlCl<sub>3</sub> ( $\chi_{AlCl_3}$ ) affects the speciation of the metal halide and thus the Lewis acidity. For example, the IL [C<sub>2</sub>mim]Cl–AlCl<sub>3</sub> is affected by the  $\chi_{AlCl_3}$  in the following way:<sup>77</sup>

- $\chi_{AlCl_3} > 0.5$ , acidic IL [Al<sub>2</sub>Cl<sub>7</sub>]<sup>-</sup> is in equilibrium with [AlCl<sub>4</sub>]<sup>-</sup>
- $\chi_{AlCl_3} < 0.5$ , basic IL, free Cl<sup>-</sup> is in equilibrium with [AlCl<sub>4</sub>]<sup>-</sup>
- $\chi_{AlCl_3} = 0.5$ , neutral IL - [AlCl<sub>4</sub>]<sup>-</sup> species

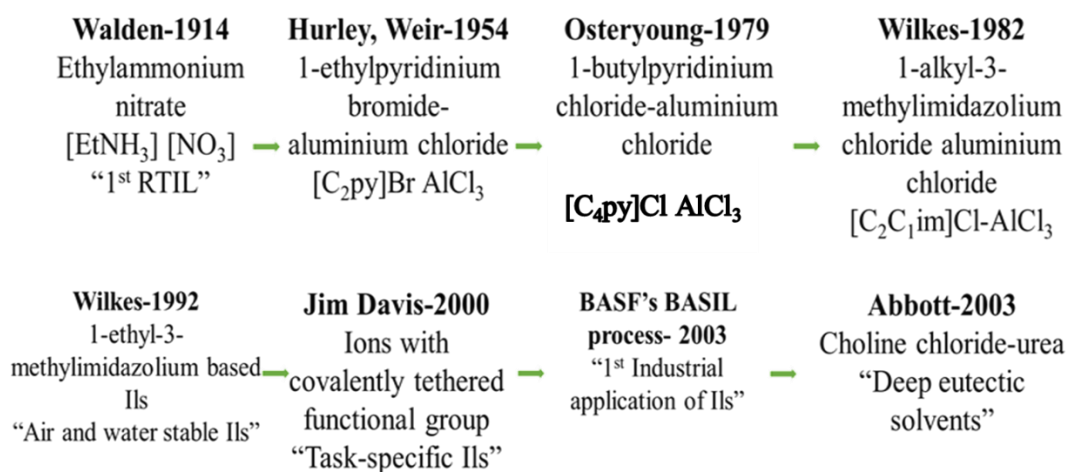


Figure 1.9: Selected moments of the history of ILs by chronological order <sup>78</sup>

In 1979 Osteryoung and Robinson introduced the 1-butylpyridinium chloride – aluminium chloride [C<sub>4</sub>py]Cl AlCl<sub>3</sub> which was liquid at room temperature for wider range of compositions.<sup>79</sup> In 1982, Wilkes synthesized, 1-alkyl-3-methylimidazolium chloride – aluminium chloride [C<sub>2</sub>C<sub>1</sub>im]Cl – AlCl<sub>3</sub>. Although this IL showed high potential for different applications, it was very sensitive to moisture.<sup>70, 80</sup> These solvents have been called “first generation” ILs.

In 1992 Wilkes and Zaworotko synthesized air and water stable ILs based on 1-ethyl-3-methylimidazolium cations.<sup>81</sup> The researchers produced mixtures of 1-ethyl-3-methylimidazolium with simple anions as tetrafluoroborate [BF<sub>4</sub>]<sup>-</sup> and acetate [OAc]<sup>-</sup> and reported their air and water stability. More recently, anions such as trifluoromethanesulfonate [CF<sub>3</sub>SO<sub>3</sub>]<sup>-</sup> and bis-trifluoromethanesulfonylimide [(CF<sub>3</sub>SO<sub>2</sub>)<sub>2</sub>N]<sup>-</sup> / [Tf<sub>2</sub>N]<sup>-</sup> have become more popular because of their higher stability compared with [BF<sub>4</sub>]<sup>-</sup> and [PF<sub>6</sub>]<sup>-</sup> that hydrolyse producing HF.<sup>82</sup> Subsequently many research groups have looked at related anions and cations and their applications, mainly in a variety of fields such as electrochemistry and transition metal catalysis.

Davis in 2000 developed the so called “task specific ionic liquids” (TSILs), which contained a covalently bonded functional group in one of the ions, rendering them selective in different applications.<sup>83</sup> In 2003 BASF developed the first industrial application in the Biphasic Acid Scavenging process (BASIL), where 1-methylimidazole substituted triethylamine as a scavenger of HCl in the production of diethoxyphenylphosphine prepared by the reaction of dichlorophenylphosphine with

ethanol.<sup>84</sup> In the same year, Abbott introduced Deep Eutectic Solvents (DESs) by mixing choline chloride and urea, opening the path to potentially less toxic and cheaper ILs.<sup>85</sup>

One common classification of ILs is into protic and aprotic. Protic ILs (PILs), are synthesized by the mixture of a Brønsted acid and a Brønsted base, as seen in **Equation 1.19**.<sup>86</sup>



This proton transfer gives unique characteristics to these solvents, resulting in proton-donor and acceptor sites, which can be the base for the development of a network of hydrogen bonds. By employing stronger acids or bases, the driving force of the proton transfer changes and so does their ionicity.<sup>87</sup> But this also means that in the case of not sufficient proton transfer, the agglomeration of neutral base and acid species is possible.<sup>86</sup> It has been suggested, that even though in these liquids, neutral molecules can exist they can still be called ionic but only if the amount of the neutral molecules is below 1%.<sup>88</sup> PILs have shown good characteristics in electrochemical and synthetic applications with a very promising result to be the elimination of the polarization of the oxygen electrode in fuel cells in these media.<sup>89</sup> Another important application is in CO<sub>2</sub> capture, which has higher solubility due to the hydrogen bonding provided by these media.<sup>90</sup>

Aprotic ILs (AILs) have been investigated more than PILs due to their low volatility. The major difference between these two classes of ILs is that PILs are volatile since the acidic proton can be abstracted by the anion at room temperatures.<sup>91</sup> They are mixtures of bulky non-symmetrical organic cations with smaller inorganic anions. They are formed via the Menshutkin type reaction, example of which is given in **Figure 1.10**.<sup>92</sup> One significant property of AILs is their “ionicity” which is the reason for their low volatility.<sup>93</sup>

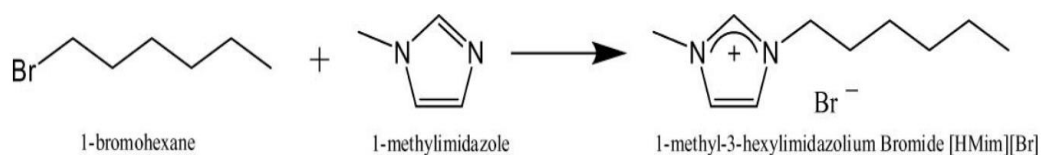


*Figure 1.10: Example of aprotic ionic liquid synthesis from the mixture of 1-bromohexane with 1-methylimidazole*<sup>94</sup>

## Synthesis and properties of ionic liquids

Currently, there is a wide range of anions and cations that are employed in the synthesis of ILs, as seen in **Figure 1.11**.

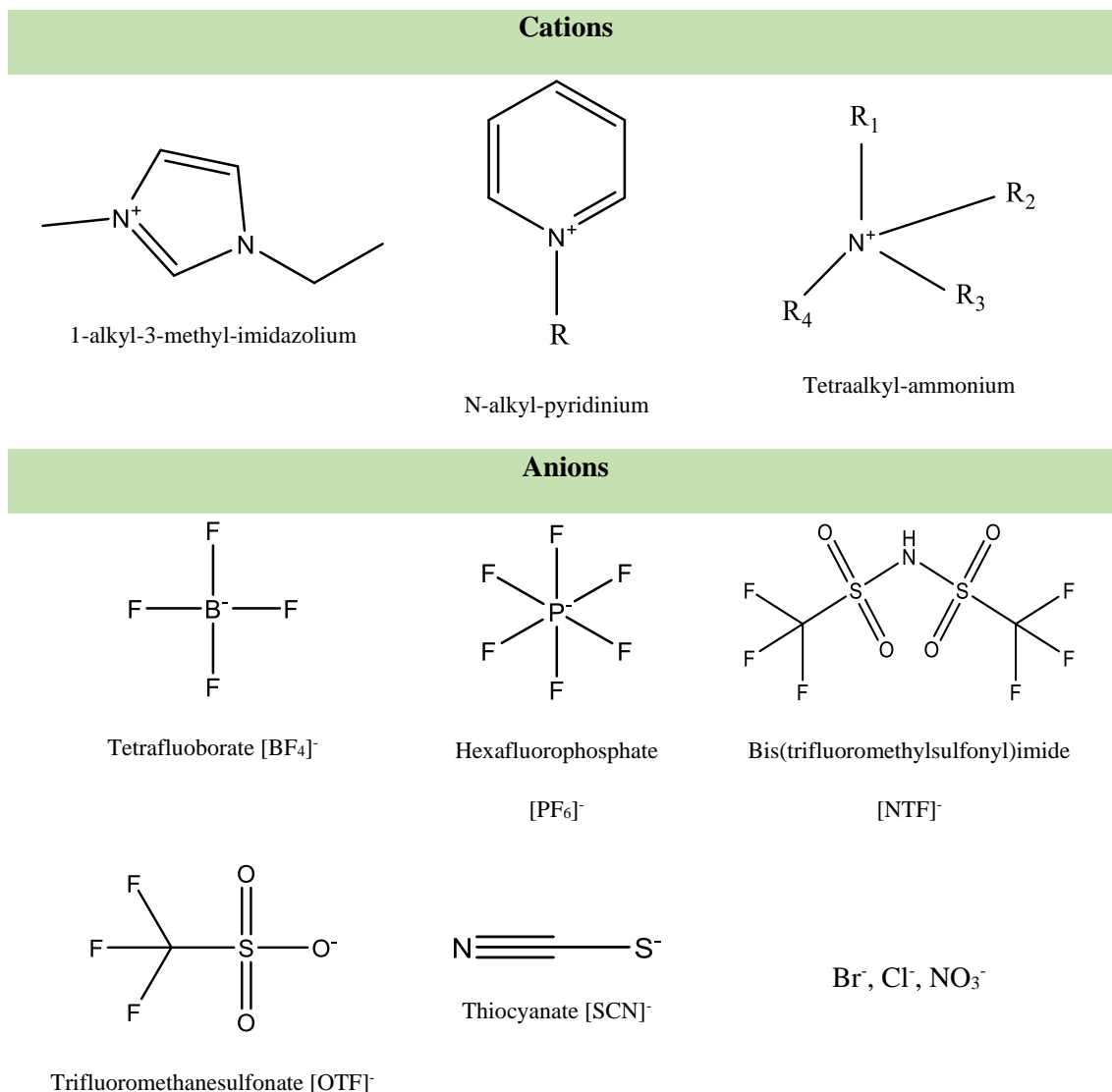


*Figure 1.11: Structures of common cations and anions for the synthesis of ILs<sup>63</sup>*

The cation in most cases is an organic compound, as imidazolium, pyridinium, pyrrolidinium, phosphonium, ammonium etc. and the anion can be either inorganic like Cl<sup>-</sup>, PF<sub>6</sub><sup>-</sup>, BF<sub>4</sub><sup>-</sup> or organic as trifluoromethyl sulfonate [CF<sub>3</sub>SO<sub>3</sub>]<sup>-</sup>, bis[(trifluoromethyl)sulfonyl]imide [(CF<sub>3</sub>SO<sub>2</sub>)<sub>2</sub>N]<sup>-</sup>, trifluoro ethanoate [CF<sub>3</sub>CO<sub>2</sub>]<sup>-</sup>.

It is estimated that up to 10<sup>18</sup> ILs can be produced by mixing different anions and cations. In general, between the ions consisting the IL, coulombic interactions predominate, resulting in high cohesive energy, which accords with their low vapour pressure. Usually the ions form clusters and aggregates, although an ideal IL has non-associated ions.<sup>95</sup>

The properties of ILs have been characterised extensively. Due to the nature of their structure, they show very different physical properties compared with aqueous molecular solvents. The main physical properties of ILs are briefly discussed.

➤ Melting point

The melting point of ILs is important because it sets the range of temperature in which these solvents can function. It defines the lower temperature of the liquid-phase diagram in which they can be utilised as solvents and the thermal decomposition marks the upper limit. It is highly affected by the size and symmetry of the ions, the charge distribution, the hydrogen bonding ability and the type of interactions between the ions.<sup>71</sup> The difference in the melting point of ILs compared to the ones of inorganic molten salts comes from the substitution of small symmetrical inorganic cations with bulky and asymmetrical ones that shift the charge distribution, causing reduction of the lattice energy and thus of the melting point. This can be explained with the fact that ions with high symmetry result in more efficient ion-ion packing in the crystal cell and so higher melting point. The ions size can also be explained by the fact that ions with increased size, leading to decrease in the Coulombic attraction forces and to increase in covalency of them leading to reduced melting point.

➤ Density

The density of ILs is an important property, not only for their industrial implementation, but also for the investigation of other properties as the heat capacity and viscosity and it has been studied more than the other physical properties. Along with the viscosity, density plays a significant role in the dispersity of the media and the contact with other reagents, which is crucial especially in catalysis.<sup>96</sup> Most of the times, the density of ILs is higher than the densities of the majority of molecular solvents and ranges between 1.05-1.35 g cm<sup>-3</sup> at ambient conditions.<sup>97</sup> The density decreases with the increase of the alkyl chain's length for all types of cations and with the increase in temperature.<sup>96,98</sup> The type of anion has a great effect on the density and the general trend shows that by increasing the molecular weight of the anion, the density increases. The type of cation also affects the density but to a lower extent compared to the anion type.

➤ Viscosity

The viscosity ( $\eta$ ) is a very crucial physical property that affects the efficiency of a solvent in metallurgical and electrochemical applications and it affects the transport properties of the systems. ILs usually exhibit high values of viscosity. However, there are ILs that exhibit relatively low viscosities almost comparable with aqueous solvents and others that are extremely viscous. The high viscosity is a disadvantage in metallurgical processes especially for the stages of stirring, mixing, mass and heat transfer and pumping as it hinders the diffusion of ions as given by the Stokes – Einstein expression (**Equation 1.20**)

$$D = \frac{kT}{6\pi\eta r} \quad \text{Equation 1.20}$$

where  $D$  is the diffusion coefficient of the substance,  $k$  is the Boltzmann constant,  $T$  is temperature,  $\eta$  is the viscosity and  $r$  is the ionic radius.

The type of interaction between the different ions; Van der Waals, hydrogen bonds or electrostatic affects and the molecular structure of the liquid all have a great effect on the viscosity.<sup>97, 99</sup> By increasing the temperature and the water content the viscosity decreases, while other contaminants such as chloride increase it. For some ILs even a small concentration of impurities may have very high impact on it.<sup>100</sup> In terms of alkyl chain, the longer the chain the more viscous the IL due to the increase in van der Waals interactions for all imidazolium, pyridinium, alkylammonium and pyrrolidinium based ILs.<sup>97, 98</sup> Likewise for the density, the viscosity is more affected by the anion than the cation of the IL.

➤ Conductivity

Conductivity ( $\sigma$ ) is very important property and considering the first applications of ILs in electrochemistry, it is understandable that it has been studied extensively. Although ILs are entirely composed of ions and it would have been apparent that the conductivity is very high, this is not true and usually aqueous solutions show higher values of conductivity. In most cases the conductivity ranges between  $10^{-5}$  to  $10^{-2}$  S cm<sup>-1</sup>.<sup>101</sup> The large size of cations leading to the inhibition of the fast mobility of the ions, along with the lack of free charge carriers due to ion pairing all explain this phenomenon.<sup>102</sup> There was an attempt to model the viscosity and conductivity of ILs by using the hole theory by Abbott et al.<sup>103</sup> It was suggested that ILs enclose holes that contribute to the movement of ions. Their size is affected by the surface tension of the liquid and by decreasing it, the

viscosity also decreases, and the conductivity rises. At ambient conditions, ILs have low conductivities, but this can be solved by increasing the temperature. Conductivity, also, depends highly on the ion size, the ion association and the viscosity of the liquid, with which it has an inversely proportional. The two properties are related with the Walden law shown in **Equation 1.21**.

$$\Lambda\eta^\alpha = C \quad \text{Equation 1.21}$$

Where  $\Lambda$  is the molar conductivity,  $C$  is a constant,  $\alpha$  is an adjustable parameter and  $\eta$  is the viscosity. As for the impurities, the water and chloride content in larger mole fractions can increase the conductivity.<sup>104</sup> The alkyl chain of the cation has an effect on the conductivity, since as discussed before it increases the viscosity of the liquid due to stronger van der Waals forces, and so the conductivity decreases. Furthermore, it has been reported that when the molecular mass, the size of the cation and the symmetry decrease, then there is a rise in the conductivity.

In general, the anion of the IL controls the chemistry of the solvent as it interacts with the metal solute and complexes with it. This means it affects the speciation and thus the reactivity and the solubility of the metal solutes.



*Figure 1.12: Colored solutions of  $\text{CuCl}_2 \cdot 2\text{H}_2\text{O}$  dissolved in different ILs and deep eutectic solvents.<sup>105</sup>*

This is illustrated in the **Figure 1.12**, where the colours of the solutions of  $\text{CuCl}_2 \cdot 2\text{H}_2\text{O}$  dissolved in different ILs and deep eutectic solvents with different anions are presented. The solutions have different colours due to the different species formed between the metal and the anion of the IL. Knowledge of metal speciation in general is very important because it gives information about reactivity and solubility of metal ions and this information is of most significance for metallurgical applications such as metal extraction

and deposition. Speciation in ILs started to be examined only in recent years, due to the difficulty of studying it, arising from the complexity of these media. In aqueous solutions the speciation is governed by the  $H^+$  and  $OH^-$  that also dominate metal solubility and their redox properties. All of these data can be correlated and illustrated in Pourbaix diagrams that have been developed for aqueous solutions and for which more information will be given in the Chapter 3. Metal ions are mainly Lewis acids and form complexes with Lewis or Brønsted bases and ILs show complexity due to the different Lewis basicity of every anion. Another reason for the poor data on speciation is the difficulty to find an appropriate technique to analyse the formed species.<sup>105</sup> In aqueous solutions, usually, the formed species are determined with the use of X-rays, by crystallising the metal complex and determining the crystal structure. In addition, other techniques such as UV-Vis, Raman and IR spectroscopy are useful in determining speciation in aqueous systems. In ILs, the crystallization of the formed species is very difficult to initiate, and the evaporation of the solvent is not possible in most cases, so different techniques are employed such as UV – Vis, NMR, EPR and EXAFS to determine the structure.

ILs show very high potential in metal processing due to their favourable properties of non-flammability, low vapour pressure, wide electrochemical potential ( $> 4\text{ V}$ )<sup>106</sup> and liquidus range, thermal and chemical stability and they can be an alternative to current metallurgical approaches.<sup>56</sup> Although, they exhibit some non-advantageous properties as low conductivity and high viscosity, by selecting the appropriate cation and anion these properties can be tuned for better results and they are very good electrolytes without the requirement of addition of other solvents.

Apart from all these favourable properties, there are some constraints in their employment industrially, with the main being their high cost and complex production process. The expensive components and process of production with the need of many purification steps, lead to the requirements of 1) reducing the cost of production 2) minimum usage , 3) high recyclability of the IL. The price of ILs has been reported to be in the range between 5-20 times more expensive than molecular solvents.<sup>107</sup>

The second constraint is their toxicity. Although, ILs have very low vapour pressure especially at ambient conditions and so the air pollution is prevented, they have significant solubility in water, which leads to the danger of contamination of environmental recipients like groundwater and then soils and sediments.<sup>108</sup> In addition, their high chemical and thermal stability might prove a potential issue due to their

persistence in the environment. ILs usually are related with green chemistry due to all the favourable properties mentioned before, but even so their toxicity is at the same level as many molecular solvents and sometimes even higher. There are many reviews on this topic, and all have concluded that the most common ILs show toxicity that varies across organisms and depends on the test conditions and the type of the liquid.<sup>108-110</sup>

#### 1.4.2 Deep eutectic solvents

Deep eutectic solvents (DESs) are defined as eutectic mixtures of quaternary ammonium salts (or in some cases quaternary phosphonium salts) with hydrogen bond donors (HBDs) and their name comes from the Greek word “εύτηκτος” that defines a substance melting easily. Coutinho et al, in a recent review on DESs, suggested that a stricter definition of a DES should be “a mixture of pure compounds whose eutectic point temperature is below that of an ideal liquid mixture” since, as he pointed out, all mixtures of compounds that are immiscible in the solid state present a eutectic point and this difference from ideality is what define a DES.<sup>111</sup> This is illustrated in **Figure 1.13** with a phase diagram of a binary mixture. For an ideal solution, at a specific ratio of two components A and B, the melting point of the mixture drops significantly and results in a eutectic point ( $T_{E, ideal}$ ). In order to characterise a liquid mixture as a DES, the eutectic point of the mixture ( $T_E$ ) should be lower than the ( $T_{E, ideal}$ ). Therefore, for a DES the difference ( $\Delta T_2$ ) between the ideal and real eutectic point should define the deep eutectic point and not the difference ( $\Delta T_1$ ) between the real eutectic point and the linear combination of the melting points of the components A and B.

The existence of a “deeper” eutectic point is the result of hydrogen bond interactions that reduce the lattice energy of the components and lead to delocalisation of the charge and the formation of non-ideal mixtures.<sup>111</sup> The depth of the depression between the ( $T_{E, ideal}$ ) to the ( $T_E$ ) depends highly on the strength of the interactions between the hydrogen bond acceptor and donor. In addition, the symmetry of the cation is another factor that affects the melting point of the system, in the same way that was mentioned before for the ILs and thus the higher the asymmetry of the cation the lower the melting point.

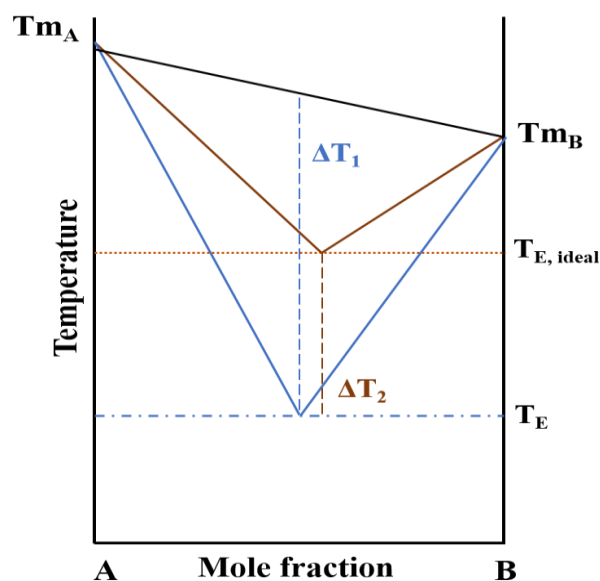


Figure 1.13: Schematic representation of the eutectic point of a binary mixture of components A and B, depending on the mole fraction of B. (adapted from ref<sup>111</sup>)

#### Synthesis and properties of deep eutectic solvents

Depending on the starting materials, there are four general types of DESs, which are shown in **Table 1.5**. The first DESs to be reported by Abbott et al., was prepared by the mixture of choline chloride with  $\text{ZnCl}_2$  in different ratios.<sup>112</sup> Example of Type I DESs can be the common chloroaluminates imidazolium ILs, but apart from  $\text{AlCl}_3$  more metal halides like  $\text{AgCl}$ ,  $\text{FeCl}_2$ ,  $\text{CuCl}_2$  etc. have been examined. Since the number of metal halides that can form DESs is limited, the Type II DESs increases the possibilities with the bigger variety of hydrated metal halides that also have lower cost. The Type III DESs are composed of a quaternary ammonium salt with the addition of a HBD, which can be selected from a variety of chemical substances, namely alcohols, amines, carboxylic acids etc. This wide range of HBDs contributes to the tunability of the DES for each specific application. The Type IV DESs is the result of the mixture of a metal halide with a HBD and an early example of this type is the mixture of  $\text{ZnCl}_2$  with urea.<sup>113</sup>

DESs unlike ILs are mixtures of ionic and molecular species but the high ionic strength (c.a. 3-5 M) and the ability to tailor the ligand properties of the HBD enable tunability for metal reactivity in solution.<sup>111</sup> DESs have low vapour pressure, are generally non-flammable, have moderate conductivity, thermal and chemical stability. Their ease of preparation by mixing the readily available components with moderate heating enables their large-scale application. In addition, some DESs can be environmentally friendly and

non-toxic. Apparently, none of these desirable properties of DESs should be generalised for all solvents since physical properties, toxicity, price etc. depend a lot on the starting materials. DESs as ILs have gained the interest of the scientific world for many applications from analytical chemistry to metallurgy and electrochemistry and due to their versatile character. These are summarised in more detailed reviews.<sup>114-116</sup>

*Table 1.5: Description of DESs types*

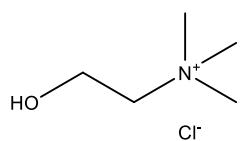
Type	Composition	
<b>Type I</b>	Quaternary ammonium salt	Metal halide
<b>Type II</b>	Quaternary ammonium salt	Hydrated metal halide
<b>Type III</b>	Quaternary ammonium salt	Hydrogen bond donor
<b>Type IV</b>	Metal halide (hydrate)	Hydrogen bond donor

**Figure 1.14** shows some of the components that can be used in Type III DES. The choice of the HBD affects the activity of protons in the DES, since the pH of the resulted DES follows the acidity of the HBD.<sup>117</sup> For example, the  $pK_a$  of the first  $H^+$  to dissociate for oxalic acid and malonic acid are 1.2 and 2.8, respectively. The pH of the resulted DESs of the mixtures of choline chloride with oxalic acid and malonic acid have been measured to be 1.32 and 2.39, respectively. On the other hand, more basic HBDs as urea lead to a DES with a pH at 8.91, so again the tunability of these solvents for specific applications is highlighted.

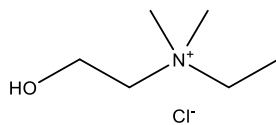
As discussed previously, DESs share a lot of physical properties with ILs. For example, the viscosity of DESs is higher compared to aqueous solutions, in the same way as ILs and this is a result of the strong hydrogen bond network in this media. Temperature, water content and the chemical nature of the constituents all are significant for the viscosity of the mixture. As an example, the viscosity of the mixture of choline chloride with glycerol is much lower than that of glycerol and it is suggested that the salt is breaking the hydrogen bond interactions in the structure of glycerol resulting in a less ordered media.<sup>118</sup>

During this thesis, only the Type III DESs are examined and discussed with the employment of choline chloride (ChCl) as the quaternary ammonium salt, due to its lower price, availability in bulk amounts, biodegradability and non-toxicity. ChCl is a supplement of vitamin B4 in chicken feed. More information about properties of DESs and applications will be provided throughout the chapters of this thesis.

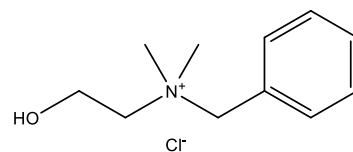
## Halide Salts



Choline Chloride

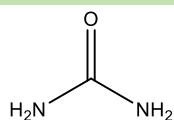


N-ethyl-2-hydroxy-N,N-dimethylethanaminium chloride



N-benzyl-2-hydroxy-N,N-dimethylethanaminium

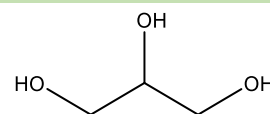
## Hydrogen Bond Donors



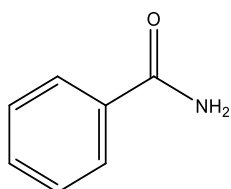
Urea



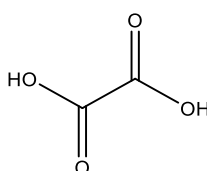
Ethylene Glycol



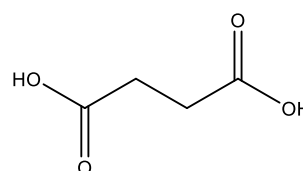
Glycerol



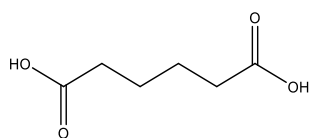
Benzamide



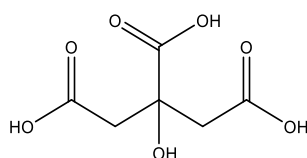
Oxalic acid



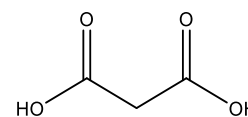
Succinic acid



Adipic acid



Citric acid



Malonic acid

Figure 1.14: Common chloride salts and hydrogen bond donors for the preparation of DES

## Metal processing in deep eutectic solvents

Binnemans in his recent review stated 10 reasons that solvometallurgy and by extension ionometallurgy should be preferred instead of the current employed processes and these are <sup>63</sup>:

- Limited water consumption
- Reduced energy consumption
- Lower consumption of acids
- Higher selectivity for leaching
- Process intensification
- Fewer problems with silica gel formation
- Compatibility with bioleaching
- Suitable for low metal containing materials
- Useful for treatment of urban waste
- New separation processes

Their emerging use in metallurgy resulted in a number of published reviews on this topic.<sup>119</sup> DESs have been investigated in both metal extraction and metal recovery. MOs processing is a big chapter of DESs, as well as the topic of this thesis. Abbott et al reported the solubility of 17 MOs in three DESs based on ChCl and compared them with the solubilities in aqueous solutions of HCl and NaCl and it was concluded that the solubilities are higher in HCl, but the DES composed of ChCl and malonic acid showed good potential and high levels of leaching affinity.<sup>120</sup>

The employment of iodine as an oxidising agent and redox catalyst in DESs, proved to be a very promising system due to its lower toxicity compared with  $\text{CN}^-$ , its fast electron transfer and high solubility ( $> 200 \text{ g kg}^{-1}$ ) compared to in water ( $0.29 \text{ g kg}^{-1}$ ).<sup>121</sup> In the DES ChCl with ethylene glycol, the redox potential of iodine was calculated and exists between 0.4 – 0.6 V, which is more positive than the redox potential of a variety of other metals such as Zn and Cu, thus making the oxidatively leaching of these metals possible.<sup>64</sup> This system of iodine in DESs has been employed in different processes as the extraction of Au and Ag from ores<sup>122</sup>, the selectively dissolution of Cu/Zn<sup>64</sup> and Ga/As<sup>123</sup>. Another

project highlighting the contribution of the tunability of DESs in metallurgy is the selective dissolution of Pb and Zn with the use of a hybrid DES consisting of ChCl with ethylene glycol and urea, resulting in high selectivity over Fe which is a contaminant.

DESs also have been employed in the extraction of rare earth elements (REEs) from NdFeB magnets and specifically the DES consisted of ChCl and lactic acid showed high leaching affinity over the REEs. Solvent extraction followed for the separation of the Fe, B, Co contaminants and subsequent solvent extraction for the separation of Nd-Dy.<sup>124</sup>

## **1.5 Thesis aims**

In this study, Type III DESs are investigated for the dissolution of MOs. The main aim of this thesis is to study the dissolution mechanism of a variety of MOs ( $\text{MnO}_2$ ,  $\text{MnO}$ ,  $\text{Fe}_2\text{O}_3$ ,  $\text{Fe}_3\text{O}_4$ ,  $\text{Co}_3\text{O}_4$ ,  $\text{CoO}$ ,  $\text{NiO}$ ,  $\text{CuO}$ ,  $\text{Cu}_2\text{O}$ ,  $\text{ZnO}$ ,  $\text{PbO}$ ), which are found in the majority of industrial residues like LIBs, in DESs consisted of different HBDs (alcohol, amine, carboxylic acids). The acidity of the solution is investigated on the solubility of the MOs and compared with the effect of the ligand abilities of the HBD. In aqueous solutions, it is known that proton exchange and surface complexation are two of the most important ways of solubilising MOs, so these methods are explored in DESs. In addition, it is expected that the use of different HBDs will provide selectivity, due to the specific interactions of metals with different HBDs. This fact is aimed to be illustrated with the extraction of metals from two EoL materials, cathode materials of a LIB and spent fluorescent lamp phosphor.

For DESs that lack of proton activity and consist of HBDs that are poor ligands and thus resulting in poor solubilities for most MOs, the electrochemical oxidation is also investigated as an alternative and novel method to solubilise MOs. The speciation after electrochemical dissolution is also investigated and the kinetics are compared with straight chemical dissolution. Electrochemical techniques such as cyclic voltammetry, chronopotentiometry and chronocoulometry are conducted using the solid state technique paint casting and are aimed to provide information about the reactivity of MOs, their stability and the rate of their electrochemical dissolution. The rate of electrochemical dissolution is also correlated with their band gap and hence conductivity.

## 1.6 References

1. Clark, I. J., *Commodity option pricing: a practitioner's guide*. John Wiley & Sons: **2014**.
2. Binnemans, K.; Jones, P. T.; Blanpain, B.; Van Gerven, T.; Yang, Y.; Walton, A.; Buchert, M., Recycling of rare earths: a critical review. *Journal of Cleaner Production* **2013**, *51*, 1-22.
3. Pillay, A. M.; Ntuli, J. K., South Africa and the Global Hydrogen Economy : The Strategic Role of Platinum Group Metals. *New Agenda: South African Journal of Social and Economic Policy* **2016**, *61* (1).
4. Skinner, B. J., Earth resources. *Proceedings of the national Academy of Sciences* **1979**, *76* (9), 4212-4217.
5. Barbalace, K., Periodic table of elements. *Environmental Chemistry. com* **2007**, 04-14.
6. Izatt, R. M., *Metal Sustainability: Global Challenges, Consequences, and Prospects*. John Wiley & Sons: **2016**.
7. Taylor, S. R.; McLennan, S. M., *The Continental Crust: Its Composition and Evolution*. *osti.gov: USA*, **1985**.
8. Revie, R. W., *Corrosion and Corrosion Control: an Introduction to Corrosion Science and Engineering*. John Wiley & Sons: **2008**.
9. Winter, M. J., *d-block Chemistry*. 2nd ed.; Oxford University Press, USA: 2015.
10. Jones, C. J., *d-and f-Block Chemistry*. Royal Society of Chemistry: 2001.
11. Rao, C. N. R.; Rao, G. S., *Transition Metal Oxides. Crystal Chemistry, Phase Transition and Related Aspects*. Springfield, Va. : NTIS: 1974.
12. Páez, A. M., Transition metal oxides: Geometric and electronic structures. *Journal of Chemical Education* **1994**, *71* (5), 381-388.
13. Kung, H. H., *Transition Metal Oxides: Surface Chemistry and Catalysis*. Elsevier: **1989**; Vol. 45.
14. Antipin, M. Y.; Tsirelson, V. G.; Flugge, M. P.; Gerr, R. G.; Struchkov, Y. T.; Ozerov, R. P., Electron density distribution in hematite,  $\alpha$ -Fe<sub>2</sub>O<sub>3</sub>, from precision X-ray diffraction data. *Doklady Akademii Nauk* **1985**, *281* (4), 854-857.
15. Yamanaka, T., Crystal structures of Ni<sub>2</sub>SiO<sub>4</sub> and Fe<sub>2</sub>SiO<sub>4</sub> as a function of temperature and heating duration. *Physics and Chemistry of Minerals* **1986**, *13* (4), 227-232.

16. Mandal, T. K.; Greenblatt, M., Transition Metal Oxides: Magnetoresistance and Half-Metallicity. In *Functional Oxides*, John Wiley & Sons, Ltd: **2010**, 257-293.
17. Santos, E.; Schmickler, W., *Catalysis in Electrochemistry: from Fundamental Aspects to Strategies for Fuel Cell Development*. John Wiley & Sons **2011**.
18. <https://www.anl.gov/article/doi-launches-its-first-lithium-ion-battery-recycling-rd-center-recell>. (accessed September 2019).
19. Free, M. L., *Hydrometallurgy: Fundamentals and Applications*. John Wiley & Sons: **2013**.
20. Marsden, J.; House, I., *The Chemistry of Gold Extraction*. 2nd ed.; Society for Mining, Metallurgy, and Exploration, Inc. (SME): **2006**.
21. Habashi, F., Fire and the art of metals: a short history of pyrometallurgy. *Mineral Processing and Extractive Metallurgy* **2005**, *114* (3), 165-171.
22. Gupta, C. K., *Chemical Metallurgy: Principles and Practice*. John Wiley & Sons: **2006**.
23. Ghosh, A.; Ray, H. S., *Principles of Extractive Metallurgy*. New Age International: **1991**.
24. Dunn, J., The oxidation of sulphide minerals. *Thermochimica Acta* **1997**, *300* (1-2), 127-139.
25. Carrillo-Pedroza, F. R.; Soria-Aguilar, M. J.; Salinas-Rodriguez, E.; Martinez-Luevantos, A.; Pecina-Trevino, T. E.; Davalos-Sanchez, A., Oxidative hydrometallurgy of sulphide minerals. In *Recent Researches in Metallurgical Engineering. From Extraction to Forming*, InTech: **2012**.
26. Lahijani, P.; Zainal, Z. A.; Mohammadi, M. and Mohamed, A. R., Conversion of the greenhouse gas CO<sub>2</sub> to the fuel gas CO via the Boudouard reaction: A review. *Renewable and Sustainable Energy Reviews*, **2015**, *41*, 615-632.
27. Ellingham, H. J. T., Reducibility of oxides and sulfides in metallurgical processes. *Journal of the Society of Chemical Industry* **1944**, *63*, 125-133.
28. Moore, J. J., *Chemical Metallurgy*. 2nd ed.; Butterworth & Co Ltd: **1990**.
29. Shamsuddin, M., *Physical Chemistry of Metallurgical Processes*. The Minerals, Metals & Materials Society: **2016**.
30. <https://www.tec-science.com/material-science/steel-making/blast-furnace-process/>. (accessed 22/10/2019).

31. Habashi, F., *A Textbook of Hydrometallurgy*. 2nd ed.; Métallurgie Extractive: **1999**; Vol. 1.
32. Mac Arthur, J. S.; Forrest, R.; Forrest, W. Improvements in obtaining gold and silver from ores and other compounds. British Patent 14174. **1889**.
33. Hilson, G.; Monhemius, A., Alternatives to cyanide in the gold mining industry: what prospects for the future? *Journal of Cleaner Production* **2006**, *14* (12-13), 1158-1167.
34. Moradi, S.; Monhemius, A., Mixed sulphide–oxide lead and zinc ores: Problems and solutions. *Minerals Engineering* **2011**, *24* (10), 1062-1076.
35. Hartley, J. M. Ionometallurgy: The Processing of Metals Using Ionic Liquids. PhD thesis, University of Leicester, **2016**.
36. Vignes, A., *Extractive Metallurgy 2: Metallurgical Reaction Processes*. John Wiley & Sons Inc: 2011.
37. Gupta, C. K.; Mukherjee, T. K., *Hydrometallurgy in Extraction Processes, Volume II*. CRC Press, Inc.: **1990**.
38. Schwertmann, U., Solubility and dissolution of iron oxides. *Plant and Soil* **1991**, *130* (1), 1-25.
39. Cornell, R. M.; Schwertmann, U., *The Iron Oxides: Structure, Properties, Reactions, Occurrences and Uses*. John Wiley & Sons: **2003**.
40. Lee, S. O.; Tran, T.; Jung, B. H.; Kim, S. J.; Kim, M. J., Dissolution of iron oxide using oxalic acid. *Hydrometallurgy* **2007**, *87* (3-4), 91-99.
41. Taxiarchou, M.; Panias, D.; Douni, I.; Paspaliaris, I.; Kontopoulos, A., Dissolution of hematite in acidic oxalate solutions. *Hydrometallurgy* **1997**, *44* (3), 287-299.
42. Oustadakis, P.; Tsakiridis, P.; Katsiapi, A.; Agatzini-Leonardou, S., Hydrometallurgical process for zinc recovery from electric arc furnace dust (EAFD): Part I: Characterization and leaching by diluted sulphuric acid. *Journal of Hazardous Materials* **2010**, *179* (1-3), 1-7.
43. Zhong, L.; Zhang, Y.; Zhang, Y., Extraction of alumina and sodium oxide from red mud by a mild hydro-chemical process. *Journal of Hazardous Materials* **2009**, *172* (2-3), 1629-1634.
44. Izutsu, K., *Electrochemistry in Nonaqueous Solutions*. 2nd ed.; WILEY-VCH Verlag GmbH & Co. KGaA: **2009**.

45. Bard, A. J., *Standard Potentials in Aqueous Solution*. International Union of Pure and Applied Chemistry: **1985**.
46. Havlík, T., *Hydrometallurgy: Principles and applications*. Cambridge International Science Publishing Ltd, Woodhead Publishing Limited and CRC Press LLC: **2008**.
47. Stefanowicz, T.; Osińska, M.; Napieralska-Zagozda, S., Copper recovery by the cementation method. *Hydrometallurgy* **1997**, *47* (1), 69-90.
48. Atkins, P.; Overton, T.; Rourke, J.; Weller, M.; Armstrong, F., *Shriver and Atkins' Inorganic Chemistry*. 5th ed.; Oxford University Press: **2010**.
49. Fu, F.; Wang, Q., Removal of heavy metal ions from wastewaters: a review. *Journal of Environmental Management* **2011**, *92* (3), 407-418.
50. Dupont, D.; Binnemans, K., Rare-earth recycling using a functionalized ionic liquid for the selective dissolution and revalorization of  $\text{Y}_2\text{O}_3\text{:Eu}^{3+}$  from lamp phosphor waste. *Green Chemistry* **2015**, *17* (2), 856-868.
51. Vander Hoogerstraete, T.; Blanpain, B.; Van Gerven, T.; Binnemans, K., From NdFeB magnets towards the rare-earth oxides: a recycling process consuming only oxalic acid. *RSC Advances* **2014**, *4* (109), 64099-64111.
52. Zürner, P.; Frisch, G., Leaching and Selective Extraction of Indium and Tin from Zinc Flue Dust Using an Oxalic Acid-Based Deep Eutectic Solvent. *ACS Sustainable Chemistry & Engineering* **2019**, *7* (5), 5300-5308.
53. Jarvenin, G., Precipitation and crystallization processes. Short Course: Introduction to Nuclear Chemistry and Fuel Cycle Separations. *Consortium for Risk Evaluation with Stakeholder Participation (CRESP)* **2008**.
54. Rengan, K.; Meyer, R. A., *Ultrafast Chemical Separations*. Board on Chemical Sciences and Technology, National Research Council: **1993**.
55. Dreisinger, D., *Aqueous Electrotechnologies: Progress in Theory and Practice*. The Minerals, Metals & Materials Society: **1997**.
56. MacFarlane, D. R.; Abbott, A. P.; Endres, F., *Electrodeposition from Ionic Liquids*. 2nd ed.; Wiley-VCH Verlag GmbH & Co. KGaA: **2017**.
57. Rice, N. M.; Irving, H. M. N. H.; Leonard, M. A., Nomenclature for liquid-liquid distribution (solvent extraction) (IUPAC Recommendations 1993). *Pure and Applied Chemistry* **1993**, *65* (11), 2373-2396.
58. Flett, D. S., Solvent extraction in hydrometallurgy: the role of organophosphorus extractants. *Journal of Organometallic Chemistry* **2005**, *690* (10), 2426-2438.

59. Kislik, V. S., *Solvent extraction: Classical and Novel approaches*. Elsevier: **2012**.
60. Helfferich, F. G., *Ion Exchange*. Dover Publications, INC: **1995**.
61. Lukey, G. C.; van Deventer, J. S. J.; Chowdhury, R. L.; Shallcross, D. C.; Huntington, S. T.; Morton, C. J., The speciation of gold and copper cyanide complexes on ion-exchange resins containing different functional groups. *Reactive and Functional Polymers* **2000**, *44* (2), 121-143.
62. Harland, C. E., *Ion Exchange: Theory and Practice*. 2nd ed.; Royal Society of Chemistry: **1994**.
63. Binnemans, K.; Jones, P. T., Solvometallurgy: an emerging branch of extractive metallurgy. *Journal of Sustainable Metallurgy* **2017**, *3* (3), 570-600.
64. Abbott, A. P.; Frisch, G.; Gurman, S. J.; Hillman, A. R.; Hartley, J.; Holyoak, F.; Ryder, K. S., Ionometallurgy: designer redox properties for metal processing. *Chemical Communications* **2011**, *47* (36), 10031-10033.
65. Sundermeyer, W., Fused salts and their use as reaction media. *Angewandte Chemie International Edition in English* **1965**, *4* (3), 222-238.
66. Brockman, C. J., Fused electrolytes—An historical sketch. *Journal of Chemical Education* **1927**, *4* (4), 512.
67. Wilkes, J. S., A short history of ionic liquids—from molten salts to neoteric solvents. *Green Chemistry* **2002**, *4* (2), 73-80.
68. Dupont, J., From molten salts to ionic liquids: a “nano” journey. *Accounts of Chemical Research* **2011**, *44* (11), 1223-1231.
69. Lorentsen, O., 125 years of the Hall-Héroult process—what made it a success. In *Molten Salts Chemistry and Technology*, John Wiley & Sons, Ltd: 2014; pp 103-112.
70. Seddon, K. R., Ionic liquids for clean technology. *Journal of Chemical Technology & Biotechnology* **1997**, *68* (4), 351-356.
71. Marsh, K.; Boxall, J.; Lichtenthaler, R., Room temperature ionic liquids and their mixtures—a review. *Fluid Phase Equilibria* **2004**, *219* (1), 93-98.
72. Buzzeo, M. C.; Evans, R. G.; Compton, R. G., Non-haloaluminate room-temperature ionic liquids in electrochemistry—A review. *ChemPhysChem* **2004**, *5* (8), 1106-1120.
73. Earle, M. J.; Seddon, K. R., Ionic liquids. Green solvents for the future. *Pure and Applied Chemistry* **2000**, *72* (7), 1391-1398.
74. Gabriel, S.; Weiner, J., Ueber einige abkömmlinge des propylamins. *Berichte der Deutschen Chemischen Gesellschaft* **1888**, *21* (2), 2669-2679.

75. Walden, P., Ueber die Molekulargrösse und elektrische Leitfähigkeit einiger geschmolzenen Salze. *Известия Российской академии наук. Серия математическая* **1914**, 8 (6), 405-422.
76. Hurley, F. H.; Wier, T. P., Electrodeposition of metals from fused quaternary ammonium salts. *Journal of the Electrochemical Society* **1951**, 98 (5), 203-206.
77. Brown, L. C.; Hogg, J. M.; Swadźba-Kwaśny, M., Lewis acidic ionic liquids. In *Ionic Liquids II*, Springer: 2017; pp 185-224.
78. Welton, T., Ionic liquids: a brief history. *Biophysical Reviews* **2018**, 10 (3), 691-706.
79. Robinson, J.; Osteryoung, R., An electrochemical and spectroscopic study of some aromatic hydrocarbons in the room temperature molten salt system aluminum chloride-n-butylpyridinium chloride. *Journal of the American Chemical Society* **1979**, 101 (2), 323-327.
80. Wilkes, J. S.; Levisky, J. A.; Wilson, R. A.; Hussey, C. L., Dialkylimidazolium chloroaluminate melts: a new class of room-temperature ionic liquids for electrochemistry, spectroscopy and synthesis. *Inorganic Chemistry* **1982**, 21 (3), 1263-1264.
81. Wilkes, J. S.; Zaworotko, M. J., Air and water stable 1-ethyl-3-methylimidazolium based ionic liquids. *Journal of the Chemical Society, Chemical Communications* **1992**, (13), 965-967.
82. Swatloski, R. P.; Holbrey, J. D.; Rogers, R. D., Ionic liquids are not always green: hydrolysis of 1-butyl-3-methylimidazolium hexafluorophosphate. *Green Chemistry* **2003**, 5 (4), 361-363.
83. H. Davis, J., James, Task-specific ionic liquids. *Chemistry Letters* **2004**, 33 (9), 1072-1077.
84. Maase, M.; Massonne, K., Biphasic acid scavenging utilizing ionic liquids: the first commercial process with ionic liquids. In *Ionic Liquids IIIB: Fundamentals, Progress, Challenges, and Opportunities*, American Chemical Society: **2005**.
85. Abbott, A. P.; Capper, G.; Davies, D. L.; Rasheed, R. K.; Tambyrajah, V., Novel solvent properties of choline chloride/urea mixtures. *Chemical Communications* **2003**, (1), 70-71.
86. Greaves, T. L.; Drummond, C. J., Protic ionic liquids: properties and applications. *Chemical Reviews* **2008**, 108 (1), 206-237.

87. Belieres, J.-P.; Angell, C. A., Protic ionic liquids: preparation, characterization, and proton free energy level representation. *The Journal of Physical Chemistry B* **2007**, *111* (18), 4926-4937.
88. MacFarlane, D. R.; Seddon, K. R., Ionic liquids-progress on the fundamental issues. *Australian Journal of Chemistry* **2007**, *60* (1), 3-5.
89. Belieres, J.-P.; Gervasio, D.; Angell, C. A., Binary inorganic salt mixtures as high conductivity liquid electrolytes for > 100 C fuel cells. *Chemical Communications* **2006**, (46), 4799-4801.
90. Xia, S.-M.; Chen, K.-H.; Fu, H.-C.; He, L.-N., Ionic liquids catalysis for carbon dioxide conversion with nucleophiles. *Frontiers in Chemistry* **2018**, *6* (462).
91. Esperança, J. M. S. S.; Canongia Lopes, J. N.; Tariq, M.; Santos, L. s. M. N. B. F.; Magee, J. W.; Rebelo, L. s. P. N., Volatility of aprotic ionic liquids-A review. *Journal of Chemical & Engineering Data* **2010**, *55* (1), 3-12.
92. Reid, J. E.; Prydderch, H.; Spulak, M.; Shimizu, S.; Walker, A. J.; Gathergood, N., Green profiling of aprotic versus protic ionic liquids: synthesis and microbial toxicity of analogous structures. *Sustainable Chemistry and Pharmacy* **2018**, *7*, 17-26.
93. Angell, C. A.; Byrne, N.; Belieres, J.-P., Parallel developments in aprotic and protic ionic liquids: Physical chemistry and applications. *Accounts of Chemical Research* **2007**, *40* (11), 1228-1236.
94. Schleicher, J. C.; Scurto, A. M., Kinetics and solvent effects in the synthesis of ionic liquids: imidazolium. *Green Chemistry* **2009**, *11* (5), 694-703.
95. Ueno, K.; Tokuda, H.; Watanabe, M., Ionicity in ionic liquids: correlation with ionic structure and physicochemical properties. *Physical Chemistry Chemical Physics* **2010**, *12* (8), 1649-1658.
96. Ochędzan-Siodłak, W.; Dziubek, K.; Siodłak, D., Densities and viscosities of imidazolium and pyridinium chloroaluminate ionic liquids. *Journal of Molecular Liquids* **2013**, *177*, 85-93.
97. Perez de los Rios, A.; Fernandez, F. J. H., *Ionic Liquids in Separation Technology*. Elsevier: **2014**.
98. Sanchez, L. G.; Espel, J. R.; Onink, F.; Meindersma, G. W.; Haan, A. B. d., Density, viscosity, and surface tension of synthesis grade imidazolium, pyridinium, and pyrrolidinium based room temperature ionic liquids. *Journal of Chemical & Engineering Data* **2009**, *54* (10), 2803-2812.

99. Gaciño, F. M.; Comuñas, M. J.; Regueira, T.; Segovia, J. J.; Fernández, J., On the viscosity of two 1-butyl-1-methylpyrrolidinium ionic liquids: Effect of the temperature and pressure. *The Journal of Chemical Thermodynamics* **2015**, *87*, 43-51.
100. Seddon, K. R.; Stark, A.; Torres, M.-J., Influence of chloride, water, and organic solvents on the physical properties of ionic liquids. *Pure and Applied Chemistry* **2000**, *72* (12), 2275-2287.
101. Endres, F., Ionic liquids: solvents for the electrodeposition of metals and semiconductors. *ChemPhysChem* **2002**, *3* (2), 144-154.
102. Díaz-Rodríguez, P.; Cancilla, J.; Matute, G.; Torrecilla, J. S., Conductivity of ionic liquids: a neural network approach. *Industrial & Engineering Chemistry Research* **2014**, *54* (1), 55-58.
103. Abbott, A. P., Application of hole theory to the viscosity of ionic and molecular liquids. *ChemPhysChem* **2004**, *5* (8), 1242-1246.
104. Ge, R.; Hardacre, C.; Nancarrow, P.; Rooney, D. W., Thermal conductivities of ionic liquids over the temperature range from 293 K to 353 K. *Journal of Chemical & Engineering Data* **2007**, *52* (5), 1819-1823.
105. Abbott, A. P.; Frisch, G.; Ryder, K. S., Metal complexation in ionic liquids. *Annual Reports Section "A"(Inorganic Chemistry)* **2008**, *104*, 21-45.
106. Park, J.; Jung, Y.; Kusumah, P.; Lee, J.; Kwon, K.; Lee, C., Application of ionic liquids in hydrometallurgy. *International Journal of Molecular Sciences* **2014**, *15* (9), 15320-15343.
107. Chen, L.; Sharifzadeh, M.; Mac Dowell, N.; Welton, T.; Shah, N.; Hallett, J. P., Inexpensive ionic liquids:[HSO<sub>4</sub>]<sup>-</sup>-based solvent production at bulk scale. *Green Chemistry* **2014**, *16* (6), 3098-3106.
108. Amde, M.; Liu, J.-F.; Pang, L., Environmental application, fate, effects, and concerns of ionic liquids: a review. *Environmental Science & Technology* **2015**, *49* (21), 12611-12627.
109. Pham, T. P. T.; Cho, C.-W.; Yun, Y.-S., Environmental fate and toxicity of ionic liquids: a review. *Water Research* **2010**, *44* (2), 352-372.
110. Zhao, D.; Liao, Y.; Zhang, Z., Toxicity of ionic liquids. *Clean–Soil, Air, Water* **2007**, *35* (1), 42-48.
111. Martins, M. A.; Pinho, S. P.; Coutinho, J. A., Insights into the nature of eutectic and deep eutectic mixtures. *Journal of Solution Chemistry* **2019**, *48* (7), 962-982.

112. Abbott, A. P.; Capper, G.; Davies, D. L.; Munro, H. L.; Rasheed, R. K.; Tambyrajah, V., Preparation of novel, moisture-stable, Lewis-acidic ionic liquids containing quaternary ammonium salts with functional side chains. *Chemical Communications* **2001**, (19), 2010-2011.
113. Abbott, A. P.; Barron, J. C.; Ryder, K. S.; Wilson, D., Eutectic-based ionic liquids with metal-containing anions and cations. *Chemistry—A European Journal* **2007**, *13* (22), 6495-6501.
114. Tang, B.; Row, K. H., Recent developments in deep eutectic solvents in chemical sciences. *Monatshefte für Chemie-Chemical Monthly* **2013**, *144* (10), 1427-1454.
115. Zhang, Q.; Vigier, K. D. O.; Royer, S.; Jerome, F., Deep eutectic solvents: syntheses, properties and applications. *Chemical Society Reviews* **2012**, *41* (21), 7108-7146.
116. Alonso, D. A.; Baeza, A.; Chinchilla, R.; Guillena, G.; Pastor, I. M.; Ramón, D. J., Deep eutectic solvents: the organic reaction medium of the century. *European Journal of Organic Chemistry* **2016**, *2016* (4), 612-632.
117. Abbott, A. P.; Alabdullah, S. S. M.; Al-Murshedi, A. Y. M.; Ryder, K. S., Brønsted acidity in deep eutectic solvents and ionic liquids. *Faraday Discussions* **2018**, *206*, 365-377.
118. Abbott, A. P.; Harris, R. C.; Ryder, K. S.; D'Agostino, C.; Gladden, L. F.; Mantle, M. D., Glycerol eutectics as sustainable solvent systems. *Green Chemistry* **2011**, *13* (1), 82-90.
119. Smith, E. L.; Abbott, A. P.; Ryder, K. S., Deep eutectic solvents (DESs) and their applications. *Chemical Reviews* **2014**, *114* (21), 11060.
120. Abbott, A. P.; Frisch, G.; Hartley, J.; Ryder, K. S., Processing of metals and metal oxides using ionic liquids. *Green Chemistry* **2011**, *13* (3), 471-481.
121. Jones, D.; Hartley, J.; Frisch, G.; Purnell, M.; Darras, L., Non-destructive, safe removal of conductive metal coatings from fossils: a new solution. *Palaeontologia Electronica* **2012**, *15* (2).
122. Jenkin, G. R.; Al-Bassam, A. Z.; Harris, R. C.; Abbott, A. P.; Smith, D. J.; Holwell, D. A.; Chapman, R. J.; Stanley, C. J., The application of deep eutectic solvent ionic liquids for environmentally-friendly dissolution and recovery of precious metals. *Minerals Engineering* **2016**, *87*, 18-24.

123. Abbott, A. P.; Harris, R. C.; Holyoak, F.; Frisch, G.; Hartley, J.; Jenkin, G. R. T., Electrocatalytic recovery of elements from complex mixtures using deep eutectic solvents. *Green Chemistry* **2015**, *17* (4), 2172-2179.
124. Riao, S.; Petranikova, M.; Onghena, B.; Vander Hoogerstraete, T.; Banerjee, D.; Foreman, M. R. S.; Ekberg, C.; Binnemans, K., Separation of rare earths and other valuable metals from deep-eutectic solvents: a new alternative for the recycling of used NdFeB magnets. *RSC Advances* **2017**, *7* (51), 32100-32113.

# Chapter 2: Experimental Procedures

2 Experimental Procedures .....	59
2.1 Materials.....	59
2.1.1 Chemicals .....	59
2.1.2 Preparation of deep eutectic solvents .....	61
2.2 Leaching experiments .....	62
2.2.1 Ultrasound assisted chemical dissolution.....	63
2.3 Analytical techniques for the characterisation of metal content .....	64
2.3.1 Inductively Coupled Plasma Mass Spectrometry ICP-MS .....	64
2.3.2 Inductively Coupled Plasma Optical Emission Spectroscopy ICP-OES .....	68
2.3.3 X-ray Fluorescence.....	68
2.4 UV-Vis Spectroscopy.....	69
2.5 Nuclear Magnetic Resonance spectroscopy (NMR).....	70
2.6 Electrochemical processes .....	71
2.6.1 Cyclic Voltammetry .....	71
2.6.2 Paint Casting.....	73
2.6.3 Chronopotentiometry.....	73
2.6.4 Chronocoulometry .....	74
2.7 Bulk electrochemical dissolution .....	74
2.8 Scanning Electron Microscopy – Energy Dispersive X-rays spectroscopy.....	76
2.9 References .....	78

## 2 Experimental Procedures

### 2.1 Materials

#### 2.1.1 Chemicals

The materials used in this thesis, along with their purity and source are listed in **Table 2.1** and **Table 2.2**.

*Table 2.1: List of chemicals used, their formula, purity and source.*

Chemical	Formula	Purity	Source
Acetic acid	C <sub>2</sub> H <sub>4</sub> O <sub>2</sub>	99%	Fisher
Betaine hydrochloride	HbetCl	99%	Acros Organics
bis(2-ethylhexyl) phosphoric acid	C <sub>16</sub> H <sub>35</sub> O <sub>4</sub> P	95 %	Acros Organics
Choline Chloride	C <sub>5</sub> H <sub>14</sub> ClNO	99%	Acros Organics
Chromium oxide	Cr <sub>2</sub> O <sub>3</sub>	99 %	Alfa Aesar
Cobalt (II) chloride hexahydrate	CoCl <sub>2</sub> ·6H <sub>2</sub> O	98%	Alfa Aesar
Cobalt (II, III) oxide	Co <sub>3</sub> O <sub>4</sub>	99%	Alfa Aesar
Cobalt (II) oxide	CoO	95%	Alfa Aesar
Copper (II) chloride dihydrate	CuCl <sub>2</sub> ·2H <sub>2</sub> O	97%	Aldrich
Copper (I) chloride	CuCl	97%	Sigma-Aldrich
Copper (II) oxide	CuO	99%	Chem Cruz
Copper (I) oxide	Cu <sub>2</sub> O	99%	Alfa Aesar
1-Decanol	C <sub>10</sub> H <sub>22</sub> O	98 %	Acros Organics
Ethylene Glycol	C <sub>2</sub> H <sub>6</sub> O <sub>2</sub>	98%	Fisher
Glycerol	C <sub>3</sub> H <sub>8</sub> O <sub>3</sub>	≥ 98%	Fisher
Glycolic acid	C <sub>2</sub> H <sub>4</sub> O <sub>3</sub>	99%	Janssen Chimica
Hydrochloric acid	HCl	37%	
Iron (III) chloride	FeCl <sub>3</sub>	98%	Acros Organics
Iron (II) chloride	FeCl <sub>2</sub>	97%	Acros Organics
Iron (III) oxide	Fe <sub>2</sub> O <sub>3</sub>	≥ 96%	Alfa Aesar
Iron (II, III) oxide	Fe <sub>3</sub> O <sub>4</sub>	97%	Aldrich
Lactic acid	C <sub>3</sub> H <sub>6</sub> O <sub>3</sub>	88%	Fisher
Lead (II) chloride	PbCl <sub>2</sub>	99%	BDH Chemicals

Table 2.2: List of chemicals used, their formula, purity and source (continued).

Chemical	Formula	Purity	Source
<b>Lead (II) oxide</b>	PbO	99.9%	Alfa Aesar
<b>Levulinic acid</b>	C <sub>5</sub> H <sub>8</sub> O <sub>3</sub>	98%	Alfa Aesar
<b>Lithium bis(trifluoromethylsulfonyl)imide</b>	LiTf <sub>2</sub> N	99%	IOLITEC
<b>Lithium chloride</b>	LiCl	99%	Alfa Aesar
<b>Lithium Nickel Manganese Cobalt oxide</b>	LiNi <sub>0.33</sub> Mn <sub>0.33</sub> Co <sub>0.33</sub> O <sub>2</sub>	98%	Aldrich
<b>Manganese (II) chloride tetrahydrate</b>	MnCl <sub>2</sub> ·4H <sub>2</sub> O	99%	Sigma Aldrich
<b>Manganese (IV) oxide</b>	MnO <sub>2</sub>	99 %	Acros Organics
<b>Manganese (II) oxide</b>	MnO	76.0- 78.0%	Alfa Aesar
<b>Nickel (II) chloride</b>	NiCl <sub>2</sub>	98%	Aldrich
<b>Nickel (II) oxide</b>	NiO	99%	Alfa Aesar
<b>Nitric acid, trace metals</b>	HNO <sub>3</sub>		Fisher
<b>Oxalic acid dihydrate</b>	C <sub>2</sub> H <sub>2</sub> O <sub>4</sub> ·2H <sub>2</sub> O	99%	Emplura
<b>Potassium hexacyanoferrate (II) trihydrate</b>	K <sub>4</sub> Fe(CN) <sub>6</sub> ·3H <sub>2</sub> O	98.5%	Acros Organics
<b>Triflic acid</b>	CF <sub>3</sub> SO <sub>3</sub> H	99%	Aldrich
<b>Urea</b>	NH <sub>2</sub> CONH <sub>2</sub>	98%	Sigma Aldrich
<b>Zinc (II) chloride</b>	ZnCl <sub>2</sub>	97%	Sigma
<b>Zinc (II) oxide</b>	ZnO	99.5%	AnalaR
<b>YOX</b>	Y <sub>2</sub> O <sub>3</sub> :Eu <sup>3+</sup>	99%	Nichia
<b>LAP</b>	LaPO <sub>4</sub> :Ce <sup>3+</sup> ,Tb <sup>3+</sup>	99%	Nichia
<b>BAM</b>	BaMg <sub>2</sub> Al <sub>16</sub> O <sub>27</sub> :Eu <sup>2+</sup>	99%	Nichia
<b>HALO</b>	(Sr, Ca) <sub>10</sub> (PO <sub>4</sub> ) <sub>6</sub> (Cl, F) <sub>2</sub> :Sb <sup>3+</sup> ,Mn <sup>2+</sup>	99%	Nichia

The experimental work for Chapter 5 was conducted at the Chemical Engineering department of KU Leuven, so the materials used were provided by the SOLVOMET group's lab. The aliphatic diluent GTL Solvent GS190 was obtained from Shell Global Solutions (Amsterdam, The Netherlands). The real lamp phosphor waste was provided by Relight Srl (Rho, Italy), whose composition is given in Chapter 5. All the components above were used as received, without any purification steps.

The LIB cathode sheets used at the end of Chapter 3 were taken from unassembled quality control EV pouch cells manufactured by Envision/AESC in July 2018 and provided by the ReLiB project. They had previously been removed from their pouches and rinsed with dimethyl carbonate (DMC) to remove any residual electrolyte and then dried in the air. The cathode sheets were kept in a sealed container in between experiments.

### 2.1.2 Preparation of deep eutectic solvents

The deep eutectic solvents (DESs) used in this study are listed in the **Table 2.3**.

*Table 2.3: List of deep eutectic solvents, their components and molar ratio*

Deep eutectic solvent (DES)	Hydrogen Bond Acceptor (HBA)	Hydrogen Bond Donor (HBD)	Molar ratio (HBA:HBD)
<b>EG:ChCl</b>	ChCl	Ethylene glycol	1:2
<b>Urea:ChCl</b>	ChCl	Urea	1:2
<b>Gly:ChCl</b>	ChCl	Glycerol	1:2
<b>OxA:ChCl</b>	ChCl	Oxalic acid dihydrate	1:1
<b>LacA:ChCl</b>	ChCl	Lactic acid	1:2
<b>AceA:ChCl</b>	ChCl	Acetic acid	1:2
<b>LevA:ChCl</b>	ChCl	Levulinic acid	1:2
<b>GlyA:ChCl</b>	ChCl	Glycolic acid	1:2

The components were mixed in a sealed container, under continuous stirring conditions and at 50 °C, until a transparent homogeneous liquid was formed.<sup>1, 2</sup> The solvents were then stored at room temperature, in order to slow down any degradation or esterification reaction between the components, since temperature has a great effect on the degradation kinetics of DESs.<sup>3</sup> In addition, the DESs were used within 3 weeks from their preparation

date. For the DES composed of oxalic acid dihydrate, which includes two carboxylic groups in its structure, the molar ratio was 1:1, as suggested by Abbott et al.,<sup>2</sup> whereas for the rest of the DESs the molar ratio was 1:2 (ChCl: HBD).

For the preparation of the mixtures EG:ChCl with triflic acid, the method used was the same as that by Alabdullah.<sup>4</sup>

## 2.2 Leaching experiments

Part of this thesis investigates the chemical dissolution of MOs. In Chapter 3 fundamental studies are conducted on the dissolution mechanism of MOs from synthetic MO powders. In the end of Chapter 3, some of the fundamental results are validated on cathode material of spent LIB, while on Chapter 5 the extraction of REEs from EoL fluorescent lamp phosphor is investigated.

For Chapter 3, in order to investigate the solubility of MOs, a weighed mass of powder was dissolved in 5 mL of solvent in a sealed glass vial, at 50 °C with continuous stirring for 48 hours. In cases where all of the powder was dissolved in the DES, an additional amount of MO was weighted and fed into the vial. Upon the completion of the dissolution, the solutions were centrifuged at 4000 rpm, using the centrifuge Centurion Scientific Pro-Research K241 and filtered with PET syringe filters (pore size 0.22 µm). In the case that precipitation of material was observed, the precipitates were rinsed with hot deionized water and dried overnight at 50 °C in an oven. Then weighed amount of them was digested in dilute HCl and the PLS was analysed with ICP-MS.

For Chapter 3, the dissolution of the synthetic  $\text{LiNi}_{0.33}\text{Mn}_{0.33}\text{Co}_{0.33}\text{O}_2$  (NMC) powder and the spent cathode of a LIB conducted in sealed glass vials, at various temperatures ranging between 25 °C – 80 °C, under stirring conditions unless otherwise stated, and with a liquid: solid ratio (L:S) of 25 mL g<sup>-1</sup>. For the dissolution of the cathode sheet 4 × 2 cm<sup>2</sup> were cut, weighed and placed in the vial. The pregnant leach solutions (PLSs) were then treated as mentioned before. For the initial characterisation of the metal content of the industrial cathode and the synthetic LiNMC powder, 0.04 g and 0.015 g of materials, respectively, were dissolved in 10 mL and 6 mL of aqua regia at 25 °C under stirring conditions for 30 minutes and the resulting solution was analysed with ICP-MS. The digestions were performed in triplicates.

For Chapter 5, the chemical characterization of the phosphors YOX and HALO was accomplished with the dissolution of 0.1 g of solid in 4 mL of 6 mol L<sup>-1</sup> HCl, under stirring conditions for 24 h at 80 °C. The characterization of the real lamp phosphor waste included its sieving using a vibratory sieve shaker Analysette 3 from Fritsch with a 125 µm sieve. Then, approximately 50 mg of solid material was placed in the microwave (MW) (Berghof Speedwave Xpert) digestion vessels (DAK-100), and 10 mL of HCl was added. Each digestion was performed in quadruplicate. The digestion method was: (1) ramping from room temperature to 145 °C in 10 min and holding for 10 min, (2) ramping to 170 °C in 5 min and holding for 10 min, (3) ramping to 200 °C in 5 min and holding for 10 min, (4) cooling down to 50 °C and hold for 20 min. The digested sample was diluted with MilliQ water to a final volume of 50 mL, and it was analysed for its metal content via ICP-OES. This method is not suitable for the characterization of the silicate fraction.

For the leaching experiments of either individual synthetic phosphors or the real waste, 0.1 - 0.3 g of material was placed in a glass vial, the lixiviant was added, and the sealed vial was placed in a sand bath at constant temperature and stirring conditions. A heated magnetic stirrer plate with a temperature controller inserted in a reference vial containing the lixiviant and was used for heating and stirring the samples. After the leaching, the samples were centrifuged at 3600 rpm and filtered using PET syringe filters (pore size 0.45 µm) to remove any remaining particulate matter.

### **2.2.1 Ultrasound assisted chemical dissolution**

Sonochemistry was first published in 1927 by Richards and Loomis<sup>5</sup>, where they proved that chemical reactions can be accelerated by sound waves. Ultrasound has found applications in diverse fields such as surface cleaning, dissolution of soils and ores, separation, welding, soldering, emulsification and atomisation of liquids, removal of chemical and biological contaminants from water, amongst others.<sup>6</sup>

Ultrasound assisted processes rely on the vibrational motion that sound induces in the medium in which is travelling through. The ultrasound waves, which usually reach frequencies of 20-100 kHz, contribute to the acoustic cavitation that is a process in which the forces binding two molecules together in a liquid state are decreased and eventually diminished. For example, if ultrasound power is applied to water, then the drops of water undergo instant compression followed by expansion, resulting in the production of

cavitation gas bubbles, due to the increase of the distance between its molecules. The bubbles then, expand until the limit of pressure is reached, ending up in their collision or collapse. During the implosion of the bubbles, high temperatures (up to 5000 K) and pressures (1500 atm) can be reached that last for less than 0.1  $\mu$ s and these extreme conditions are responsible for the positive effect of ultrasound in chemical reactions. The extreme temperature and pressure contribute to the significant increase of the activity of these bubbles, which then act as micro-reactors and generate activated molecules and free radicals that under normal conditions would not exist in the solution.<sup>6,7</sup>

In this investigation, ultrasound assisted leaching was tested on the cathodes of spent LIBs of Chapter 3. The initial hypothesis was that ultrasound would contribute to the faster dissolution of the MOs from the electrode surface. Cathode electrode sheets of  $4 \times 2 \text{ cm}^2$  were cut, weighed and placed in a beaker along with 20 mL of OxA:ChCl. A sonic horn (20 kHz, 1250 W), made from titanium alloy from the Branson Ultrasonics company, was inserted in the beaker, which was placed in a water bath, to prevent the overheating of the solution and the beaker. The level of power (translated in power %) used was 70 % of the maximum power the sonic horn could provide. The experiments were carried out for different times scales, ranging between 1-15 minutes. After the completion of the experiments, the remaining solid electrode materials were washed with hot de-ionized water and dried in an oven at 45 °C. The pregnant leach solution was then filtered, in order to avoid the existence of dispersed fine particles and then analysed with ICP-MS.

## **2.3 Analytical techniques for the characterisation of metal content**

### **2.3.1 Inductively Coupled Plasma Mass Spectrometry ICP-MS**

ICP-MS is a common and powerful analytical technique for the characterisation of the metal content of either solids or solutions, whose first instrument was launched in 1983, after the extensive work of different scientists such as Houk<sup>8</sup>, Douglas<sup>9</sup> and Gray<sup>10</sup> amongst others. The advantage of this method is that is highly sensitive, so it is very useful for trace metals analysis as it can detect elements existing in part per billion (ppb) – part per trillion (ppt) concentrations in solution or solids. Due to its high sensitivity, it finds applications in the quality control of highly pure materials, in the detection of heavy and toxic metals and also in geology, geochemistry, semi-conductors industry, food industry and forensic science.<sup>11</sup> ICP-MS provides the advantage of analysing multi-

element solutions with high accuracy and analysing individual isotopes of elements and compare them.

The principle of ICP-MS is the combination of two processes a) the atomization and then ionization of the elements and b) their identification using a mass spectrometer. As seen in the **Figure 2.1** samples are inserted in the sample carrier as aerosol droplets. In this stage, argon plasma of temperature around 5500-5800 °C contributes to the dissociation of molecules and their atomization. For that reason, ICP-MS is a technique, which is not dependent on the metal speciation in solution, and the results taken refer to the total mass of an element in the solution. After the atomization and ionization of the elements, they are inserted in a mass spectrometer that serves as a filter.

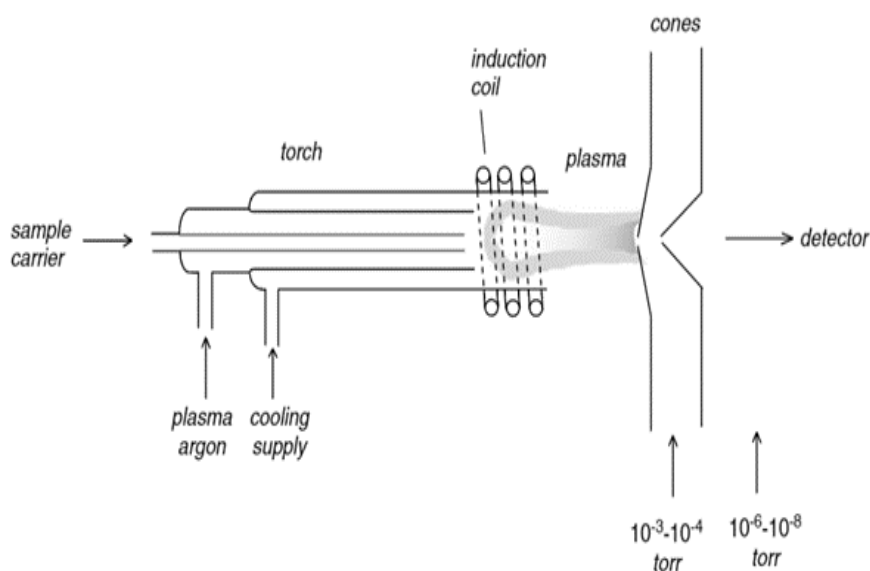
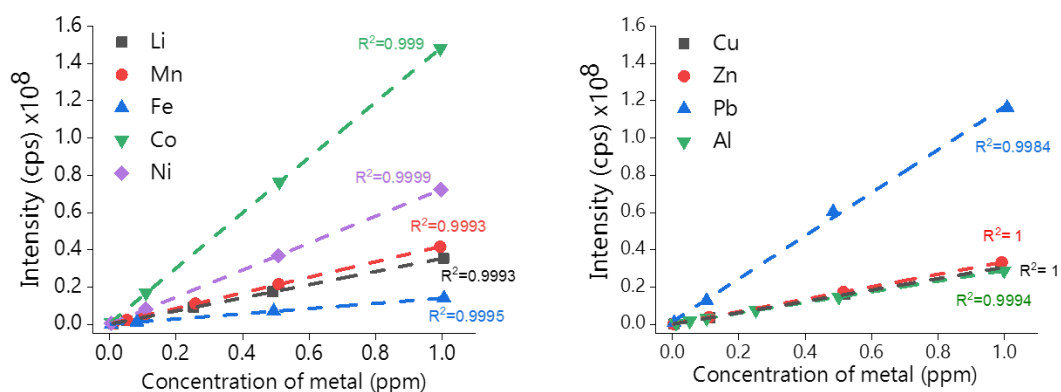


Figure 2.1: Graphical presentation of ICP-MS instrumentation.<sup>11</sup>

Most ICP-MS instruments employ a quadrupole mass spectrometer, which can filter the different elements existing in the argon plasma by allowing only one mass-to-charge ( $m/z$ ) ratio to flow through the spectrometer.<sup>12</sup> The ions then exit the mass spectrometer and strike the dynode of an electron multiplier, which actually acts as the detector of each element. By striking on the dynode, each ion produces an impact in the form of electrons that are amplified so that the pulse is measurable. Then, the software correlates the intensity of the pulses produced by each sample to those of solutions of standard concentrations. The calibration solutions are prepared for every metal and the concentrations are selected to be within the range of expected concentrations of metals in

the samples. In **Figure 2.2**, calibration plots prepared for all the metals under investigation are shown.



*Figure 2.2: Calibration plots for different metals in 2% HNO<sub>3</sub> using ICP-MS*

The calibration lines were produced, by dilution of a stock synthetic multi-element solution (Standard solution 2A purchased from SPEX CertiPrep, with initial concentration 10 ppm), which included all the metals under investigation in 2% HNO<sub>3</sub>, resulting in different concentration between 10 ppb to 1000 ppb. The R<sup>2</sup> of the calibration lines is 0.999 for most of them, indicating the accuracy of the instrument. In addition, it was also very essential to determine if the instrument accurately measures concentrations of metals from samples prepared in DESs. For that reason, the metals investigated were dissolved in different concentrations in EG:ChCl and then diluted in 2% HNO<sub>3</sub> in order to be analysed by ICP-MS. In **Figure 2.3**, the correlation between the theoretically expected ppm of metals in the different solutions in EG:ChCl with the actual measured ppm by the instrument is shown.

It is apparent that for most metals the instrument can accurately measure concentrations from samples initially dissolved in DESs, with small exceptions for Zn that showed slightly lower accuracy. The instrument can therefore be employed for the chemical analysis of the samples produced in the following chapters. For this investigation, before the analysis of the samples calibration lines of each element were constructed in 2% HNO<sub>3</sub> for concentrations between 10 – 1000 ppb. The internal standards (spikes) used in each sample were always Rh and La (0.1 ppm). The use of internal standards is not compulsory in ICP-MS, but it can improve the accuracy of the results by setting a reference that can be used to correct variabilities between the calibration solutions and

the unknown samples. Also, each sample was diluted 1000 times in 2% HNO<sub>3</sub>, and if needed an extra 100 times dilution followed.

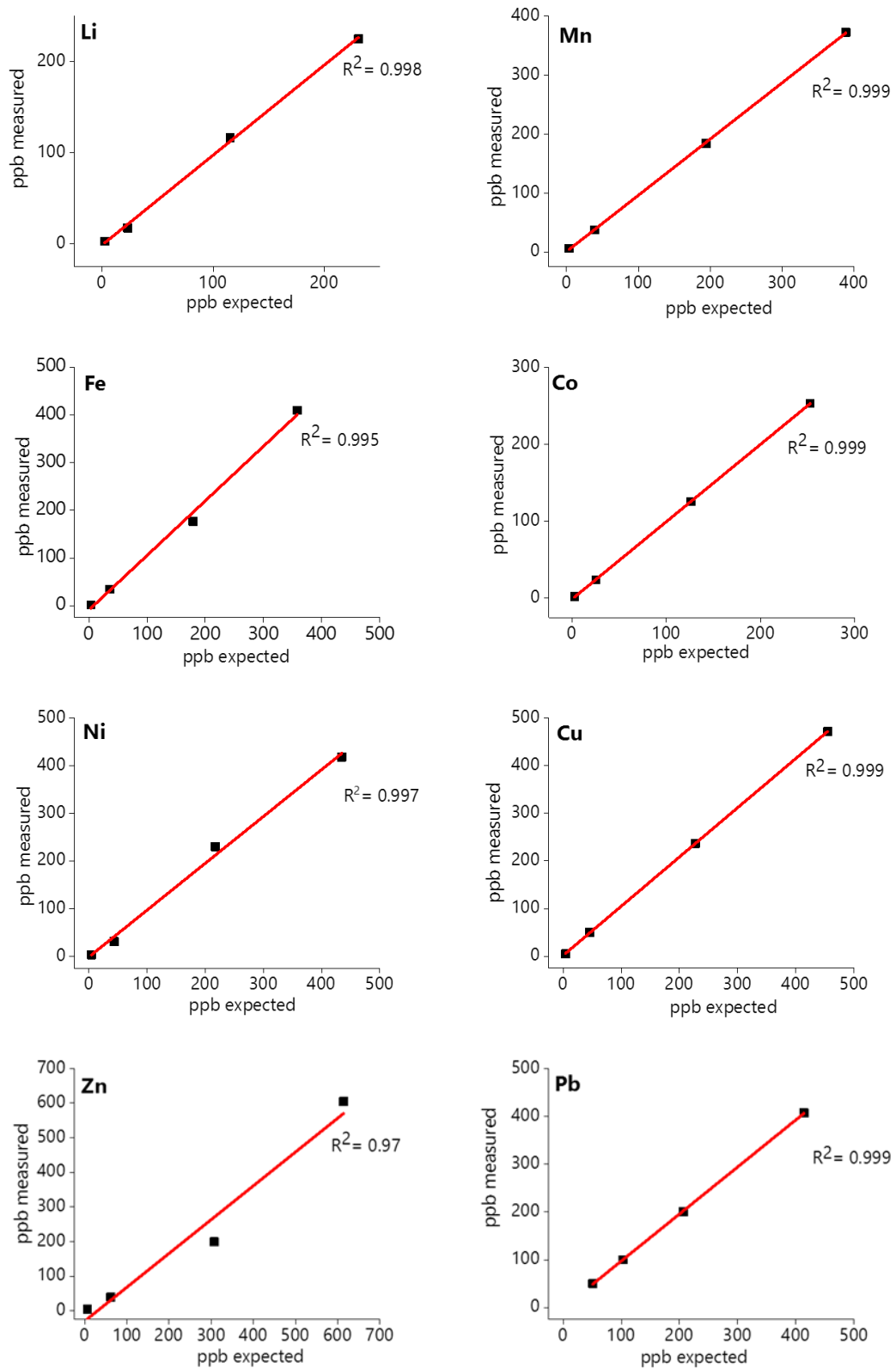


Figure 2.3: Correlation of measured concentrations of different metals, dissolved in EG:ChCl, by ICP-MS with the theoretical expected concentrations.

### **2.3.2 Inductively Coupled Plasma Optical Emission Spectroscopy ICP-OES**

ICP-OES is another common analytical technique for measuring concentration of metals in solutions. As a first step, in the same manner as during an ICP-MS analysis that mentioned before, the heat provided by the plasma torch contributes to the atomization and ionization of the elements. The distinguishing difference between the two methods of ICP-OES and ICP-MS are the ways to identify the elements present in the sample. ICP-OES detects the light emitted by the elements, which are in their excited state after the heating step associated with the plasma torch. Each element emits light at different wavelength and that means that the emitted light from the plasma zone is polychromatic. This polychromatic emission, then needs to be separated so that different elements and their intensity can be identified, and this is accomplished by either a monochromator, which can detect the light emitted at a specific wavelength or a polychromator that can detect light at different wavelengths at the same time. Actually, ICP-OES provides the flexibility to measure the concentration of all the elements in the solution at a specific wavelength, but this may also result in interferences of different elements that show emission of light at very close wavelengths.<sup>13</sup>

ICP-OES was only used for the experimental work conducted at KU Leuven (Chapter 6), as mentioned before. The sample preparation for the ICP-OES analysis was as follows: the samples were diluted with 2 vol% HNO<sub>3</sub> to have a final metal concentration lower than 50 ppm, and indium (5 ppm) was used as the internal standard. The spectral lines (wavelengths in nm) selected for quantification were: yttrium 324.227; calcium 315.887; europium 381.967; iron 238.204; lanthanum 408.672; cerium 413.764; and barium 233.527.

### **2.3.3 X-ray Fluorescence**

X-ray fluorescence provides with both qualitative and quantitative information about a solid or liquid sample. First, the sample is irradiated by high energy X-rays, which contributes to the release of one core shell electron, leaving a hole. The atom then regains stability by an outer orbital electron relaxing into the vacant position shell hole. This movement of the electron from the higher energy state to the lower one of the inner shells releases energy in the form of photons, which is actually the difference in energy between the two quantum states of this electron and is specific for each element.<sup>14</sup> This energy is then measured by the detector and the identification of the element and its concentration follows, since each element has electronic transitions that have specific energy.

XRF was used only for Chapter 5, to analyse the metal content of the organic phases after the solvent extraction of rare earth elements. The organic samples were diluted 10 times in ethanol, and indium was used as an internal standard using a concentration similar to that of the analyte. The measurements were performed following an optimised methodology. The samples were measured on polished quartz glass disks. To prevent the pipetted sample droplet from moving and spreading on the carrier, 30  $\mu\text{L}$  of a silicon solution in isopropanol (SERVA Electrophoresis GmbH, Heidelberg, Germany) was added on the carrier surface and dried for 5 min at 80  $^{\circ}\text{C}$  in a hot air oven. A small droplet (2.5  $\mu\text{L}$ ) of the prepared solution was added onto the hydrophobised carrier. Then, the carrier was dried in a hot air oven for 30 min at 80  $^{\circ}\text{C}$ .<sup>15</sup>

## 2.4 UV-Vis Spectroscopy

One of the most widely employed techniques for the identification of soluble species is the UV- Visible spectroscopy. The principle of this method relies on the absorbance of energy, in the form of light (200 – 800 nm) from the sample. During the analysis, light with initial intensity  $I_o$  is passing through a sample and light with final intensity  $I$  is leaving the sample, since some of the energy is absorbed by the sample. The ratio of  $\frac{I}{I_o}$  is called the transmittance ( $T$ ) of light and it is actually the first value that is collected by the instrument. Then, the transmittance is translated into absorbance ( $A$ ) with the **Equation 2.1**.

$$A = -\log(T) \quad \text{Equation 2.1}$$

The absorbance is more important, since it is directly proportional to the concentration of the species by the Beer-Lambert law, which is shown in **Equation 2.2**.

$$A = \varepsilon \times C \times l \quad \text{Equation 2.2}$$

Where  $\varepsilon$  is the extinction coefficient ( $\text{mol}^{-1} \text{dm}^3 \text{cm}^{-1}$ ),  $C$  is the concentration of the solute ( $\text{mol dm}^{-3}$ ) and  $l$  is the path length of the sample holder (cm).

UV-Vis spectroscopy is employed in analytical chemistry mainly in order to give information about the concentration of molecules in the sample. In this thesis, however, it was used to provide information about the species of metals ions formed in the different solutions of DESs, by comparing their spectra with other spectra of solutions of known speciation. For that purpose, a Mettler Toledo UV5 Bio spectrometer and quartz cell with a path length of 10 mm were used for all the samples. In cases where the sample was very

concentrated, and where dilution of the sample resulted in a change of colour and hence of metal species, quartz slides with a path length of 1 mm were used.

## 2.5 Nuclear Magnetic Resonance spectroscopy (NMR)

Nuclear magnetic resonance (NMR) spectroscopy is the study of molecules, upon their placement in a strong magnetic field, by measuring the interaction of the nuclei of the sample molecules after excitation with radiofrequency ( $Rf > 10^6$  to  $10^8$  Hz) electromagnetic radiation.<sup>16</sup> NMR signal can be observed only by atoms whose nuclei possess the property of spin. This happens when a nucleus can have more than one energy states under a magnetic field and thus the quantum spin number ( $I$ ) is not zero. This number is influenced by the number of protons and neutrons in the nucleus. This technique lies on the Zeeman effect under which, when a nucleus that possess a spin, it then align itself according of its energy states under a magnetic field. The charged nuclei generates a magnetic field and possess a magnetic moment. When the spin returns to its original energy level, energy is emitted at the same frequency. The resonant frequency is dependent upon the magnetic field at the nucleus, which in turn is affected by electron shielding and thus chemical environment and so information about the chemical environment can be derived by the resonant frequency.<sup>17</sup>

NMR was discovered by Isidor Isaac Rabi at the Columbia University during 1930s.<sup>18</sup> His work was further developed by Felix Bloch and Edward Purcell that simultaneously demonstrated NMR in condensed matter, during 1940s.<sup>19</sup> The first NMR spectrometers became commercial by the end of 1950s.<sup>16</sup>

It can give qualitative information about the molecule, even if it is unknown by compare the spectra with ones reported in open spectral libraries, since each spectrum is unique for a molecule. It can also give information about the purity of a sample. In addition, it provides further information for the properties of the organic molecule such as diffusion, solubility, phase change etc.

For this investigation, a nuclear magnetic resonance (NMR) spectrometer (Bruker Ascend 300) operating at 300 MHz was used to record NMR spectra in the Chemical engineering department of KU Leuven. All NMR measurements were executed in deuterated methanol as the solvent.

## 2.6 Electrochemical processes

### 2.6.1 Cyclic Voltammetry

Cyclic voltammetry is one of the most common and basic techniques used in electroanalytical chemistry and it is useful for the quantitative and qualitative characterisation of redox species in an electrolyte. It is a potentiostatic technique, meaning that the potential is an externally controlled parameter, which is linearly scanned between two fixed values  $E_1$  to  $E_2$  and backwards, at a constant rate:  $v = \frac{dE}{dt}$  called scan rate.<sup>20</sup> The current resulting from the change in potential is recorded and reported in plots called cyclic voltammograms (CVs), an example of which is given in **Figure 2.4**.

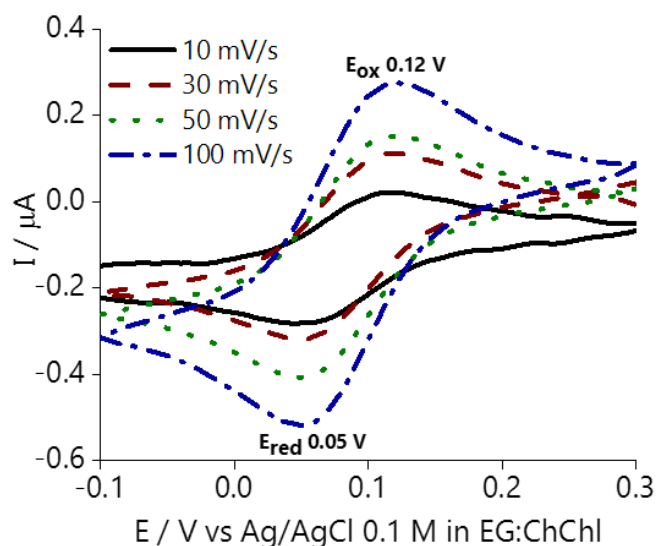
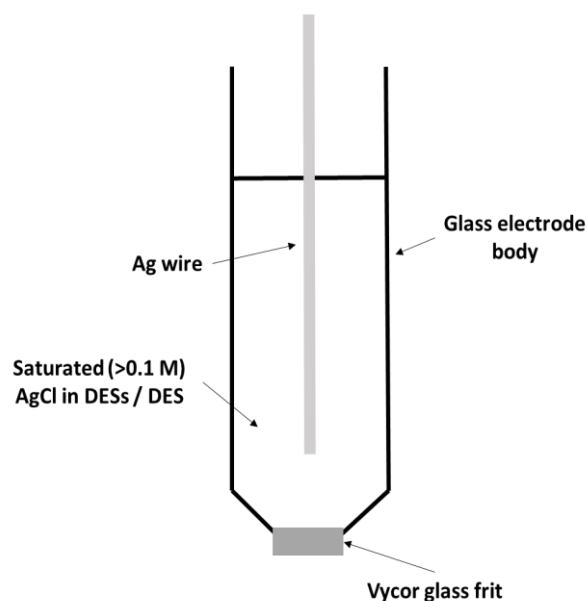


Figure 2.4: Cyclic voltammogram of 10mM  $K_4[Fe(CN)_6] \cdot 3H_2O$  dissolved in EG:ChCl at different scan rates from 10 to 100 mV/s.



The setup of any voltammetry technique (e.g. cyclic, linear) requires a three-electrode system including the working (WE), counter (CE) and reference (RE) electrode. The redox reactions are occurring at the surface of the WE. The RE allows the control of the potential applied at the WE and it must consist of an electrochemically reversible couple with Nernstian behaviour and be chemically stable over time. The CE closes the current circuit and usually is an inert electrode like platinum or graphite and because the current flows between the WE and CE, its surface needs to be bigger than the one of WE so that is not opposing any limitations to the kinetics.

During the cyclic voltammetry experiment, peaks are forming at the CV whenever an oxidation or a reduction of species occurs, rendering cyclic voltammetry a very important technique for the determination of the standard potential of half-cell reactions.<sup>21</sup> For example, in **Figure 2.4** the CV of  $K_4[Fe(CN)_6] \cdot 3H_2O$  dissolved in EG:ChCl is shown. Two peaks are apparent, the oxidation peak ( $E_{ox}$ ) at 0.12 V, where ferrocyanide  $[Fe(CN)_6]^{4-}$  is oxidised to ferricyanide  $[Fe(CN)_6]^{3-}$  by the following **Equation 2.3**, and the reduction peak ( $E_{red}$ ) at 0.05 V, where the opposite reaction occurs.



*Figure 2.5: Schematic presentation of reference electrode used in all electrochemical experiments*

All of the CV experiments carried out using an IVIUMnSTAT multichannel potentiostat/galvanostat together with the corresponding Ivium software. The CVs were performed at room temperature (otherwise stated) with the below setup of electrodes:

- Working electrode - Pt flag 0.32 cm<sup>2</sup>
- Counter electrode - Pt flag *ca* 1 cm<sup>2</sup>
- Reference electrode – Ag wire (1 mm) immersed in a saturated solution of AgCl in EG:ChCl. **Figure 2.5** shows a schematic representation of the reference electrode used, which has been developed and investigated by Hartley.<sup>22</sup>

The WE and CE were rinsed with deionized H<sub>2</sub>O and dried with acetone prior to use. Also, before each CV, linear sweep voltammogram was performed in order to remove any possible contaminants on the surface of the WE.

### 2.6.2 Paint Casting

The electrochemical study of the metal oxides in powder form was accomplished by using a novel technique developed by Abbott et al,<sup>23</sup> called paint casting. During this method, the synthetic powders of MOs were ground with pestle and mortar, until very fine particles were produced and were then mixed with a small amount of DES. The paste was “painted” on the Pt WE that was bent at 90°. One limitation was the quantity of the paste painted on the WE; it had to be ensured that the amount was the smallest possible to obtain a clear redox couple, otherwise a high resistivity current was produced. The setup used for this analysis is shown in **Figure 2.6**. By employing the paint casting method, both soluble and non-soluble or conductive and non-conductive materials can be electrochemically studied.



*Figure 2.6: Paint casting method paste obtained from the mixing of powder of mineral or metal compound with a DES (left) and WE bended at 90 °C holding the paste (right).<sup>23</sup>*

More information about this method and its possibilities are given in Chapter 4.

### 2.6.3 Chronopotentiometry

Chronopotentiometry was conducted using the paint casting method, in order to measure the open circuit potential (OCP) of MOs and gain information about their stability and affinity to dissolve chemically in EG:ChCl. This method can give information about the oxidation or reduction reactions when no current is flowing in the system and is widely employed in the corrosion science.<sup>24</sup>

The OCP is the potential of the WE in respect to the reference electrode, where no external electric potential is applied. Hence, the plots of chronopotentiometry illustrate the change in galvanic potential over time and gives information about the potential of the electroactive materials at equilibrium. In order to investigate the OCP, the same three electrode system as during the CV was employed. Same weighed amount of MO powder slurry was painted on the WE and the results were recorder for over an hour and a half.

#### 2.6.4 Chronocoulometry

Chronocoulometry was also conducted using the paint casting method. The weighed MOs slurries were painted on the WE. A constant voltage applied to the WE and the charge passed was measured as a function of time.

The charge can be obtained using the integrated Cottrell equation, given in **Equation 2.4**

$$Q = \frac{2nFAD^{\frac{1}{2}}[M]}{\frac{1}{2}} t^{\frac{1}{2}} \quad \text{Equation 2.4}$$

Where  $Q$  is the total charge consumed in C,  $n$  is the number of electrons transferred,  $F$  is the Faraday constant ( $96485 \text{ C mol}^{-1}$ ),  $A$  is the area of the electrode surface in  $\text{cm}^2$ ,  $D$  is the diffusion coefficient of the species in  $\text{cm}^2 \text{ s}^{-1}$ ,  $t$  is the time in s and  $[M]$  is the concentration of the metal ions in  $\text{mol cm}^{-3}$ .<sup>25</sup>

The chronocoulometry can provide with information about diffusion coefficients of the species involved in the electrochemical process and also can give information about the rate of these reactions.

### 2.7 Bulk electrochemical dissolution

The electrochemical dissolution of MOs was conducted in a cell presented in **Figure 2.7**. The idea behind this experiment is similar to that of paint casting, since the powder of MO was placed on the surface of the anode, which was immersed in the DES. The cell of bulk anodic dissolution consisted of a two-electrode system, with both anode and cathode being an iridium oxide coated titanium mesh electrode. The leaching experiments were carried out at  $50 \text{ }^\circ\text{C}$  for 48 hours, using 15 mL of solvent and a constant voltage of 2.7 V was provided by a bench power supply. Afterwards the PLSs were treated as in the case of the chemical dissolution.

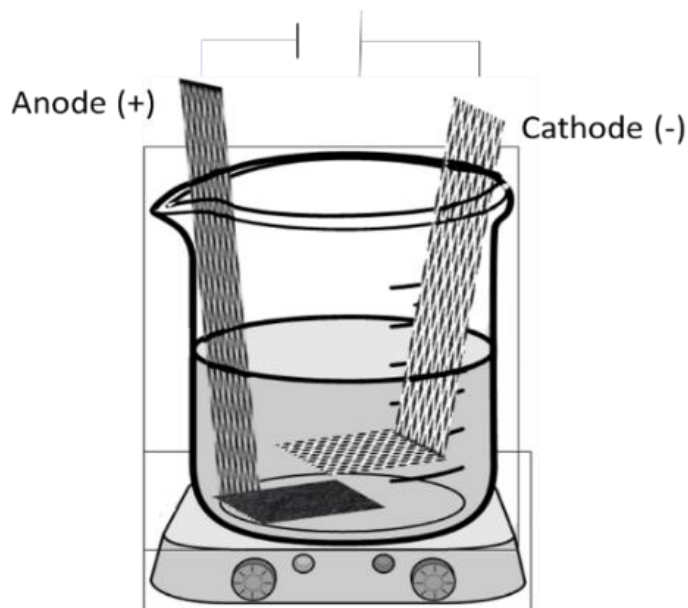


*Figure 2.7: Schematic presentation of the bulk dissolution experiment*

The bulk electrochemical dissolution and deposition were investigated in the cell of the **Figure 2.8**.

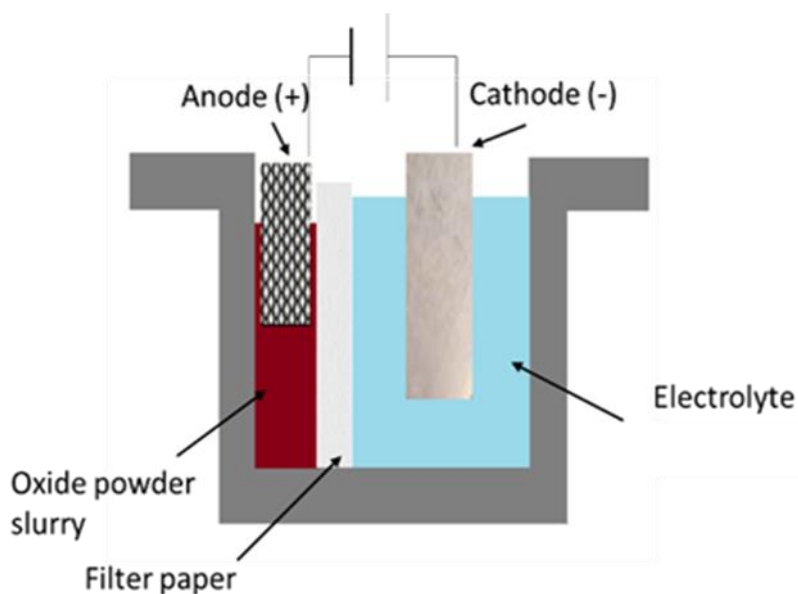


*Figure 2.8: Cell of bulk electrochemical dissolution and deposition*

The same electrodes are used as in the previous cell of bulk dissolution and constant voltage of 2.5 V was applied again by a bench power supply. Prior to the experiment the Ni plates were rinsed with hot deionized water, followed by rinsing with acetone and roughening of the surface with 100 grit sandpaper. The Ni plates before the experiment were kept in a seal vial filled with acetone, in order to eliminate the possibility of oxide formation on the surface. By the end of the experiment, the PLSs were also treated as

after the chemical dissolution and the Ni plates were placed in a vial with hot deionized water to dissolve the remaining DES from the surface.

## 2.8 Scanning Electron Microscopy – Energy Dispersive X-rays spectroscopy

Scanning Electron Microscopy (SEM) is a versatile tool for the investigation of the morphology and microstructure of materials and when coupled with the Energy Dispersive X-ray analysis it can also provide information about chemical composition.<sup>26</sup> During the analysis, a high-energy (2-40 keV) electron beam strikes the specimen's surface. When the electrons encounter the atoms of the specimen, then secondary, backscattered, Auger electrons and X-rays are produced from different depths of the specimen, which various detectors are then collecting.

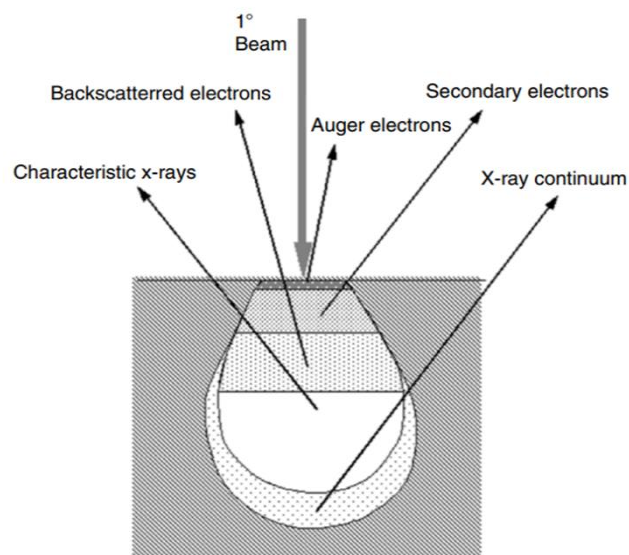


*Figure 2.9: Schematic representation of the various signals produced from different regions of the specimen, after the interaction of the incident electron beam with the surface of the specimen during SEM analysis.<sup>26</sup>*

The secondary electrons emission (SE) is the most widely used; these electrons possess low energy (3-5 eV), and they are escaping from a region of only few nanometres ( $\approx 10$  nm) from the surface, presented also in **Figure 2.9**.<sup>26</sup> SE analysis is useful for obtaining information about surface roughness and texture and gives the highest spatial resolution images, because the probe beam has the same size as the area under investigation. Backscattered electrons are the electrons that have undergone scattering events before escaping the surface of the specimen with energy levels larger than 50 eV and from a deeper area of the specimen, as seen in **Figure 2.9**. The images obtained from BSE

analysis are not as of high resolution as from SE, because the area of analysis is larger than the probe size. With BSE analysis, information about composition can be accomplished, since elements of higher atomic mass give a brighter contrast.<sup>27</sup>

Energy dispersive X-ray (EDX) analysis is usually functioning in conjunction with SEM and provides information about the chemical composition of specific areas selected on the surface of the specimen. During the analysis, X-rays are emitted from the sample after an electron beam of high energy has stroked the surface of the specimen. When the electron beam hits the surface, then core shell electrons escape their orbitals, resulting in vacancies in the electronic structure that are filled by electrons of higher energy. This movement of the electrons produces X-rays.

In this investigation, SEM was used in order to obtain images of the surface morphology of the cathodes of lithium ion batteries of Chapter 5 and NMC powder before and after leaching. The microscope employed was a FEI Quanta 650 FEG in secondary electron (SE) mode, with an Everhart Thornley detector coupled with an EDX software (Aztec). The EDX results obtained at 20 keV and are presented in weight and atomic percentages.

## 2.9 References

1. Abbott, A. P.; Capper, G.; Davies, D. L.; Munro, H. L.; Rasheed, R. K.; Tambyrajah, V., Preparation of novel, moisture-stable, Lewis-acidic ionic liquids containing quaternary ammonium salts with functional side chains. *Chemical Communications* **2001**, (19), 2010-2011.
2. Abbott, A. P.; Boothby, D.; Capper, G.; Davies, D. L.; Rasheed, R., Deep eutectic solvents formed between choline chloride and carboxylic acids: Versatile alternatives to ionic liquids. *Journal Of The American Chemical Society* **2004**, *126* (29), 9142-9147.
3. Rodriguez Rodriguez, N.; van den Bruinhorst, A.; Kollau, L. J.; Kroon, M. C.; Binnemans, K., Degradation of deep-eutectic solvents based on choline chloride and carboxylic acids. *ACS Sustainable Chemistry & Engineering* **2019**, *7* (13), 11521-11528.
4. Alabdullah, S. S. M. pH Measurements in Ionic Liquids. PhD thesis, University of Leicester, **2018**.
5. Richards, W. T.; Loomis, A. L., The chemical effects of high frequency sound waves I. A preliminary survey. *Journal of the American Chemical Society* **1927**, *49* (12), 3086-3100.
6. Mason, T. J.; Peters, D., An introduction to the uses of power ultrasound in chemistry. In *Practical Sonochemistry: Power Ultrasound Uses and Applications*, 2nd ed.; Woodhead Publishing: **1999**.
7. Mason, T. J., Theory, applications and uses of ultrasound in chemistry. In *Sonochemistry*, Ellis Horwood Ltd.: **1988**.
8. Houk, R. S., Mass spectrometry of inductively coupled plasmas. *Analytical Chemistry* **1986**, *58* (1), 97A-105A.
9. Douglas, D. J.; French, J., Elemental analysis with a microwave-induced plasma/quadrupole mass spectrometer system. *Analytical Chemistry* **1981**, *53* (1), 37-41.
10. Gray, A. L.; Date, A. R., Inductively coupled plasma source mass spectrometry using continuum flow ion extraction. *Analyst* **1983**, *108* (1290), 1033-1050.
11. Ammann, A. A., Inductively coupled plasma mass spectrometry (ICP MS): a versatile tool. *Journal of mass spectrometry* **2007**, *42* (4), 419-427.
12. Elmer, P., The 30-minute Guide to ICP-MS. *Perkin Elmer, Shelton CT* **2001**, 1-8.

13. Boss, C.; Fredeen, K. J., *Concepts, Instrumentation and Techniques in Inductively Coupled Plasma Optical Emission Spectrometry*. 3rd ed.; Perkin Elmer Corporation: **2004**.
14. Beckhoff, B.; Kanngießer, B.; Langhoff, N.; Wedell, R.; Wolff, H., *Handbook of Practical X-ray Fluorescence Analysis*. Springer Science & Business Media: **2007**.
15. Regadío, M.; Riaño, S.; Binnemans, K.; Vander Hoogerstraete, T., Direct analysis of metal ions in solutions with high salt concentrations by total reflection X-ray fluorescence. *Analytical Chemistry* **2017**, 89 (8), 4595-4603.
16. Rahman, A.-u.; Choudhary, M. I.; Wahab, A.-t., The Basics of Modern NMR Spectroscopy. In *Solving Problems with NMR Spectroscopy*, 2nd ed.; Elsevier: **2016**.
17. Breitmaier, E.; Voelter, W., *<sup>13</sup>C NMR-Spectroscopy. Methods and applications*. Weinheim, Bergstr: Verlag Chemie: **1974**.
18. Rabi, I. I., Space quantization in a gyrating magnetic field. *Physical Review* **1937**, 51 (8), 652-654.
19. Bloch, F., Nuclear induction. *Physical review* **1946**, 70 (7-8), 460-474.
20. Izutsu, K., *Electrochemistry in Nonaqueous Solutions*. 2nd ed.; WILEY-VCH Verlag GmbH & Co. KGaA: **2009**.
21. Evans, D. H.; O'Connell, K. M.; Petersen, R. A.; Kelly, M. J., Cyclic voltammetry. *Journal of Chemical Education* **1983**, 60 (4), 290-294.
22. Hartley, J. M. Ionometallurgy: the processing of metals using ionic liquids. PhD thesis, University of Leicester, **2013**.
23. Abbott, A. P.; Bevan, F.; Baeuerle, M.; Harris, R. C.; Jenkin, G. R., Paint casting: A facile method of studying mineral electrochemistry. *Electrochemistry Communications* **2017**, 76, 20-23.
24. Frangini, S.; De Cristofaro, N., Analysis of the galvanostatic polarization method for determining reliable pitting potentials on stainless steels in crevice-free conditions. *Corrosion science* **2003**, 45 (12), 2769-2786.
25. Zoski, C. G., Cottrell Equation. In *Handbook of electrochemistry*, Elsevier: **2007**.
26. Zhou, W.; Apkarian, R.; Wang, Z. L.; Joy, D., Fundamentals of scanning electron microscopy (SEM). In *Scanning Microscopy for Nanotechnology*, Springer: **2006**; pp 1-40.
27. Vernon-Parry, K., Scanning electron microscopy: an introduction. *III-Vs Review* **2000**, 13 (4), 40-44.

# Chapter 3: Chemical dissolution of metal oxides in deep eutectic solvents

3 Chapter.....	81
3.1 Introduction.....	81
3.1.1 Metallurgical processing of metal oxides.....	81
3.1.2 Aims .....	84
3.2 Chemical dissolution of metal oxides in DESs.....	85
3.2.1 Dissolution of metal oxides in ethylene glycol: choline chloride .....	86
3.2.2 Effect of pH on dissolution in ethylene glycol: choline chloride.....	91
3.2.3 Ligand effect on dissolution.....	96
3.3 Dissolution kinetics.....	105
3.4 Dissolution of cathode materials of LIBs.....	107
3.4.1 Importance of LIBs recycling.....	107
3.4.2 Characterisation of cathode materials .....	110
3.4.3 Dissolution of the cathode materials in OxA:ChCl.....	112
3.5 Conclusions.....	121
3.6 References .....	124

## 3 Chapter

### 3.1 Introduction

Metal oxides (MOs) represent a very large group of compounds, which exist in nature as primary ores of metals as for example hematite- $\text{Fe}_2\text{O}_3$  and magnetite- $\text{Fe}_3\text{O}_4$ . In addition, MOs are important technological materials that are found in EoL products e.g. LIBs, catalysts and fluorescent lamps. They also exist in low metal containing industrial residues, as for example in the fayalitic slag and red mud, from where they either need to be recycled or will behave as contaminants and their extraction needs to be prevented. Their abundance naturally led to extensive studies of their dissolution and extraction by pyrometallurgical or hydrometallurgical methods. Both these methods show high environmental footprints that needs to be limited, as described in **Chapter 1**. Another issue that the state-of-the art extraction methods need to face is the increasing complexity of the metal deposits and the EoL materials that need to be processed and recycled. Samples with lower concentrations and lower value make pyrometallurgy unsuitable, while the flowsheets of hydrometallurgical methods consist of many subsequent steps that require use of large amounts of chemicals. While mineral acids such as  $\text{H}_2\text{SO}_4$  will always be the cornerstone of metal processing due to their low cost (much is produced from the scrubbing of flue gas) there is a need to characterise alternative media which may be more selective. Thus, in this Chapter, DESs are investigated as lixivants for the extraction of metals from MOs, due to their tuneable character.

#### 3.1.1 Metallurgical processing of metal oxides

The MOs under investigation are  $\text{MnO}_2$ ,  $\text{MnO}$ ,  $\text{Fe}_2\text{O}_3$ ,  $\text{Fe}_3\text{O}_4$ ,  $\text{Co}_3\text{O}_4$ ,  $\text{CoO}$ ,  $\text{NiO}$ ,  $\text{CuO}$ ,  $\text{Cu}_2\text{O}$ ,  $\text{ZnO}$  and  $\text{PbO}$ . The reason behind the choice of these MOs is that some of them exist in low metal containing residues, with Fe, Cu, Zn and Pb oxides to be found together in waste streams such as the fayalitic slag or the electric arc furnace dust. Other MOs such as Mn, Co and Ni coexist either in ores in sea nodules<sup>1</sup> or in finished materials like cathode materials in secondary batteries.<sup>2,3</sup> The MOs under investigation are not only abundant minerals of their respective oxides, but they also take part in many high end technological applications, such as batteries, fuel cells, catalysts, cathode ray tubes, etc. **Table 3.1** presents the main applications and countries of primary production.

Table 3.1: Main applications and countries-producers of metal oxides under investigation

Metal Oxide	Main applications	Producers
<b>MnO<sub>2</sub></b> & <b>MnO</b>	<ul style="list-style-type: none"> <li>▪ main mineral of Mn (pyrolusite)<sup>4</sup></li> <li>▪ primary batteries (Zn/MnO<sub>2</sub>, Mg/MnO<sub>2</sub>)<sup>2</sup></li> <li>▪ secondary batteries (LIBs)<sup>3</sup></li> <li>▪ catalysis<sup>5</sup></li> </ul>	South Africa, Russia
<b>Fe<sub>2</sub>O<sub>3</sub></b> & <b>Fe<sub>3</sub>O<sub>4</sub></b>	<ul style="list-style-type: none"> <li>▪ main minerals of Fe (hematite, magnetite)</li> <li>▪ pigment industry</li> <li>▪ purification of water</li> <li>▪ ferrites production</li> <li>▪ production of Portland cement</li> <li>▪ cathode ray tubes</li> <li>▪ magnetic inks, ferrofluids, contrast agents in sensitive magnetic resonance imaging and in magnetic recording media.<sup>6</sup></li> </ul>	China, Brazil, India, Australia and Russia
<b>Co<sub>3</sub>O<sub>4</sub></b> & <b>CoO</b>	<ul style="list-style-type: none"> <li>▪ secondary batteries (LIBs)<sup>3</sup></li> <li>▪ fuel cells and electrochemical capacitors<sup>7</sup></li> <li>▪ ceramics industry</li> </ul>	Democratic Republic of Congo <sup>8</sup>
<b>NiO</b>	<ul style="list-style-type: none"> <li>▪ secondary batteries (LIBs)<sup>3</sup></li> <li>▪ supercapacitors<sup>9</sup></li> <li>▪ electrochromic devices, gas sensors and solar cells<sup>10</sup></li> </ul>	Indonesia, Philippines, Canada, Russia, New Caledonia
<b>CuO</b> <b>Cu<sub>2</sub>O</b>	<ul style="list-style-type: none"> <li>▪ mineral of Cu (cuprite)</li> <li>▪ catalysis, photocatalysis, gas sensors, solar cells and cathode ray tubes.<sup>11</sup></li> </ul>	Chile, China and Peru
<b>ZnO</b>	<ul style="list-style-type: none"> <li>▪ mineral of Zn (zincite)</li> <li>▪ optoelectronics<sup>12</sup>, photocatalysis<sup>13</sup></li> <li>▪ textile and rubber industry<sup>13</sup></li> <li>▪ pharmaceutical and cosmetic industry<sup>13</sup></li> </ul>	China, Australia, Peru, India and USA
<b>PbO</b>	<ul style="list-style-type: none"> <li>▪ lead acid batteries<sup>14</sup></li> <li>▪ glass industry</li> <li>▪ cathode ray tubes</li> </ul>	China, Australia and USA

One route for the extraction of metals from their MOs is pyrometallurgy which was described in **Chapter 1**. Due to the great stability and the high lattice energy of MOs, their melting point is also large, rendering the pyrometallurgical processes energy intensive, with smelting temperatures usually > 1200 °C. The second group of methods employed is hydrometallurgy, which is actually widely used when the concentration of

metals in the mineral or the EoL material is low and the matrix of the material is rather complex. For most MOs, when they are found in nature in deposits like for the case of  $\text{Fe}_2\text{O}_3$  and  $\text{Fe}_3\text{O}_4$ , the obvious route of processing is pyrometallurgy. However, hydrometallurgy is used when metals need to be recycled from complex EoL materials like LIBs or other electronics, because it can be designed to be selective. For example, the pyrometallurgical industrially implemented process of Umicore for the recycling of spent LIBs, which will be discussed later, has shown that pyrometallurgy cannot be selective, since Al and Li cannot be extracted.<sup>15, 16</sup> In addition, the economic viability of this process is highly dependent on the existence of expensive metals in the battery such as Co, due to the great energy consumption and cost of this method. For that reason, hydrometallurgy can be useful for the recycling of either EoL products or low metal containing waste streams because it will allow recovery of all elements in a less energy intensive process.

For the oxides of Mn, the hydrometallurgical path, most of the time, includes the reductive dissolution in iron sulfate  $\text{FeSO}_4$  solutions, with the presence or not of sulphuric acid  $\text{H}_2\text{SO}_4$ .<sup>17</sup> Another reducing agent used for extraction of Mn is sulphur dioxide  $\text{SO}_2$ .<sup>18</sup> Organic acids such as oxalic acid and tartaric acid, and inorganic acids such as HCl and  $\text{HNO}_3$  have also been employed for the acidic leaching of Mn from  $\text{MnO}_2$ .<sup>4</sup>

For iron oxides, acidic hydrometallurgy is used and recent work has shown that oxalic acid is promising for dissolving the higher oxidation state oxide due to its reducing abilities.<sup>19-22</sup> During the dissolution in presence of oxalic acid, two parallel reactions are occurring; a) the oxidation of oxalate to form either carbonic acid  $\text{H}_2\text{CO}_3$  or carbon dioxide  $\text{CO}_2$ , and b) the reduction of hematite to iron (II) oxalate.

Cobalt oxides and sulfides are found together in many minerals, but they are always produced as by-products from copper and nickel mining. Sulfidic ores are usually roasted first, and the oxidised materials are leached using dilute  $\text{H}_2\text{SO}_4$ . Precipitation of other metals is usually carried out by control of pH with lime or ammonia. Most cobalt rich deposits are found in the Democratic Republic of Congo.<sup>23</sup>

The hydrometallurgical studies for the processing of nickel from its ores are focused mainly on the recovery process. Solvent extraction is widely investigated, in order to separate nickel from cobalt and iron that most of the times are found together, especially in laterites, followed by electrowinning of pure nickel.<sup>24</sup> Apart from the inorganic acids,

organic acids have also been tested for the extraction of Ni, with citric acid to be one of the most efficient.<sup>25</sup>

Copper is mainly processed from the mineral  $\text{CuFeS}_2$ . For the oxidised minerals of copper, the state-of-the art process is first the dissolution in concentrated  $\text{H}_2\text{SO}_4$  resulting in a complex pregnant leach solution (PLS) with many contaminants, from which then Cu is recovered through the steps of solvent extraction and finally electrowinning.<sup>26</sup>

The most important deposits of zinc are also sulfides like sphalerite ( $\text{ZnS}$ ), which is mainly processed pyrometallurgically with its roasting to  $\text{ZnO}$ , followed by smelting. On the other hand, the hydrometallurgical path of  $\text{ZnO}$  requires the use of weak sulphuric acid, resulting in a complex PLS that first needs to be purified and then Zn is recovered from it by electrolysis.<sup>27</sup>

Finally, lead is mainly extracted by pyrometallurgy from sulphidic minerals like galena ( $\text{PbS}$ ). It can also be roasted, to produce  $\text{PbSO}_4$ , which is insoluble in water, whereas contaminants such as  $\text{CuSO}_4$  and  $\text{ZnSO}_4$  are soluble and so they can be easily separated.<sup>28</sup> Another path for the hydrometallurgical extraction of lead oxides is the reductive dissolution in acidic bromine and iodide solutions.<sup>29, 30</sup>

Of course, all of the above processes are not unique for each MO, with many different systems which have also been examined. Technological advancements render EoL materials increasingly complex with more components complicating separation. This chapter looks at ionometallurgical processes for the separation of metal oxides.

### **3.1.2 Aims**

This study investigates the chemical dissolution of various MOs, namely  $\text{MnO}_2$ ,  $\text{MnO}$ ,  $\text{Fe}_2\text{O}_3$ ,  $\text{Fe}_3\text{O}_4$ ,  $\text{Co}_3\text{O}_4$ ,  $\text{CoO}$ ,  $\text{NiO}$ ,  $\text{CuO}$ ,  $\text{Cu}_2\text{O}$ ,  $\text{ZnO}$  and  $\text{PbO}$  in different DESs. As it is known and proven by Pourbaix diagrams, the dissolution of MOs in aqueous systems is highly dependent on the proton activity and on the speciation on the surface of the metal oxide. Therefore, it is prudent to investigate the role of proton activity in ionic systems as DESs and observe if it is as important as in aqueous solutions, since MOs dissolution is highly dependent upon the pH of the solution.

Apart from the pH, the effect of the complexation ability of the HBD of the DES on the solubility of MOs is predicted to be significant, since speciation has a significant impact on the solubility of metal compounds. Hence, this assumption again is investigated with

the main aim to be the comparison of the effect of pH and speciation on dissolution of MOs. A second reason to use different HBDs is to study the possibility to develop selective processes for the extraction of MOs.

The rate of dissolution of MOs in DESs has not yet widely examined. Thus, kinetic studies of  $\text{MnO}_2$ ,  $\text{MnO}$ ,  $\text{Co}_3\text{O}_4$ ,  $\text{CoO}$  and  $\text{NiO}$ , which are MOs incorporated in LIBs, are studied in four systems: a) EG:ChCl, b) EG:ChCl with 0.1 M triflic acid, c) LevA:ChCl, and d) OxA:ChCl. These four systems were selected in order to investigate the difference of the effect of pH and the complexation abilities of the HBD on the rate of dissolution and to find a possible point of selectivity.

By the end of this investigation, the results of the fundamental studies of the dissolution of MOs are validated on a real EoL material. The dissolution of a synthetic mixture of LiNMC material, a mixture of  $\text{MnO}_2$ ,  $\text{Co}_3\text{O}_4$  and  $\text{NiO}$  that is widely used as active material in the cathodes of LIBs and of an industrial cathode are investigated in oxalic acid-choline chloride that showed the higher potential of selectivity.

### **3.2 Chemical dissolution of metal oxides in DESs**

In hydrometallurgy, most MO dissolution processes use mineral acids which are corrosive and need neutralisation and purification prior to their disposal. The selectivity in aqueous solutions can be relatively poor and the dissolution most of the times results in complex PLSs from where the pure metal is recovered after several steps and using various complexing agents. DESs offer a largely non-aqueous solution which can be tuneable for specific physical and chemical solvent properties using different HBDs or mixtures of HBDs, depending on the metals of interest.

Ionometallurgy has previously used for the chemical dissolution of MOs. ILs have been employed in the processing of MOs due to their promising properties such as high thermal and chemical stability, non-flammability, wide liquidus window and tunability.<sup>31-38</sup> ILs are able to provide selectivity towards targeted metals by alternating their components, however constraints related to their toxicity and their complex and costly production process prevent their industrial implementation.

The dissolution of MOs has been investigated in DESs<sup>39-44</sup> and preliminary studies by Abbott et al showed that the dissolution of MOs was higher in DESs that incorporated acidic HBDs. It has been suggested that the protons act as oxygen acceptors, breaking the

metal-oxide bonds, which probably is why acidic DESs have higher leaching rates than those without.<sup>45</sup> DESs have also been employed for dissolution of MOs from EoL products and other waste streams as spent cathodes of lithium ion batteries,<sup>46</sup> spent fluorescent lamps,<sup>47</sup> NdFeB magnets<sup>48</sup>, zinc flue dust<sup>49</sup> and zinc arc furnace dust.<sup>50</sup>

The preliminary studies have only been carried out with a limited number of DESs and metal oxides and the preliminary studies did not take account of pH or speciation. In this investigation, proton activity of the DES and the complexation abilities of the HBDs are considered for their effect on dissolution. The literature review on the dissolution of MOs in **Chapter 3.1**, shows that the pH of the system needs to be in the acidic region and that is why most solvents used are either inorganic acids as HCl, HNO<sub>3</sub> or organic acids like oxalic acid, tartaric acid, citric acid, etc. Moreover, for the higher oxidation state MOs, reductive conditions are also essential. In this chapter, the chemical dissolution of MOs in various DESs is examined.

### **3.2.1 Dissolution of metal oxides in ethylene glycol: choline chloride**

The dissolution of MOs was first examined in EG:ChCl. This DES is one of the first solvents of the Type III DESs together with Urea:ChCl.<sup>51</sup> EG:ChCl has been extensively studied due to its low viscosity and high conductivity at ambient conditions, compared with the majority of the DESs.<sup>51, 52</sup> In addition, the solubility of MOs in this DES was studied before,<sup>39</sup> so the whole process of dissolution and chemical analysis of the samples can be compared with the past reported results and verified.

The solubilities of the MOs in EG:ChCl determined within this work are presented **Table 3.2** and compared with the ones reported by Abbott et al.<sup>39</sup> in previous research, and are in good agreement for most of the MOs. Some discrepancies, especially for CuO and Cu<sub>2</sub>O, are probably due to the different chemical analysis methods or from possible differences in the particle size and crystallinity of the solid powder. The solubility of PbO was not investigated by Abbott, but a recent study by Payne et al.<sup>53</sup> reported the solubility to be  $4453 \pm 10 \text{ mg L}^{-1}$  at room temperature, which is almost double that reported in this investigation. This difference is justified from either the choice of the authors to use ICP-OES analysis, the water content of the DES, or the polymorph of PbO used, which can be either litharge (tetragonal crystal structure) or massicot (orthorhombic crystal structure). The two structures of PbO show different Pb-O bond lengths, as the tetragonal structure show a bond length of 0.232 nm and the orthorhombic 0.2358 nm, along with

differences in valence bands.<sup>54</sup> In this investigation the massicot polymorph was used, as shown in **Table 3.3**.

*Table 3.2: Gibbs energy of formation, lattice energy (expressed as U and U/x) and solubility of various MOs in EG:ChCl after 48 h at 50 °C.*

<b>Metal Oxide</b>	$\Delta G_f^{55}$ (kJ mol <sup>-1</sup> )	U <sup>56</sup> (kJ mol <sup>-1</sup> )	U/x (kJ mol <sup>-1</sup> )	Solubility (mg L <sup>-1</sup> )	Solubility (mg L <sup>-1</sup> ) by Abbott et al. <sup>39</sup>
<b>MnO<sub>2</sub></b>	-464.4	12970	12970	24 ± 2.33	0.6
<b>MnO</b>	-362.9	3745	3745	35 ± 3	12
<b>Fe<sub>2</sub>O<sub>3</sub></b>	-742.8	14774	7387	0.13 ± 0.03	0.7
<b>Fe<sub>3</sub>O<sub>4</sub></b>	-1016.1	18742	6247	0.24 ± 0.03	15
<b>Co<sub>3</sub>O<sub>4</sub></b>	-802.2	18067 <sup>57</sup>	6022	3 ± 0.56	18.6
<b>CoO</b>	-214.1	3910	3910	75 ± 11	16
<b>NiO</b>	-211.7	4012	4012	13 ± 0	9
<b>CuO</b>	-128.4	4050	4050	251 ± 16	4.6
<b>Cu<sub>2</sub>O</b>	-168.6	3189	1594	1675 ± 223	394
<b>ZnO</b>	-318.4	3971	3971	578 ± 41	469
<b>PbO</b>	-190	3433	3433	1670 ± 24	-

It is clear that EG:ChCl is a poor lixiviant for most MOs, due mostly to its neutral environment (pH of around 7)<sup>58</sup> and/or the poor complexing abilities of the EG. In this stage, it would be useful to understand why some MOs show higher or lower affinity to dissolve in such a poor solvent, without considering differences related to speciation. The speciation of the metals in EG:ChCl is mainly governed by the very high chloride content ( $\approx 4.8$  M depending on the preparation of the DES)<sup>59</sup> resulting in metal chloro complexes. The speciation of metals in EG:ChCl and the rest of the ionic systems studied in this work will be discussed later.

Thus, the main question is why some MOs dissolve more readily than others. MOs, in general, are stable compounds due to their ionic bond between the oxygen anion and the metal cation. The strength of this ionic bond is measured by the lattice energy. MOs have high lattice energies and strong ionic bonds and usually show close packed crystal structures such as the ones shown in **Table 3.3**. A highly packed crystal structure means

that the distance between the ions is small, resulting in higher lattice energy, as shown from the **Equation 3.1**.

$$U = k \times \frac{Q_1 \times Q_2}{r} \quad \text{Equation 3.1}$$

$U$  is the lattice energy,  $k$  is a proportionality constant that highly depends on the chemical environment,  $Q_1$ ,  $Q_2$  are the charges of the cation and anion, and  $r$  is the distance between the ions.

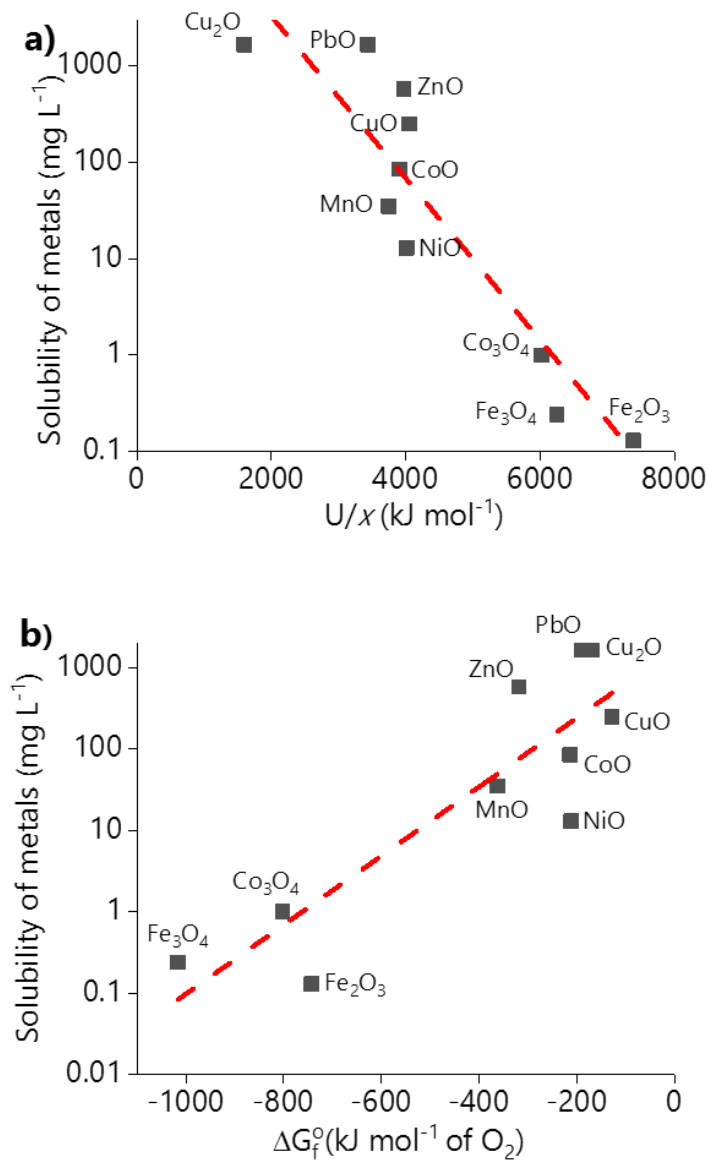


*Figure 3.1: a) Effect of lattice energy and b) effect of Gibbs energy of formation of metal oxides on their solubility in EG:ChCl. Conditions:  $T = 50\text{ }^\circ\text{C}$ ,  $t = 48\text{h}$ ,  $L:S=30$  and  $500\text{ rpm}$*

MOs that are composed of metal cations in their higher oxidation state like  $\text{MnO}_2$  ( $\text{Mn}^{4+}$ ) and  $\text{Fe}_2\text{O}_3$  ( $\text{Fe}^{3+}$ ) are expected to be more stable and difficult to dissolve, due to their higher charge (**Equation 3.1**). Also, the smaller size of the  $\text{Me}^{3+}$  ends up in higher Lewis acidity of the MO. Differences in the crystal structure (**Table 3.3**) and lattice energy will result in differences in their stability and affinity to dissolve. In **Figure 3.1a**, the solubility of MOs is correlated with the lattice energy divided by the moles of the metal ( $U/x$ ) and a general downward trend is observed, meaning that an increased lattice energy results in low solubilities.

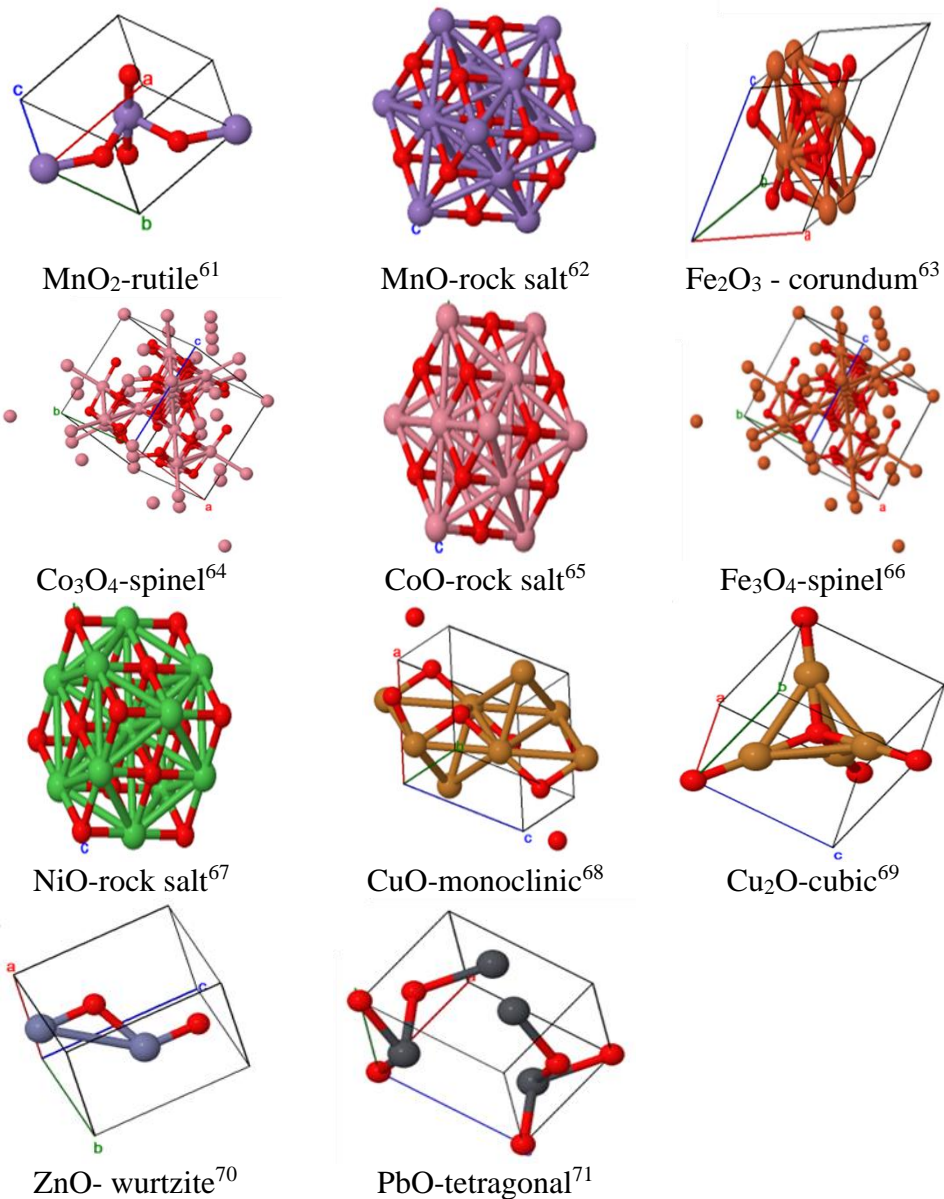
Fan et al.<sup>38</sup> investigated the solubility of REE oxides in the [Hbet][Tf<sub>2</sub>N] IL and proposed a general rule that oxides with  $U > 10000 \text{ kJ mol}^{-1}$  are insoluble, while oxides with  $U < 7000 \text{ kJ mol}^{-1}$  are soluble in the IL. Here, the same trend appears with a noticeable exception of the solubility of  $\text{MnO}_2$  that is almost 100 times higher than the  $\text{Fe}_2\text{O}_3$ ,  $\text{Fe}_3\text{O}_4$  and 10 times higher than  $\text{Co}_3\text{O}_4$ , while they all show high lattice energies. Similar exceptions have been reported by Ruck<sup>57</sup> and Chandrakumar<sup>60</sup> working with ILs, resulting in the idea that apart from the lattice energy other factors also influence the solubility, such as the crystal structure, the energy of formation of the metal oxide and the possible change in coordination number of the metal ion in the produced compound.

In addition, the Gibbs energy of formation ( $\Delta G_f^\circ$ ) is another tool to predict the solubility of MOs, because it gives information on their stability. As mentioned in Chapter 1, Ellingham diagrams are a very useful type of graphs used to predict the ease of reduction of MOs. It is known that the more negative the Gibbs energy, the more stable is the oxide. In **Table 3.2**, the Gibbs energy of formation for the MOs is shown (calculated using HSC 9) and in **Figure 3.1b** the correlation between  $\Delta G_f^\circ$  with their solubility in EG:ChCl is also presented. An upward trend is observed, meaning that the lower the energy of formation of the MOs, the higher their affinity to dissolve. Few exceptions are observed in this trend.

It is clear from both graphs, that both the Gibbs energy of formation and the lattice energy of the oxides have a significant effect on their solubility. The same patterns have been observed in aqueous solutions and with this preliminary investigation it is proven that the same trends apply in DESs.

Table 3.3: Crystal structure of the metal oxides under investigation

(red: oxygen atoms)



The solubility product constant was also calculated for the dissolution of MOs in EG:ChCl and shown in **Table 3.4**. It is apparent that the  $K_{sp}$  is very small especially for the high oxidation state MOs and the reason for that is that in EG:ChCl the low  $H^+$  activity limits its ability to act as an  $O^{2-}$  acceptor and drive the reaction forward. Similar values of  $K_{sp}$  have been reported for aqueous solutions, since the hydration energy of the water is not sufficient enough to surpass the high lattice energy of MOs.<sup>72-77</sup> Actually, for most of the oxides the  $K_{sp}$  in water is very close with the one in EG:ChCl, since the  $K_{sp}$  for MnO<sub>2</sub>, Fe<sub>2</sub>O<sub>3</sub>, Fe<sub>3</sub>O<sub>4</sub>, NiO, CuO, ZnO and PbO were found to be in the range of  $10^{-14}$ ,  $10^{-$

<sup>37</sup>,  $10^{-38}$ ,  $10^{-9}$ ,  $10^{-7}$ ,  $10^{-6}$  and  $10^{-7}$  respectively. Significant research has been conducted for the determination of the solubility of MOs in water, with many studies focusing on subcritical and supercritical water, water with different additions of lixivants and acids or bases and at different temperatures.

*Table 3.4: Calculated  $K_{sp}$  for metal oxides in EG:ChCl at 50°C*

<b>Metal oxide</b>	<b><math>K_{sp}</math></b>
<b>MnO<sub>2</sub></b>	$1.63 \times 10^{-10}$
<b>MnO</b>	$4.17 \times 10^{-7}$
<b>Fe<sub>2</sub>O<sub>3</sub></b>	$3.01 \times 10^{-28}$
<b>Fe<sub>3</sub>O<sub>4</sub></b>	$3.5 \times 10^{-38}$
<b>Co<sub>3</sub>O<sub>4</sub></b>	$2.60 \times 10^{-27}$
<b>CoO</b>	$1.37 \times 10^{-6}$
<b>NiO</b>	$5.22 \times 10^{-8}$
<b>CuO</b>	$1.57 \times 10^{-5}$
<b>Cu<sub>2</sub>O</b>	$7.61 \times 10^{-6}$
<b>ZnO</b>	$7.81 \times 10^{-5}$
<b>PbO</b>	$6.5 \times 10^{-5}$

In the next section, the investigation of the addition of protons is studied as an enhancement of MOs solubility.

### **3.2.2 Effect of pH on dissolution in ethylene glycol: choline chloride**

The effect of pH has been extensively studied in aqueous chemistry and many years of collection of thermodynamic data (e.g. Gibbs energies of formation, thermodynamic equilibrium relationships, Nernst equations) are processed and presented in Pourbaix (E vs pH) diagrams.<sup>78</sup> The Pourbaix diagrams give information about thermodynamically predominant species depending on the potential and pH of the solution. They find applications in the field of corrosion engineering and in metallurgy, as they help the prediction of soluble phases of metals and conditions of pH and potential that may provide selectivity between different metals. However, they suffer from two drawbacks; the lack of kinetic information and the assumption that pH is constant in the bulk solution and at the metal or reaction products surface. In **Figure 3.2** an example of Pourbaix diagram is given for the system of iron without any complexing agents in the system.

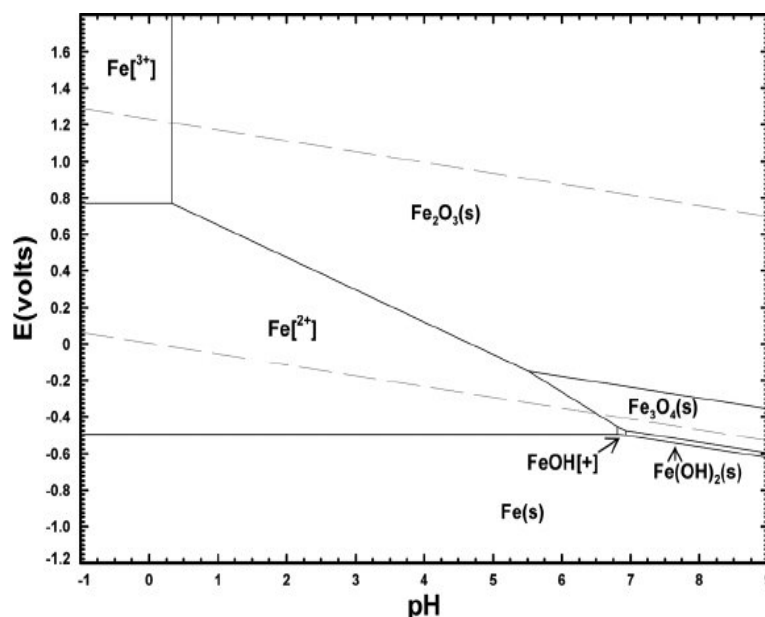


Figure 3.2: Pourbaix diagram of iron in aqueous solution without the presence of complexing agents at 25 °C. Each line represents solubility limits of 0.001 M for soluble species.<sup>79</sup>

Different information can be derived from it, for example in order to transform Fe<sub>2</sub>O<sub>3</sub> into soluble Fe<sup>3+</sup> species a very low pH of less than 1 is required or the transformation of Fe<sup>2+</sup> to Fe<sup>3+</sup> occurs at 0.77 V, which is the standard redox potential of this reaction. More detailed information about standard potentials will be given in Chapter 4.

It would be really useful to develop Pourbaix diagrams in ionic media such as DESs, in order to predict the stable phases of a metal under certain conditions of potential and proton activity. However, this is extremely difficult because of the activity of water, which in all the software packages is taken as 1, but is different in every IL or DESs. In addition, there is a lack of thermodynamic data behind the different speciation of metals in these solutions. The vast array of possible ILs or DESs make the task of collecting suitable data almost impossible.

During this investigation, the effect of pH of the DESs on the solubility of the selected MOs is evaluated. In order to examine the effect of actual pH without the presence of additional complexing agents, solutions of EG:ChCl of different pH were prepared by adding different amounts of trifluoromethanesulfonic acid (TFSA). The DES EG:ChCl resulted in poor solubilities of most MOs and also its pH has been measured to be close to neutral.<sup>58</sup> TFSA is a super acid with  $pK_a \approx -15$ , while it has very poor complexing abilities that render it the best candidate for this investigation. Alabdullah et al., has

reported that by adding  $10^{-1}$ ,  $10^{-2}$ ,  $10^{-3}$  and  $10^{-4}$  M of TFSA in EG:ChCl, resulted in solutions of pH 1, 2, 3 and 4, as TFSA completely dissociates in the DES.<sup>80</sup>

*Table 3.5: Proposed reactions of metal oxides dissolution in EG:ChCl with TFSA*

$MnO_2 + 4Cl^- + 4H^+ \rightarrow [MnCl_4]^{2-} + 2H_2O$
$MnO + 4Cl^- + 2H^+ \rightarrow [MnCl_4]^{2-} + H_2O$
$Fe_2O_3 + 4Cl^- + 6H^+ \rightarrow 2[FeCl_4]^- + 3H_2O$
$Fe_3O_4 + 12Cl^- + 8H^+ \rightarrow 3[FeCl_4]^- + 4H_2O$
$Co_3O_4 + 12Cl^- + 8H^+ \rightarrow 3[CoCl_4]^{2-} + 4H_2O$
$CoO + 4Cl^- + 2H^+ \rightarrow [CoCl_4]^{2-} + H_2O$
$NiO + 4Cl^- + 2H^+ \rightarrow [Ni(EG)_3]^{2+} + H_2O$
$CuO + 4Cl^- + 2H^+ \rightarrow [CuCl_4]^{2-} + H_2O$
$Cu_2O + 4Cl^- + 2H^+ \rightarrow [CuCl_4]^{2-} + H_2O$
$ZnO + 4Cl^- + 2H^+ \rightarrow [ZnCl_4]^{2-} + H_2O$
$PbO + 4Cl^- + 2H^+ \rightarrow [PbCl_4]^{2-} + H_2O$

In **Figure 3.3** the concentrations of the metal oxide dissolved in solutions of EG:ChCl of different acidity is shown. As it can be seen from the proposed reactions in the **Table 3.5**, not all MOs require the same amount of protons to thermodynamically dissolve. MOs with the metal in higher oxidation state require higher amounts of  $H^+$ , more specifically  $MnO_2$ ,  $Fe_2O_3$ ,  $Fe_3O_4$  and  $Co_3O_4$  require 4, 6 and 8  $H^+$  respectively for the dissolution of one mole of the respective oxide. The rest of the investigated MOs with metals in lower oxidation states require only  $2H^+$  for each mole of dissolved oxide. So, if it assumed that in the different solutions of EG:ChCl only the proton activity is influencing the dissolution of MOs, then the concentrations of dissolved MOs should be as close to the theoretical lines, constructed and shown in **Figure 3.3**, as possible. All the calculations of the theoretical and experimental concentrations of metals are presented in the Appendix (**Table 7.2**).

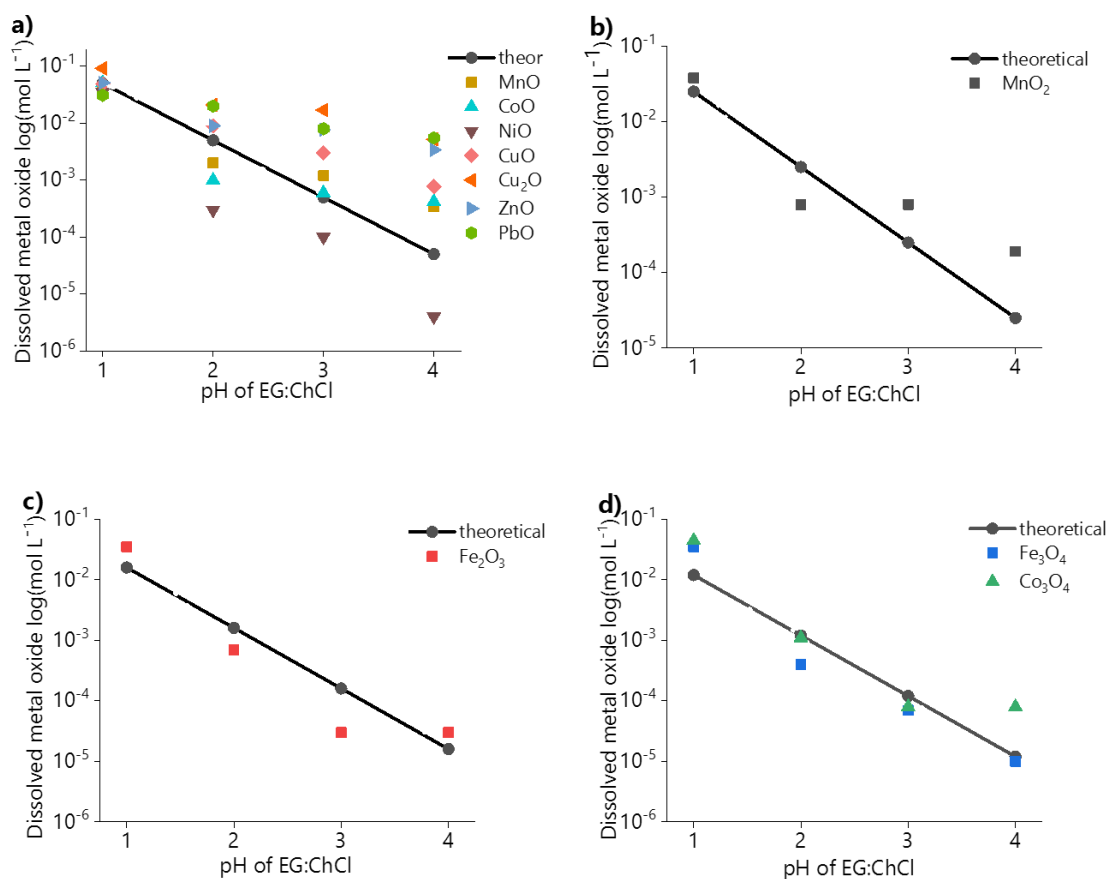
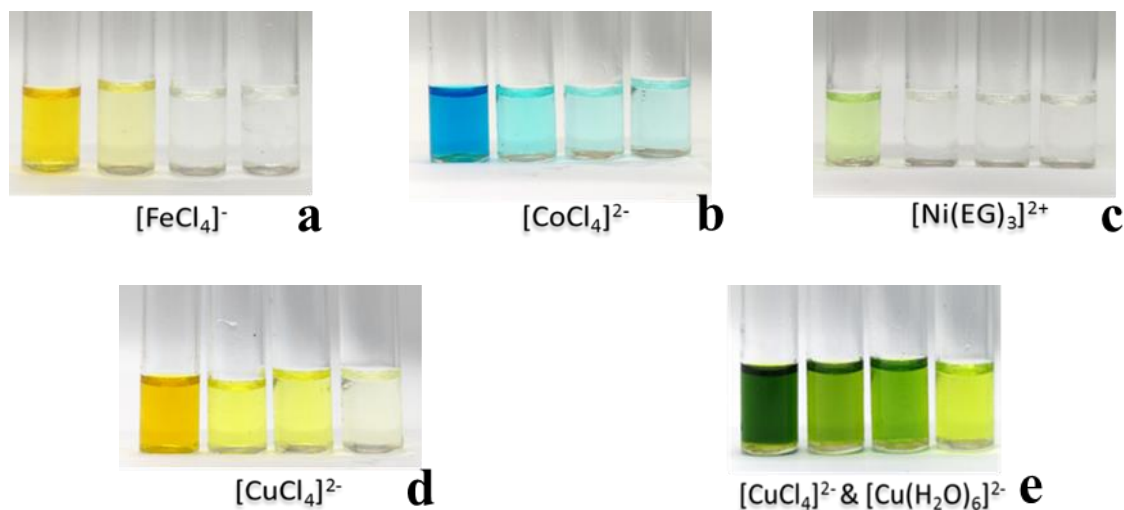


Figure 3.3: Effect of on the solubility of selected metal oxides in EG:ChCl compared to theoretical solubility (solid line) for a)  $2[H^+]$ , b)  $4[H^+]$ , c)  $6[H^+]$  and d)  $8[H^+]$  systems. Conditions:  $T = 50\text{ }^\circ\text{C}$ ,  $t = 48\text{h}$ ,  $L:S=30$  and  $500\text{ rpm}$

As expected, all oxides show a downward trend, meaning that as the pH increases the concentration of dissolved metal oxide decreases. According to Le Chatelier's principle, the higher the  $H^+$  the more the equilibrium is pushed towards metal ions in solution. The solubility of  $Fe_2O_3$ ,  $Fe_3O_4$  and  $Co_3O_4$  are close to the theoretical values, resulting in the assumption that their dissolution is highly influenced by the proton activity. On the other hand, the concentration of the dissolved  $CuO$ ,  $Cu_2O$ ,  $ZnO$  and  $PbO$  lies always above the theoretical line, which correlates well with their moderately high solubility even in pure EG:ChCl. One possible reason of their high dissolution affinity even in low acidic environment is the high concentration of  $Cl^-$  in the DES that is able to form complexes with the metals, showing that the equilibria shown in Table 3.5 are not the only ones that need to be considered.

The case of  $NiO$  is interesting because its concentration is always lower than the theoretical one, even though thermodynamically it requires the same amount of  $H^+$  as for the rest of the oxides. Except from its concentration in the most acidic solution of

EG:ChCl, which is very close to the theoretical value, for the rest of the solutions the concentration is almost 100 times less than it expected to be. One explanation can be the speciation of Ni in the solution, which as presented in **Figure 3.4** forms the complex  $[\text{Ni}(\text{EG})_3]^{2+}$ , that is different from all the rest of the oxides that show complexes with the  $\text{Cl}^-$  of the ChCl. The speciation was studied by Hartley using EXAFS measurements of  $\text{NiCl}_2 \cdot 6\text{H}_2\text{O}$  dissolved in EG:ChCl, for which the same apple green colour of solution was observed.<sup>81</sup> The resulting species means that  $\text{Ni}^{2+}$  has a preference towards the oxygen of the EG rather than the  $\text{Cl}^-$ , which could be attributed to its oxophilicity even though it is less oxophilic than Mn, Fe and Co.<sup>82</sup> It is assumed that these resulted Ni species are not favourable in mild acidic conditions and higher amounts of  $\text{H}^+$  are needed in order to react with the  $\text{O}^{2-}$  and break the bond of the oxide. In that case Ni is then free to make complexes with the HBD.



*Figure 3.4: Difference in the colour of solutions of dissolved a)  $\text{Fe}_2\text{O}_3$ , b)  $\text{Co}_3\text{O}_4$ , c)  $\text{NiO}$ , d)  $\text{CuO}$  and e)  $\text{Cu}_2\text{O}$  in solutions of EG:ChCl with TFSA and the proposed metal species. pH 1, 2, 3 and 4 from left to right.*

In these systems is very difficult to measure the equilibrium of the reactions because the activity of water is not known and it is not appropriate to assume it is unity, as in aqueous systems. Instead, in calculations of the equilibrium constants in DESs the activity of  $\text{Cl}^-$  should be unity, due to its existence in excess in the DES. This fact means that the activity of  $\text{H}^+$  is the limiting factor.

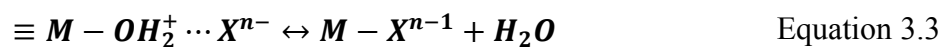
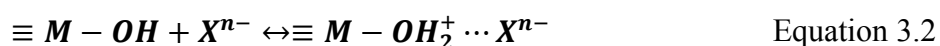
The speciation of metal chlorides in EG:ChCl was studied by Hartley using extended X-ray absorption fine structure (EXAFS) spectroscopy. In this investigation all the resulting solutions were tested with UV-vis spectroscopy and the spectra were compared with the

ones of the respective metal chlorides. Selected samples of MOs dissolved in the different solutions of EG:ChCl with TFSA are shown in **Figure 3.4**. It can be observed that the solutions of Fe<sub>2</sub>O<sub>3</sub>, Co<sub>3</sub>O<sub>4</sub>, NiO, CuO and Cu<sub>2</sub>O are coloured in the solution of pH 1, with the colour fading when pH increases, i.e. metal oxide solubility decreases. The solutions of the rest of the MOs are given in Appendix (**Figure 7.1**). The solutions of MnO<sub>2</sub>, MnO, ZnO and PbO are not presented, because they were colourless.

The UV-Vis spectra of the metals dissolved in EG:ChCl with 0.1 M TFSA is shown in Appendix (**Figure 7.3 and Figure 7.4**) and it is observed that the spectra are identical with the respective metal chlorides. So, all MOs, except from NiO, form tetrachloride complexes in solution, and this was important for this study as no complexation with the TFSA<sup>-</sup> occurred to prevent the observation of the actual effect of pH.

### 3.2.3 Ligand effect on dissolution

Another way to dissolve MOs in aqueous systems, apart from the protonation of O<sup>2-</sup>, is the surface complexation. Organic acids such as oxalic acid, citric acid, lactic acid, etc. have proven to be efficient lixivants for MOs, due to formation of complexes with the metals. Actually, as presented in **Equation 3.2** and **Equation 3.3**, the complexation by organic anions require two steps. First the anion is chemisorbed on the active OH sites of the hydrated metal. Then if the metal-ligand anion complexes are more stable than the metal-OH complex, the anion is substituting the OH sites and the reaction is pushed to the forward direction.<sup>78</sup> Organic acids with higher chelating efficiencies, like oxalic acid, result in higher dissolution yields.



The use of organic acids for the dissolution of MOs in DESs has been reported before. Abbott et al. observed that the dissolution of selected MOs in a malonic acid-ChCl resulted in higher leaching efficiencies than in EG:ChCl and urea:ChCl, and they assumed that the high proton activity in the malonic acid DES was the main reason for the dissolution of MOs.<sup>39</sup> Here it is assumed that apart from the proton activity in the DES, the choice of the chelating agent and the speciation play a crucial role on the dissolution as well.

In order to investigate what is effect of the carboxylic acid addition on the dissolution of MOs, the system EG:ChCl with addition of lactic acid was examined. Alabdullah has

measured the pH of the LacA:ChCl to be in the range of 2-3, with methods already published.<sup>58</sup> At this stage, LacA ( $1.3 \text{ mol L}^{-1}$ ) was added to EG:ChCl until the pH of the solution reached the value of 3. The choice of LacA was taken because it is a chelating agent, proven to be efficient in extracting metals from MOs in both aqueous solutions and DESs,<sup>48, 83, 84</sup> but in the same time is a weaker organic acid than oxalic acid for example, that would produce metal precipitates. In that way, it is easier to understand the effect of the carboxylic acid on the dissolution affinity of MOs.

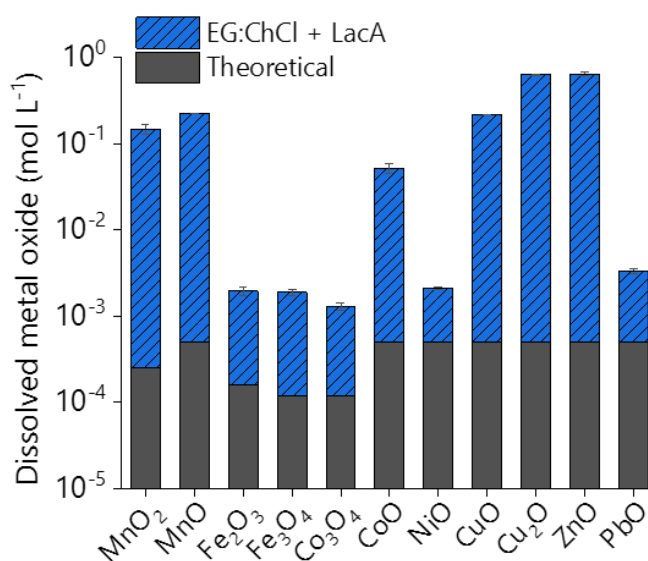


*Figure 3.5: Difference of the effect of the addition of LacA in EG:ChCl compared with proton activity.*

The solution of EG:ChCl after the addition of  $1.3 \text{ mol L}^{-1}$  LacA had a pH of 3. If LacA contributed only by adding protons in the solution, then the concentration of the dissolved MOs should be close to the theoretical concentration calculated by the contribution of only  $\text{H}^+$ , as in the previous section. However, from **Figure 3.5**, it is clear that the concentration for all MOs is higher than the theoretical values. More specifically, for  $\text{Cu}_2\text{O}$  and  $\text{ZnO}$  the concentration was  $>1000$  times higher and for  $\text{MnO}_2$ ,  $\text{MnO}$  and  $\text{CuO}$   $> 400$  times higher due to the contribution of LacA. These very high concentrations of Cu and Zn oxides may be justified from the stability of their respective Cu and Zn lactate complexes. The stability has been measured in aqueous solutions and it was reported that Pb forms the most stable complexes followed by Zn and then Cu with lactic acid compared with the rest of the divalent metals.<sup>85</sup> It would be expected that PbO would

also show much higher dissolution, but due to the formation of solid lead precipitates, the concentration was only 5 times higher.

In order to visually compare the difference of the surface complexation with just proton activity in DESs, the concentration of the dissolved metal oxide in EG:ChCl with  $10^{-3}$  M TFSA and EG:ChCl with LacA are compared in **Figure 3.6**.

In both systems the pH is the same. It is clear that the stronger ability of the lactate anion to form complexes with the metals compared with the very weak ligand abilities of TFSA, results in higher concentrations of dissolved MOs. This shows the importance of the surface complexation as method of dissolution of MOs in DESs.

The speciation of the metals in both EG:ChCl with LacA and EG:ChCl with  $10^{-3}$  M TFSA resulted in solutions of the same colour and speciation as for the metal chlorides solutions in EG:ChCl, which as discussed before formed tetrachloro complexes, except for Ni. It is assumed that as for aqueous solutions, when the proton binds the oxygen on the oxide surface, these hydrated intermediate species are active sites for the adsorption of the lactate anion, which then binds the metal ion. This mechanism contributes to the higher yield of reaction as it drives it to the forward direction. Once the metal-lactate anion species are diffused into the bulk solution, the  $\text{Cl}^-$  substitutes the lactate anion due to its much higher activity in solution. Actually, the concentration of  $\text{Cl}^-$  is almost 5 times higher than the concentration of the lactic acid in this case.

Having proved that the addition of a ligand in the DES improves the dissolution of MOs, the next step was to investigate the employment of different HBDs. The HBDs used were representative of the most widely used compounds in DESs, such as carboxylic acids, alcohols and amine, and more specifically the DES investigated were mixtures of ChCl with oxalic acid dihydrate, lactic acid, levulinic acid, acetic acid, ethylene glycol, glycerol and urea with molar ratios already reported in the experimental section (Chapter 2).

At this stage, two hypotheses were tested. First, the employment of acidic DESs will result in higher dissolution of MOs, with the dissolution to be influenced by the  $\text{pK}_a$  of the carboxylic acids and their proton activity. Secondly, discrepancies from general trends will be reported for MOs resulted from specific interactions of metals with the HBD.

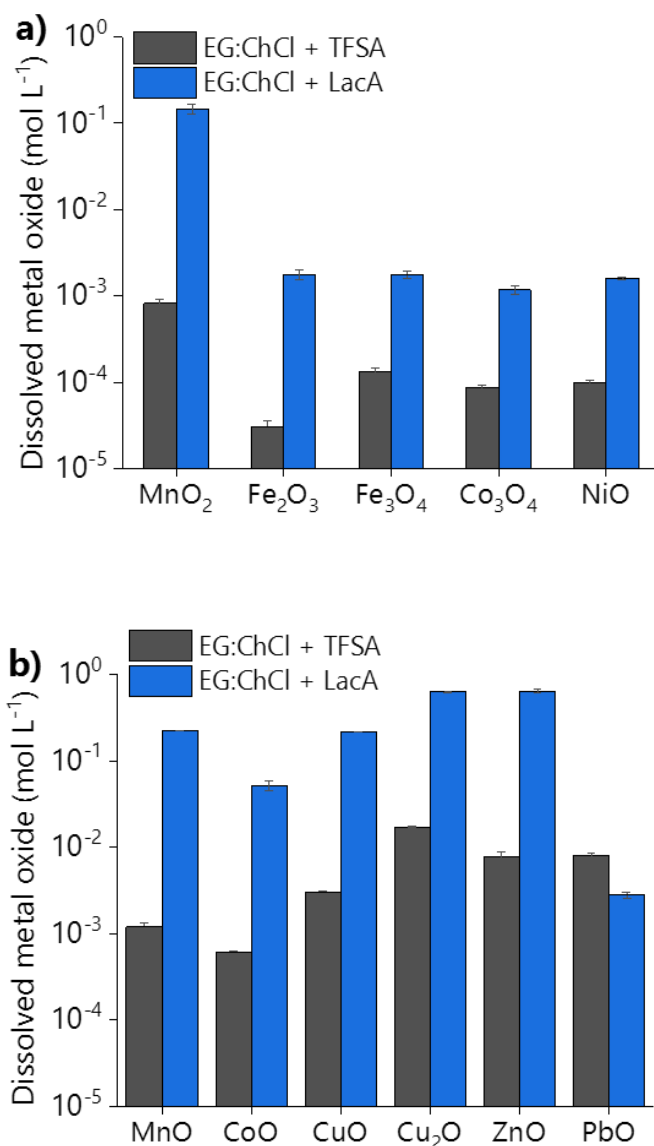


Figure 3.6: Difference in metal oxide concentration in EG:ChCl with  $10^{-3}M$  TFSA and EG:ChCl with lactic acid. Both solutions have the same pH of 3. a) poorly soluble and b) soluble metal oxides. Conditions:  $T = 50\text{ }^{\circ}C$ ,  $t = 48h$ ,  $L:S=30$  and  $500\text{ rpm}$

In **Figure 3.7**, the concentrations of the dissolved MOs are compared against the different DESs. The graphs are split into two parts, the left part represents the effect of the  $pK_a$  and acidity of the carboxylic acids, while the right side represents the MOs concentration in neutral to basic DESs with weak ligands. The first conclusion that can be drawn is that with the exception of PbO, all other MOs dissolve better in the acidic DESs, as expected. PbO showed lower concentrations due to precipitation of  $0.650\text{ g L}^{-1}$ ,  $0.932\text{ g L}^{-1}$  and  $0.887\text{ g L}^{-1}$  of Pb in the precipitates during the dissolution in OxA:ChCl, LacA:ChCl and AceA:ChCl, respectively.

For the analysis of the left part of the graphs, first, it is important to consider the difference in the  $pK_a$  of the acids used. The  $pK_a$  of OxA, LacA, LevA and AcA in aqueous solutions is 1.25, 3.86, 4.32 and 4.75, respectively. Alabdullah has characterised the  $pK_a$  of many carboxylic acids in EG:ChCl and drew the conclusion that acids in DESs are a little less acidic due to their buffer behaviour resulting from the high concentration of basic  $Cl^-$  and so the  $pK_a$  values are 0.5 units higher than in water.<sup>80</sup> However, even though they have slightly higher values in the DES media, their difference would be the same. So, it would be expected that the dissolution of MOs would follow the trend OxA:ChCl > LacA:ChCl > LevA:ChCl > AceA:ChCl.

For OxA:ChCl this is the case for only the higher oxidation state MOs, because OxA is not only highly acidic but is also a good reducing agent, resulting in the easier dissolution of the higher oxidation state oxides as they are reduced in solution.<sup>86</sup> The rest of the MOs showed lower dissolution in OxA:ChCl than the other carboxylic acids, due to their precipitation.

The trend that was mentioned before (LacA:ChCl > LevA:ChCl > AceA:ChCl) is followed for the rest of the acidic DESs and especially for the dissolution of the higher oxidation state MOs. Exemptions include NiO and MnO, which follow the opposite trend and show the higher dissolution affinity in AceA:ChCl, and CoO and ZnO, which show their highest dissolution in LevA:ChCl. ZnO showed precipitation in both LacA:ChCl and AceA:ChCl with 0.9 and 0.8 g L<sup>-1</sup> Zn to be present in the precipitates, respectively.

For the right side of the graph, the dissolution of MOs in EG:ChCl, Gly:ChCl and Urea:ChCl is very low because these DESs do not contain free protons to react with  $O^{2-}$  and also include weak ligands, thus as expected their ability to dissolve MOs is low. Alabdullah has measured the pH of EG:ChCl (5.93-6.89), Gly:ChCl (6.97-7.5) and urea:ChCl (8.31-8.91) using spectroscopy and electrochemistry.<sup>58</sup> The exceptions of CuO, Cu<sub>2</sub>O, ZnO and PbO that showed relatively high dissolution in urea:ChCl is justified from the formation of metal-urea species, as it will be discussed later.

Returning to the analysis of the dissolution in OxA:ChCl, samples of the precipitates are shown in Appendix (**Figure 7.2**) and compared with precipitates resulting from dissolution in aqueous oxalic acid solution. The analysis of the precipitates showed that 1.5, 0.8, 0.43, 1.3, 2.2, 2.7 and 0.65 g L<sup>-1</sup> of metals precipitated during the dissolution of MnO<sub>2</sub>, MnO, CoO, CuO, Cu<sub>2</sub>O, ZnO and PbO respectively, most probably in the form of

oxalates if compared with the precipitates resulting from the dissolution in aqueous oxalic acid.

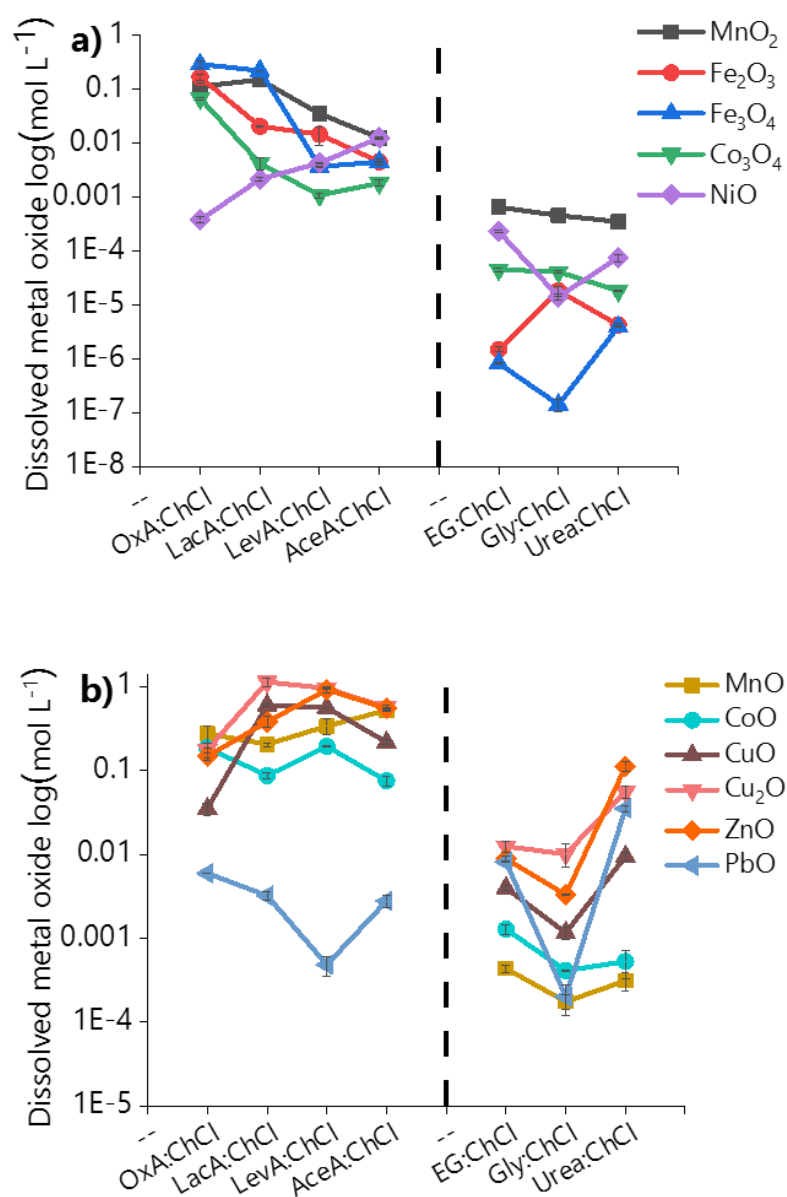


Figure 3.7: Effect of different HBDs on the concentration of dissolved a) poorly soluble and b) soluble metal oxides. Conditions:  $T = 50\text{ }^{\circ}\text{C}$ ,  $t = 48\text{h}$ ,  $L:S=30$  and  $500\text{ rpm}$

The dissolution of MOs was also investigated in aqueous solution of oxalic acid with concentration of 1.8M oxalic acid, mimicking the concentration of the DES. The concentrations of the dissolved MOs in the aqueous oxalic acid solution and in OxA:ChCl are compared in **Table 3.6**.

Table 3.6: Comparison of dissolution of metal oxides in OxA:ChCl and aqueous solution of 1.8 M oxalic acid. (errors indicate one standard deviation ( $\sigma$ ))

Metal oxide	Dissolved metal in OxA:ChCl (mg L <sup>-1</sup> )	Dissolved metal in aqueous oxalic acid 1.8M (mg L <sup>-1</sup> )
<b>MnO<sub>2</sub></b>	6123 ± 900	715.1 ± 17
<b>MnO</b>	16648 ± 200	650 ± 4
<b>Fe<sub>2</sub>O<sub>3</sub></b>	18638 ± 2700	8582 ± 1200
<b>Fe<sub>3</sub>O<sub>4</sub></b>	48185 ± 6600	10500 ± 600
<b>Co<sub>3</sub>O<sub>4</sub></b>	11099 ± 500	52 ± 4
<b>CoO</b>	9658 ± 1900	34.9 ± 5
<b>NiO</b>	21.8 ± 3	13.9 ± 0.3
<b>CuO</b>	2215 ± 360	26.5 ± 2
<b>Cu<sub>2</sub>O</b>	22447 ± 4400	88.3 ± 2
<b>ZnO</b>	96540 ± 260	46.0 ± 9
<b>PbO</b>	1228 ± 2	123 ± 9

It is clear that all MOs show higher dissolution in the DES, compared with the aqueous oxalic acid solution, except for NiO which is poorly soluble in both solvents. In the aqueous solution, precipitation of metals occurred, resulting in very low metal content in solution, with the exception of Fe<sub>2</sub>O<sub>3</sub> and Fe<sub>3</sub>O<sub>4</sub> which did not precipitate, but even so the concentration was higher for both of them in the DES. In the DES, even though precipitation of metals was observed, the metal content in solution was still high. It is assumed that this occurs due to the high Cl<sup>-</sup> content, which forms complexes with the metals that remain in solution. After a specific concentration of metal in solution the metal forms species with the oxalate anion, which then precipitate.

The same mechanism is assumed to happen with the other DESs that showed precipitation, and this is confirmed from the UV-Vis studies of the solutions of MOs that showed that most of them end up in tetrachloride complexes in solution. The UV-Vis spectra and the solutions of MOs are presented in Appendix (**Figure 7.3 and Figure 7.4**) and in **Figure 3.8** where the examples of Co<sub>3</sub>O<sub>4</sub> and NiO are shown.

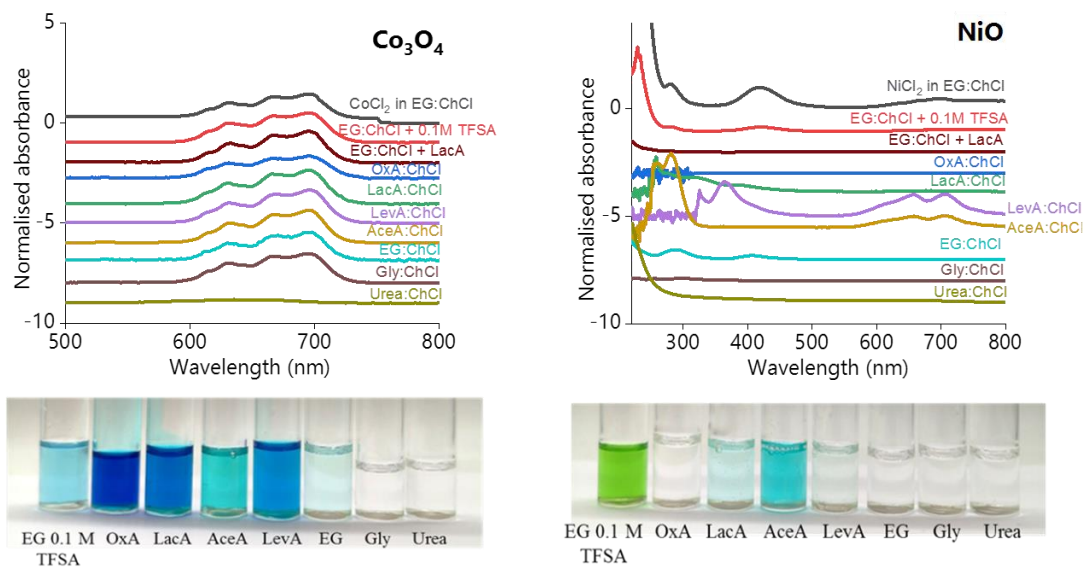


Figure 3.8: UV-Vis spectra of  $\text{Co}_3\text{O}_4$  and  $\text{NiO}$  and comparison of their coloured solutions upon dissolution in different DESs.

The choice of these MOs was made in order to show that some MOs show a dependency on the HBD and some result in the same speciation regardless of the HBD used. One example of non-dependency on the HBD is  $\text{Co}_3\text{O}_4$  as shown in **Figure 3.8**. It is clear that the dissolution of  $\text{Co}_3\text{O}_4$  resulted in blue solutions and with spectra consisting of the same peaks at 633 nm, 667 nm and 692 nm which are associated with  $[\text{CoCl}_4]^{2-}$  species in all DESs,<sup>81</sup> except urea:ChCl where the concentration was so low that the spectra is flat. The same behaviour was observed for CoO.

$\text{Fe}_2\text{O}_3$  and  $\text{Fe}_3\text{O}_4$  show the same peaks at 240 nm, 316 nm and 363 nm for all the acidic DESs, whose spectra are identical with the solution of  $\text{FeCl}_3$  in EG:ChCl, which forms  $[\text{FeCl}_4]^{2-}$  species.<sup>81</sup> In the rest of DESs, the spectra of both oxides are flat lines due to the very low Fe concentration.

$\text{PbO}$  also shows the same peak in the ultraviolet region at around 272 nm in all DESs, which is associated with  $[\text{PbCl}_4]^{2-}$ , similarly to that observed in aqueous HCl solutions.<sup>87, 88</sup> A solvatochromic shift to longer wavelengths is observed with increasing pH, as for urea:ChCl the peak is at 272 nm and goes to 276 nm for EG:ChCl and 280 for LevA:ChCl.

$\text{MnO}$  and  $\text{MnO}_2$  both show for all the acidic DESs a pattern of weak *d-d* transitions peaks with the main ones at 357 nm, 432 nm and 447 nm. Similar peaks have been reported in aqueous solutions for the solutions of  $\text{MnCl}_2$ .<sup>89</sup> Together with the EXAFS studies of

Hartley et al.,<sup>81</sup> it is concluded that Mn shows the same speciation in all DESs which is  $[\text{MnCl}_4]^{2-}$ .

In contrast, there are MOs whose speciation is influenced by the HBD. In **Figure 3.8** the solutions of NiO together with the associated UV-Vis spectra are presented. As mentioned before, NiO in EG:ChCl results in  $[\text{Ni}(\text{EG})_3]^{2+}$  complex, which has a characteristic apple green associated colour and the main absorption peak is at 424 nm. However, in LevA:ChCl and AceA:ChCl the colour of the solution is blue and the peak at 424 nm was not observed, while peaks at 657 nm and 708 nm were observed. It has been reported, previously, that Ni forms thermochromic complexes, meaning that the speciation changes depending on the temperature and Abbott et al. showed that in EG:ChCl the  $[\text{Ni}(\text{EG})_3]^{2+}$  species are gradually transformed to  $[\text{NiCl}_4]^{2-}$  with an increase in temperature.<sup>90</sup> The blue coloured solutions of Ni at 120 °C showed the same peaks as the ones reported at LevA: ChCl and AceA: ChCl, concluding that in these DESs Ni is complexed with  $\text{Cl}^-$ .

CuO and  $\text{Cu}_2\text{O}$  also show difference in speciation, as in urea: ChCl the spectra and colour of solution are different than in the other DESs. The same peak at around 406 nm which is ascribed to the  $[\text{CuCl}_4]^{2-}$  species is present in all the DESs, except urea: ChCl. However, not all solutions show the same yellow colour associated with  $[\text{CuCl}_4]^{2-}$ , and the solutions LacA:ChCl, LevA:ChCl and AceA:ChCl show green colour, which has been reported before to be a mixture of  $[\text{CuCl}_4]^{2-}$  and water by Binnemans et al.<sup>91</sup> Using EXAFS they reported that a green solution means that the water content is increased and water molecules are able to enter the coordination sphere of the  $\text{Cu}^{2+}$  along with  $\text{Cl}^-$ . It is assumed that due to the very high amount of  $\text{Cu}^{2+}$  dissolved in these DESs, the water content is increased in the solution and so can form complexes with the  $\text{Cu}^{2+}$ . In addition, it could be assumed that the green colour may arise from a mixed chloride/HBD coordination that would have the same O-coordination effects on colour. In urea:ChCl; however, they show a different pale blue colour and a peak at 265 nm. There is previous report by Rimsza et al. mentioning that  $[\text{Cu}(\text{urea})]^{2+}$  is a favourable complex in this DES.<sup>92</sup>

So, it appears that the high  $\text{Cl}^-$  content of the DESs influences the speciation of the metals, with a few exceptions, while the acidity of the solvent and the complexing abilities of the HBD affect the dissolution affinity of the MOs. Speciation is a very critical aspect of any

dissolution process because the coordination of the metal and the lattice energy of the formed species influence its solubility and stability in the solvent. Moreover, different species of the same metal may have very different reactivities when considering electrowinning processes for example, thus the speciation of the metal is very critical and needs to be controlled. At this stage, it is worth noticing some examples of selectivity, which was the second hypothesis to be tested. The interactions of the metals with the HBDs, either favourable or unfavourable, may lead to systems where the DES is selective towards some metals over others.

As it appears in **Figure 3.7**, the dissolution of PbO in the acidic DESs is low, due to its precipitation, while Fe<sub>2</sub>O<sub>3</sub>, Fe<sub>3</sub>O<sub>4</sub>, CuO, Cu<sub>2</sub>O and ZnO show very high concentrations. This is a possible beneficial system for the separation of Pb from the rest of metals, which are coexisting in low metal containing industrial residues as the fayalitic slag of the copper production. The opposite system occurs for urea:ChCl, where PbO and ZnO show high concentrations, while Fe<sub>2</sub>O<sub>3</sub> and Fe<sub>3</sub>O<sub>4</sub> have negligible dissolution. Actually urea:ChCl has been employed before by Abbott for the selective dissolution of Pb and Zn from arc furnace dust.<sup>50</sup> Another example of selectivity is the dissolution of Co<sub>3</sub>O<sub>4</sub>, MnO<sub>2</sub> and NiO in OxA:ChCl, which resulted in very high concentrations of Co and Mn and negligible dissolution of Ni. This system is also very important when considering recycling of cathode materials of LIBs, which many of them incorporate mixtures of MnO<sub>2</sub>, Co<sub>3</sub>O<sub>4</sub> and NiO, as will be discussed later.

### 3.3 Dissolution kinetics

All of the above experiments were conducted for a fixed time of 48 h, to ensure that the systems were at equilibrium, but practical dissolution experiments require fast dissolution so kinetic experiments were carried out on MnO<sub>2</sub>, MnO, Co<sub>3</sub>O<sub>4</sub>, CoO and NiO in four different DESs. These MOs were chosen due to their relatively high economic value compared with the rest of MOs investigated, and they are also widely used as cathode materials in LIBs, whose recycling is considered critical. As for the DESs, four systems were investigated, EG:ChCl, EG:ChCl with 0.1 M TFSA, LevA:ChCl and OxA:ChCl.

The dissolution of the MOs was first investigated in EG:ChCl. This DES achieves very low dissolution of MOs, due to the absence of acidic activity and because EG is a weak ligand. However, a possible problem could be the slow kinetics of dissolution of MOs in DESs and so very long times are required for extraction of metals to be achieved.

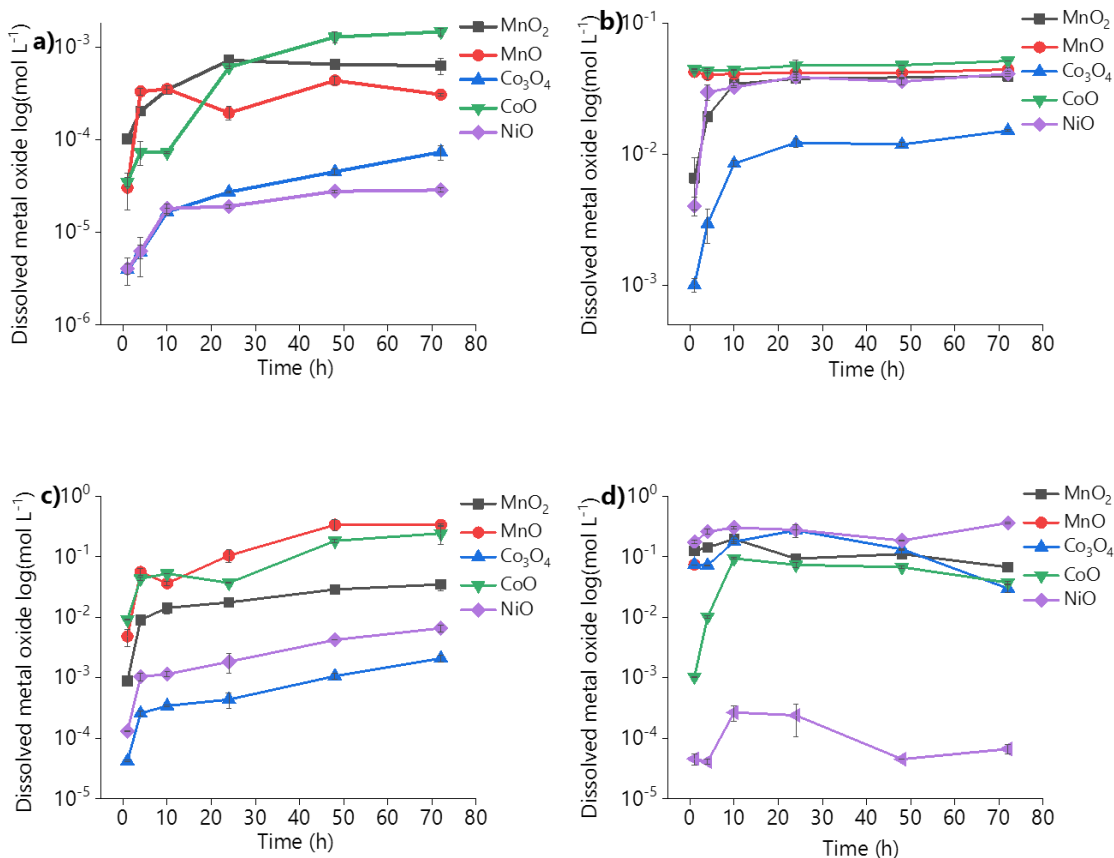


Figure 3.9: Kinetics of the dissolution of selected metal oxides in a) EG:ChCl, b) EG:ChCl with the addition of  $10^{-1}$  M TFSA, c) LevA:ChCl, d) OxA:ChCl. Conditions:  $T = 50$  °C,  $L:S=30$  and 500 rpm

As observed in **Figure 3.9a**, this is not the case, as the concentration of all MOs seems to get stable after 48h, except for  $\text{Co}_3\text{O}_4$  which slowly increases even after 48h. Some MOs show faster dissolution with the highest concentration to be reported at the 4<sup>th</sup> h and 10<sup>th</sup> h for MnO and NiO, respectively. Thus, the dissolution in EG:ChCl is not low due to slow rate of dissolution, but for all the thermodynamic reasons mentioned before.

The EG:ChCl with 0.1 M TFSA was studied in order to examine how the high proton activity influences the kinetics. It is apparent that the dissolution is very fast, especially for MnO and CoO that are reaching the highest concentration in the 1<sup>st</sup> h of dissolution.  $\text{MnO}_2$ ,  $\text{Co}_3\text{O}_4$  and NiO require 10 h to reach their solubility level. This may be justified from the different crystal structure and lattice energy of the first oxides and the different dissolution mechanism for NiO, which was discussed before. It is also obvious for all MOs that once they consumed all the required amount of  $\text{H}^+$  (**Table 3.5**) their dissolution came to an end, because without  $\text{H}^+$  in EG:ChCl the reaction of dissolution cannot be pushed forward.

The system of LevA:ChCl was used as an example of DES that in its media MOs are dissolved through both protonation and surface complexation. However, LevA is a poorer ligand than OxA, so it would help to examine the kinetics in a medium that incorporates intermediate levels of proton activity and complexation. The dissolution seems to be slower, as for all MOs the concentration slowly increases until the 72<sup>nd</sup> h. The same long hours of dissolution have been observed for a mixture of Y and Eu oxide (Y<sub>2</sub>O<sub>3</sub>:Eu),<sup>93</sup> as it will be discussed later in Chapter 5. A reason for the longer hours of dissolution is the higher viscosity of LevA:ChCl compared with EG:ChCl with 0.1M TFSA that may influence negatively the diffusion due to poorer mass transport.

Last but not least, the dissolution in OxA:ChCl shows a rather more complex behaviour. The highest concentration of all MOs is reached between 5 to 10 h of dissolution. However, the concentration of all dissolved MOs starts to slowly decrease and especially for MnO, due to precipitation of oxalate complexes. The difference in dissolution affinity of NiO compared to the rest of MOs is also very clearly observed, which opens an alternative route of selective extraction of Co and Mn from LIBs.

### **3.4 Dissolution of cathode materials of LIBs**

#### **3.4.1 Importance of LIBs recycling**

The decarbonisation of transport necessitates a wholesale conversion from the internal combustion engine to devices based on electrical storage of electricity produced from renewable resources. LIBs are seen as the cornerstone in the revolution of electric vehicles. LIBs are superseding other secondary batteries such as nickel metal hydrides (NiMH) due to their superior energy density. Many LIBs have a reliance on critical metals such as Co and Ni and the projected expansion in the electric vehicle fleet means that a circular economy in these metals is essential to enable sufficient supply.<sup>94</sup>

Up until now, both pyrometallurgy and hydrometallurgy have been employed for the recycling of metals from LIBs. As far as pyrometallurgy is concerned, Umicore has industrially implemented a method for recycling metals from both LIBs and NiMH batteries since 2006.<sup>15, 16</sup> The process of Umicore involves the feed of spent batteries together with coke, slag formers (MgO, CaO) and some amount of MOs in a vertical shaft furnace, in which there are three thermal zones; 1) the preheating zone where the electrolyte evaporates (< 300 °C) , 2) the pyrolyzing zone where the plastic caps and casing are melted (≈700 °C) and 3) the smelting zone at which, with the aid of oxygen

enriched air, the targeted metals Co, Ni and Cu are forming a metal alloy and the impurities such as Fe and Ca are gathered in the slag phase (1200-1450 °C). One disadvantage of this process is that Al and Li show a higher affinity to the slag phase and because their recovery from this phase is not efficient in terms of the energy consumption and economy of the process, they do not return to the supply chain. Umicore's process is viable only when the feed comprises of high Co and Ni content waste and also depends a lot on the price of these metals.<sup>16</sup> This process only operates economically because a significant gate fee is applied to process spent batteries. Pyrometallurgical processes also need to be able to handle polymetallic and more complex materials which will be used in the next generation of batteries.<sup>95</sup>

In contrast, hydrometallurgical approaches are known for their ability to be selective towards different metals and several variants have been applied on semi-commercial scale (1000-5000 t/a). A general flowsheet of hydrometallurgical processing of LIBs is presented in **Figure 3.10**.

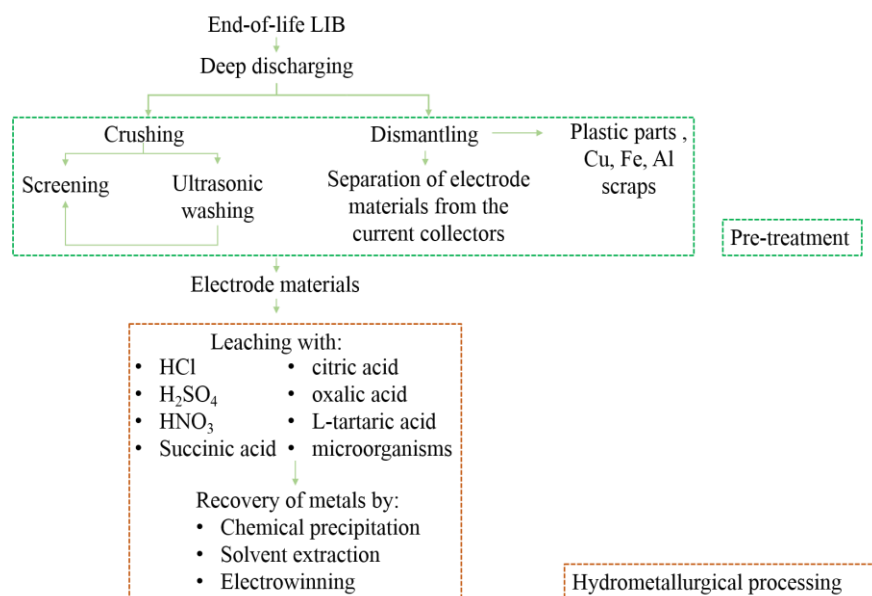


*Figure 3.10: General flowsheet of hydrometallurgical recycling of LIBs, adapted from ref<sup>96</sup>*

Different leaching agents have been investigated, the most common of which are HCl, HNO<sub>3</sub>, and H<sub>2</sub>SO<sub>4</sub>. The addition of H<sub>2</sub>O<sub>2</sub> has been proved to increase significantly the yield of Co, because it promotes the reduction of Co<sup>3+</sup> to Co<sup>2+</sup> and thus the easier breakage of the bond of Co with oxygen. In some reports, prior to acidic leaching, NaOH or LiOH are employed for the dissolution of Al, in order to reduce the contaminants of the final products.<sup>97, 98</sup> In addition to inorganic acids, organic acids like citric acid, maleic acid,

ascorbic acid, L-tartaric acid and oxalic acid have also proven to be successful in extracting metals from spent LIBs. The leaching of metals from spent LIBs has been reviewed many times.<sup>99-102</sup> Recovery of metals from the PLS is obtained by the use of different approaches. Precipitation using NaOH contributes to the separation of contaminants like Cu, Al, Fe and Mn by forming metal hydroxides.<sup>103, 104</sup> Solvent extraction is also widely used, especially for the separation of Co / Ni and Co / Li, with PC88A and Cyanex 272 to have the highest extraction efficiencies for Co.<sup>105</sup> Electrowinning is another method, in which either whole compound of LiCoO<sub>2</sub> can be deposited on Ni plate, or individual elements can be recovered in high purity.<sup>106</sup> Bioleaching also has been considered with the use of bacteria, but this route is in its infancy and will not be discussed further in this thesis.

The recycling of metals or other components from spent batteries in ILs or DESs is not a widely studied field. A few research projects in the literature have been published, such as the use of EG:ChCl for the leaching of Co, Ni and Mn from NMC cathode materials.<sup>46</sup> Also, the IL 1-Butyl-3-methyl-imidazolium-tetrafluoroborate has been employed for the dissolution of the PVDF material that holds the cathode electrode material to the current collector.<sup>107</sup>

There is also the approach of the recycling of the different LIBs components, with the use only of separation methods. During this process, spent discharged batteries are fed to a container together with CO<sub>2</sub>, under high temperature and pressure conditions. The first step includes the recovery of the electrolyte with the aid of CO<sub>2</sub>, which can then be recycled to new batteries. Afterwards, the different metals are separated by physicochemical properties such as density and conductivity. This technique is beneficial due to the ability to recycle all the components of the cell, but its major issue relies on the quality of the recycled components and the levels of efficiency they will provide to the new batteries.<sup>108</sup>

The studies of the MOs dissolution in the previous sections of this chapter, showed that selective extraction of metals is achievable in DESs during the extraction process, which is a very important advantage compared to the aqueous solutions. This selectivity is achieved via the metal speciation and whether the formed species are soluble or if they precipitate out of solution. As mentioned before, OxA:ChCl showed the ability of rapidly dissolving very high concentrations of MnO<sub>2</sub>, MnO, Co<sub>3</sub>O<sub>4</sub> and CoO, while NiO

dissolution is very small. More specifically, the concentration of dissolved  $\text{MnO}_2$  and  $\text{Co}_3\text{O}_4$  were almost 300 and 200 times higher than the concentration of NiO.

Hence, the question developed is if this selectivity in extraction of Co and Mn can be achieved from a mixture of them and from a real EoL product. The dissolution in OxA:ChCl was examined for a synthetic mixture of LiNMC and for a commercial cathode sheet. The mixed oxide LiNMC is one of the most widely used, due to the high specific energy and lifespan, but the use of Co increases its cost.<sup>109</sup>

### 3.4.2 Characterisation of cathode materials

Prior to the dissolution process, the characterisation of both the LiNMC powder and the cathode sheet took place. Both materials were digested in an *aqua regia* bath at ambient conditions for 30 minutes. Almost instantly the solutions turned to green due to the dissolution of the metals. After 10 minutes, the LiNMC powder was fully dissolved. The same happened for the cathode material, which was fully delaminated and the active material, along with the Al foil were digested. The remaining solid that was not dissolved in *aqua regia*, which was assumed to be a mixture of the conductive additive and the binder, was weighed and it accounted for 5.8 wt.% of the cathode.

The PLS after the digestion of the LiNMC powder and the cathode were analyzed, and the chemical composition is presented in **Table 3.7**. The results provided information about the molar ratio of the metals, with the synthetic powder consisting of  $\text{Ni}_{0.3}\text{Mn}_{0.4}\text{Co}_{0.3}$ , while the active material of the cathode sheet consists of  $\text{Ni}_{0.4}\text{Mn}_{0.3}\text{Co}_{0.2}$ .

*Table 3.7: Metal content of the cathode*

<b>Metal</b>	<b>Wt.% of the LiNMC powder</b>	<b>Wt.% of the cathode sheet</b>
Al	-	$12.6 \pm 1.3$
Li	$6 \pm 0.85$	$7.34 \pm 0.9$
Co	$17.5 \pm 0.81$	$13.3 \pm 1.6$
Ni	$16 \pm 0.6$	$26 \pm 3.3$
Mn	$19.8 \pm 0.82$	$15 \pm 2.1$
Total	60	74

The surface of the cathodic sheet was also analyzed under microscope and in **Figure 3.11** the morphology of the cathode under 5000x magnification is presented. The cathode,

most of the times, includes the active material along with small amount of binder that holds it to the current collector and conductive additives.

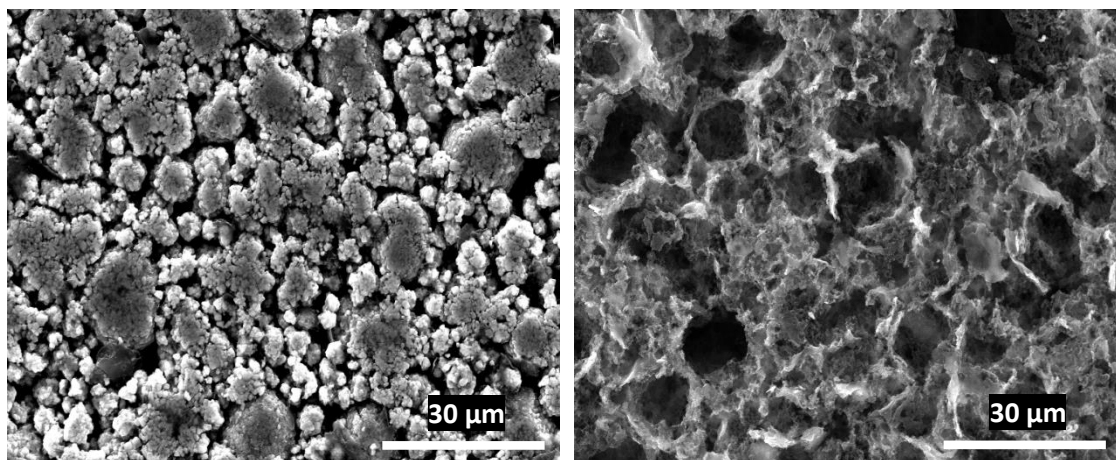


*Figure 3.11: Morphology of the initial cathode (left) and cathode after digestion in aqua regia (right) using scanning electron microscopy (x5000)*

In the cathode small particles of the active material are present, which in some cases have been aggregated into larger particles due to their mixing with the binder. The particle size of the MOs is on average  $0.6 \mu\text{m}$  in diameter. EDAX analysis showed the presence of Ni, Mn, Co, F, O, C and negligible amounts of Al, as presented in **Table 3.8**. The EDAX analysis provided supportive information on which molar ratio the metals are present in the active material.

According to the **Table 3.8**, the active material consists of:  $\text{Ni}_{0.4}\text{Mn}_{0.3}\text{Co}_{0.2}$ , which agrees with the prior chemical analysis. Elemental mapping of the scan area, presented in Appendix (**Figure 7.5**), showed that all the elements are evenly distributed across the surface, with carbon to show some spots of higher concentration.

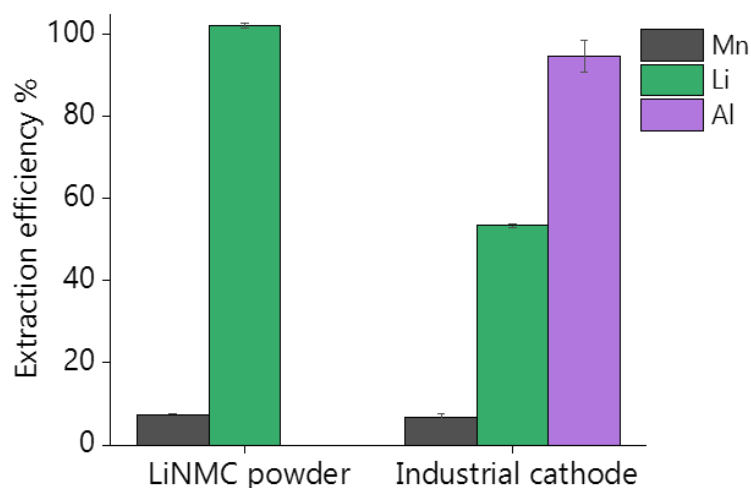
The remaining solid after the digestion in *aqua regia* was also examined under microscope and shown in **Figure 3.11**. The EDAX analysis showed that it consisted mainly of C, F and  $\text{O}_2$  and negligible amount of Al, as presented in **Table 3.8**. The existence of F and C concludes that polyvinylidene difluoride (PVDF) was employed as binder, material that is widely used in the industrial manufacture of LIBs. The C results from the presence of carbon black that is mixed with PVDF, functioning as a conducting additive. The surface of the remaining solid is covered with evenly distributed holes that the leached metals left behind, which if compared with the morphology of the initial cathode, show the same sizes.

Table 3.8: EDAX analysis of the initial cathode and remaining solid after digestion in aqua regia.

Element	Initial Cathode	Remaining solid
	Wt. %	Wt. %
C	21.59	63.6
F	3.80	29.9
O	26.34	4.7
Al	0.22	1.3
Ni	21.92	-
Mn	13.80	-
Co	11.98	-
<b>Total</b>	100	100

### 3.4.3 Dissolution of the cathode materials in OxA:ChCl

After characterization of the materials, both the dissolution of the synthetic powder and the industrial cathode were first investigated in an aqueous oxalic acid solution 1.8 M, as it was crucial to observe the behaviour of the aqueous oxalic acid solution, because there are occasions that the pure HBDs behave in a very similar manner to the DES, as will be discussed in Chapter 5. In **Figure 3.12** the extraction efficiency of the NMC powder and the industrial cathode are presented. The extraction efficiency of Co and Ni were negligible, while that of Mn reaches 7 % from both materials. The dissolution of the synthetic powder led to the recovery of  $\approx 70$  % of Co, Ni and Mn in the mixed precipitate, while no precipitation of metals occurred from the dissolution of the cathode. In the aqueous solutions the resulted species of Mn, Co and Ni will be of course different compared to the DES. The very low solubility of Co, Ni and Mn oxalates in aqueous systems leads to their precipitation. In addition, it seems that Li and Al remain in solution, with 100 % Li to be extracted from the NMC powder and 50 % of Li and 100 % of Al from the cathode. Since Li oxalate is highly insoluble in water, it appears that Li forms hydrated species. The solubility of LiOH in water is high of around  $138 \text{ g L}^{-1}$  at  $60 \text{ }^\circ\text{C}$ .<sup>110</sup> This system is selective and beneficial for Li and Al. The fact also that no metals are recovered from the cathodic sheet, renders the examination of this DES to be highly interesting.



*Figure 3.12: Extraction efficiency of metals from both the LiNMC synthetic powder and the industrial cathode in aqueous 1.8 M oxalic acid. Conditions: Time=24 h, Temperature=80 °C, L:S=30 and 500 rpm*

In the next part, the DES is examined for its ability to extract metals from the two different materials using the same conditions for the dissolution process. First, the parameter of the temperature was examined due to its importance for an enhanced mass transport of ions, especially in a rather viscous solvent as OxA:ChCl (35 Cp at 40°C). It is reported that upon heating, the viscosity of OxA:ChCl is significantly decreased.<sup>111</sup> **Figure 3.13a** and **Figure 3.13b** show the effect of the temperature on the dissolution of LiNMC powder and the cathode sheet after 24 h.

It is clear that for both materials, increased temperature of 80 °C is required for the full extraction of Mn and 90 % extraction of Co and a little less of Al from the industrial cathode, while the extraction of Li seems to remain rather stable at 20 %. On the other hand, the extraction efficiency of Ni is negligible for all different temperatures for both materials, validating the previous preliminary results of solubilities in OxA:ChCl.

The influence of temperature on recycling of metals from LIBs was mentioned in another study by Ajayan et al.,<sup>46</sup> in which the recycling of LiCoO<sub>2</sub> material was investigated in EG:ChCl. It was reported that high temperature conditions were crucial for the extraction of Co and Li, as they investigated temperatures up to 220 °C. However, such high temperatures need to be avoided when employing carboxylic based DESs, due to the esterification between the alcohol of the ChCl and the carboxyl group of the HBD.<sup>112</sup>

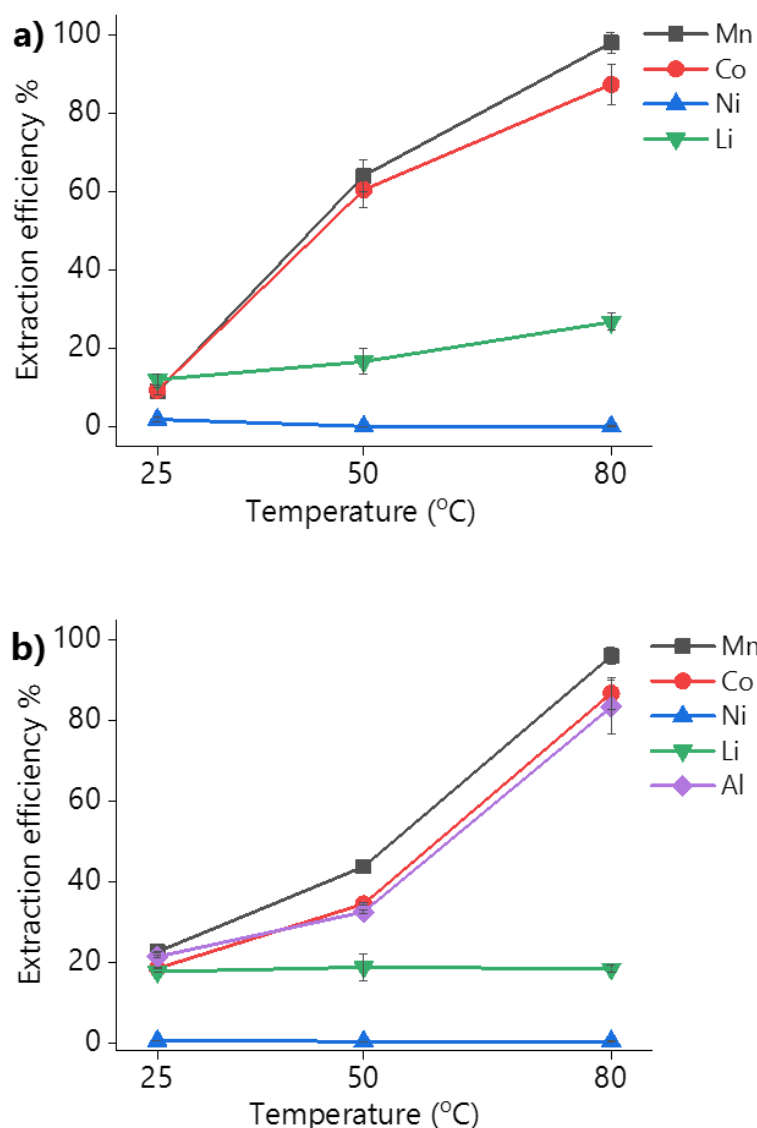


*Figure 3.13: Effect of temperature on the dissolution of a) LiNMC synthetic powder and b) industrial cathode sheet in OxA:ChCl. Conditions: Time=24 h, L:S=30 and 500 rpm (for a) and no stirring (for b)*

Rodriguez has reported the esterification reaction between the carboxylic acid and the alcohol group of the choline and mentioned that a high temperature results in increased yield of the esterification reaction.<sup>112</sup> In fact, it was mentioned that upon formation of OxA:ChCl 10 mol % of choline is esterified, which increases to 29 mol % if heated for 2 h at 80 °C. Nonetheless, for an industrial implementation of such a system for the recycling of cathode materials, a more stable cation would be required. At this stage, the investigation in OxA:ChCl will follow, as this is a preliminary investigation for the recycling of Co and Mn from cathode materials.

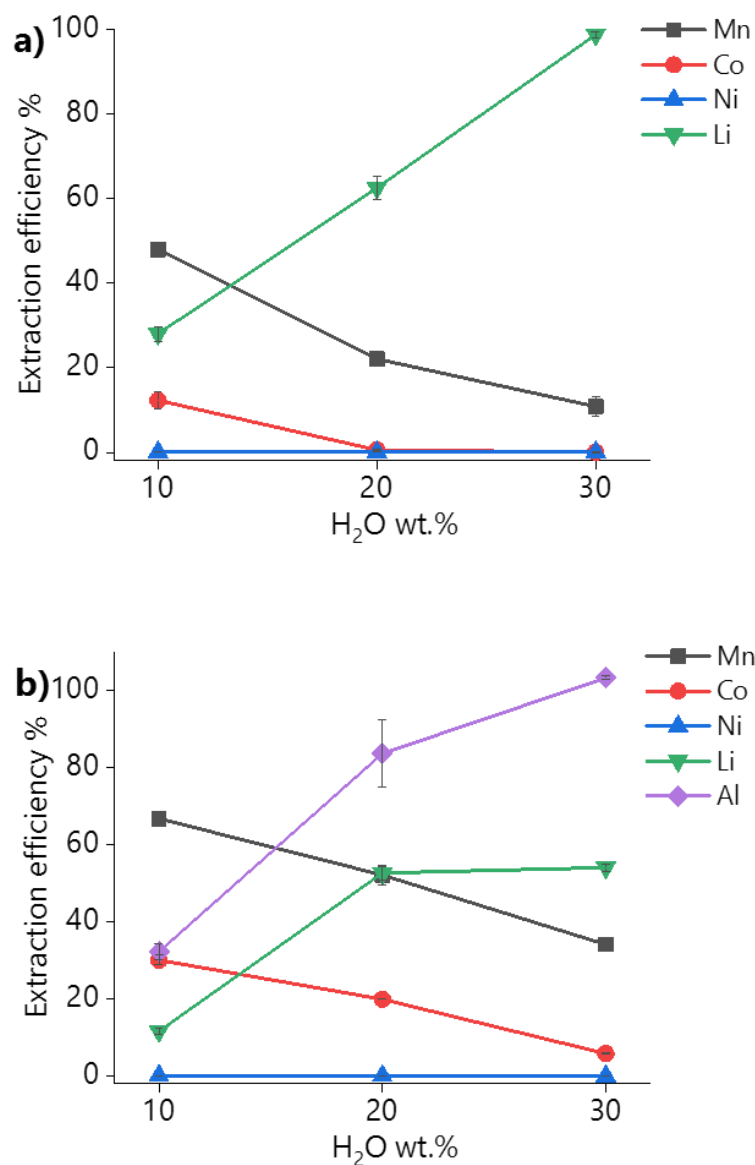


Figure 3.14: Effect of H<sub>2</sub>O wt.% in OxA:ChCl on the extraction efficiency of a) LiNMC synthetic powder and b) industrial cathode sheet. Conditions: Temperature=80 °C, Time=24 h, L:S=30 and 500 rpm.

A way to tackle the problem of esterification and high viscosity of DESs, is to add water to the DES, which will decrease the yield of the esterification and the viscosity. The addition of water needs to be moderate, since studies have shown that 40 wt.% of water transforms the DES into an aqueous solution with dissolved components of the DESs.<sup>113</sup> This then will lead to changes in metal ion speciation, since in the DES around 4.2 M of Cl<sup>-</sup> and in aqueous solutions 55.6 mol L<sup>-1</sup> of water, thus in an increase amount of water the metals from the cathode materials either would not dissolve or would precipitate as oxalates since the activity of Cl<sup>-</sup> would be much lower. Different amounts of water content

(10, 20 and 30 wt.%) in the DES were tested, to investigate the effect on the extraction efficiency and if the addition of water will result in differences in selectivity.

The results are presented in **Figure 3.14a** and **b**. Both materials show very similar behaviour. First, it is observed that the extraction of Ni is unaffected by the addition of water, while Li extraction increased to 100 % when 30 wt.% of water was added from the powder and 60 % from the cathode sheet. Interestingly, the extraction efficiency of Co and Mn declined with the addition of water, due to their precipitation of metals as oxalate complexes, with a significant decrease in solubility observed for Co compared to Mn. The maximum recovery of Mn, Co and Ni in the precipitates was recorded at the OxA:ChCl with 30 wt.% addition of water and it was at the level of 15 %, 25 % and 26% respectively. This is an example of how the coordination environment can alter the speciation and hence the solubility and selectivity of the system. From these experiments, it was observed that Mn, Co and Ni behave similarly upon addition of water in the DES, which might be beneficial for a recycling process because later the mixed metal oxalate can be calcined at 950 °C back to their mixed oxide form.<sup>47</sup>

Next, the kinetics of metal extraction were studied. The previous reported results showed that the dissolution in OxA:ChCl was quite fast, with very high concentrations of Mn and Co to be obtained in 5 h. In **Figure 3.15a** and **b**, the kinetic investigation of the dissolution of the LiNMC in pure OxA:ChCl and OxA:ChCl with 20 wt.% water is shown. It would be rational to test the 30 wt.% of water rather than 20 wt.%, because higher selectivity of Li was achieved. However, the choice over 20 wt.% was taken due to the fact that part of choline would be esterified, producing water as a by-product, and the fact previously mentioned that after the 40 wt.% of water the DES is no longer an ionic medium but an aqueous one.

Significant differences are observed when OxA:ChCl and the mixture with water are used. Without addition of water, almost total digestion of Co and Mn is observed and almost no Ni is dissolved and with the maximum selectivity to be observed at the 5<sup>th</sup> h of dissolution. A separation process could be envisaged whereby NMC was dissolved in OxA:ChCl enabling separation of Ni. The addition of water would enable the Co to precipitate and leaving Mn in solution. This is a supportive fact of the hypothesis that by tuning the DES selectivity in the recycling process is achievable.

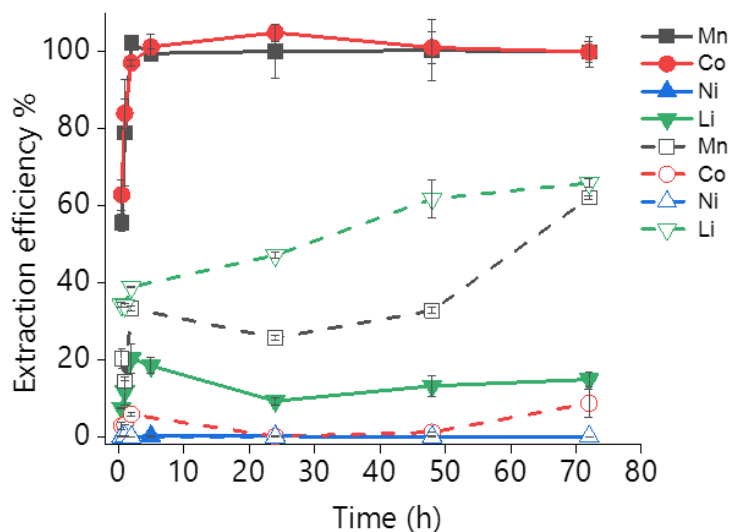


Figure 3.15: Effect of time on the extraction efficiency of LiNMC synthetic powder in OxA:ChCl (solid) and OxA:ChCl with 20 wt.% H<sub>2</sub>O (dashed). Conditions: Temperature=80 °C, L:S=30 and 500 rpm

The kinetics of the industrial cathode were also investigated under both static and stirred conditions. As was observed for the LiNMC, Ni remained insoluble and Li extraction remained poor, regardless of leaching conditions, whilst the other elements were strongly influenced by temperature and stirring rate. The kinetics of the dissolution of the cathode in OxA:ChCl under stirred and static conditions at 80 °C are presented in **Figure 3.16**.

Ni and Li are behaving the same way under both conditions as used for the LiNMC powder. Full extraction of Mn from the cathode material occurs after 24 h under static conditions and after 48 h under stirring conditions, while Co only has a maximum extraction efficiency of 92 % after 48 h under static conditions, but is fully extracted at the same time under stirring conditions. Last but not least, the extraction efficiency of Al reaches 100 % after 48 h of dissolution for both systems. Compared to the LiNMC powder, the dissolution is slower possibly due to the difference in the surface area, since the metals need to be dissolved from very fine particles exposing their hole surface to the solvent in the case of the powder and from the surface of the sheet not exposing the whole area and the also from the decreased mass transport during the static conditions.

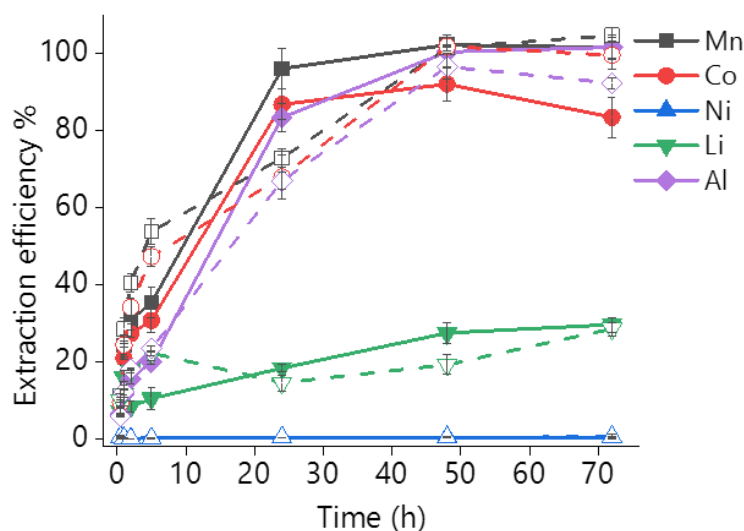
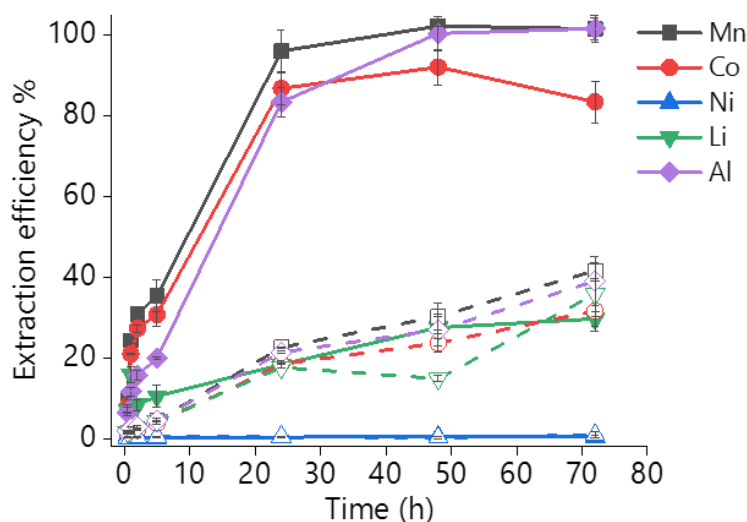


Figure 3.16: Effect of time on the extraction efficiency of the industrial cathode in OxA:ChCl under static (solid) and stirred conditions (dashed). Conditions: Temperature=80 °C, L:S=30

At this stage it would be interesting to understand how the OxA:ChCl attacks the surface of the cathode, with one assumption being that the Al foil is digested first, rapidly delaminating the cathode, or it attacks the MO particles on the surface of the cathode. For that reason, the kinetic studies of the cathode dissolution were investigated also at lower temperatures, in order to slow the rate of dissolution and under static conditions. **Figure 3.17** compares the extraction of metals from the cathode 25 and 80 °C.

As expected, the rate of dissolution at 80°C is much higher than at ambient conditions, with Mn, Co and Al reaching an extraction efficiency of 40, 30 and 40 % respectively, after 72 h at 25 °C. What is interesting is that for both systems the rate of dissolution of Mn, Co and Al is very similar, meaning that the solvent does not show a preferential behaviour over a specific metal. In Appendix (**Figure 7.6** and **7.7**) the images of the cathodes after certain times of dissolution at the two different temperatures are shown. It appears that OxA:ChCl attacks the edges of the cathode, from where the dissolution starts, but not because the dissolution of Al is favoured, but due to the faults and cracks existing at the edges, increasing the surface area and favouring the reaction of dissolution. The fact that the dissolution starts from faults at the surface and the reaction is not even for all the cathode's surface, is supported also from the microscope image of the cathode after 30 mins of dissolution at 25 °C, presented in **Figure 7.8**. It is shown that the area A, which resembles the bulk surface of the cathode has high amounts of Mn, Co and Ni, while as

it gets closer to the points C and D the amount of Mn and Co decreases because they have been digested from these points. The SEM image shown in **Figure 7.8** shows a starting point of dissolution close to the edge of the cathode, **Figure 7.9** shows also some points on the bulk surface that have started to expose the Al foil, due to the metals being digested. A pre-treatment step for the formation of artificial cracks on the surface of the sheet would be beneficial for the kinetics.



*Figure 3.17: Comparison of the rate of extraction of metals from the commercial cathode in OxA:ChCl at 25 °C (dashed) and 80 °C (solid). Conditions: L:S=30 and no stirring*

The dissolution of the cathode was also investigated using ultrasound assisted dissolution in OxA:ChCl to increase the rate of dissolution of the metals. Ultrasound assisted processes have not been widely investigated in DESs. **Figure 3.18**, shows the extraction efficiency of the cathode using an ultrasound assisted process. It is apparent that the ultrasound indeed assisted the rate of dissolution, as the extraction efficiency of Co and Mn reach almost 5 % extraction in the 1<sup>st</sup> minute of dissolution, compared to 10 % extraction after 30 minutes under stirring conditions at 80 °C. After 15 minutes the extraction efficiency of Mn and Co reached 30 %, with Al and Li to reach lower efficiencies in the level of 20 %. The extraction of Ni was negligible in this system as well. The cathodes after ultrasound dissolution are shown in Appendix (**Figure 7.10**). They have a rather different surface than the ones resulted from silent dissolution, with the appearance of some crater-like holes from where the dissolution initiates. So, during

ultrasound dissolution the solvent locally attacks the surface at the cracks or faults on the surface, as mentioned previously for the normal dissolution as well.

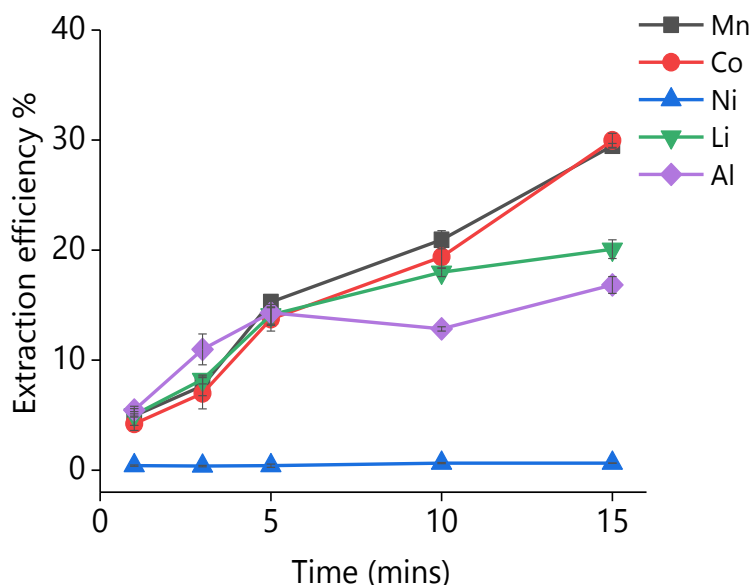


Figure 3.18: Extraction efficiency of metals from the industrial cathode using ultrasound assisted dissolution in OxA:ChCl.

The ultrasound extraction was investigated only for 15 minutes, because during the dissolution heating of the solution occurred with the temperature increasing from room temperature to 55, 62, 70, 87 and 100 °C after 1, 3, 5, 10 and 15 minutes, respectively. The high viscosity of the DES together with the limited water content rendered the ultrasound dissolution not to be as effective as it could be in an aqueous solution. The same issue has been reported in another ultrasound assisted project relating to copper redox kinetics in EG:ChCl, where it was reported that the limiting factor of the kinetics in the ultrasound process was the viscosity of the DES.<sup>114</sup> In aqueous systems, ultrasound assisted processes have focused mainly for the separation of the active material from the Al foil,<sup>115</sup> with less research on the actual assistance on the process of extraction of metals.<sup>116, 117</sup> In general, the aqueous dissolution processes are rather fast due to the employment of very acidic lixivants such as sulfuric acid coupled with H<sub>2</sub>O<sub>2</sub>. The use of ultrasonic dissolution is justified when milder solvents are employed for the enhancement of the kinetics of dissolution.

Depending on the targeted metal and metal compound, different selective processes have been shown just from the investigation of one DES. Alternating properties such as water content of the solvent can target the selectivity of the process towards specific metals. Whilst selecting the solvent, the upcoming process of metal recovery also needs to be

considered. Recovery can either be with a precipitating agent, e.g. oxalic acid, or with solvent extraction to an aqueous layer and then precipitation back with oxalic acid. Actually, the addition of water was shown to act as a precipitating agent for Co and Mn, a fact that may lead to a green process of recycling of all active materials and Al from the cathode.

### 3.5 Conclusions

Concluding, this chapter investigated the employment of DESs as an alternative pathway for the extraction of metals from their respective MOs. The solubility of MOs was investigated first in EG:ChCl, which consists of a weakly coordinating ligand and has a neutral pH. It was observed that the solubility of MOs was very low, with the exception of Cu<sub>2</sub>O, ZnO and PbO that showed higher levels of dissolution than the rest of MOs. In general MOs showed a dependency and the same trend observed in aqueous solutions of lowering dissolution affinity when the lattice energy and the enthalpy of formation is higher and vice versa. The solubility product of MOs was also calculated, and the values were in the same range as in for pure water solutions.

Next the dissolution of MOs was studied in EG:ChCl with different amounts of triflic acid that resulted in solutions of pH 1, 2, 3 and 4. As expected, the dissolution of MOs was highly dependent on the acidic activity. CuO, Cu<sub>2</sub>O, ZnO and PbO showed higher concentrations than the theoretical calculated for the amount of H<sup>+</sup> in solution, most likely due to contributions from the high Cl<sup>-</sup> content. On the other hand, NiO seemed to dissolve less than theoretically expected for the less acidic solutions and one explanation could be the speciation of Ni in solution, as it formed complexes with the EG, counter to the rest of MOs which formed tetrachloro complexes. The concentration of the rest of the dissolved MOs seemed to be close to the theoretical ones, showing the dependency of the dissolution on the proton activity.

Subsequently, the dissolution of MOs was investigated in a solution of EG:ChCl with lactic acid that had a pH of 3, and the concentrations were compared with the solutions of EG:ChCl with triflic acid of the same pH. The concentration in the EG:ChCl with lactic acid was also compared with the theoretical expected concentration if the dissolution was only dependent on the proton activity, and it was observed that for all MOs the dissolution was much higher due to the contribution of lactic acid as a ligand. It was also concluded that once the protons of the solution are attached on the oxide, they form intermediate species

that can act as active sites for the attachment of the ligand. The Me-L then detaches from the surface of the metal oxide and once it reaches the bulk solution then the metal preferentially makes complexes with the  $\text{Cl}^-$ , due to its very high activity in the DES.

After showing the effect of the surface complexation on the dissolution of MOs, the employment of different HBDs was followed. The alcohol based DESs resulted in very low dissolution of MOs, while the Urea:ChCl system showed greater concentrations even though its proton activity is less than the alcohol based DESs. This was justified from the ligand abilities of the urea to make surface complexes that detach the metal from the MO. For CuO, Cu<sub>2</sub>O and ZnO also the species formed in solution were metal-urea complexes. The carboxylic based DESs resulted in the higher concentrations of dissolved MOs with ones having a lower pKa to be more effective lixivants. Oxalic acid based DES was expected to show the higher concentrations, however this was not the case due to the precipitation of metals resulted from the strong interaction of the metal with the oxalic acid. An interesting result observed was the selectivity of oxalic acid towards Co and Mn over Ni, that could be beneficial in a process of extracting metals from active materials of LIBs.

The rate of dissolution is also a very crucial parameter, that is why it was examined in EG:ChCl, EG:ChCl with 0.1 M triflic acid, LevA:ChCl and OxA:ChCl. It was concluded that in EG:ChCl the rate of dissolution is fast meaning that thermodynamics prevent the dissolution of MOs in this DES and not the kinetics. The dissolution in the acidic EG:ChCl showed that the rate is very fast, with the dissolution stopping when all the  $\text{H}^+$  has been consumed. Longer time is required in order to reach the solubility levels in LevA:ChCl. For OxA:ChCl a more complex behaviour exists due to the precipitation of metals, with the rate of dissolution to be relatively high.

The dissolution of a synthetic mixture of LiNMC and of an industrially manufactured cathode were tested in OxA:ChCl. The result of selectivity was validated in both these materials with Ni dissolution to be negligible in all systems tested. The effect of temperature and water content on the dissolution were investigated. Interestingly, the change in water content resulted in change in the solubility of the metal ion species and hence the selectivity of the system. A higher water content helped the precipitation of Co and Mn and the fully extraction of Li and Al. In terms of kinetics, 5h and 24 h are needed for the full extraction of Co and Mn from the powder and the cathode sheet, respectively.

It was also concluded that OxA:ChCl attacks both the edges of the cathode sheet but also attacks the surface locally where cracks or faults are existing, without showing a preference on the dissolution of Al or the MO particles. The ultrasound assisted dissolution was also investigated for the industrial cathode, for which indeed increased the rate of dissolution. However, the high viscosity and the low water content of the DES render the ultrasonic processes not as efficient and may result in the decomposition of the DES due to its extreme heating after longer hours of dissolution.

### 3.6 References

1. Burns, R. G.; Burns, V. M., The mineralogy and crystal chemistry of deep-sea manganese nodules, a polymetallic resource of the twenty-first century. *Philosophical Transactions of the Royal Society of London. Series A, Mathematical and Physical Sciences* **1977**, 286 (1336), 283-301.
2. Reddy, T.; Linden, D., *Linden's Handbook of Batteries*. McGraw-hill New York: **2011**; Vol. 4.
3. Scrosati, B.; Abraham, K.; van Schalkwijk, W. A.; Hassoun, J., *Lithium Batteries: Advanced Technologies and Applications*. John Wiley & Sons, Inc: **2013**; Vol. 58.
4. Zhang, W.; Cheng, C. Y., Manganese metallurgy review. Part I: Leaching of ores/secondary materials and recovery of electrolytic/chemical manganese dioxide. *Hydrometallurgy* **2007**, 89 (3-4), 137-159.
5. Miao, L.; Wang, J.; Zhang, P., Review on manganese dioxide for catalytic oxidation of airborne formaldehyde. *Applied Surface Science* **2019**, 466, 441-453.
6. Ali, A.; Zafar, H.; Zia, M.; ul Haq, I.; Phull, A. R.; Ali, J. S.; Hussain, A., Synthesis, characterization, applications, and challenges of iron oxide nanoparticles. *Nanotechnology, Science and Applications* **2016**, 9, 49-67.
7. Yuan, C.; Wu, H. B.; Xie, Y.; Lou, X. W., Mixed transition-metal oxides: design, synthesis, and energy-related applications. *Angewandte Chemie International Edition* **2014**, 53 (6), 1488-1504.
8. Tijsseling, L.; Dehaine, Q.; Rollinson, G.; Glass, H., Flotation of mixed oxide sulfide copper-cobalt minerals using xanthate, dithiophosphate, thiocarbamate and blended collectors. *Minerals Engineering* **2019**, 138, 246-256.
9. Xia, X.; Tu, J.; Mai, Y.; Chen, R.; Wang, X.; Gu, C.; Zhao, X., Graphene sheet/porous NiO hybrid film for supercapacitor applications. *Chemistry–A European Journal* **2011**, 17 (39), 10898-10905.
10. Danjumma, S. G.; Abubakar, Y.; Suleiman, S., Nickel Oxide (NiO) Devices and Applications: A Review. *International Journal of Engineering Research & Technology*, **2019**, 8 (4), 461-467.
11. Zhang, Q.; Zhang, K.; Xu, D.; Yang, G.; Huang, H.; Nie, F.; Liu, C.; Yang, S., CuO nanostructures: synthesis, characterization, growth mechanisms, fundamental properties, and applications. *Progress in Materials Science* **2014**, 60, 208-337.

12. Yu, X.; Marks, T. J.; Facchetti, A., Metal oxides for optoelectronic applications. *Nature Materials* **2016**, *15* (4), 383-396.
13. Kołodziejczak-Radzimska, A.; Jesionowski, T., Zinc oxide-from synthesis to application: a review. *Materials* **2014**, *7* (4), 2833-2881.
14. Karami, H.; Karimi, M. A.; Haghdar, S.; Sadeghi, A.; Mir-Ghasemi, R.; Mahdi-Khani, S., Synthesis of lead oxide nanoparticles by sonochemical method and its application as cathode and anode of lead-acid batteries. *Materials Chemistry and Physics* **2008**, *108* (2-3), 337-344.
15. <https://csm.unicore.com/en/recycling/battery-recycling/our-recycling-process/>. (accessed 12/09/2019).
16. Cheret, D.; Santen, S. Battery recycling. U.S. Patent No. 7,169,206. 30 Jan., **2007**.
17. Vu, H.; Jandova, J.; Lisa, K.; Vranka, F., Leaching of manganese deep ocean nodules in FeSO<sub>4</sub>-H<sub>2</sub>SO<sub>4</sub>-H<sub>2</sub>O solutions. *Hydrometallurgy* **2005**, *77* (1-2), 147-153.
18. Norman, L. D.; Kirby, R. C., *Review of Major Proposed Processes for Recovering Manganese from United States Resources (in Three Parts): 1. Pyrometallurgical Processes*. US Bureau of Mines: **1962**; Vol. 1.
19. Taxiarchou, M.; Pnias, D.; Douni, I.; Paspaliaris, I.; Kontopoulos, A., Dissolution of hematite in acidic oxalate solutions. *Hydrometallurgy* **1997**, *44* (3), 287-299.
20. Salmimies, R.; Mannila, M.; Kallas, J.; Häkkinen, A., Acidic dissolution of magnetite: experimental study on the effects of acid concentration and temperature. *Clays and Clay Minerals* **2011**, *59* (2), 136-146.
21. Salmimies, R.; Vehmaanperä, P.; Häkkinen, A., Acidic dissolution of magnetite in mixtures of oxalic and sulfuric acid. *Hydrometallurgy* **2016**, *163*, 91-98.
22. Lee, S. O.; Tran, T.; Park, Y. Y.; Kim, S. J.; Kim, M. J., Study on the kinetics of iron oxide leaching by oxalic acid. *International Journal of Mineral Processing* **2006**, *80* (2-4), 144-152.
23. Shengo, M. L.; Kime, M.-B.; Mambwe, M. P.; Nyembo, T. K., A review of the beneficiation of copper-cobalt-bearing minerals in the Democratic Republic of Congo. *Journal of Sustainable Mining* **2019**, *18* (4), 226-246.
24. Agatzini-Leonardou, S.; Tsakiridis, P.; Oustadakis, P.; Karidakis, T.; Katsiapi, A., Hydrometallurgical process for the separation and recovery of nickel from sulfate heap leach liquor of nickeliferrous laterite ores. *Minerals Engineering* **2009**, *22* (14), 1181-1192.

25. Tzeferis, P.; Agatzini-Leonardou, S., Leaching of nickel and iron from Greek non-sulfide nickeliferous ores by organic acids. *Hydrometallurgy* **1994**, *36* (3), 345-360.
26. Jones, D. L. Hydrometallurgical copper extraction process. U.S. Patent 5,223,024. 29 Jun, **1993**.
27. Filippou, D., Innovative hydrometallurgical processes for the primary processing of zinc. *Mineral Processing and Extractive Metallurgy Review* **2004**, *25* (3), 205-252.
28. Habashi, F. In *Hydrometallurgy of lead*, Zinc and Lead Metallurgy - 47th Annual Conference of Metallurgists of CIM, **2008**.
29. Lin, Y.-P.; Valentine, R. L., Reductive dissolution of lead dioxide (PbO<sub>2</sub>) in acidic bromide solution. *Environmental science & technology* **2010**, *44* (10), 3895-3900.
30. Wang, Y.; Wu, J.; Wang, Z.; Terenyi, A.; Giammar, D. E., Kinetics of lead (IV) oxide (PbO<sub>2</sub>) reductive dissolution: Role of lead (II) adsorption and surface speciation. *Journal of Colloid and Interface Science* **2013**, *389* (1), 236-243.
31. Nockemann, P.; Thijs, B.; Pittois, S.; Thoen, J.; Glorieux, C.; Van Hecke, K.; Van Meervelt, L.; Kirchner, B.; Binnemans, K., Task-specific ionic liquid for solubilizing metal oxides. *The Journal of Physical Chemistry B* **2006**, *110* (42), 20978-20992.
32. Nockemann, P.; Thijs, B.; Parac-Vogt, T. N.; Van Hecke, K.; Van Meervelt, L.; Tinant, B.; Hartenbach, I.; Schleid, T.; Ngan, V. T.; Nguyen, M. T., Carboxyl-functionalized task-specific ionic liquids for solubilizing metal oxides. *Inorganic Chemistry* **2008**, *47* (21), 9987-9999.
33. Wellens, S.; Vander Hoogerstraete, T.; Möller, C.; Thijs, B.; Luyten, J.; Binnemans, K., Dissolution of metal oxides in an acid-saturated ionic liquid solution and investigation of the back-extraction behaviour to the aqueous phase. *Hydrometallurgy* **2014**, *144*, 27-33.
34. Dupont, D.; Raiguel, S.; Binnemans, K., Sulfonic acid functionalized ionic liquids for dissolution of metal oxides and solvent extraction of metal ions. *Chemical Communications* **2015**, *51* (43), 9006-9009.
35. Dai, S.; Shin, Y.; Toth, L.; Barnes, C., Comparative UV-Vis studies of uranyl chloride complex in two basic ambient-temperature melt systems: The observation of spectral and thermodynamic variations induced via hydrogen bonding. *Inorganic Chemistry* **1997**, *36* (21), 4900-4902.

36. Bell, R. C.; Castleman, A.; Thorn, D., Vanadium oxide complexes in room-temperature chloroaluminate molten salts. *Inorganic Chemistry* **1999**, *38* (25), 5709-5715.
37. Davris, P.; Balomenos, E.; Panias, D.; Paspaliaris, I., Selective leaching of rare earth elements from bauxite residue (red mud), using a functionalized hydrophobic ionic liquid. *Hydrometallurgy* **2016**, *164*, 125-135.
38. Fan, F.-L.; Qin, Z.; Cao, S.-W.; Tan, C.-M.; Huang, Q.-G.; Chen, D.-S.; Wang, J.-R.; Yin, X.-J.; Xu, C.; Feng, X.-G., Highly Efficient and Selective Dissolution Separation of Fission Products by an Ionic Liquid [Hbet][Tf<sub>2</sub>N]: A New Approach to Spent Nuclear Fuel Recycling. *Inorganic Chemistry* **2018**, *58* (1), 603-609.
39. Abbott, A. P.; Capper, G.; Davies, D. L.; McKenzie, K. J.; Obi, S. U., Solubility of metal oxides in deep eutectic solvents based on choline chloride. *Journal of Chemical and Engineering Data* **2006**, *51* (4), 1280-1282.
40. Abbott, A. P.; Frisch, G.; Hartley, J.; Ryder, K. S., Processing of metals and metal oxides using ionic liquids. *Green Chemistry* **2011**, *13* (3), 471-481.
41. Abbott, A. P.; Capper, G.; Davies, D. L.; Rasheed, R. K.; Shikotra, P., Selective extraction of metals from mixed oxide matrixes using choline-based ionic liquids. *Inorganic Chemistry* **2005**, *44* (19), 6497-6499.
42. Rodriguez Rodriguez, N.; Machiels, L.; Binnemans, K., p-Toluenesulfonic Acid-Based Deep-Eutectic Solvents for Solubilising Metal Oxides. *ACS Sustainable Chemistry & Engineering* **2019**, *7* (4), 3940-3948.
43. Yang, H.; Reddy, R. G., Electrochemical deposition of zinc from zinc oxide in 2:1 urea/choline chloride ionic liquid. *Electrochimica Acta* **2014**, *147*, 513-519.
44. Sldner, A.; Zach, J.; Knig, B., Deep eutectic solvents as extraction media for metal salts and oxides exemplarily shown for phosphates from incinerated sewage sludge ash. *Green Chemistry* **2019**, *21* (2), 321-328.
45. Abbott, A.; Capper, G.; Davies, D.; Shikotra, P., Processing metal oxides using ionic liquids. *Mineral Processing and Extractive Metallurgy* **2006**, *115* (1), 15-18.
46. Tran, M. K.; Rodrigues, M.-T. F.; Kato, K.; Babu, G.; Ajayan, P. M., Deep eutectic solvents for cathode recycling of Li-ion batteries. *Nature Energy* **2019**, *4* (4), 339.
47. Dupont, D.; Binnemans, K., Rare-earth recycling using a functionalized ionic liquid for the selective dissolution and revalorization of Y<sub>2</sub>O<sub>3</sub>:Eu<sup>3+</sup> from lamp phosphor waste. *Green Chemistry* **2015**, *17* (2), 856-868.

48. Riaño, S.; Petranikova, M.; Onghena, B.; Vander Hoogerstraete, T.; Banerjee, D.; Foreman, M. R. S.; Ekberg, C.; Binnemans, K., Separation of rare earths and other valuable metals from deep-eutectic solvents: a new alternative for the recycling of used NdFeB magnets. *RSC Advances* **2017**, *7* (51), 32100-32113.
49. Zürner, P.; Frisch, G., Leaching and Selective Extraction of Indium and Tin from Zinc Flue Dust Using an Oxalic Acid-Based Deep Eutectic Solvent. *ACS Sustainable Chemistry and Engineering* **2019**, *7* (5), 5300-5308.
50. Abbott, A. P.; Collins, J.; Dalrymple, I.; Harris, R. C.; Mistry, R.; Qiu, F.; Scheirer, J.; Wise, W. R., Processing of electric arc furnace dust using deep eutectic solvents. *Australian Journal of Chemistry* **2009**, *62* (4), 341-347.
51. Abbott, A.; Capper, G.; Swain, B.; Wheeler, D., Electropolishing of stainless steel in an ionic liquid. *Transactions of the IMF* **2005**, *83* (1), 51-53.
52. Bahadori, L.; Manan, N. S. A.; Chakrabarti, M. H.; Hashim, M. A.; Mjalli, F. S.; AlNashef, I. M.; Hussain, M. A.; Low, C. T. J., The electrochemical behaviour of ferrocene in deep eutectic solvents based on quaternary ammonium and phosphonium salts. *Physical Chemistry Chemical Physics* **2013**, *15* (5), 1707-1714.
53. Ballantyne, A. D.; Hallett, J. P.; Riley, D. J.; Shah, N.; Payne, D. J., Lead acid battery recycling for the twenty-first century. *Royal Society Open Science* **2018**, *5* (5), 171368.
54. Terpstra, H. J.; De Groot, R. A.; Haas, C., Electronic structure of the lead monoxides: Band-structure calculations and photoelectron spectra. *Physical Review B* **1995**, *52* (16), 11690-11697.
55. Roine, A., HSC Chemistry 10 [Software]. Outotec: Research Center, Pori, Finland, 2019.
56. Haynes, W. M., *CRC handbook of chemistry and physics*. 95th ed.; CRC press: 2014.
57. Richter, J.; Ruck, M., Dissolution of metal oxides in task-specific ionic liquid. *RSC Advances* **2019**, *9* (51), 29699-29710.
58. Alabdullah, S. S. M. pH Measurements in Ionic Liquids. PhD thesis, University of Leicester, **2018**.
59. Smith, E. L.; Abbott, A. P.; Ryder, K. S., Deep eutectic solvents (DESs) and their applications. *Chemical Reviews* **2014**, *114* (21), 11060.
60. Jayachandran, K.; Gupta, R.; Chandrakumar, K.; Goswami, D.; Noronha, D.; Paul, S.; Kannan, S., Remarkably enhanced direct dissolution of plutonium oxide in task-

specific ionic liquid: insights from electrochemical and theoretical investigations. *Chemical Communications* **2019**, 55 (10), 1474-1477.

61. Rogers, D. B.; Shannon, R. D.; Sleight, A. W.; Gillson, J. L., Crystal chemistry of metal dioxides with rutile-related structures. *Inorganic Chemistry* **1969**, 8 (4), 841-849.

62. Shaked, H.; Faber Jr, J.; Hitterman, R., Low-temperature magnetic structure of MnO: a high-resolution neutron-diffraction study. *Physical Review B* **1988**, 38 (16), 11901.

63. Pauling, L.; Hendricks, S. B., The crystal structures of hematite and corundum. *Journal of the American Chemical Society* **1925**, 47 (3), 781-790.

64. Roth, W., The magnetic structure of  $\text{Co}_3\text{O}_4$ . *Journal of Physics and Chemistry of Solids* **1964**, 25 (1), 1-10.

65. Tombs, N.; Rooksby, H., Structure of monoxides of some transition elements at low temperatures. *Nature* **1950**, 165 (4194), 442.

66. Bragg, W., The structure of magnetite and the spinels. *Nature* **1915**, 95 (2386), 561-561.

67. Cairns, R.; Ott, E., X-ray studies of the system nickel-oxygen-water. I. Nickelous oxide and hydroxide<sup>1</sup>. *Journal of the American Chemical Society* **1933**, 55 (2), 527-533.

68. Tunell, G.; Posnjak, E.; Ksanda, C., Geometrical and optical properties, and crystal structure of tenorite. *Zeitschrift für Kristallographie-Crystalline Materials* **1935**, 90 (1-6), 120-142.

69. Hafner, S.; Nagel, S., The electric field gradient at the position of copper in  $\text{Cu}_2\text{O}$  and electronic charge density analysis by means of K-factors. *Physics and Chemistry of Minerals* **1983**, 9 (1), 19-22.

70. Xu, Y.-N.; Ching, W., Electronic, optical, and structural properties of some wurtzite crystals. *Physical Review B* **1993**, 48 (7), 4335.

71. Dickinson, R. G.; Friauf, J. B., The crystal structure of tetragonal lead monoxide. *Journal of the American Chemical Society* **1924**, 46 (11), 2457-2463.

72. Swain, H.; Lee, C.; Rozelle, R., Determination of the solubility of manganese hydroxide and manganese dioxide at 25. deg. by atomic absorption spectrometry. *Analytical Chemistry* **1975**, 47 (7), 1135-1137.

73. Tremaine, P. R.; Von Masscow, R.; Shierman, G. R., A calculation of Gibbs free energies for ferrous ions and the solubility of magnetite in  $\text{H}_2\text{O}$  and  $\text{D}_2\text{O}$  to 300 C. *Thermochimica Acta* **1977**, 19 (3), 287-300.

74. Taylor, P.; Owen, D. G. *Oxidation of magnetite in aerated aqueous media*; Atomic Energy of Canada Ltd.: **1993**.
75. Dirkse, T. P., *Copper, Silver, Gold & Zinc, Cadmium, Mercury Oxides & Hydroxides*. Elsevier: **2016**; Vol. 23.
76. Dirkse, T. P. *Zinc Oxide and Hydroxide, NIST Critical Evaluation*; Calvin College, Michigan USA: **1984**.
77. Garrett, A.; Vellenga, S.; Fontana, C., The solubility of red, yellow, and black lead oxides (2) and hydrated lead oxide in alkaline solutions. The character of the lead-bearing ion. *Journal of the American Chemical Society* **1939**, *61* (2), 367-373.
78. Pantias, D.; Taxiarchou, M.; Paspaliaris, I.; Kontopoulos, A., Mechanisms of dissolution of iron oxides in aqueous oxalic acid solutions. *Hydrometallurgy* **1996**, *42* (2), 257-265.
79. Eisele, T.; Gabby, K., Review of reductive leaching of iron by anaerobic bacteria. *Mineral Processing and Extractive Metallurgy Review* **2014**, *35* (2), 75-105.
80. Abbott, A. P.; Alabdullah, S. S. M.; Al-Murshedi, A. Y. M.; Ryder, K. S., Brønsted acidity in deep eutectic solvents and ionic liquids. *Faraday Discussions* **2018**, *206*, 365-377.
81. Hartley, J. M.; Ip, C.-M.; Forrest, G. C. H.; Singh, K.; Gurman, S. J.; Ryder, K. S.; Abbott, A. P.; Frisch, G., EXAFS study into the speciation of metal salts dissolved in ionic liquids and deep eutectic solvents. *Inorganic Chemistry* **2014**, *53* (12), 6280-6288.
82. Kepp, K. P., A quantitative scale of oxophilicity and thiophilicity. *Inorganic Chemistry* **2016**, *55* (18), 9461-9470.
83. Senanayake, G.; Childs, J.; Akerstrom, B.; Pugaev, D., Reductive acid leaching of laterite and metal oxides—a review with new data for Fe (Ni, Co) OOH and a limonitic ore. *Hydrometallurgy* **2011**, *110* (1-4), 13-32.
84. Li, L.; Fan, E.; Guan, Y.; Zhang, X.; Xue, Q.; Wei, L.; Wu, F.; Chen, R., Sustainable recovery of cathode materials from spent lithium-ion batteries using lactic acid leaching system. *ACS Sustainable Chemistry & Engineering* **2017**, *5* (6), 5224-5233.
85. Thun, H.; Guns, W.; Verbeek, F., The stability constants of some bivalent metal complexes of  $\alpha$ -hydroxyisobutyrate and lactate. *Analytica Chimica Acta* **1967**, *37*, 332-338.
86. Lee, S. O.; Tran, T.; Jung, B. H.; Kim, S. J.; Kim, M. J., Dissolution of iron oxide using oxalic acid. *Hydrometallurgy* **2007**, *87* (3-4), 91-99.

87. Merritt Jr, C.; Hershenson, H.; Rogers, L., Spectrophotometric determination of bismuth, lead, and thallium with hydrochloric acid. *Analytical Chemistry* **1953**, 25 (4), 572-577.
88. Liao, Y.-S.; Chen, P.-Y.; Sun, I.-W., Electrochemical study and recovery of Pb using 1: 2 choline chloride/urea deep eutectic solvent: A variety of Pb species PbSO<sub>4</sub>, PbO<sub>2</sub>, and PbO exhibits the analogous thermodynamic behavior. *Electrochimica Acta* **2016**, 214, 265-275.
89. Suleimenov, O.; Seward, T., Spectrophotometric measurements of metal complex formation at high temperatures: the stability of Mn (II) chloride species. *Chemical Geology* **2000**, 167 (1-2), 177-192.
90. Abbott, A. P.; Ballantyne, A.; Harris, R. C.; Juma, J. A.; Ryder, K. S.; Forrest, G., A comparative study of nickel electrodeposition using deep eutectic solvents and aqueous solutions. *Electrochimica Acta* **2015**, 176, 718-726.
91. De Vreese, P.; Brooks, N. R.; Van Hecke, K.; Van Meervelt, L.; Matthijs, E.; Binnemans, K.; Van Deun, R., Speciation of copper (II) complexes in an ionic liquid based on choline chloride and in choline chloride/water mixtures. *Inorganic Chemistry* **2012**, 51 (9), 4972-4981.
92. Rimsza, J. M.; Corrales, L. R., Adsorption complexes of copper and copper oxide in the deep eutectic solvent 2: 1 urea–choline chloride. *Computational and Theoretical Chemistry* **2012**, 987, 57-61.
93. Pateli, I. M.; Abbott, A.; Binnemans, K.; Rodriguez Rodriguez, N., Recovery of yttrium and europium from spent fluorescent lamps using pure levulinic acid and the deep eutectic solvent levulinic acid-choline chloride. *RSC Advances* 2020, 10 (48), 28879–28890.
94. Alves Dias, P.; Blagoeva, D.; Pavel, C.; Arvanitidis, N. *Cobalt: Demand-Supply Balances in the Transition to Electric Mobility*; Publications Office of the European Union, Luxembourg **2018**.
95. Chagnes, A.; Pospiech, B., A brief review on hydrometallurgical technologies for recycling spent lithium-ion batteries. *Journal of Chemical Technology & Biotechnology* **2013**, 88 (7), 1191-1199.
96. Huang, B.; Pan, Z.; Su, X.; An, L., Recycling of lithium-ion batteries: Recent advances and perspectives. *Journal of Power Sources* **2018**, 399, 274-286.

97. Nan, J.; Han, D.; Zuo, X., Recovery of metal values from spent lithium-ion batteries with chemical deposition and solvent extraction. *Journal of Power Sources* **2005**, *152*, 278-284.
98. Nan, J.; Han, D.; Yang, M.; Cui, M.; Hou, X., Recovery of metal values from a mixture of spent lithium-ion batteries and nickel-metal hydride batteries. *Hydrometallurgy* **2006**, *84* (1-2), 75-80.
99. Zheng, X.; Zhu, Z.; Lin, X.; Zhang, Y.; He, Y.; Cao, H.; Sun, Z., A mini-review on metal recycling from spent lithium ion batteries. *Engineering* **2018**, *4* (3), 361-370.
100. Lv, W.; Wang, Z.; Cao, H.; Sun, Y.; Zhang, Y.; Sun, Z., A critical review and analysis on the recycling of spent lithium-ion batteries. *ACS Sustainable Chemistry & Engineering* **2018**, *6* (2), 1504-1521.
101. Li, L.; Zhang, X.; Li, M.; Chen, R.; Wu, F.; Amine, K.; Lu, J., The recycling of spent lithium-ion batteries: a review of current processes and technologies. *Electrochemical Energy Reviews* **2018**, *1* (4), 461-482.
102. Ordoñez, J.; Gago, E.; Girard, A., Processes and technologies for the recycling and recovery of spent lithium-ion batteries. *Renewable and Sustainable Energy Reviews* **2016**, *60*, 195-205.
103. Chen, L.; Tang, X.; Zhang, Y.; Li, L.; Zeng, Z.; Zhang, Y., Process for the recovery of cobalt oxalate from spent lithium-ion batteries. *Hydrometallurgy* **2011**, *108* (1-2), 80-86.
104. Meshram, P.; Pandey, B.; Mankhand, T., Hydrometallurgical processing of spent lithium ion batteries (LIBs) in the presence of a reducing agent with emphasis on kinetics of leaching. *Chemical Engineering Journal* **2015**, *281*, 418-427.
105. Kang, J.; Senanayake, G.; Sohn, J.; Shin, S. M., Recovery of cobalt sulfate from spent lithium ion batteries by reductive leaching and solvent extraction with Cyanex 272. *Hydrometallurgy* **2010**, *100* (3-4), 168-171.
106. Dutta, D.; Kumari, A.; Panda, R.; Jha, S.; Gupta, D.; Goel, S.; Jha, M. K., Close loop separation process for the recovery of Co, Cu, Mn, Fe and Li from spent lithium-ion batteries. *Separation and Purification Technology* **2018**, *200*, 327-334.
107. Zeng, X.; Li, J., Innovative application of ionic liquid to separate Al and cathode materials from spent high-power lithium-ion batteries. *Journal of Hazardous Materials* **2014**, *271*, 50-56.

108. Georgi-Maschler, T.; Friedrich, B.; Weyhe, R.; Heegn, H.; Rutz, M., Development of a recycling process for Li-ion batteries. *Journal of Power Sources* **2012**, *207*, 173-182.
109. Muneer, T.; Kolhe, M.; Doyle, A., *Electric Vehicles: Prospects and Challenges*. Elsevier: **2017**.
110. Stephen, E.; Miller, P. D., Solubility of Lithium Hydroxide in Water and Vapor Pressure of Solutions above 220° F. *Journal of Chemical and Engineering Data* **1962**, *7* (4), 501-505.
111. Florindo, C.; Oliveira, F. S.; Rebelo, L. P. N.; Fernandes, A. M.; Marrucho, I. M., Insights into the synthesis and properties of deep eutectic solvents based on cholinium chloride and carboxylic acids. *ACS Sustainable Chemistry & Engineering* **2014**, *2* (10), 2416-2425.
112. Rodriguez Rodriguez, N.; van den Bruinhorst, A.; Kollau, L. J.; Kroon, M. C.; Binnemans, K., Degradation of deep-eutectic solvents based on choline chloride and carboxylic acids. *ACS Sustainable Chemistry & Engineering* **2019**, *7* (13), 11521-11528.
113. Hammond, O. S.; Bowron, D. T.; Edler, K. J., The effect of water upon deep eutectic solvent nanostructure: An unusual transition from ionic mixture to aqueous solution. *Angewandte Chemie International Edition* **2017**, *56* (33), 9782-9785.
114. Mandroyan, A.; Mourad-Mahmoud, M.; Doche, M.-L.; Hihn, J.-Y., Effects of ultrasound and temperature on copper electro reduction in Deep Eutectic Solvents (DES). *Ultrasonics Sonochemistry* **2014**, *21* (6), 2010-2019.
115. Li, J.; Shi, P.; Wang, Z.; Chen, Y.; Chang, C.-C., A combined recovery process of metals in spent lithium-ion batteries. *Chemosphere* **2009**, *77* (8), 1132-1136.
116. Zhu, S.-g.; He, W.-Z.; Li, G.-M.; Xu, Z.; Zhang, X.-j.; Huang, J.-W., Recovery of Co and Li from spent lithium-ion batteries by combination method of acid leaching and chemical precipitation. *Transactions of Nonferrous Metals Society of China* **2012**, *22* (9), 2274-2281.
117. Li, L.; Zhai, L.; Zhang, X.; Lu, J.; Chen, R.; Wu, F.; Amine, K., Recovery of valuable metals from spent lithium-ion batteries by ultrasonic-assisted leaching process. *Journal of Power Sources* **2014**, *262*, 380-385.

# Chapter 4: Electrochemical dissolution of metal oxide in deep eutectic solvents

4 Chapter.....	135
4.1 Introduction.....	135
4.1.1 Oxidative dissolution of metal oxides .....	135
4.1.2 Aims .....	138
4.2 Electrochemical studies of metal oxides .....	138
4.2.1 Paint casting of MOs .....	138
4.2.2 Chronopotentiometry.....	149
4.2.3 Chronocoulometry .....	150
4.3 Bulk anodic dissolution of MOs .....	154
4.4 Bulk anodic deposition.....	161
4.5 Conclusions .....	163
4.6 References .....	165

## 4 Chapter

### 4.1 Introduction

From the previous Chapter, it was concluded that the dissolution of MOs in DESs is highly influenced by the proton activity of the solvent, due to the reaction of  $H^+$  with the oxide moiety and its detachment from the MO surface. However, their dissolution is even more dependent on the presence of a ligand in solution, which can be the HBD of the DES, resulting in surface complexation and detachment of the Me-L species from the surface of the MO. This fact shows the importance of speciation for the dissolution of MOs. Hence, the tuneability of DESs can significantly affect the selectivity of processes due to specific interactions of metals with different HBDs. That was illustrated with the process of extracting selectively Co and Mn from a cathode of LIB, without dissolving Ni in OxA:ChCl.

When the investigated solvent does not include any of these characteristics, neither high proton activity nor a suitable ligand, then the MO solubility is low. Of course, there are oxides such as  $Cu_2O$ ,  $ZnO$  and  $PbO$  that even in a non-coordinating solvent like EG:ChCl or Gly:ChCl they show significant solubilities. This was justified from their ionic character, low lattice energy and enthalpy of formation, which all led to their higher dissolution of the metal ion via complexation with  $Cl^-$ .

The Pourbaix diagrams have shown that the dissolution of a MO can be either with the alternation of pH or with the change in the potential of the system or with the combination of the two. Thus, an alternative way that can tackle the issue of very low MOs solubilities in poor lixiviants, is using electrochemical dissolution and the application of voltage to the system to enhance the dissolution rate. This can be done by either reducing or oxidising potentials depending on the Pourbaix diagram for the metal. The efficiency of this approach depends on the possible oxidation states of the metal and the conductivity of the MO. The dissolution of MOs with the use of oxidising agents has been studied in aqueous solutions, but the research is not that extensive as for the reducing dissolution.

#### 4.1.1 Oxidative dissolution of metal oxides

Research on the electrochemical dissolution of MOs has been focused mainly on reducing the metal cation of the MO. MOs such as  $Al_2O_3$ ,  $SiO_2$  and  $MgO$  are non-reducible due to their low conductivity, lack of different redox states and low chemical

reactivity due to their high covalent character. This chapter will focus on metal oxides with lower band gap (energy difference between the conduction and valence band) which leads to higher conductivity and chemical reactivity, which will be discussed later.<sup>1</sup>

As mentioned in Chapter 3, reducing agents like oxalic acid enhance the dissolution of MOs and actually it was proven that an ideal lixiviant for MOs would be an acidic solution that incorporates a strong ligand, which can also act as a reducing agent, especially for the high-valency MOs. Very few lixiviant can show both these characteristics but oxalic acid, lactic acid, tartaric acid and citric acid all do. Some other reducing systems studied in aqueous chemistry for the increase in the rate of MOs dissolution are hydroquinone, metallic Zn, Na<sub>2</sub>SO<sub>3</sub>, Na<sub>2</sub>S<sub>2</sub>O<sub>4</sub>, Fe<sup>2+</sup> and Cr<sup>3+</sup>.<sup>2,3</sup> The need for reducing conditions can be directly seen from a Pourbaix diagram. In **Figure 4.1** the Pourbaix diagrams of Fe and Cr are given in aqueous solutions, without the existence of complexing agents. These two examples were chosen due to their distinguish difference in behaviour. It is obvious and has already been discussed that Fe dissolves more efficiently under reducing conditions. However, Cr can be dissolved either under reducing or oxidizing conditions. For example, Cr<sub>2</sub>O<sub>3</sub> can be transformed into CrO<sub>4</sub><sup>2-</sup> by oxidation, because chromium can appear in Cr<sup>6+</sup> oxidation state. Actually, it is also reported that the electrochemical dissolution of oxides is faster than the slow surface complexation reactions.<sup>4</sup>

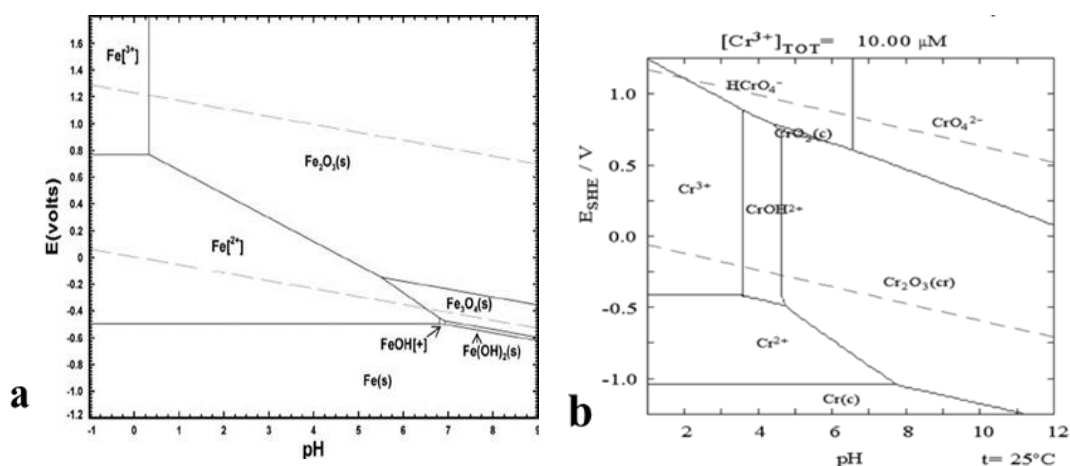


Figure 4.1: Pourbaix diagrams in aqueous solutions of a) 1  $\mu\text{M}$  Fe<sup>5</sup> and b) 10  $\mu\text{M}$  Cr.<sup>6</sup>

The oxidative dissolution of Cr<sub>2</sub>O<sub>3</sub> has been widely studied.<sup>7-9</sup> Segal et al.<sup>8</sup> investigated the dissolution of oxide films on steel containing a mixture of Ni<sub>x</sub>, Fe<sub>y</sub>, Cr<sub>3-x-y</sub>O<sub>4</sub> with the use of MnO<sub>4</sub><sup>-</sup> and various concentration of H<sup>+</sup> at 90 °C. It was reported that at optimum conditions >85 % of Cr was extracted, with <10 % and <30 % coextraction for Fe and Ni, respectively. This was logical since iron oxides are known to be dissolve faster under

reducing conditions, and that is the reason that oxalic acid is one of the most efficient lixivants for Fe<sub>2</sub>O<sub>3</sub> and Fe<sub>3</sub>O<sub>4</sub> dissolution. For NiO, though, it has been reported that the rate of dissolution in acidic solutions is enhanced under the presence of oxidising agents or with anodic polarisation.<sup>10, 11</sup> The oxidative dissolution of UO<sub>2</sub> has also been reported with the use of MnO<sub>4</sub><sup>-</sup> and carbonate solutions.<sup>12-14</sup> The oxidative dissolution of RuO<sub>2</sub>·xH<sub>2</sub>O was reported by Mills et al.<sup>15</sup>, in which report RuO<sub>4</sub> was formed as the corrosion product of the reaction between RuO<sub>2</sub>·xH<sub>2</sub>O with several oxidising agents including Ce<sup>4+</sup>, BrO<sub>3</sub><sup>-</sup>, IO<sub>4</sub><sup>-</sup>, MnO<sub>4</sub><sup>-</sup>, MnO<sub>2</sub> powder and PbO<sub>2</sub> powder with the first four to result in very fast oxidation.

There are many strong oxidants such as F<sub>2</sub>, Cl<sub>2</sub>, HNO<sub>3</sub>, H<sub>2</sub>SO<sub>4</sub>, Ce<sup>4+</sup>, MnO<sub>4</sub><sup>-</sup>, BrO<sub>3</sub><sup>-</sup>, IO<sub>4</sub><sup>-</sup> with their oxidising strength translated into their standard potential compared with H<sub>2</sub>, showing on **Table 4.1**.

*Table 4.1: Standard potential of common oxidising agents*

<b>Oxidising agent</b>	<b>Standard Electrode Potential E° (V) at 25 °C in aqueous solutions</b>
<b>Fe<sup>3+</sup></b>	0.77
<b>NO<sub>3</sub><sup>-</sup></b>	0.96
<b>Br<sub>2</sub></b>	1.07
<b>O<sub>2</sub></b>	1.23
<b>Cr<sub>2</sub>O<sub>7</sub><sup>2-</sup></b>	1.33
<b>Cl<sub>2</sub></b>	1.36
<b>Ce<sup>4+</sup></b>	1.44
<b>MnO<sub>4</sub><sup>-</sup></b>	1.49
<b>F<sub>2</sub></b>	2.87

In this investigation, the oxidative dissolution of MOs in DESs is studied, but instead of an oxidising agent, which is proven in the literature to not work for the MOs of this study, the employment of electrochemical anodic dissolution in EG:ChCl is studied. The rate of dissolution using electrochemical dissolution of MOs is proven to be enhanced in aqueous solutions, because the surface complexation reactions have slow kinetics. Hence, the

hypothesis is that the rate of the dissolution will increase in EG:ChCl, which is a poor chemical lixiviant, by oxidation of the oxide moiety to a more reactive species (as superoxide) that then can weaken the bond between the oxide and metal acting as the driving force of the dissolution.

#### **4.1.2 Aims**

This chapter investigates the oxidative electrochemical dissolution of MOs in DESs, as an alternative way of dissolution in EG:ChCl, which is a neutral solvent that does not contain any strong ligand to promote the surface complexation reactions on MOs. Actually, this study is a continuation of previous studies of Bevan and Al Bassam<sup>16, 17</sup> that studied the anodic dissolution of Cu and Fe sulfide minerals (CuS, Cu<sub>2</sub>S, CuFeS<sub>2</sub>, FeS<sub>2</sub> etc.) in EG:ChCl. These studies found that sulfur redox chemistry controlled dissolution. In the current study the aim was to determine whether, oxides are also electroactive and can also be dissolved electrolytically. So, the electrochemical oxidation is investigated as a potential tool for the increase in the rate of dissolution in EG:ChCl, by oxidising the oxide part of the compound to a more reacting species.

Voltammetry will be studied to determine whether the oxides are electroactive and see whether information about the electroactive species can be determined. Chronopotentiometric and chronocoulometric studies of the MOs will be attempted by using paint casting. These methods provide information about the stability and the open circuit potential (OCP) of the MOs and the rate of their electrochemical dissolution. The band gap of the MOs will be correlated to the rate of their dissolution.

Next, the bulk anodic dissolution of MOs will be examined, and the dissolution of metal quantified to determine whether the anodic dissolution can provide higher rate and yields of dissolution in EG:ChCl, compared to chemical dissolution. Bulk electrolysis will also enable proof that the dissolved metal can also be electrolytically recovered on the cathode as has been shown previously for copper and lead sulfides.<sup>16, 18</sup>

## **4.2 Electrochemical studies of metal oxides**

### **4.2.1 Paint casting of MOs**

The electrochemical study of solid compounds, especially minerals, has been demonstrated and is complex due to the presence of contaminants and anisotropic effects.<sup>19, 20</sup> Voltammetric studies of minerals are difficult due to problems associated with sample preparation. One technique employed is the use of a compact crystal of a mineral

which is limited to conductive solids.<sup>21</sup> In this technique, a single crystal of the solid material is attached to a wire (current collector) using a conductive resin or epoxy the mineral and wire are then cast in an insulating resin and polished to produce a flat sample. The preparation of the electrode can be laborious and usually produces voltammograms with low resolution, due to the low conductivity resulting in Ohmic artefacts. In addition, the exposure of only one single crystal face of the solid gives limited electrochemical information about the bulk solid. Al Bassam<sup>17</sup> showed that the cyclic voltammetry of different crystals of pyrite ( $\text{FeS}_2$ ) in EG:ChCl, which resulted in cyclic voltammograms (CVs) with different redox peaks. It was also shown that for pyrite different crystal faces etch at different rates.

Carbon paste electrodes (CPEs)<sup>21,22</sup> are an alternative method of preparing samples. Modified CPEs, produce a paste of both graphite as a conductive additive and the material of interest, which are ground with an organic binder such as silicon oil. These so-called carbon paste electroactive electrode (CPEEs) were developed by Kuwana and French.<sup>23</sup> Although, the electrochemical characterization with this method was possible, issues related to the decay of the metal compound have been experienced and so the electrodes have a short lifespan. An alternative technique called voltammetry of microparticles (VMP)<sup>24,25</sup> employed a paraffine-impregnated graphite electrode, in whose cross-section the microparticles of conductive or not solid compounds were mechanically immobilised. This technique resulted in fast and clear redox signals but suffers from the issue of difficulties in quantitative analysis due to the difficult assessment of the amount of exposed metal surface.<sup>25</sup>

The most widely electrochemical method used for the characterization of solid compounds is cyclic voltammetry, CV. In order to gain reliable and reproducible results from the solid analysis, the particle size of the solid needs to remain constant, the surface of the solid and the working electrode or the electrolyte need to be in good contact to eliminate any resistance issues.<sup>21</sup> In this sense, the method of paint casting<sup>26</sup>, enables electrodes to be easily prepared by grinding the solid with a viscous DESs and applying the paste to an electrode surface. The fluidity of the paste is easily adjusted by adding either more solid or liquid.



*Figure 4.2: Setup of the paint casting method. Paste of solid material mixed with EG:ChCl (left) and three electrode system with the paste painted on the working electrode (right)*

The relatively high viscosity of the DESs contributes to the binding of the ground solid on the working electrode (WE), which is bent at 90°, as shown in **Figure 4.2** and also helps for its adhesion on the electrode when immersed in the solution. In addition, Bevan reported that the DES is able to wet the surface of the solid better than an aqueous solution of sodium chloride.<sup>16</sup>

The paint casting method was used for the first time on the mineral galena (PbS) using the DES EG:ChCl, whose CV is presented in **Figure 4.3**.<sup>26</sup> Three oxidation and two reduction peaks are apparent. The peaks of C1 and C2 are only visible when the oxidation of PbS has passed the voltage at point A3, where the oxidation of PbS occurs, resulting in the formation of Pb<sup>II</sup> species in the double layer. Subsequently, the Pb<sup>II</sup> species are deposited on the Pt working electrode at C1, from where they are stripped back at A1. The oxidation peak at A2 is assumed to be due to the stripping of a Pb-Pt alloy formed on the electrode. An interesting observation lies at the point C2, where a second reduction peak is observed. It was assumed that this peak is attributed to the reduction of S species formed after the oxidation of PbS.<sup>16, 27</sup> Bevan also studied the electrochemistry of S powder using paint casting, showing that this technique can work with more resistive materials, as shown in **Figure 4.3**. The reduction of S<sub>8</sub> has been reported to produce the polysulfides S<sub>6</sub><sup>2-</sup> and S<sub>4</sub><sup>2-</sup> in ILs.<sup>28</sup>

The redox couples of both constituents, the metal and non-metal part of the compound, can be seen in the CV giving very useful information for the subsequent electrochemical extraction of the metal. The same behaviour of sulfides was reported from Al Bassam<sup>17</sup>

that studied the electrochemistry of different iron sulfide and arsenide minerals using paint casting. The importance of paint casting was further illustrated in its application on transition metal tellurides and selenides from Bevan<sup>16</sup>. The CVs showed both the redox couple for the Se and Te and the other metals, giving useful information for the development of selective extraction processes.

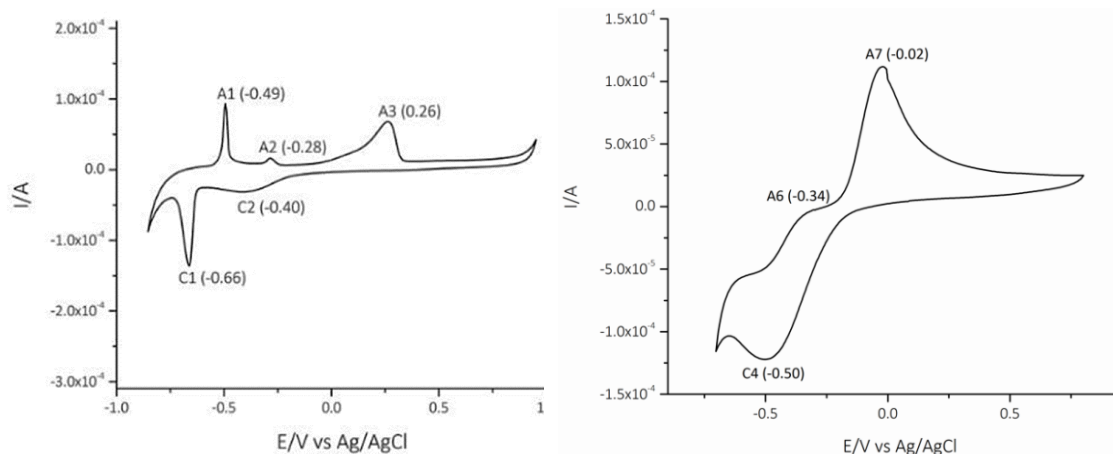


*Figure 4.3: Cyclic voltammogram of paint casted PbS (left) and S powder (right) in EG:ChCl.<sup>26</sup>*

In this chapter, paint casting method was used to investigate the electrochemistry of ten MOs in EG:ChCl. It is important to investigate if, as for the metal chalcogenides (sulfides, selenides and tellurides), the CVs of MOs solids will show two different redox couples; for the metal and for the oxide species. As a first stage, the paint casting is employed on the oxides of Fe, Cu and Pb to have direct comparison with the sulfides that were studied by Bevan and Al Bassam. The metal sulfides, in general, are more conductive than the MOs or hydroxides, so it was expected to obtain weaker electrochemical response and not as clear redox signals from the MOs investigated.<sup>29</sup>

In this examination, EG:ChCl was employed as the electrolyte for the paint casting method. The CV of the pure EG:ChCl is given in **Figure 4.4** and no redox behaviour is observed, with its electrochemical window to be around 2.2 V (-1 to 1.2 V) with respect to Ag/AgCl. The paint casting method was also investigated in Urea:ChCl, but the low conductivity and higher viscosity of this DES compared to EG:ChCl produced CVs with poorly resolved redox peaks. The more acidic DESs were not chosen, because of the narrow potential window. Hence, the high conductivity and low viscosity of EG:ChCl, combined with its high air and moisture stability rendering it the best candidate among the rest of DESs for this investigation.

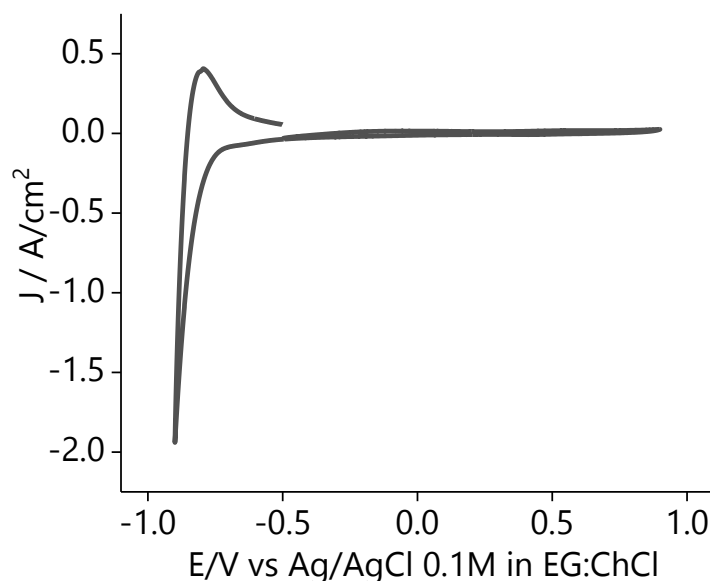
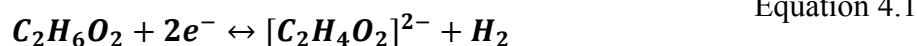


Figure 4.4: Cyclic voltammogram of pure EG:ChCl with a 0.32 cm<sup>2</sup> Pt flag WE, a Pt flag CE and an Ag/AgCl (0.1 M in EG:ChCl) RE. Scan rate: 10 mV s<sup>-1</sup>

In **Figure 4.5**, the CVs of paint casted Fe<sub>2</sub>O<sub>3</sub> and Fe<sub>3</sub>O<sub>4</sub> are presented. Both CVs show the highly reactive and quasi reversible redox couple of Fe<sup>II</sup>/ Fe<sup>III</sup>. The reactivity of Fe<sup>III</sup> as an oxidising agent is enhanced in the presence of high Cl<sup>-</sup> media and this maybe the reason of the clear redox couple shown in the CV, even though the solubility of these oxides is very low in EG:ChCl. The anodic peak at 0.43 V is assigned to the oxidation of Fe<sup>II</sup> to Fe<sup>III</sup> and the inverse reduction peak at 0.31 V is attributed to the reduction of Fe<sup>III</sup> to Fe<sup>II</sup>. The difference between the cathodic and anodic peak is around 120 mV, meaning that the redox couple behaves quasi reversible. The same shape and quasi-reversibility was observed by Kanatharana et al.<sup>30</sup> in dimethylformide. The same redox peaks have been reported for the CV of paint casted FeS<sub>2</sub> and FeCl<sub>3</sub> and also from the solution of FeCl<sub>3</sub> in EG:ChCl.<sup>17</sup> This shows that the paint casting method can be used for direct comparison of solid and solution electrochemistry. The absence of the redox signals for the couple Fe<sup>II</sup>/Fe<sup>0</sup> in the CV was discussed from Hartley<sup>31</sup> and Spathariotis<sup>32</sup> and it was pointed out that the reduction of Fe is below the cathodic limit of the DES, since at more negative potentials than -1 V the degradation of EG:ChCl occurs releasing H<sub>2</sub> gas, as the **Equation 4.1** shows.



What is interesting in the CVs of the iron oxides, is a second quasi-reversible redox couple with an oxidation peak at -0.15 V and a reduction peak at -0.24 V. This redox couple was

not observed in the CVs of  $\text{FeCl}_3$  solution or for paint casted  $\text{FeS}_2$ . More discussion on this peak will be given later.

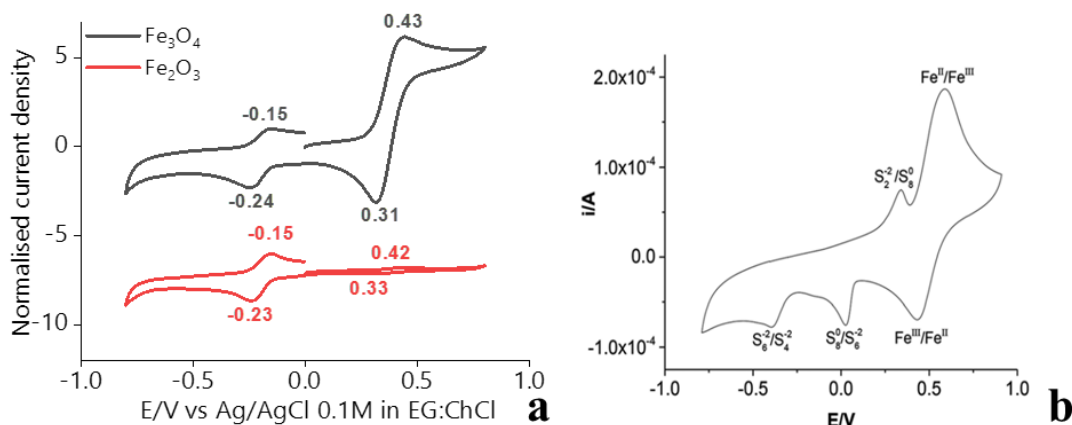


Figure 4.5: a) CV of paint casted solid  $\text{Fe}_2\text{O}_3$  and  $\text{Fe}_3\text{O}_4$  in EG:ChCl, with a  $0.32 \text{ cm}^2$  Pt flag WE, a Pt flag CE and an Ag/AgCl (0.1 M in EG:ChCl) RE. Scan rate:  $10 \text{ mV s}^{-1}$  b) Analogous CV for  $\text{FeS}_2$  by ref<sup>20</sup>

In **Figure 4.6**, the CVs of paint casted CuO and  $\text{Cu}_2\text{O}$  are presented and compared with the one reported from Bevan for paint casted  $\text{Cu}_2\text{S}$ . Again, both oxides show a very similar redox behaviour, with two redox couples. The CV started at 0 V and first was swept anodically until the point of 0.8 V and reversed. In this region, a typical redox species reaction is observed for both CVs. The anodic peak at 0.46 V is assigned to the oxidation of  $\text{Cu}^{\text{I}}$  to  $\text{Cu}^{\text{II}}$  and the cathodic peak at 0.37 V is assigned to the reduction of the  $\text{Cu}^{\text{II}}$  species to  $\text{Cu}^{\text{I}}$ . The difference in the anodic and cathodic peak is 90 mV, rendering it a quasi-reversible system. The same fact has been reported from Abrantes et al.,<sup>33</sup> that studied the electrochemistry of copper in aqueous chloride media and observed a difference of 128 mV. Moving to more negative potentials, a second redox couple is observed that has a typical shape for a nucleation and stripping process. The cathodic peak at -0.47 V is attributed to the deposition of  $\text{Cu}^0$  on Pt WE, while the sharper anodic peak at -0.22 V is assigned to the stripping of  $\text{Cu}^0$  from the surface of the electrode and its oxidation to  $\text{Cu}^+$  at -0.22 V. Overall, the same shape of the peaks related to the redox species of Cu have been reported for paint casted  $\text{Cu}_2\text{S}$ , as shown in **Figure 4.6**. In the CV of  $\text{Cu}_2\text{S}$  one more redox peak is observed in the middle of the redox couples of Cu, which is associated with the electrochemistry of S. The same shape and position of the redox peaks for Cu have also been reported for the paint casted  $\text{CuCl}_2$ , CuS and the solution of  $\text{CuCl}_2$  in EG:ChCl.<sup>16, 34, 35</sup>

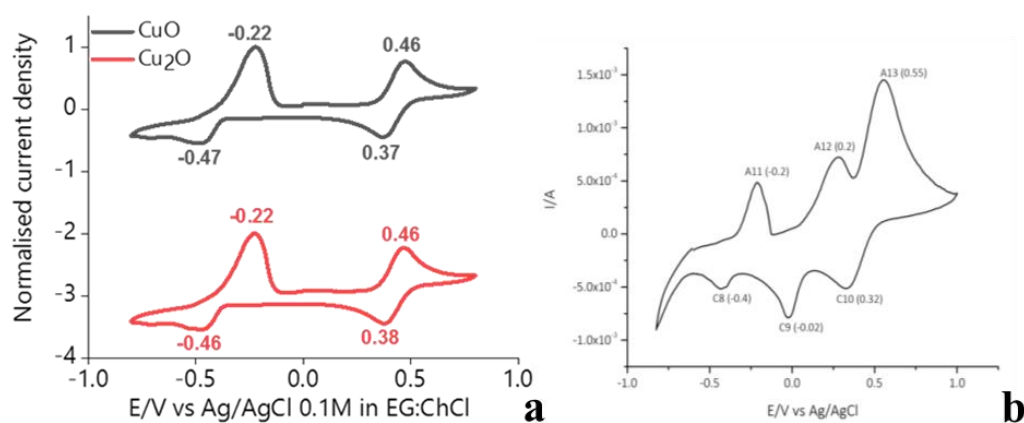


Figure 4.6: Cyclic voltammogram of a) paint casted solid CuO and Cu<sub>2</sub>O in EG:ChCl, with a 0.32 cm<sup>2</sup> Pt flag WE, a Pt flag CE and an Ag/AgCl (0.1 M in EG:ChCl) RE. Scan rate: 10 mV s<sup>-1</sup> and b) Analogous CV for Cu<sub>2</sub>S by ref<sup>16</sup>

Next, the paint casting was employed on PbO, was studied and this is shown in **Figure 4.7**. The CV of PbO is rather more complicated than the rest of MOs studied. There is a clear deposition peak of Pb at -0.64 V that agrees with the one reported from Bevan for the paint casted PbS.<sup>26</sup> However, for PbO there is a second sharper peak at -0.79 V, which is more negative than the deposition peak in the CV of PbS in **Figure 4.3**.

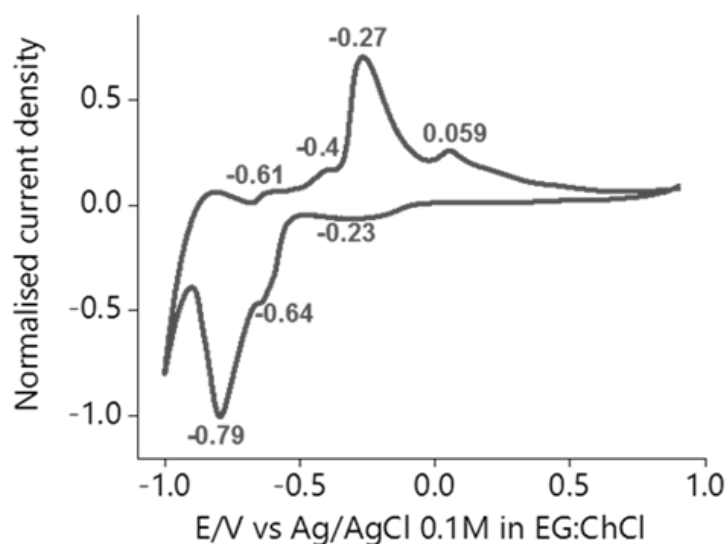


Figure 4.7: Cyclic voltammogram of painted casted PbO in EG:ChCl, with a 0.32 cm<sup>2</sup> Pt flag WE, a Pt flag CE and an Ag/AgCl (0.1 M in EG:ChCl) RE. Scan rate: 10 mV s<sup>-1</sup>.

Hua et al.<sup>36</sup> studied the electrochemistry of solid PbO in EG:ChCl, using a PbO pellet held on a Ti mesh working electrode with a cotton thread. The deposition peak observed

by Hua et al was at -0.7 V with respect to Ag/AgCl. The stripping of Pb from the WE was reported from Bevan to be assigned to the voltage of -0.49 V, but in the CV of PbO the stripping happens at two subsequent steps starting from -0.61 V and finishing at -0.4 V. The next oxidation peak is attributed to the stripping of a Pb-Pt alloy. Sun et al.<sup>27</sup> investigated the CV of Pb compounds on Pt, Au and GC electrodes and it was reported that only for the CV obtained on the Pt WE there are two oxidation peaks, one for the stripping of Pb and one for the stripping of the Pb-Pt alloy. Once again, in the CV of the paint casted PbO the reduction peak at -0.23 V is observed, as for the iron oxides.

This investigation of the solid state CV of Fe<sub>2</sub>O<sub>3</sub>, Fe<sub>3</sub>O<sub>4</sub>, CuO, Cu<sub>2</sub>O and PbO in EG:ChCl showed that the paint casting as a method can be used for the investigation of the electrochemistry of solid MOs. In addition, paint casting gives the opportunity to compare different solid compounds of the same metal (e.g. oxides, sulfides, chlorides) and also with their solutions. Hence, changes in speciation and subsequently reactivity of the metal species can be observed between different compounds.

Bevan and Al-Bassam only studied the paint casting of Fe, Cu, Zn and Pb compounds, and no attention has been given to compounds of metals like Co, Ni and Mn. Spathariotis has concluded that the solution electrochemistry of CoCl<sub>2</sub> shows an irreversible behaviour in DESs, while NiCl<sub>2</sub> shows a semi irreversible behaviour agreeing with prior results from Hartley that also suggested that MnCl<sub>2</sub> shows an irreversible behaviour.<sup>31, 32</sup> This difference in electrochemical behaviour between the metals investigated, was suggested to be due to difference in speciation and the species formed on the surface of the WE. Hartley concluded that if the species formed on the WE were not pure tetrachloride complexes and instead included the HBD, then the redox behaviour would be different. For ZnCl<sub>2</sub>, it was shown that voltammetry is highly dependent on its concentration in solution because at low concentrations (<0.1 M) the electrochemistry is kinetically hindered.<sup>32</sup> In addition to that, solid ZnO is an insulator meaning that no response is expected to appear in the CV. Hence, it is anticipated that the paint casting method will not give clear redox couples for ZnO. **Figure 4.8** shows the CVs for paint cast samples of MnO<sub>2</sub>, MnO, Co<sub>3</sub>O<sub>4</sub>, CoO, NiO and ZnO in EG:ChCl.

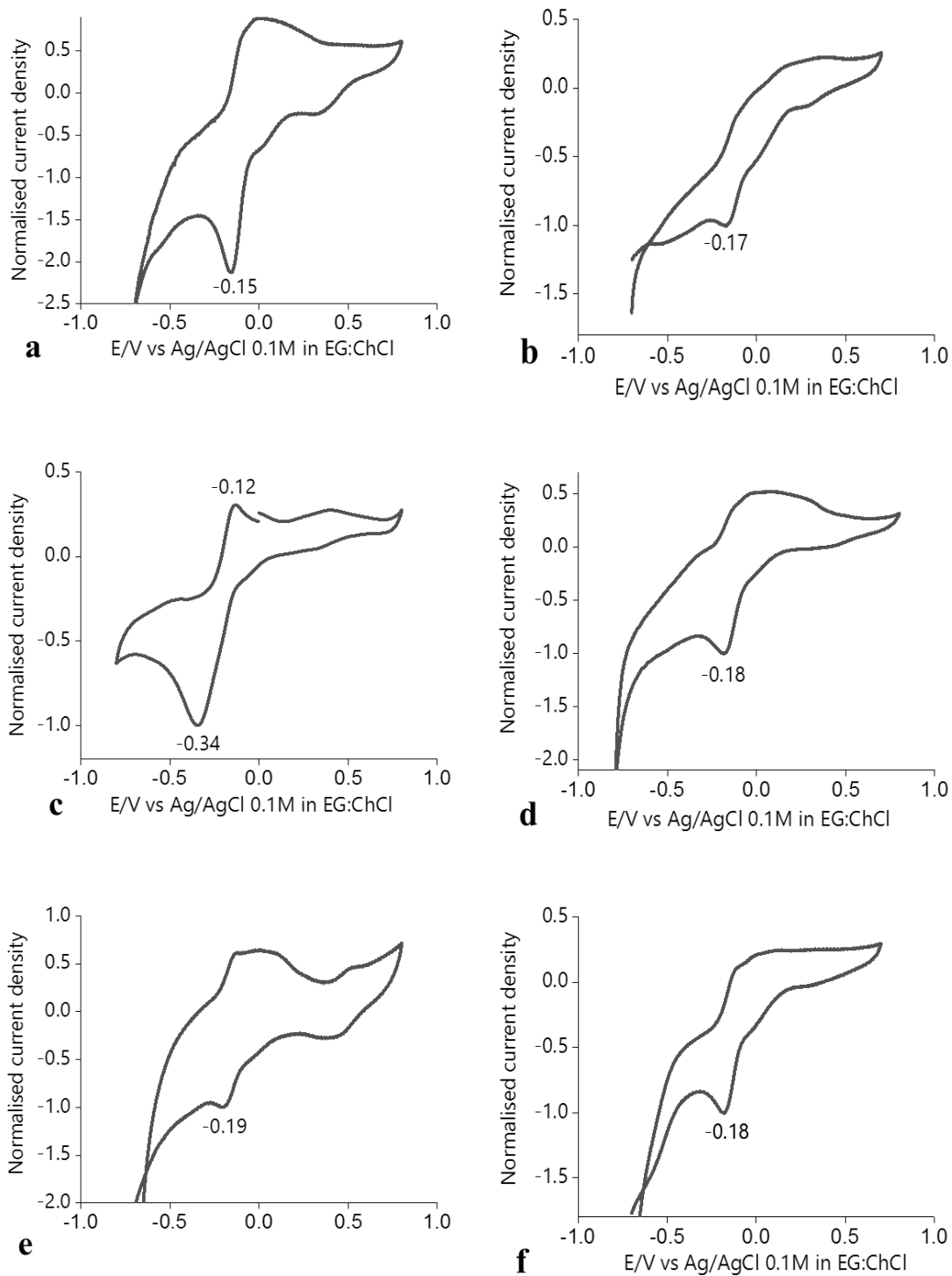


Figure 4.8: Cyclic voltammograms of paint casted a)  $MnO_2$ , b)  $MnO$ , c)  $Co_3O_4$ , d)  $CoO$ , e)  $NiO$  and f)  $ZnO$  in EG:ChCl with a  $0.32\text{ cm}^2$  Pt flag WE, a Pt flag CE and an Ag/AgCl (0.1 M in EG:ChCl) RE. Scan rate:  $10\text{ mV s}^{-1}$

While none of the CVs are particularly well resolved it can be seen that all have similar redox properties with a reduction peak at  $\approx -0.18\text{ V}$ . This is also the case of the  $Fe_2O_3$ ,

Fe<sub>3</sub>O<sub>4</sub> and PbO, with a slight shift towards positive potentials. The anodic peak which for the iron oxides was clear, for the rest of MOs is distinct but not as well formed.

The same behaviour has been reported for paint cast lanthanide oxides in EG:ChCl by Stodd.<sup>37</sup> The voltammetry of paint casted Er<sub>2</sub>O<sub>3</sub>, CeO<sub>2</sub>, Gd<sub>2</sub>O<sub>3</sub>, Sm<sub>2</sub>O<sub>3</sub>, Yb<sub>2</sub>O<sub>3</sub> and Pr<sub>2</sub>O<sub>3</sub> showed the same reduction peak at  $\approx -0.2$  V and an oxidation peak at  $-0.1$  V vs Ag/AgCl. Stodd also investigated the effect of paste loading on the WE and it was concluded that with higher loading on the electrode, both the anodic and cathodic peak at these voltages were enhanced.

The lack of distinct redox processes does not mean that the metal oxides are inert. Results below show that bulk electrolysis of all of these samples leads to solutions with metal concentrations of between 0.01 and 0.1 mol L<sup>-1</sup> which are in most cases are orders of magnitude higher than those observed by chemical dissolution. The poor resolution of the CVs in **Figure 4.8** are probably due to the higher resistivities of the oxides compared to the other chalcogenides.

As mentioned before, this redox peak could be assigned to the formation of oxide electroactive species on the surface of MO, as superoxide (O<sub>2</sub><sup>-</sup>), which could be the product of the oxidation of oxide after giving one electron. The literature has focused mainly on the reduction of oxygen for the formation of superoxide. Hayyaan et al.<sup>38</sup> has studied the generation of superoxide in the ILs 1-butyl-1-methylpyrrolidinium trifluoromethanesulfonate and 1-butyl-2,3-dimethylimidazolium and its stability by dissolving KO<sub>2</sub> in them. It was reported that the generation of O<sub>2</sub><sup>-</sup> happened at  $-1$  V with respect to Ag/AgCl with no oxidation peak being present for both ILs, meaning that the generated superoxide was not stable in these media. The same peak has been observed by Sawyer et al.<sup>39</sup> It was also mentioned that the stability of O<sub>2</sub><sup>-</sup> is greatly dependent upon contaminants present in the ILs and that is why all the CVs were performed in a glovebox under controlled environment. The pH of the solvent is also reported to be a crucial parameter, since a proton source can lead to fast disproportionation of the superoxide species.<sup>38</sup> Weidner et al.<sup>40</sup> reported the generation of superoxide at  $-0.46$  V in respect to Ag/AgCl in 1,2-dimethyl-3-n-butylimidazolium hexafluorophosphate with the presence of oxygen with no existence of an oxidation peak on a GC electrode. This potential is the closest value to the one reported in this Chapter. Sawyer et al.<sup>41</sup> has concluded that the electrode material and the solvent have a great impact on the reversibility and the peak

separation and that the reduction potential of  $O_2/O_2^-$  shifts to more negative values when there is decrease in the solvating properties of the electrolyte.

In order to investigate the generation of superoxide in the DES media, the dissolution of  $KO_2$  in EG:ChCl followed and the UV-Vis spectra are shown in **Figure 4.9**. A single peak is observed at around 279 nm, which is close to the already published values of nm for superoxide in other solvents, which are in the range of 255-275 nm.<sup>38</sup> The use of  $KO_2$  for the localization of superoxide in solution is common in aqueous solutions, where the peak attributed to  $O_2^-$  is at 245 nm in water and 255 in acetonitrile.<sup>42</sup> The existence of a superoxide peak in the spectra obtained in EG:ChCl means that superoxide can be stable in DESs. It would be important in future to examine the lifetime of this species in DESs.

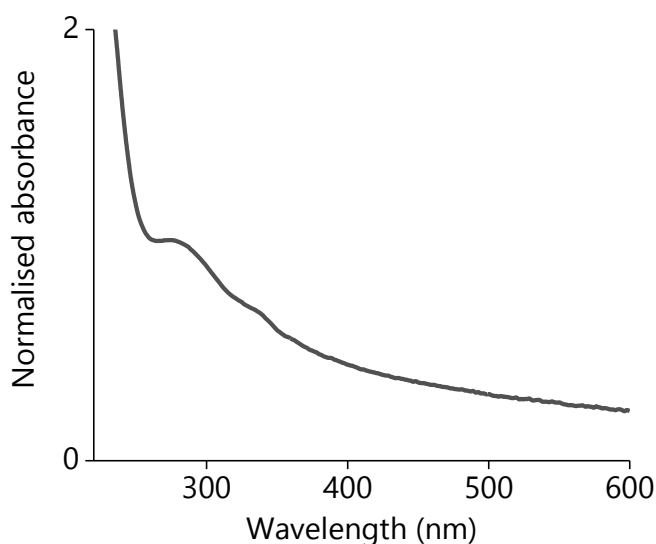


*Figure 4.9: UV-Vis spectra of solution of  $KO_2$  after chemical dissolution in EG:ChCl.*

The fact that the paint casting CVs were carried out in an ambient environment, with a significant water content in the DES (c.a. 1 wt.%), which would decrease the stability of the superoxide. This decreases the likelihood that this peak is related to superoxide generation however electron paramagnetic resonance (EPR) measurements for the solution, would be able to confirm the existence of the radical species of superoxide.<sup>42</sup>

Another explanation of the existence of this peak could also be the oxidation of the Pt WE surface. However, the potential measured here is far enough from the already known potentials of the oxide and hydroxide formation on single crystal Pt electrodes (above 0.8 V vs NHE) and also the shape of the redox couple is different.<sup>43</sup> The Pt surface also is a

well-known catalyst for the electrooxidation of ethylene glycol and other organic solvents and intense investigation has been conducted on this topic.<sup>44</sup> It is worth to mention that the surface area of the Pt WE during paint casting is high (0.32 cm<sup>2</sup>), increasing a possible catalytic activity. The existence of a transition MO also on the surface of the WE could also enhance this catalytic electrooxidation of the component of the DES that might did not react in the mixture. As future work, the paint casting of MOs would be attempted on different WEs such as Au, but the cost of such an electrode is high. Overall, the justification of this peak requires more work. The one conclusion that can be drawn is that this peak is independent on the metal part.

#### **4.2.2 Chronopotentiometry**

Chronopotentiometry measures the potential of an electrode as a function of time and was carried out for the MOs in EG:ChCl, using the paint casting method. A paste of MO was painted on the WE and the changes in voltage were measured while zero current was passing through the cell. This electrochemical test is useful, in order to form predictions about the reactivity of metal compounds when chemically dissolved. The characterization of OCP is typically carried out for the corrosion of metals and for the prediction of the charge/discharge batteries' performance.<sup>45</sup> It is, however, not generally carried out for metal compounds. In general, the OCP measurement after some time of the WE immersion in the electrolyte, gives useful information about the stability of the WE in a medium.

Al Bassam first employed this method to study the chemical reactivity of iron sulfide minerals.<sup>17</sup> The OCP curves obtained in EG:ChCl were in accordance with the results obtained from the chemical dissolution of the minerals. In the same way, the observation of the OCP after 1 h of the immersion of the MO paste in EG:ChCl showed the stability of the MOs and their tendency to chemically dissolve. When the OCP of the electrode is stable and high, the electrolyte is not able to change the equilibrium established and the material is relatively stable and shows resistance to any corrosion reactions from the electrolyte that is surrounding it. On the other hand, when the OCP changes over time it shows that the material is prone to chemical dissolution in the electrolyte. The change in metal ion concentration in solution with time affects the potential through the Nernst equation.

The OCP curves in EG:ChCl of the paint casted MOs are shown in **Figure 4.10**. Two groups of MOs are observed that behave differently. Firstly, the OCP curves for Fe<sub>3</sub>O<sub>4</sub>, Co<sub>3</sub>O<sub>4</sub> and NiO seem to stay stable even after 1 h in EG:ChCl, which means that they have no tendency to chemically dissolve. On the other hand, the curves for CuO, Cu<sub>2</sub>O, ZnO and PbO all show a decrease in potential with time. Thus, these MOs show a more unstable behaviour in EG:ChCl and would predict higher chemical solubility, which confirms the chemically reactivity already be shown in Chapter 3.

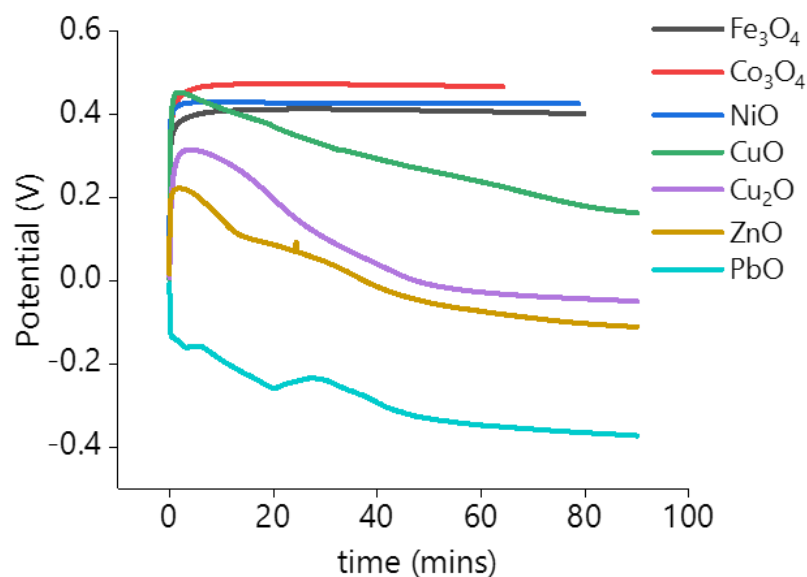


*Figure 4.10: Open circuit potential of metal oxides paint casted in EG:ChCl, with a 0.32 cm<sup>2</sup> Pt flag WE, a Pt flag CE and an Ag/AgCl (0.1 M in EG:ChCl) RE.*

This is a positive result for the paint casting method, because it means that it can be used for the characterization of metal compounds or minerals in a specific lixiviant, predicting their affinity to dissolve in it.

#### 4.2.3 Chronocoulometry

Chronocoulometry measures the charge passed through an electrode as a function of time and gives a measure of process kinetics. Chronocoulometry was used with the paint casting method to investigate the rate of electrochemical dissolution of MOs. In the same way as for the voltammetry, pastes of MOs ( $\approx 13$  mg) were painted on the WE. However, at this stage a fixed potential of 1.2 V was applied to the cell for 30 mins, with the electrochemical test occurring at 50 °C, in order to directly compare the results with the bulk anodic dissolution, which will be discussed later. This process was again firstly

tested by Al Bassam<sup>17</sup> that studied the charge passed at a fixed potential and time for different iron sulfide and arsenide minerals.

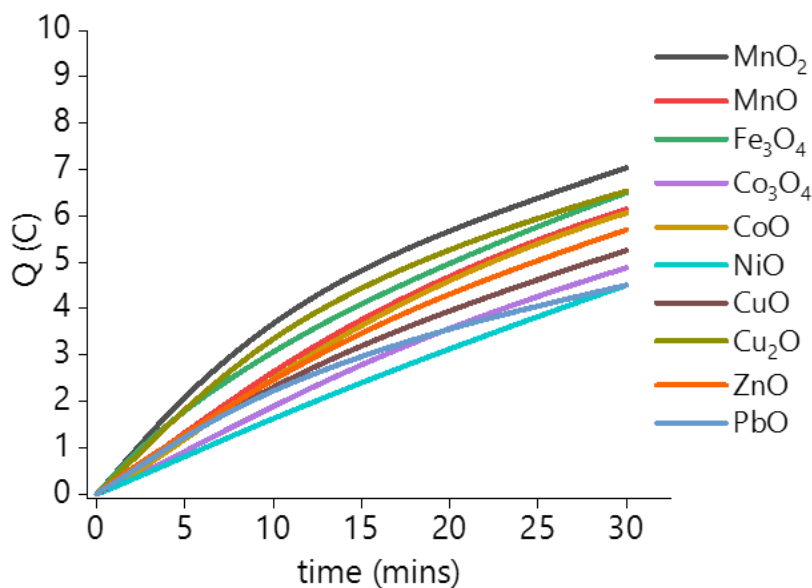


Figure 4.11: Chronocoulometric plots for paint casted metal oxides in EG:ChCl

In **Figure 4.11** the charge passed in the fixed time of 30 mins during the chronocoulometric study for the paint casted MOs, is shown. The results for Fe<sub>2</sub>O<sub>3</sub> are not presented, because its lower density rendered the use of 13 mg of powder on the WE very difficult. The MOs investigated did not show very large discrepancies in the rate of electrochemical dissolution in EG:ChCl. The highest charge passed was reported for MnO<sub>2</sub> with 7 C followed by Fe<sub>3</sub>O<sub>4</sub> with 6.5 C, while the slowest rate was observed for NiO and PbO with 4.5 C. However, the difference between the highest and lowest charge passed is only 2.5 C. Bevan also studied the chronocoulometry of different copper chalcogenides.<sup>16</sup> In that report the highest and lowest charge were reported for Cu<sub>2</sub>Te and Cu<sub>2</sub>Se, respectively, and the difference between the two copper chalcogenides was as high as 17 C. In the case of iron sulfide and arsenide minerals tested by Al Bassam, the highest rate was observed for marcasite, which is the orthorhombic structure of pyrite (FeS<sub>2</sub>), and the lowest charge for loellingite (FeAs<sub>2</sub>) with a difference of 5 C.<sup>17</sup>

In both these previous studies, it was assumed that differences in the electrochemical rate were due to the diverse band gaps of the metal compounds. The hypothesis here lies on the fact that the band gap of MOs will affect the ease of injection or extraction of electrons from the bulk material and hence the rate of dissolution.

In general, band gaps can be used as a tool to predict the conductivity and the electrochemical reactivity of solid compounds. **Figure 4.12** shows a schematic representation of the band gap. A metal compound with a large band gap behaves as an insulator, with the insulating properties coming from the fact that the excitation of the valence electrons towards the conduction band is energetically difficult resulting in compounds that are chemically inert. On the other side, metals are electrical conductors, since the valence and conduction bands are overlapping. The intermediate compounds called semiconductors show a lower band gap than the insulators, but the excitation of the electrons from the valence band is not as energetically favoured as for the conductors. The electrons move from the valence band (highest occupied molecular orbital-HOMO) to the conduction band (lowest unoccupied molecular orbital-LUMO), but the ease of this move is dependent upon the gap between the two orbitals, hence the band gap. When voltage is applied to semiconducting materials, then the valence electrons are excited and generate current, which would then result to the oxidation and dissolution of the material.

In **Table 4.2** the band gap of the MOs is given. There are transition MOs that behave as semiconductors such as  $\text{Fe}_3\text{O}_4$ , for which there are references of metallic behaviour with very low band gap of 0.2 eV.<sup>46</sup> In addition,  $\text{Cu}_2\text{O}$  and  $\text{CuO}$  are well-known p-type semiconductors, and the former was used in the first semiconductor material in storage devices.<sup>47-49</sup> On the other hand, metal oxides such as  $\text{ZnO}$  behaves as an insulator with a wide band gap.<sup>47</sup>

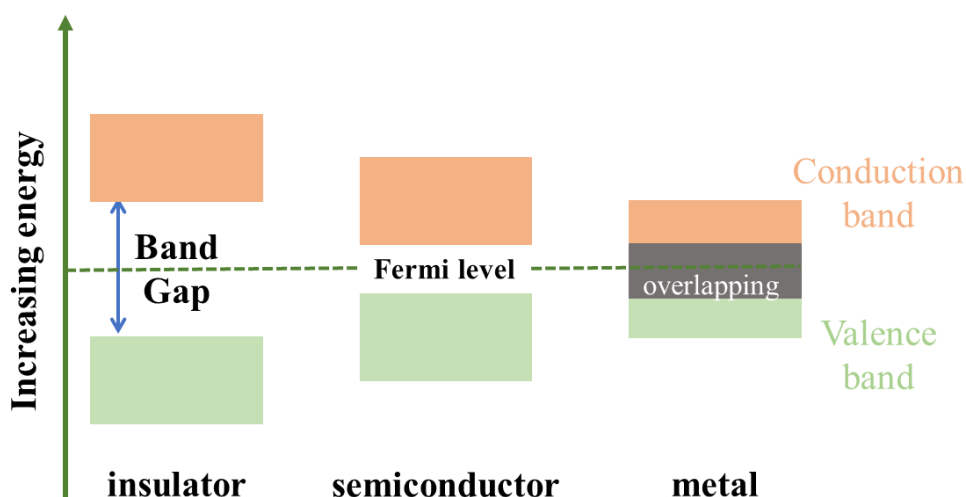


*Figure 4.12: Schematic representation of band gap*

However, there are transition MOs such as MnO, CoO and NiO with partially filled d-shells which behave as Mott insulators.<sup>50</sup> Mott insulators are materials that should be conductors of electricity if considered using conventional band theory, due to an odd number of electrons per unit cell, however in reality they behave as insulators, due to correlation effects such as electron-electron repulsions and magnetic moments formed in the solid.<sup>51</sup> This was first observed and reported by de Boer and Verwey in 1937.<sup>47</sup> Then Mott justified this behaviour by interactions between electrons and the magnetic moments that are formed in the solid from the attempt of electrons to avoid each other in order to minimise their Coulomb repulsion.<sup>52, 53</sup>

*Table 4.2: Band gap of metal oxides under investigation*

<b>Metal Oxide</b>	<b>Band Gap (eV)</b>
<b>MnO<sub>2</sub></b>	1.33 <sup>54</sup>
<b>MnO</b>	3.5 <sup>55</sup>
<b>Fe<sub>3</sub>O<sub>4</sub></b>	0.2 <sup>46</sup>
<b>Co<sub>3</sub>O<sub>4</sub></b>	2.4 <sup>55</sup>
<b>CoO</b>	3.3 <sup>55</sup>
<b>NiO</b>	3.5 <sup>55</sup>
<b>CuO</b>	1.6 <sup>55</sup>
<b>Cu<sub>2</sub>O</b>	2.2 <sup>55</sup>
<b>ZnO</b>	3.37 <sup>56</sup>
<b>PbO</b>	3.21 <sup>57</sup>

As for the previous studies, the charge passed was correlated with the band gap of the MOs, as illustrated in **Figure 4.13**. There is a general decrease in charge passed with increasing band gap i.e. the more conducting oxides are more easily oxidised than the more insulating oxides.

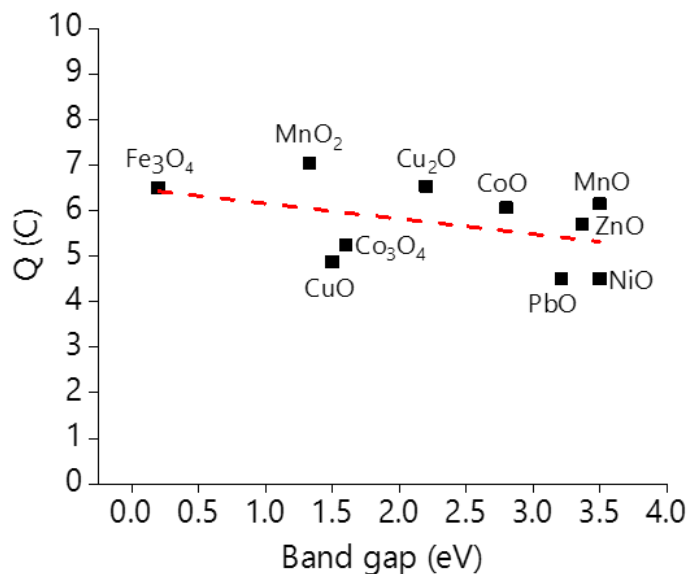


Figure 4.13: Effect of the band gap of metal oxides on the charge passed during chronocoulometry.

Most MOs comply to the downward trend, but the effect of the band gap is not as noteworthy as in the case of copper chalcogenides studied by Bevan, even though the difference in the band gap was maybe smaller for some compounds.<sup>16</sup> This fact may provide an extra support that the electrochemical dissolution of metal oxides in EG:ChCl follows a similar mechanism, as it will be described later. The discrepancy may also be in the band gap data as different methods and different samples will produce different values.

### 4.3 Bulk anodic dissolution of MOs

Bulk electrolysis enables the concentration of metal dissolving in solution to be quantified. It also enables experiments which demonstrate the ability to recover the metal in a pure state. The idea of the paste casting of MOs on the WE was employed again with a different configuration. In Chapter 2 (Figure 2.7) the cell of the electrochemical bulk dissolution of MOs was presented. In this cell two iridium oxide coated titanium mesh electrodes were used as the anode and cathode. The oxidative dissolution of a MO slurry was examined by applying a constant voltage of 2.7 V between the two electrodes for 48 h at 50 °C and at the same solid: liquid ratio as for the chemical dissolution in Chapter 3 was used, in order to have direct comparison.

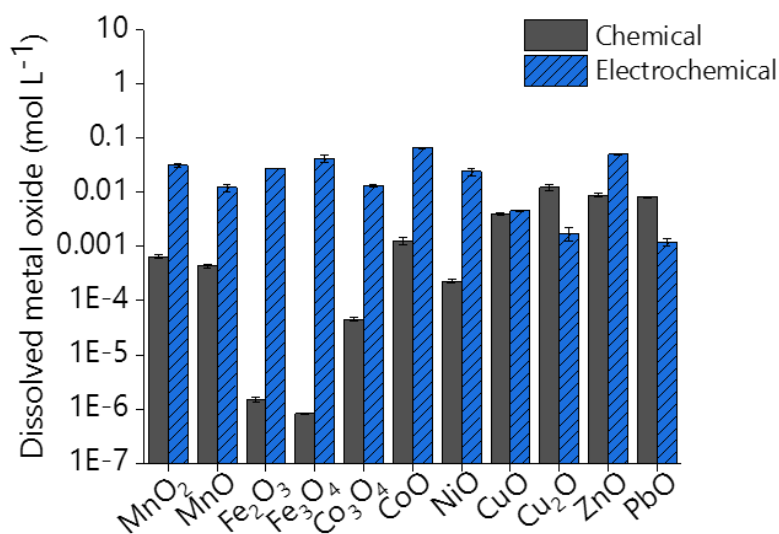
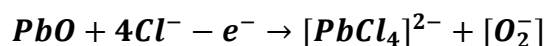


Figure 4.14: Comparison of chemical and electrochemical dissolution of metal oxides in EG:ChCl. Conditions: Conditions for electrochemical dissolution:  $T = 50\text{ }^{\circ}\text{C}$ ,  $t = 48\text{h}$ ,  $L:S=30$ , and constant  $V = 2.7\text{ V}$

In **Figure 4.14**, the concentrations of the dissolved MOs in EG:ChCl are shown and compared with the chemical dissolution in the same solvent, which was discussed in Chapter 3. It is clear that for most MOs, except from Cu<sub>2</sub>O and PbO, the electrochemical solubilities are in most cases significantly higher than the chemical solubility. This shows that in EG:ChCl, which as mentioned before is a poor solvent for MOs, enhancement of the dissolution can occur by electrochemical oxidation. It should be noted that Chapter 3 shows that dissolution is mass transport limited and the experiments carried out in this chapter are unstirred, which probably accounts for a lower possible electrochemical dissolution of MOs.

This enhancement is extremely noticeable for Fe<sub>2</sub>O<sub>3</sub>, Fe<sub>3</sub>O<sub>4</sub>, Co<sub>3</sub>O<sub>4</sub> and NiO, for which the electrochemical dissolution provided 18510, 51800, 292 and 106 times higher dissolution of the respective MOs in EG:ChCl than straight chemical dissolution. The much higher electrochemical dissolution for Fe<sub>3</sub>O<sub>4</sub> could be attributed to its low band gap enabling higher electrical conductivity.

The oxidative dissolution of MOs in EG:ChCl is assumed to happen due to the oxidation of oxide resulting in reactive superoxide species on the surface of the bulk MO. A proposed reaction would be the one below **Equation 4.2**, for PbO for example.



The oxide ( $O^{2-}$ ) can give one electron and be oxidised to the radical superoxide species with the form of  $O_2^-$ , in which the oxidation state is  $-1/2$ . A second oxidation step could be the oxidation of superoxide to oxygen gas ( $O_2$ ). The assumption that the driving force of the electrochemical dissolution is the oxidation of the non-metal part of the MO can be drawn because many of the metal oxides are either in their highest oxidation state or do not have another oxidation state e.g. ZnO. The metal cannot lose any further electrons, hence cannot be oxidised. In addition to that, Bevan and Al Bassam have also reported the oxidation of sulfur to soluble polysulfides to be the driving force for the oxidative dissolution of copper and iron sulfides.<sup>16, 17</sup>

Superoxides have been mostly studied as the product of the oxygen reduction reaction, where oxygen can take one electron and form a superoxide, as previously described.<sup>42</sup> The formation of the radical superoxide by the oxidation of the metal oxide is not that widely studied or understood. One reason for the prevention of the study on superoxides is that they are unstable in most solutions, especially in water, where the solvation is very high and disproportionation occurs at a very fast rate ( $10^7 - 10^{10} M^{-1} s^{-1}$ ) and also they are only stable below 104 °C.<sup>42, 58</sup> It is reported and expected that superoxide radicals with unpaired electrons are highly reactive in many solvents.<sup>42</sup> However, it has a rather high stability in some aprotic solvents like acetone and pyridine and it has lower reactivity in isopropanol.<sup>59</sup> To some extent the stability of the superoxide is not important if the metal-oxygen bond is changed which enables the metal to be released into solution which is clearly happening in bulk electrolysis.

There are several ways of generating superoxide in solution with the most common and easiest method being the electrochemical reduction of oxygen. However, there are other methods such as the dissolution of salts that include the superoxide like  $KO_2$  or  $NaO_2$ , but their affinity to dissolve is low in most organic solvents.<sup>60</sup> It is reported that the addition of tetraalkylammonium salts can increase their solubility levels and the addition of quaternary ammonium salts can increase the stability of electrochemically generated superoxide and also increase its nucleophilicity.<sup>58</sup> This is particularly interesting in this case, since EG:ChCl consists of choline chloride which is a quaternary ammonium salt and hence it can stabilize the superoxide generated during the electrooxidation. As it was shown previously in **Figure 4.9**, the solution of  $KO_2$  in EG:ChCl gave a peak in its UV-

Vis spectra similar to the one expected from the literature in organic solvents, so a superoxide can indeed be stable in a DES.

Another reported method to produce superoxide, is during charge transfer reactions between oxygen and a surface either directly or photoinduced.<sup>42</sup> The adsorption of oxygen species at an oxide surfaces has been reported to be also catalytic for oxidation reactions at solid-liquid interfaces.<sup>61</sup> It was reported that insulating MgO doped with  $\text{Co}^{2+}$  could absorb oxygen resulting in species of  $\text{Co}^{3+} \text{O}_2^-$ , whose formation had a reversible behaviour.<sup>61</sup> However, the electrochemical oxidation of the oxide to the superoxide was not reported. It is proposed here that during the electrochemical oxidation of the MOs, the oxidation of oxide to superoxide occurs, which renders the bonds at the surface of the MO weaker and thus the metals can make complexes with  $\text{Cl}^-$  like during chemical dissolution, but in this case the dissolution is much faster because there is an extra driving force.

In Appendix (**Figure 7.12** and **Figure 7.13**) the UV-Vis spectra and the coloured solutions after anodic dissolution are presented and compared with the ones obtained from chemical dissolution to investigate whether there were changes in the speciation of the metal during the different processes. The change in the intensity of the colour of  $\text{Fe}_3\text{O}_4$ ,  $\text{Fe}_2\text{O}_3$  and  $\text{NiO}$  is greatly noticeable after electrochemical dissolution, a fact that is in agreement with the concentrations of the metals. For the rest of the MOs the colour turned to darker blue in the case of  $\text{Co}_3\text{O}_4$  and  $\text{CoO}$  and darker yellow for  $\text{CuO}$  and  $\text{Cu}_2\text{O}$ .

As for the speciation of the metals in solution, it is observed from the UV-Vis spectra that the dissolution of  $\text{MnO}_2$ ,  $\text{MnO}$ ,  $\text{Co}_3\text{O}_4$ ,  $\text{CoO}$ ,  $\text{CuO}$ ,  $\text{Cu}_2\text{O}$  and  $\text{PbO}$  resulted in tetrachloro complexes, as discussed in Chapter 3 and the spectra after chemical and electrochemical dissolution in EG:ChCl are essentially identical, with the exception of the Mn oxides for which no peaks were obvious after chemical dissolution. However, the electrochemical dissolution of  $\text{NiO}$ , as for the chemical dissolution, did not lead to tetrachloro complexes but instead it resulted in the “green apple” coloured solution that Hartley analysed with EXAFS and showed  $\text{Ni}(\text{EG})_3^{2+}$  to be the main species present.<sup>62</sup>

In the case of  $\text{Fe}_3\text{O}_4$ , it is apparent that the solution after anodic dissolution does not show the typical three peaks spectra of  $[\text{FeCl}_4]^{2-}$ . Instead it shows a peak at  $\approx 303 \text{ nm}$  and the colour is dark brown rather than yellow. The same peak has been reported by Al Bassam for the solution formed from the anodic dissolution of pyrrhotite ( $\text{Fe}_{(1-x)}\text{S}$ ) in EG:ChCl,

for which it was suggested that Fe had formed complexes with the oxygen of the HBD and also a same peak has already reported for an aqueous solution containing glycine after oxidative dissolution of pyrrhotite.<sup>17, 63</sup> In aqueous solution, it was reported that the glycine was absorbed at the oxidised surface and formed a species with Fe<sup>3+</sup>. One possible reason for that is the fact that Fe and Ni are highly oxophilic, so they are highly dependent upon the HBD.<sup>64</sup> For Fe<sub>2</sub>O<sub>3</sub> no distinctive peaks are observed in the UV-Vis spectra, while the colour of the solution is identical with the one of the anodically dissolved pyrrhotite.

From **Figure 4.14** it is observed that the concentrations of dissolved Cu<sub>2</sub>O and PbO after electrochemical dissolution were lower than after chemical dissolution and for CuO the concentrations were at the same level. This happened because during the anodic dissolution of these oxides Cu and Pb were deposited on the cathode. As seen in Appendix (**Figure 7.14**) a thick grey deposit was formed during PbO anodic dissolution that was consisted of 46 atomic % of Pb and 54 atomic % of oxygen and a typical brown colour deposit for Cu<sub>2</sub>O with 71 atomic % of Cu and 23 atomic % of oxygen. Similar results were obtained for CuO. This is an interesting result, because it means that from a solid MO slurry Cu and Pb can be dissolved, form tetrachloro complexes and then directly deposit in a metallic form as the SEM and EDX results suggested. In some repeated experiments deposition of Mn from MnO<sub>2</sub> and MnO also occurred during electrochemical oxidation, for which deposits the EDX analysis reported around 11 atomic % of Mn and 87 atomic % oxygen. This positive result was further investigated by employing another type of cell, which will be discussed later.

What is worth mentioning as well is the lack of selectivity of this process. All MOs dissolve to roughly the same concentration in EG:ChCl, reinforcing the statement that their dissolution is driven by the reaction of oxide and not the metal and the slight differences between them result from kinetic factors due probably to their conductivity. To put a perspective on the actual efficiency of the electrochemical dissolution, the comparison with the concentrations derived from the chemical dissolution in EG:ChCl with 0.1 mol L<sup>-1</sup> TFSA was very crucial and given in **Figure 4.15**.

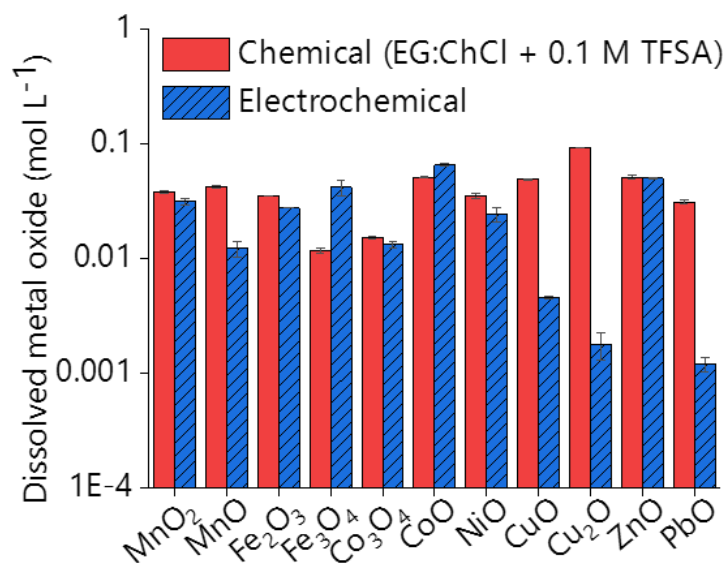


Figure 4.15: Comparison of concentrations of dissolved metal oxides after chemical dissolution in EG:ChCl with addition of 0.1 mol L<sup>-1</sup> TFSA and electrochemical dissolution in EG:ChCl. Conditions for electrochemical dissolution:  $T = 50\text{ }^{\circ}\text{C}$ ,  $t = 48\text{h}$ ,  $L:S=30$ , and constant  $V = 2.7\text{ V}$

It is observed that except for Fe<sub>3</sub>O<sub>4</sub> and CoO, all the rest of MOs show higher concentrations after chemical dissolution in the acidic EG:ChCl. One possible reason for that apart from the high affinity of MOs to dissolve in acidic environments, is the fact that the anodic dissolution occurred under static conditions. Al Bassam has previously shown that the anodic dissolution of mineral slurries in EG:ChCl is hindered due to passivation of the surface when no stirring exists.<sup>17</sup> For that reason, another type of cell was designed in which the anode was slowly stirred by placing the digestion cell on an orbital shaker and maintain both of the electrodes at a fixed position.<sup>17</sup> It was also suggested that the kinetics of dissolution were diffusion controlled.

For that reason, kinetic studies of selected MOs, whose kinetics were studied also for their chemical dissolution in EG:ChCl are presented in **Figure 4.16**.

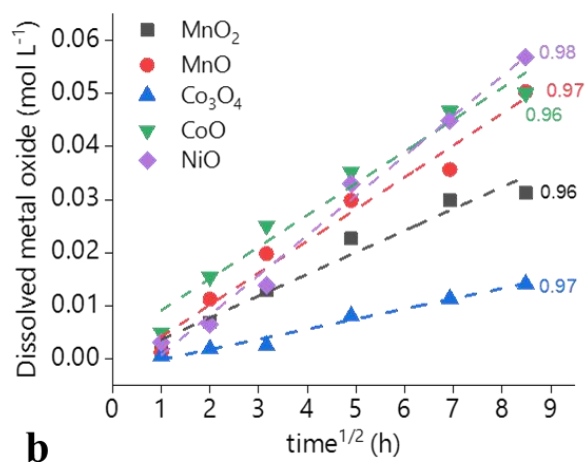
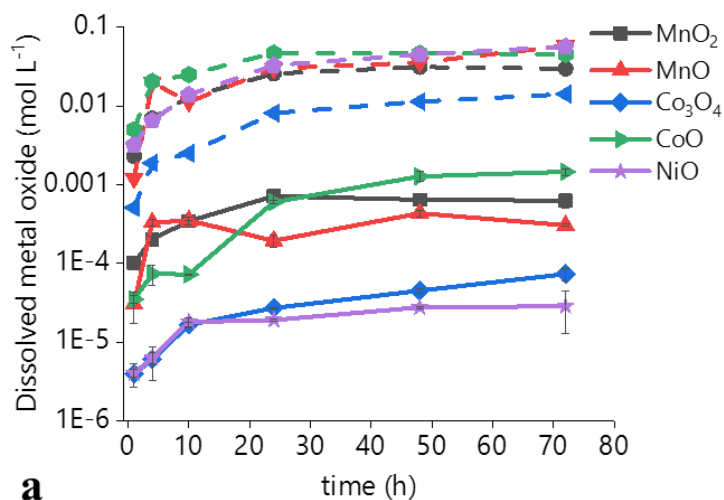


Figure 4.16: a) Kinetic studies of selected MOs after electrochemical dissolution (dashed lines) and chemical dissolution (solid lines) in EG:ChCl (logarithmic scale).

b) Diffusion model plot of concentration depending on time. Conditions for electrochemical dissolution:  $T = 50\text{ }^{\circ}\text{C}$ ,  $L:S=30$ , and constant  $V = 2.7\text{ V}$

For all MOs investigated the concentration rapidly increases in the first 10<sup>th</sup> h and then very slowly increases until the 24<sup>th</sup> h, after which only very small dissolution occurs due to passivation of the electrode surface. The passivation is justified from the static conditions of dissolution and so the results are in accordance for the ones of Al Bassam.<sup>17</sup>

The diffusion model<sup>65</sup> shown in **Equation 4.3** was used on the kinetic data,

$$C = C_o + 2k_p t^{1/2} \quad \text{Equation 4.3}$$

where  $C$  is the concentration of dissolved MO,  $t$  is the time of reaction,  $K_p$  is the reaction rate constant ( $\text{M s}^{-1/2}$ ).

It is observed from **Figure 4.16b**, that for all MOs the  $R^2$  of their trend is rather higher close to 0.99 so it can be concluded that the electrochemical dissolution is diffusion controlled.

#### **4.4 Bulk anodic deposition**

As mentioned in the previous section, the electrochemical dissolution of MOs provided enhanced dissolution in EG:ChCl, with all metals, except Fe and Ni, forming tetrachloro complexes. It was also observed that during the anodic dissolution of CuO, Cu<sub>2</sub>O and PbO the metals were first dissolved and then deposited on the cathode. A separated cell presented in Chapter 2 (Figure 2.8) was used. In the anodic compartment, the MOs are dissolved electrochemically and the metal tetrachloro species or metal-glycolate species diffuse through the filter paper to the cathodic compartment where they are electrodeposited on a Ni plate. Al Bassam reported that the use of a filter paper hinders the diffusion of the metal species, but this study is only a preliminary attempt to see if such a cell would work on MOs and no optimisation has occurred.<sup>17</sup>

In **Figure 4.17**, the masses of the deposits on the Ni plate after the bulk electrolysis of the different MOs are presented. As expected, CuO and Cu<sub>2</sub>O showed the higher amount of deposition, which relates well with the results obtained by Spathariotis for the electrodeposition of Cu from the solution of CuCl<sub>2</sub> in EG:ChCl.<sup>32</sup> Copper has the most positive reduction potential and does not passivate through reaction with the DES. Abbott reported that Cu can be deposited easily and with high current efficiency, forming bright deposits when the concentration of the Cu species are between 0.01-1 mol L<sup>-1</sup>, but when the concentration is lower, then black deposits are formed.<sup>66</sup> With the rest of the MOs, significantly less metal was recovered. This is due to the relatively low metal ion concentration which makes electrodeposition inefficient particularly in unstirred systems.  
<sup>32</sup> Most of these metals also passivate particularly at low metal ion concentrations.<sup>67</sup>

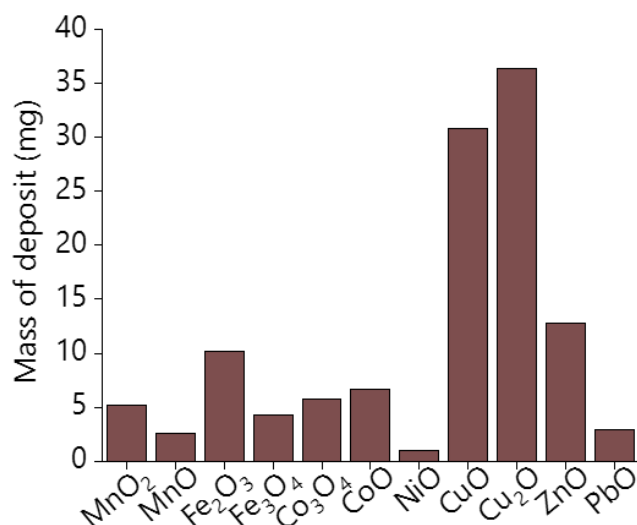


Figure 4.17: Mass of deposit on Ni plate after bulk anodic electrolysis of metal oxides in EG:ChCl. Conditions:  $T = 50\text{ }^{\circ}\text{C}$ ,  $L:S=30$ , and constant  $V = 2.5\text{ V}$

In Appendix (**Table 7.3**), the plates after the anodic deposition of metals on a Ni plate are presented. It is observed, that for CuO and Cu<sub>2</sub>O bright deposits are obtained, and EDX analysis showed that pure copper is deposited with negligible amount of oxygen. These results are in accordance with the report from Bevan who carried out analogous experiments using CuS and Cu<sub>2</sub>S.<sup>16</sup> For PbO and ZnO, pure metallic deposits were also observed on the Ni plate with negligible amounts of oxygen due to the formation of an oxide layer from the atmosphere, agreeing with the results previously obtained for PbS.<sup>16</sup> Also, these results are in accordance with the reported data from Spatharotis, that observed compact deposits of pure metals from the deposition of Cu and Pb from solutions of their chlorides.<sup>32</sup> It can be also observed that larger amounts of metal with higher purity were obtained from the MOs that have the most ionic character and dissolve better in EG:ChCl. For the rest of the MOs, poor quality, non-adherent, flaky and sometimes cracked deposits are observed.<sup>32</sup>

This investigation was not focused on the optimisation of the electrodeposition process, since the recovery is not the aim of this thesis. However, the examination of the bulk anodic electrolysis of MOs is a field that is relatively novel, and it was attempted to show that even for MOs that are not as conductive as metal sulfides, the anodic dissolution and subsequent deposition is possible. This method actually would be beneficial for the processing of oxide mixtures and especially those with a high value. An interesting result was obtained from Bevan, where the selective recovery of Cu from Fe from the mineral

of chalcopyrite ( $\text{CuFeS}_2$ ) was obtained using the same logic but with a more sophisticated designed cell in EG:ChCl.<sup>18</sup>

## 4.5 Conclusions

In this chapter the electrochemical dissolution of MOs was studied in DESs. The enhancement of the rate of the dissolution in a poor lixiviant by employing anodic dissolution of MOs is a novel field. It is shown that all ten metal oxides studied could be electrochemically oxidised and it was postulated that like the metal sulfide, selenide and telluride studies previously carried out in our group, dissolution occurred due to oxidation of the chalcogenide. It was suggested that oxide could be oxidise to superoxide, but further studies are required to fully understand the mechanism.

Firstly, the paint casting method was employed for the characterization of the reactivity of the pastes of MOs in EG:ChCl and the investigation of their electrochemical response during cyclic voltammetry. It was reported that the redox peaks of  $\text{Fe}^{\text{III}}/\text{Fe}^{\text{II}}$  from  $\text{Fe}_2\text{O}_3$  and  $\text{Fe}_3\text{O}_4$ ,  $\text{Cu}^{\text{II}}/\text{Cu}^{\text{I}}$  and  $\text{Cu}^{\text{I}}/\text{Cu}^0$  from  $\text{CuO}$  and  $\text{Cu}_2\text{O}$  and also the  $\text{Pb}^0$  and the stripping peaks of  $\text{Pb}$  and  $\text{Pb-Pt}$  alloy were all observed during the CV of the pastes. For all the other MOs, one common peak was observed as in the case of iron oxides as well, which can be related to the redox peaks of  $\text{O}^{2-}/\text{O}_2^-$  species on the surface or the redox activity of the DES catalysed by the Pt surface and the presence of the transition MOs. Of course, more spectroscopic evaluation are needed like EPR for the investigation of the possible generation of superoxide.

The method of paint casting was also used as a preliminary tool to examine whether the MOs can be dissolved by applying 1.2 V for a fixed time in EG:ChCl and the rate of their dissolution was correlated with their band gaps. It was reported that indeed a higher band gap would lead to a lower dissolution and vice versa. However, the differences between the values of charge passed between the MOs were rather small, meaning the effect of band gap was not great, as in the case of copper and iron sulfides, previously reported. The chronopotentiometry of MOs was also tested using the paint casting method and the results obtained were in perfect agreement with the results from Chapter 3, in the sense that the OCP of  $\text{Cu}_2\text{O}$ ,  $\text{PbO}$  and  $\text{ZnO}$  was lower than from the rest of MOs and it was decreasing over time, which meant that they had a higher affinity for chemical dissolution in EG:ChCl as shown in Chapter 3. Thus, paint casting can actually work for the electrochemical characterisation of MOs and different electrochemical techniques like

CV, chronocoulometry and chronopotentiometry can provide with accurate results in DESs.

One of the most interesting aspects of this chapter was the investigation of an alternative way of dissolving MOs by employing an electrochemical anodic dissolution of MOs slurries. It was reported that the dissolution in EG:ChCl, which in Chapter 3 was concluded that it is a poor lixiviant and it can provide higher concentrations of dissolved MOs only when its acidity is increased or with the addition of a complexing agent, could be enhanced by applying a constant voltage of 2.7 V in the system. This enhancement was for some oxides exceptionally great, for example for  $\text{Fe}_2\text{O}_3$  and  $\text{Fe}_3\text{O}_4$  it provided more than 10000 times fold higher concentration of dissolved metals after electrochemical dissolution compared to just chemical and for other like  $\text{Co}_3\text{O}_4$  and NiO more than 100 times. The driving force of this dissolution could not be the oxidation of the metal, since most metals were in their highest oxidation state so it was proposed that the driving force was the oxidation of oxide resulting in the formation of superoxide radical species that would be more reactive and could weaken the bond of the metal-oxide. The rate of the dissolution was also proven to be diffusion limited. The enhancement of the electrochemical dissolution was at the same levels as the enhancement from the addition of 0.1 M TFSA, which was discussed in Chapter 3. However, all MOs were dissolved in the same levels and no selectivity can be obtained from this process, enhancing the conclusion that the anodic dissolution is not metal dependent but instead it is driven by the reaction of the oxide.

Speciation studies showed that with the exception of iron oxides, the rest of them did not show any difference speciation from that formed by chemical dissolution. For iron oxides a specie of iron with oxygen from EG is proposed, which is in agreement with the literature data.

Last but not least, bulk anodic electrolysis of a MO slurry in EG:ChCl enabled samples of pure metal to be recovered on a Ni cathode. These preliminary results showed that this process is feasible in DESs even for insulating MOs like ZnO or NiO and confirmed that all most metal chalcogenides can be electrodisolved.

## 4.6 References

1. Ruiz Puigdollers, A.; Schlexer, P.; Tosoni, S.; Pacchioni, G., Increasing oxide reducibility: the role of metal/oxide interfaces in the formation of oxygen vacancies. *Acs Catalysis* **2017**, 7 (10), 6493-6513.
2. Chiarizia, R.; Horwitz, E., New formulations for iron oxides dissolution. *Hydrometallurgy* **1991**, 27 (3), 339-360.
3. Senanayake, G.; Childs, J.; Akerstrom, B.; Pugaev, D., Reductive acid leaching of laterite and metal oxides—a review with new data for Fe (Ni, Co) OOH and a limonitic ore. *Hydrometallurgy* **2011**, 110 (1-4), 13-32.
4. Grygar, T., Phenomenological kinetics of irreversible electrochemical dissolution of metal-oxide microparticles. *Journal of Solid State Electrochemistry* **1998**, 2 (3), 127-136.
5. Eisele, T.; Gabby, K., Review of reductive leaching of iron by anaerobic bacteria. *Mineral Processing and Extractive Metallurgy Review* **2014**, 35 (2), 75-105.
6. Mahiya, S.; Lofrano, G.; Sharma, S., Heavy metals in water, their adverse health effects and biosorptive removal: A review. *International Journal of Chemistry* **2014**, 3 (1), 132-149.
7. Grygar, T.; Bezdička, P., Electrochemical dissolution of Cr III and Cr IV oxides. *Journal of Solid State Electrochemistry* **1998**, 3 (1), 31-38.
8. Segal, M. G.; Williams, W. J., Kinetics of metal oxide dissolution. Oxidative dissolution of chromium (III) oxide by potassium permanganate. *Journal of the Chemical Society, Faraday Transactions 1: Physical Chemistry in Condensed Phases* **1986**, 82 (10), 3245-3254.
9. Reartes, G. B.; Morando, P. J.; Blesa, M. A.; Hewlett, P. B.; Matijevic, E., Reactivity of chromium oxide in aqueous solutions. 1. Oxidative dissolution. *Chemistry of Materials* **1991**, 3 (6), 1101-1106.
10. Grygar, T.; Jandová, J.; Klímová, Z., Dissolution reactivity of NiO obtained by calcination of pure and contaminated Ni-hydroxides. *Hydrometallurgy* **1999**, 52 (2), 137-149.
11. Yohe, D.; Riga, A.; Greef, R.; Yeager, E., Electrochemical properties of nickel oxide. *Electrochimica Acta* **1968**, 13 (6), 1351-1358.
12. Filippov, A., Oxidation of Uranium Dioxide with Manganates and Permanganates in Carbonate Solutions. *Radiochemistry* **2001**, 43 (3), 259-264.

13. Peper, S. M.; Brodnax, L. F.; Field, S. E.; Zehnder, R. A.; Valdez, S. N.; Runde, W. H., Kinetic study of the oxidative dissolution of UO<sub>2</sub> in aqueous carbonate media. *Industrial & Engineering Chemistry Research* **2004**, *43* (26), 8188-8193.
14. Wang, Z.; Xiong, W.; Tebo, B. M.; Giammar, D. E., Oxidative UO<sub>2</sub> dissolution induced by soluble Mn (III). *Environmental science & technology* **2014**, *48* (1), 289-298.
15. Mills, A.; Giddings, S.; Patel, I., Corrosion of ruthenium dioxide hydrate by Ce IV ions and other oxidants. *Journal of the Chemical Society, Faraday Transactions 1: Physical Chemistry in Condensed Phases* **1987**, *83* (8), 2317-2329.
16. Bevan, F. R. Electrochemical Processing of Metal Chalcogenides in Deep Eutectic Solvents. PhD thesis, University of Leicester, **2019**.
17. Al-Bassam, A. Z. M. H. Mineral processing using deep eutectic solvents. PhD thesis, University of Leicester, **2018**.
18. Anggara, S.; Bevan, F.; Harris, R. C.; Hartley, J.; Frisch, G.; Jenkin, G.; Abbott, A. P., Direct Extraction of Copper from Copper Sulfide Minerals using Deep Eutectic Solvents. *Green Chemistry* **2019**, *21* (23), 6502-6512.
19. Sander, M.; Hofstetter, T. B.; Gorski, C. A., Electrochemical analyses of redox-active iron minerals: A review of nonmediated and mediated approaches. *Environmental Science & Technology* **2015**, *49* (10), 5862-5878.
20. Abbott, A. P.; Al-Bassam, A. Z.; Goddard, A.; Harris, R. C.; Jenkin, G. R.; Nisbet, F. J.; Wieland, M., Dissolution of pyrite and other Fe–S–As minerals using deep eutectic solvents. *Green Chemistry* **2017**, *19* (9), 2225-2233.
21. Grygar, T.; Marken, F.; Schröder, U.; Scholz, F., Electrochemical analysis of solids. A review. *Collection of Czechoslovak Chemical Communications* **2002**, *67* (2), 163-208.
22. Adams, R. N., Carbon paste electrodes. *Analytical Chemistry* **1958**, *30* (9), 1576-1576.
23. Kuwana, T.; French, W., Electrooxidation or Reduction of Organic Compounds into Aqueous Solutions Using Carbon Paste Electrode. *Analytical Chemistry* **1964**, *36* (1), 241-242.
24. Bertocello, P., Electrochemistry of Polymeric Thin Films Prepared by Langmuir-Blodgett Technique. *Progress in Electrochemistry Research* **2005**, 67.
25. Scholz, F.; Nitschke, L.; Henrion, G., A new procedure for fast electrochemical analysis of solid materials. *Naturwissenschaften* **1989**, *76* (2), 71-72.

26. Abbott, A. P.; Bevan, F.; Baeuerle, M.; Harris, R. C.; Jenkin, G. R., Paint casting: A facile method of studying mineral electrochemistry. *Electrochemistry Communications* **2017**, *76*, 20-23.
27. Liao, Y.-S.; Chen, P.-Y.; Sun, I.-W., Electrochemical study and recovery of Pb using 1: 2 choline chloride/urea deep eutectic solvent: A variety of Pb species PbSO<sub>4</sub>, PbO<sub>2</sub>, and PbO exhibits the analogous thermodynamic behavior. *Electrochimica Acta* **2016**, *214*, 265-275.
28. Manan, N. S.; Aldous, L.; Alias, Y.; Murray, P.; Yellowlees, L. J.; Lagunas, M. C.; Hardacre, C., Electrochemistry of sulfur and polysulfides in ionic liquids. *The Journal of Physical Chemistry B* **2011**, *115* (47), 13873-13879.
29. Jin, S., Are metal chalcogenides, nitrides, and phosphides oxygen evolution catalysts or bifunctional catalysts? ACS Publications: **2017**.
30. Kanatharana, P.; Spritzer, M. S., Cyclic voltammetry of the Iron (II)-Iron (III) couple in dimethylformamide. *Analytical Chemistry* **1974**, *46* (7), 958-959.
31. Hartley, J. M. Ionometallurgy: The Processing of Metals Using Ionic Liquids. PhD thesis, University of Leicester, **2016**.
32. Spathariotis, S. Recovery of metals using deep eutectic solvents. PhD thesis, University of Leicester, **2020**.
33. Abrantes, L.; Araujo, L.; Levi, M., Voltammetric studies on copper deposition/dissolution reactions in aqueous chloride solutions. *Minerals Engineering* **1995**, *8* (12), 1467-1475.
34. Abbott, A. P.; Frisch, G.; Hartley, J.; Ryder, K. S., Processing of metals and metal oxides using ionic liquids. *Green Chemistry* **2011**, *13* (3), 471-481.
35. Al-Murshedi, A.; Hartley, J.; Abbott, A.; Ryder, K., Effect of water on the electrodeposition of copper on nickel in deep eutectic solvents. *Transactions of the IMF* **2019**, *97* (6), 321-329.
36. Ru, J.; Hua, Y.; Wang, D.; Xu, C.; Li, J.; Li, Y.; Zhou, Z.; Gong, K., Mechanistic insight of in situ electrochemical reduction of solid PbO to lead in ChCl-EG deep eutectic solvent. *Electrochimica Acta* **2015**, *186*, 455-464.
37. Stodd, S. Lanthanide based deep eutectic solvents. PhD thesis, University of Leicester, **2018**.
38. Hayyan, M.; Mjalli, F. S.; AlNashef, I. M.; Hashim, M. A., Stability and kinetics of generated superoxide ion in trifluoromethanesulfonate anion-based ionic liquids. *International Journal of Electrochemical Science*, **2012**, *7*, 9658-9667.

39. Sawyer, D. T.; Roberts Jr, J. L., Electrochemistry of oxygen and superoxide ion in dimethylsulfoxide at platinum, gold and mercury electrodes. *Journal of Electroanalytical Chemistry (1959)* **1966**, 12 (2), 90-101.
40. AlNashef, I. M.; Leonard, M. L.; Kittle, M. C.; Matthews, M. A.; Weidner, J. W., Electrochemical generation of superoxide in room-temperature ionic liquids. *Electrochemical and Solid-State Letters* **2001**, 4 (11), D16-D18.
41. Sawyer, D. T.; Sobkowiak, A.; Roberts, J. L., *Electrochemistry for Chemists*. Wiley: **1995**.
42. Hayyan, M.; Hashim, M. A.; AlNashef, I. M., Superoxide ion: generation and chemical implications. *Chemical Reviews* **2016**, 116 (5), 3029-3085.
43. Angerstein-Kozłowska, H.; Conway, B.; Sharp, W., The real condition of electrochemically oxidized platinum surfaces: Part I. Resolution of component processes. *Journal of Electroanalytical Chemistry and Interfacial Electrochemistry* **1973**, 43 (1), 9-36.
44. Mello, G. A.; Fernandes, P. H.; Giz, M. J. d.; Camara, G. A., Ethylene glycol electro-oxidation on platinum-free surfaces: how the composition of PdRuRh surfaces influences the catalysis. *Journal of the Brazilian Chemical Society* **2017**, 28 (6), 1123-1131.
45. Kimura, K. W.; Wilhelm, R.; Besli, M. M.; Kim, S.; Usubelli, C.; Ziegler, J. C.; Klein, R.; Christensen, J.; Gorlin, Y., Interrelationship Between the Open Circuit Potential Curves in a Class of Ni-Rich Cathode Materials. *Journal of The Electrochemical Society* **2020**, 167 (4), 040510.
46. Liu, H.; Di Valentin, C., Band gap in magnetite above Verwey temperature induced by symmetry breaking. *The Journal of Physical Chemistry C* **2017**, 121 (46), 25736-25742.
47. de Boer, J. H.; Verwey, E. J., Semi-conductors with partially and with completely filled 3d-lattice bands. *Proceedings of the Physical Society* **1937**, 49 (4S), 59.
48. Nolan, M.; Elliott, S. D., The p-type conduction mechanism in Cu<sub>2</sub>O: a first principles study. *Physical Chemistry Chemical Physics* **2006**, 8 (45), 5350-5358.
49. Rahnama, A.; Gharagozlou, M., Preparation and properties of semiconductor CuO nanoparticles via a simple precipitation method at different reaction temperatures. *Optical and Quantum Electronics* **2012**, 44 (6-7), 313-322.
50. Lany, S., Semiconducting transition metal oxides. *Journal of Physics: Condensed Matter* **2015**, 27 (28), 283203.

51. Mott, N.; Zinamon, Z., The metal-nonmetal transition. *Reports on Progress in Physics* **1970**, *33* (3), 881.
52. Mott, N. F., The basis of the electron theory of metals, with special reference to the transition metals. *Proceedings of the Physical Society. Section A* **1949**, *62* (7), 416.
53. Roy, S. B., *Mott Insulators*. IOP Publishing: **2019**.
54. LeBlanc, S.; Fogler, H. S., The role of conduction/valence bands and redox potential in accelerated mineral dissolution. *AIChE Journal* **1986**, *32* (10), 1702-1709.
55. Lany, S., Band-structure calculations for the 3 d transition metal oxides in G W. *Physical Review B* **2013**, *87* (8), 085112.
56. Klingshirn, C., The luminescence of ZnO under high one-and two-quantum excitation. *Physica Status Solidi (b)* **1975**, *71* (2), 547-556.
57. Terpstra, H. J.; De Groot, R. A.; Haas, C., Electronic structure of the lead monoxides: Band-structure calculations and photoelectron spectra. *Physical Review B* **1995**, *52* (16), 11690-11697.
58. Moorcroft, M. J.; Hahn, C. E.; Compton, R. G., Electrochemical studies of the anaesthetic agent enflurane (2-chloro-1, 1, 2-trifluoroethyl difluoromethyl ether) in the presence of oxygen: reaction with electrogenerated superoxide. *Journal of Electroanalytical Chemistry* **2003**, *541*, 117-131.
59. Mohammad, M.; Khan, A.; Subhani, M.; Bibi, N.; Ahmad, S.; Saleemi, S., Kinetics and electrochemical studies on superoxide. *Research on Chemical Intermediates* **2001**, *27* (3), 259-267.
60. Merritt, M. V.; Sawyer, D. T., Electrochemical studies of the reactivity of superoxide ion with several alkyl halides in dimethyl sulfoxide. *The Journal of Organic Chemistry* **1970**, *35* (7), 2157-2159.
61. Anpo, M.; Che, M.; Fubini, B.; Garrone, E.; Giamello, E.; Paganini, M. C., Generation of superoxide ions at oxide surfaces. *Topics in Catalysis* **1999**, *8* (3-4), 189.
62. Hartley, J. M.; Ip, C.-M.; Forrest, G. C. H.; Singh, K.; Gurman, S. J.; Ryder, K. S.; Abbott, A. P.; Frisch, G., EXAFS study into the speciation of metal salts dissolved in ionic liquids and deep eutectic solvents. *Inorganic Chemistry* **2014**, *53* (12), 6280-6288.
63. Duinea, M. I.; Sandu, A. M.; Petcu, M. A.; Dăbuleanu, I.; Cârâc, G.; Chiriță, P., Aqueous oxidation of iron monosulfide (FeS) in the presence of glycine. *Journal of Electroanalytical Chemistry* **2017**, *804*, 165-170.

64. Kepp, K. P., A quantitative scale of oxophilicity and thiophilicity. *Inorganic Chemistry* **2016**, *55* (18), 9461-9470.
65. Stumm, W.; Wollast, R., Coordination chemistry of weathering: Kinetics of the surface-controlled dissolution of oxide minerals. *Reviews of Geophysics* **1990**, *28* (1), 53-69.
66. Abbott, A. P.; El Ttaib, K.; Frisch, G.; McKenzie, K. J.; Ryder, K. S., Electrodeposition of copper composites from deep eutectic solvents based on choline chloride. *Physical Chemistry Chemical Physics* **2009**, *11* (21), 4269-4277.
67. Alesary, H. F.; Cihangir, S.; Ballantyne, A. D.; Harris, R. C.; Weston, D. P.; Abbott, A. P.; Ryder, K. S., Influence of additives on the electrodeposition of zinc from a deep eutectic solvent. *Electrochimica Acta* **2019**, *304*, 118-130.

# Chapter 5: Recycling of REEs from spent fluorescent lamps using deep eutectic solvents

5 Chapter.....	172
5.1 Introduction.....	172
5.1.1 Rare earth elements and the importance of their recycling.....	172
5.1.2 Fluorescent lamps and their recycling.....	175
5.1.3 Aims.....	180
5.2 Extraction of REEs from spent fluorescent lamps using solvometallurgy.....	181
5.2.1 Selection of deep eutectic solvent for the extraction of REEs from phosphors.....	181
5.2.2 Optimization of dissolution parameters.....	185
5.2.3 Dissolution of synthetic mixture of phosphors.....	188
5.2.4 Dissolution of real lamp phosphor waste.....	189
5.2.5 Comparison with other hydrometallurgical and solvometallurgical processes.....	192
5.3 Recovery of REEs from lamp phosphor.....	194
5.3.1 Recovery using precipitation with oxalic acid.....	194
5.3.2 Recovery using solvent extraction.....	197
5.4 Conclusions.....	198
5.5 References.....	200

## 5 Chapter

### 5.1 Introduction

Rare earth elements (REEs) contain the series of 15 lanthanides along with yttrium (Y) and scandium (Sc), which all show similar chemical properties and ionic radii.<sup>1</sup> In reality, the term “rare” is mistaken, as these metals are rather abundant in the Earth’s crust and are no more rarer than the platinum group metals, as for example rhodium which is the most rare metal in the Earth’s crust. The issue with the extraction of REEs lies on their costly and complex mining, mainly due to their conjoint occurrence. Their very similar chemical properties render their mining and their later metallurgical extraction processes very intensive, in terms of chemicals and energy required. Thus, alternative sources are needed to be investigated like EoL products, spent batteries or fluorescent lamps. As shown in the Chapter 3, DESs can be selective for the extraction of some metals from their oxides, for which aqueous acidic acids are not able to provide selectivity. Thus, in this Chapter DESs are employed and specific interactions of the HBD is expected to provide selectivity in the extraction of REEs from spent fluorescent lamp phosphors.

#### 5.1.1 Rare earth elements and the importance of their recycling

REEs are divided into two categories. The light REEs (LREEs): lanthanum (La), cerium (Ce), praseodymium (Pr), neodymium (Nd) and samarium (Sm), and the heavy REEs (HREEs): yttrium (Y), europium (Eu), gadolinium (Gd), terbium (Tb), dysprosium (Dy), holmium (Ho), erbium (Er), thulium (Tm), ytterbium (Yb) and lutetium (Lu). The LREEs tend to be more abundant than the heavy REEs (HREEs), as well as the REEs with even atomic number  $Z$  (Oddo – Harkin’s rule).<sup>2</sup> More specifically Ce, La and Nd show the highest crustal abundance while Eu, Tb, Ho, Tm and Lu seem to be the scarcest REEs.<sup>2</sup>

Another problem related to the processing of their ores, apart from the fact that they are co-found in geological deposits, is that they usually exist in non-exploitable concentrations. They are identified in different minerals like silicates, phosphates, carbonates, oxides etc., but never in a pure form.<sup>2</sup> In addition, due to very fast technological changes, a “balance” problem occurs as the supply of individual REEs is not at the same level with the market demand, resulting in an even more complex extraction.<sup>3</sup> Currently, for example, there is high demand for Pr but its extraction requires the co-extraction of Ce and La, which are already abundant and so need to be stockpiled, increasing the cost of mining.

The main minerals of REEs are shown in **Table 5.1**. Monazite and bastnaesite are the main minerals for LREEs as Ce, La and Nd, with bastnaesite being the main source of Ce. There are also occasions where Ce has been substituted by Y in bastnaesite. Monazite is also a significant source of Ce and La, but it consists of higher amounts of Nd, which currently makes it more economically interesting. On the other hand, xenotime is the main source of HREEs like Y, Eu, and Ho etc. As shown in the **Table 5.1**, Europe or UK are definitely not in the mining and refining part of the REEs market, a fact that is more visually clear from the **Figure 5.1** showing the world production of REE oxides. The main REEs producers are China and the USA, followed by other countries like India, Australia, Russia and Malaysia.

*Table 5.1: Main economically processed minerals of REEs*

Mineral	Formula	REE content %	Occurrence
<b>Xenotime</b>	YPO <sub>4</sub>	61	Brazil, California, Malaysia, Norway, Pakistan Sweden
<b>Monazite</b>	(Ce, La, Nd, Th)PO <sub>4</sub>	65	Australia, Brazil, India, USA
<b>Bastnaesite</b>	(Ce, La) (CO <sub>3</sub> )F	75	Australia, Brazil, Canada, China, USA

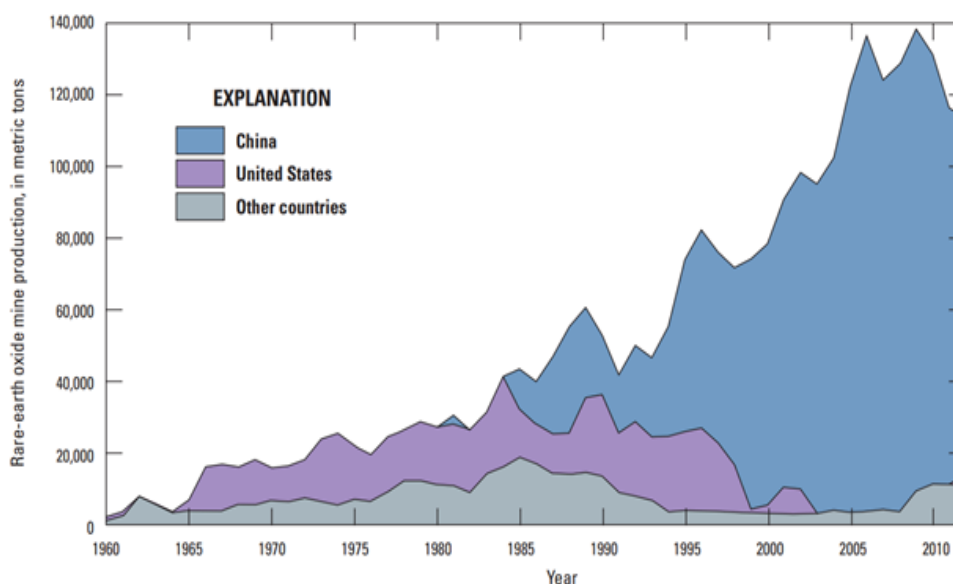


*Figure 5.1: World mine production of rare earth oxides from country, per year (1960-2012).<sup>4</sup>*

REEs are considered as strategic metals for countries that aim to build their future on greener technologies, thus showing high demand.<sup>5</sup> Their employment in emerging low

carbon technologies such as wind turbines, fluorescent lamps, NdFeB permanent magnets, rechargeable NiMH batteries and catalysts, combined with their scarcity in Europe, explains the reason why the European Commission has reported them in the reports of 2011,<sup>6</sup> 2014,<sup>7</sup> and 2017<sup>8</sup> as the most critical raw materials, with the highest supply risk. Moreover, the US Department of Energy (DoE) concluded that the five most critical REEs are Nd, Eu, Tb, Dy and Y in their report of 2011.<sup>9</sup> The projected criticality matrix for the time period of 2015-2025, combining the supply risk and the importance of technological metals, was also measured in the report of DoE and presented in **Figure 5.2**. It is clear that the most critical metals from this report are in complete agreement with the reports of the European Commission.

Currently, the major producer of REEs is China, which possess the 40% of REEs reserves and holds the primacy of their production (> 90%), leading to Europe's great vulnerability to the price changes and embargos upon REEs.<sup>7, 10</sup> The price of REEs is continuously shifting and currently the most expensive REEs are Dy, Pr and Tb, followed by Eu.<sup>11</sup>

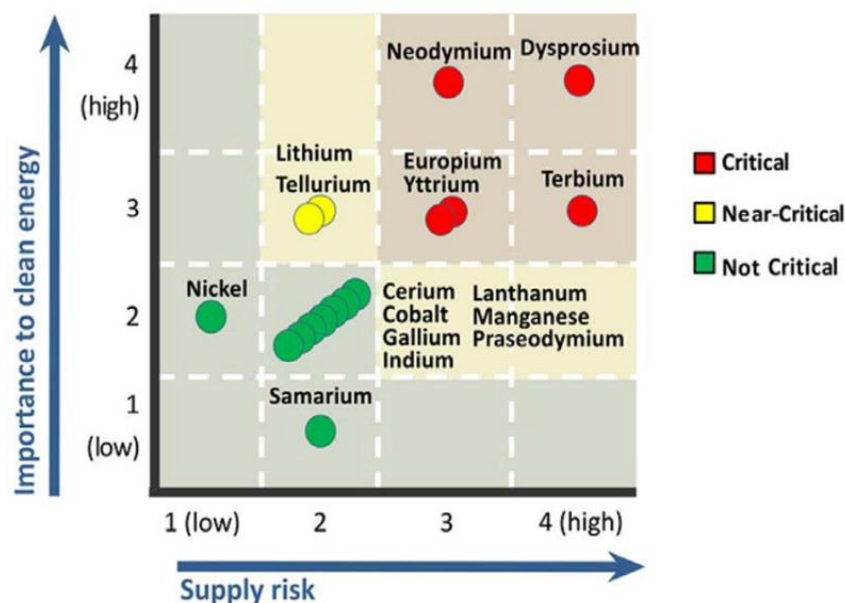
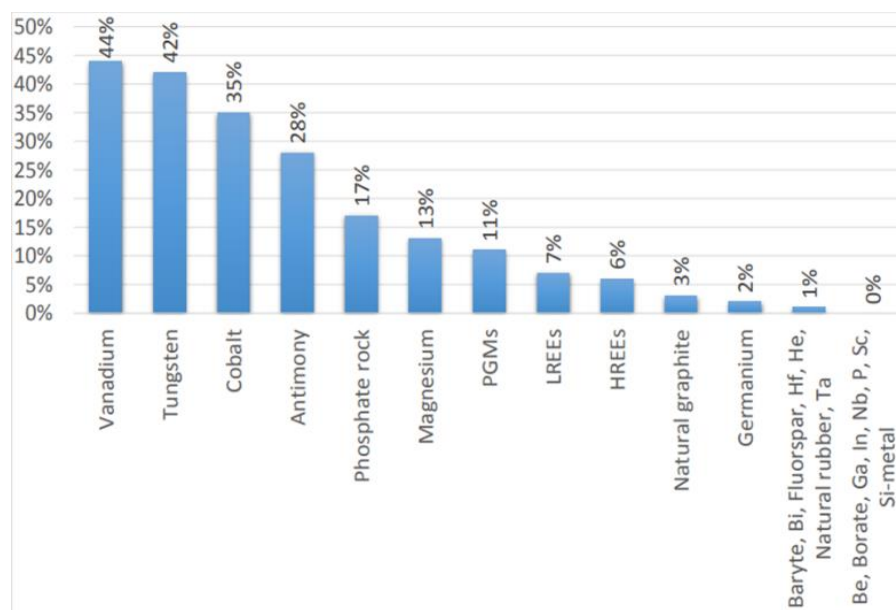


Figure 5.2: Criticality Matrix for the time period 2015-2025.<sup>9</sup>

It is anticipated that demand for REEs will grow even more following the intensified need for development of low carbon technologies. It has been projected that every year the demand for REEs will be increasing by 10%, but this number is just an approximation since the technological improvements cannot always be forecasted accurately.<sup>12</sup> As mentioned before, with the exception of some Scandinavian countries that possess deposits of REEs, UK and Europe are in definite need of seeking alternative sources of

REEs. These sources can be metallurgical slags (e.g. slags from recycling of precious metals from electronic scrap),<sup>13</sup> landfilled residues containing high amounts of REEs (e.g. bauxite residue by product of aluminium production)<sup>14</sup> or EoL products (e.g. fluorescent lamps and NdFeB permanent magnets).<sup>15,16</sup> Although a high amount of materials that can be identified as alternative sources of REEs exists, their recycling rate is still low due to their low toxicity and due to difficulties in selective recycling, as they are usually present in minor concentrations in very complex materials, as shown in **Figure 5.3**. Up until 2017, only 6% of HREEs and 7% of LREEs were recycled from EoL products in Europe, which is a very small number, considering their scarcity.



*Figure 5.3: Contribution of recycling of different technological metals in European metal chain.<sup>8</sup>*

This research work aims to examine the possibility of recycling REEs from EoL fluorescent lamps wastes.

### 5.1.2 Fluorescent lamps and their recycling

Fluorescent lamps have been established many years in the lightning market and have been promoted as a greener and more energy efficient replacement of the common incandescent lamps. In **Figure 5.4**, the inner part of a fluorescent lamp is presented along with its different constituents. Before their recycling, it is crucial to understand how these lamps function.

A fluorescent lamp functions under low pressure and is filled with inert gas like Ar. It simply works by applying a voltage between the two electrodes (cathodes) of the lamp,

resulting in movement of electrons from one end of the lamp towards the other. This electrical energy is transforming the liquid mercury into gaseous atoms, which then collide with electrons or charged atoms inside the tube. These collisions transfer energy to the mercury gas atoms, followed by excitement of their electrons to higher energy levels. Once the mercury gas atoms return back to their stable energy levels, they release energy in the form of light photons. These light photons fall in the ultraviolet wavelength range, so they need to be transformed into light that the human eye can see. The phosphor powder comes in at this stage to assist this transformation. The phosphors are substances that when they are exposed to light, they fluoresce, and they give off light in the visible range. So, when the ultraviolet light from the mercury gas atoms hits the phosphors, then this energy excites their electrons and once they fall back to their original states, they release visible light. Different manufacturers use different phosphors or ratio of phosphors depending on the targeted colour and warmth of light.

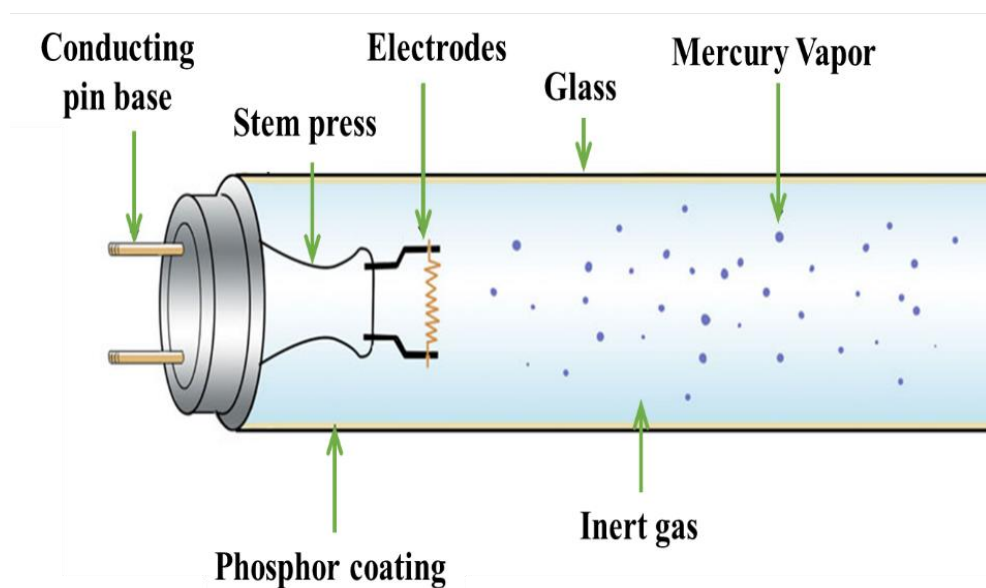


*Figure 5.4: Inner part of a fluorescent lamp and the individual constituents, reproduced from reference <sup>17</sup>*

Currently, the market of fluorescent lamps is decreasing due to the development and increased use of light emitting diodes (LEDs) that show higher efficiency and lifetime span compared with fluorescent lamps and do not contain mercury. This means that replacement of vast amounts of fluorescent lamps is expected.<sup>18</sup> It is also regulated for many countries to gather fluorescent lamps for recycling, as their disposal generates issues due to their mercury content.<sup>19</sup>

In addition, EoL fluorescent lamps incorporate heavy REEs as Y, Eu and Tb, which as mentioned before belonging to the category of the most critical metals in Europe, leading to the increase of their value and recycling interest. Recycling of these REEs may also contribute to the metal chain closing and might be a solution to the “balance” problem.<sup>20</sup> Although, plenty of studies have focused on the extraction and recovery of REEs from phosphor wastes, only  $\approx 1\%$  was recycled in 2011, due to challenging development of an environmentally friendly and economically viable strategy for recovery of highly pure ( $>99.999\%$ ) REEs from complex mixtures.<sup>21</sup>

There are three approaches for the recycling of fluorescent lamps: 1) direct reuse of the lamp phosphor powder into new fluorescent lamps, 2) physicochemical separation of the individual phosphor fractions and their reuse into new lamps, and 3) chemical dissolution of lamp phosphor waste for the extraction and recovery of individual REEs.<sup>22</sup> The last approach resembles the methods of chemical dissolution of REEs from their ores. Prior to the recovery of REEs, pre-treatment steps are required for the separation of other components such as glass particles, electrodes, aluminium end caps and mercury.<sup>21</sup> Usually crushing of the lamps occurs before any further process, leading to minimisation of the volume of lamps, but also to contamination of the phosphor waste with glass particles. Different routes for mercury removal have been developed and thermal distillation at  $800\text{ }^{\circ}\text{C}$  is one of the most common approaches even though it is energy intensive.<sup>23</sup>

Most lamp phosphor powders consist of certain fractions, whose chemical composition along with the wt.% in the phosphor fraction and value are summarized in **Table 5.2**.<sup>16</sup> Each lamp phosphor fraction has different economic value and dissolution proneness. HALO has the lowest intrinsic value, since it includes no REEs and dissolves very easily even in dilute acidic solutions at ambient conditions.<sup>22</sup> YOX shows very high recycling interest, as it consists only from Y and Eu and represents almost the 20 wt. % of a lamp phosphor powder. It dissolves in mild conditions, but requires more elevated temperatures in the range of  $60\text{-}90\text{ }^{\circ}\text{C}$ .<sup>21</sup> The rest of the phosphors (BAM, CAT, and LAP) contain different REEs and Sb. Their existence in very low wt.% in the phosphor powder along with the harsh conditions required for their successful processing, renders the flowsheet of their dissolution very complex, chemical and energy intensive and sometimes not economically viable. Apart from the phosphor fractions, the lamp phosphor wastes

contain significant amount of silica (SiO<sub>2</sub>), due to the glass parts, and alumina (Al<sub>2</sub>O<sub>3</sub>) that exists in the barrier layer of the lamp.

*Table 5.2: Typical phosphor fractions, their chemical composition, wt.% (with the rest to be SiO<sub>2</sub>) and economic value.*

Phosphor	Chemical composition	Wt.% in the lamp phosphor	Value
<b>HALO</b>	(Sr, Ca) <sub>10</sub> (PO <sub>4</sub> ) <sub>6</sub> (Cl, F) <sub>2</sub> :Sb <sup>3+</sup> ,Mn <sup>2+</sup>	40-50	low
<b>YOX</b>	Y <sub>2</sub> O <sub>3</sub> :Eu <sup>3+</sup>	20	high
<b>LAP</b>	LaPO <sub>4</sub> :Ce <sup>3+</sup> ,Tb <sup>3+</sup>	6-7	high
<b>BAM</b>	BaMgAl <sub>10</sub> O <sub>17</sub> :Eu <sup>2+</sup>	5	high

The extraction and recovery of REEs from phosphor wastes have been tested by different hydrometallurgical and solvometallurgical approaches. The hydrometallurgical route includes the steps of acidic leaching, precipitation and solvent extraction. Currently, the recovery of REEs from lamp phosphor powder is accomplished with the use of different dissolution steps. A direct dissolution step of REEs from lamp phosphors leads to the co-dissolution of impurities like calcium, iron, silicon, zinc and phosphorus.<sup>22</sup> Occasionally, alkali conversion at 800 °C with NaOH contributes to the transformation of the stable green phosphors to soluble oxides.<sup>24</sup>

In **Figure 5.5**, the patented flowsheet of Siemens is shown, illustrating the different dissolution steps for the extraction of metals from the different phosphor fractions.<sup>25</sup> It is clear that different steps are required for the selective processing of the different fractions of the phosphors. However, the adoption of subsequent steps at different conditions does not always result in fully selective processes. As will be reported later in this chapter, the dissolution of YOX in dilute HCl at ambient conditions results in almost 10% loss of Y and Eu in this first step.

The recovery of the REEs occurs in two steps of solvent extraction with extractants like Cyanex 923<sup>26</sup> and tributyl phosphate<sup>27</sup> and precipitation with the use of oxalic acid.<sup>21</sup> Then the REE oxalates are calcined and transformed into oxides, which can be reused in the industry of fluorescent lamps.

## Example of industrial flowsheet (Siemens, 2012):

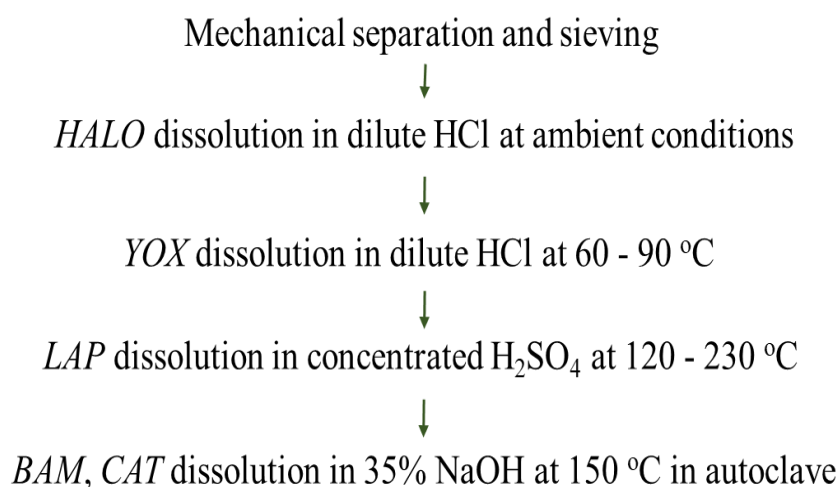


*Figure 5.5: Industrial patented flowsheet for the selective processing of the different phosphor fractions, adapted from ref<sup>25</sup>*

Some solvometallurgical studies have focused on this area of REEs extraction, but none of them has surpassed the lab scale. Selective extraction of Y and Eu using a functionalized ionic liquid betainium bis(trifluoromethylsulfonyl)imide [Hbet][Tf<sub>2</sub>N] and recovery by an acidic aqueous phase or generation of the red phosphor by precipitation with oxalic acid and thermal calcination of the oxalate at 850 °C showed very promising results.<sup>28</sup> Dissolution of the green phosphor LAP with the use of concentrated methanesulphonic acid resulted in high dissolution efficiencies for La, Ce and Tb in very short time periods ( $\approx 1$  h). Eventually, using two steps of recovery by solvent extraction with di-(2-ethylhexyl)phosphoric acid (DEHPA) and precipitation using oxalic acid, followed with the calcination of the precipitates, pure Tb<sub>4</sub>O<sub>7</sub>, CeO<sub>2</sub> and La<sub>2</sub>O<sub>3</sub> were formed.<sup>29</sup>

The use of DESs for the recycling of REEs from fluorescent lamp wastes has not yet been reported. However, preliminary processing of REE oxides in DESs has been carried out by Stodd,<sup>30</sup> in which EG:ChCl was employed for the dissolution of various REE oxides. All of the REE oxides tested were found to be electrochemically active in EtGly:ChCl and all showed similar response in their CVs justified by the redox couple of oxide/superoxide rather than the redox behaviour of the metal. The anodic dissolution of REE oxides was reported, which resulted in various solubilities for the different REEs, as shown in **Table 5.3**. In addition, the dissolution of EoL NdFeB supermagnets by electrochemical dissolution was also investigated and the results showed fast dissolution

of all the components, but no selectivity was accomplished during the dissolution step. The recovery of Nd and Dy from the pregnant leach solution was tested by electrodeposition and oxalic acid precipitation, with the latter to show high selectivity towards Nd and Dy against Fe.

*Table 5.3: Solubility of REE oxides in EG:ChCl of 0.2 g of oxide in a paste at a current density of 2 mA cm<sup>-2</sup> for 24 hours. (reproduced from Stodd<sup>30</sup>)*

Rare earth element oxide	Solubility (ppm)
CeO <sub>2</sub>	4
Nd <sub>2</sub> O <sub>3</sub>	131
Sm <sub>2</sub> O <sub>3</sub>	176
Gd <sub>2</sub> O <sub>3</sub>	99
Pr <sub>2</sub> O <sub>3</sub>	16

### 5.1.3 Aims

In this work, the possibility of extraction and recovery of REEs from lamp phosphor powder wastes using DESs is investigated for the first time. The main aim is to show that by employing DESs in a complex material as the fluorescent lamp phosphor powder, selective extraction of REEs can be achieved. It is also expected, according to the results of Chapter 3, that the carboxylic acid based DESs will be able to extract more of REEs from their oxides, for example Y and Eu from Y<sub>2</sub>O<sub>3</sub>:Eu<sup>3+</sup>. The screening of different DESs takes place on synthetic individual phosphor fractions, due to no previous study on the recycling of lamp phosphors in DESs existing. Then, the most well behaved DES, in terms of selectivity of extraction and highest dissolution affinity of YOX, is compared with the pure HBD, meaning without the use of choline chloride, in order to investigate if the use of a DES is indeed justified, as the purpose of this work is not to promote the unreasonable use of DESs but to practically show that by employing a mixture of choline chloride with a HBD results in higher or more selective extraction.

Afterwards, the dissolution parameters (temperature, water content and time) are optimised. The optimised parameters are then validated on both synthetic and real lamp phosphor waste. The recovery of the dissolved REEs is also studied by employing both the methods of solvent extraction and precipitation with the use of oxalic acid.

## 5.2 Extraction of REEs from spent fluorescent lamps using solvometallurgy

In Chapter 1, the concept of solvometallurgy and its benefits were discussed. The main advantage provided by the employment of molecular solvents, ILs or DESs is the selective dissolution of metals from complex matrices, for which pyrometallurgy is definitely not suitable and hydrometallurgy requires complicated and chemically intensive flowsheets. This was shown in more detail in Chapter 3.

DESs have been used in the extraction of many industrial EoL materials as lithium ion batteries (LIBs),<sup>31</sup> lead acid batteries,<sup>32</sup> NdFeB magnets<sup>33</sup> and semiconductors (GaAs).<sup>34</sup> To date, no previous research has been carried out on the extraction of REEs from spent fluorescent lamps.

### 5.2.1 Selection of deep eutectic solvent for the extraction of REEs from phosphors

In this investigation, and as a continuity from the previous chapters, the DESs employed are mixtures of ChCl with various HBDs, namely oxalic acid dihydrate, glycolic acid, levulinic acid, ethylene glycol and urea.<sup>1</sup> As a starting point, the suitability of DESs as lixivants for REE phosphors was tested by measuring the solubility of the individual phosphors (YOX, HALO, LAP and BAM) in a variety of DESs. For the phosphors LAP and BAM, the solubility of metals was negligible in all DESs tested, so no other analysis was conducted for these materials.

*Table 5.4: Chemical composition of the synthetic YOX and HALO phosphors.*

Element	Concentration (wt.%)
YOX phosphor	
Y	70.93
Eu	4.23
HALO phosphor	
Ca	38.06
Sr	0.06
Sb	1.05
Mn	1.06
PO <sub>4</sub>	55.71

<sup>1</sup> The inconsistency in the use of exactly the same DESs as in Chapter 3 or the use of different analytical techniques is because this work was part of a 3 months secondment at KU Leuven,

The composition of the synthetic phosphors YOX and HALO was determined via digestion in HCl at 60 °C for 24 h, followed by ICP-OES analysis and the composition is presented in **Table 5.4**. Due to the identical dissolution behaviour of Y and Eu from the YOX phosphor, all the following graphs present the extraction efficiency of Y. In respect with HALO, the dissolution efficiencies presented in the graphs refer to Ca, because it accounts for almost the 40 wt.% of the metal content, unless stated.

The screening of DESs included most of the widely used group of HBDs (carboxylic acid, alcohol and amide). From the results of Chapter 3, the YOX phosphor, which is an oxide of Y and Eu is expected to dissolve more in the carboxylic acid based DESs, as it was described that both the acidity of the solvent, but most importantly the surface complexation of the HBD lead to increased yield of dissolution. Fan et al.<sup>35</sup> has also reported that the low lattice energy of Y and Eu oxides resulted in high solubilities in the water saturated IL betainium bis(trifluoromethylsulfonyl)imide [Hbet][Tf<sub>2</sub>N], same as observed also in Chapter 3 for the d and p-block oxides in DESs.

In **Figure 5.6**, the solubility of YOX and HALO using different DESs are compared. The addition of 10 vol.% of water was added to decrease the viscosity of the solvents. The extraction of YOX in solution was found be negligible in all the DESs (<1%), except for LevA:ChCl, in which was about 70 %.

Contrarily to what has been previously reported, carboxylic acid-based DESs did not result in high amount of Y and Eu in solution, neither the amide-based nor polyol-based DESs. The unexpected low solubility of YOX in GlyA:ChCl and OxA:ChCl compared to Urea:ChCl and EG:ChCl will be discussed further. The extraction efficiency of HALO was very low in all the DESs, independently of the HBD employed, except for OxA:ChCl in which Ca was precipitated and  $40\% \pm 2.3$  of Mn and  $60\% \pm 1.4$  Sb were extracted, under the same conditions. Thus, the employment of OxA:ChCl for the processing of phosphor wastes would be justified if the targeted metals were Mn and Sb.

When YOX was leached with GlyA:ChCl and OxA:ChCl, it was noticed that the volume of solids after the dissolution was larger than at the beginning. The first hypothesis was that the metals present in the phosphor were leached, and subsequently precipitated as metal glycolates or oxalates, respectively.

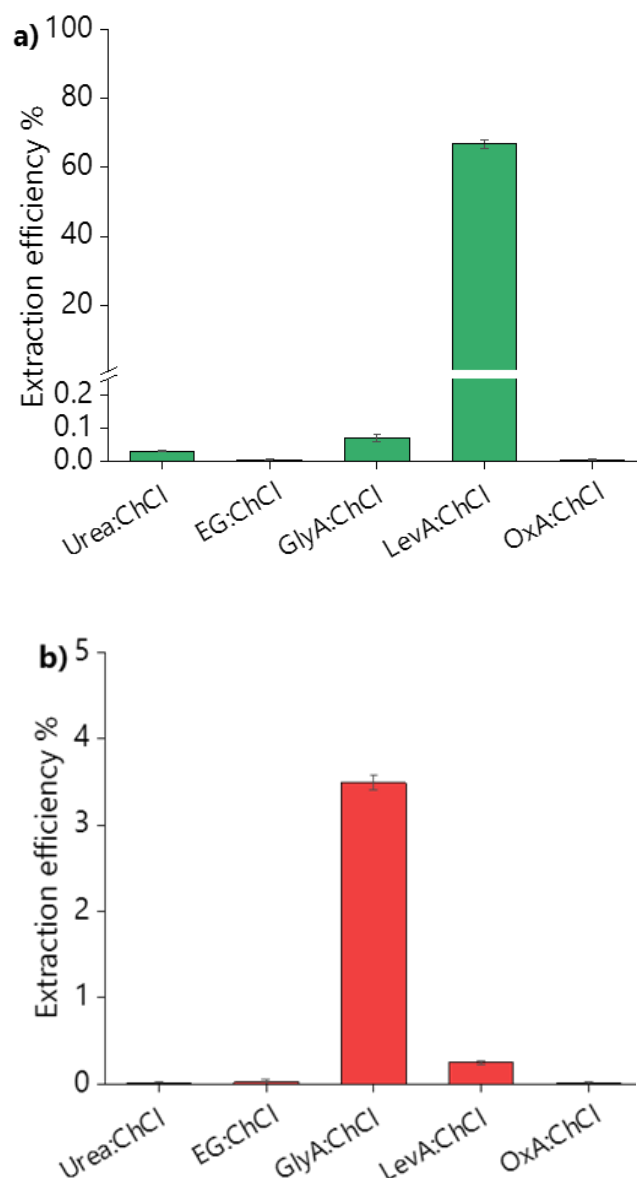
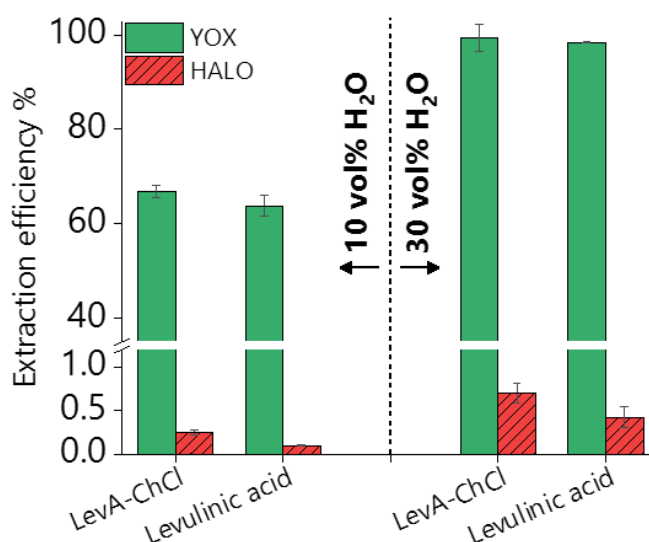


Figure 5.6: Effect of the hydrogen-bond donor type on the extraction efficiency of (a) YOX and (b) HALO lamp phosphors. Conditions:  $H_2O$  vol.% = 10;  $T = 80^\circ C$ ;  $t = 48$  h;  $L:S = 10$  and 500 rpm.

The  $^1H$  NMR and  $^{13}C$  spectra of the OxaA:ChCl and the GlyA:ChCl were recorded before and after the dissolution and presented in Appendix (**Figure 7.15**). The integration of the spectra showed that 45 % of the glycolic acid and 41 % of the oxalic acid were lost during the dissolution. These losses are higher than what could be expected for the full transformation or the REEs into glycolates or oxalates (i.e. carboxylic acid/(Y, Eu) = 1.5). The following carboxylic acid/REE ratio was obtained: glycolic acid/(Y, Eu) = 3 and oxalic acid/(Y, Eu) = 2. This means that all the YOX was transformed into oxalates/glycolates. This result is very interesting, as for example direct production of yttrium oxalate is beneficial. However, during the dissolution of real lamp phosphor waste

the newly formed compound would be mixed with the remaining residue (HALO, silicates, LAP, and BAM) and the complex separation of the glycolates/oxalates from the remaining residue would be required. The  $^1\text{H}$  NMR spectra of LevA:ChCl, after extraction of YOX, was also recorded before and after the dissolution, presented in Appendix (**Figure 7.15**) and it was observed that the DES was stable during the dissolution process. Therefore, neither Y nor Eu precipitated as levulinates. The high solubility of YOX in LevA:ChCl could be explained by ligation of the metal in a high chloride medium or by complexation with levulinic acid, with the method described in Chapter 3. In order to confirm either one of the two hypotheses, the dissolution of YOX and HALO in pure levulinic acid followed.



*Figure 5.7: Comparison of YOX and HALO extraction efficiency in LevA:ChCl and pure levulinic acid with the addition of 10 wt.% and 30 wt.% H<sub>2</sub>O. Conditions: T = 80 °C; t = 48 h; L:S = 10 and 500 rpm.*

In **Figure 5.7** the comparison of both YOX and HALO dissolved in LevA:ChCl and pure levulinic acid (10 and 30 H<sub>2</sub>O vol.%) is presented. The extraction of YOX is similar in both lixivants suggesting that the chloride has negligible effect on metal solubility, i.e. carboxylate complexes dominate speciation. As for HALO, its extraction efficiency is almost negligible in both solvents. Therefore, the addition of another chemical to the levulinic acid to form a DES might not be justified, from both an economic and environmental point of view. To validate this assumption, subsequent studies compare the dissolution with levulinic acid and LevA:ChCl, as well as the effect of both lixivants on the metal recovery step.

### 5.2.2 Optimization of dissolution parameters

Upon the completion of the DES screening and its comparison with the pure HBD, the DES LevA:ChCl and the pure levulinic acid were selected as promising lixiviants for the selective extraction of Y and Eu, considering the negligible co-dissolution of HALO phosphor. Subsequently, optimization of the following significant dissolution parameters was carried out:

- Water content
- Time
- Temperature

Firstly, the effect of water content in both the DES and in levulinic acid was investigated. In **Figure 5.8**, the effect of the water content on the extraction efficiency of YOX and HALO is presented.

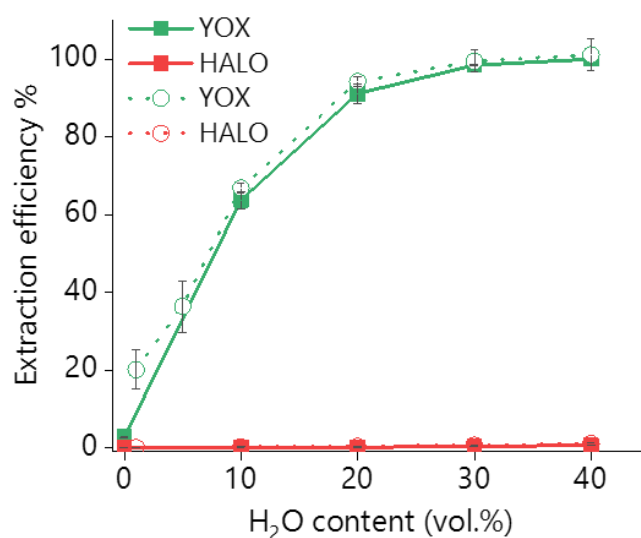


*Figure 5.8: Effect of the water content on the extraction efficiency of YOX and HALO using levulinic acid (solid line) and LevA:ChCl (dotted line). Conditions:  $T = 80\text{ }^{\circ}\text{C}$ ,  $t = 48\text{ h}$ ,  $L:S = 10$  and  $500\text{ rpm}$ .*

It is apparent that the impact of the water content is similar for both lixiviants: increasing the water content significantly increases the solubility of YOX, while that of HALO is barely affected. A possible reason is that the presence of water facilitates the proton transfer between the carboxylic acid and the Y/Eu oxide to form the carboxylate complex. The increase of the solubility of metal oxides as a function of the water content has been previously reported for IL systems.<sup>36</sup> Another possible explanation is that by increasing

the water content, the viscosity of the solvent decreases, leading to enhanced mass transport and thus augmented solubility.

Without addition of water, the solubility of YOX is remarkably higher using LevA:ChCl (20%) than using levulinic acid (2.7%). This could be attributed to the higher water content of the LevA:ChCl, due to the hygroscopicity of the ChCl, and to the esterification reaction between ChCl and levulinic acid, which is enhanced by the high dissolution temperatures (50–80 °C).<sup>37</sup> The extraction efficiency of YOX for both lixivants is more than 90%, when the water content is 30 vol.%, thus this water content was used for subsequent studies. Apart from the high extraction of Y and Eu with higher water content, it is expected that the addition of water prevents the esterification, since it is a product of this reaction. In fact, the degree of esterification after the dissolution with a water content of 30 vol.%, calculated from Appendix (**Figure 7.15c**) (following a procedure previously reported) only accounts for 2 mol%.<sup>37</sup>

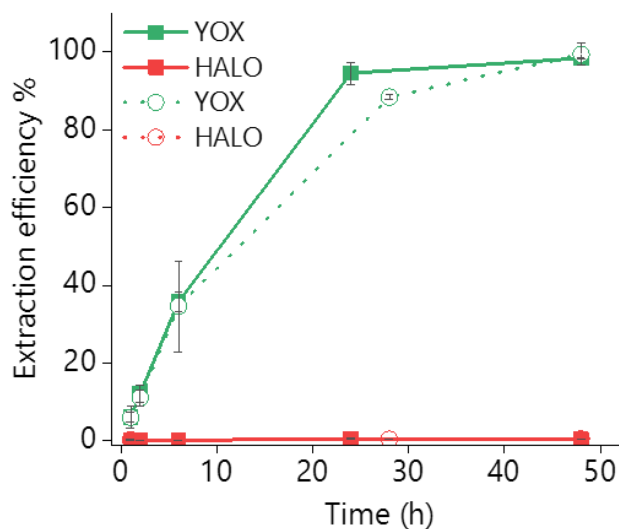


*Figure 5.9: Kinetics of the dissolution of YOX and HALO in levulinic acid (solid line) and LevA:ChCl (dotted line). Conditions:  $T = 80\text{ }^{\circ}\text{C}$ ;  $L:S = 10$ ;  $\text{H}_2\text{O vol.}\% = 30$ ; and 500 rpm*

Moreover, a higher water content would decrease the cost of the lixiviant. However, it has been reported that for DESs, the transition from an ionic mixture to an aqueous solution of its components is at around 40 H<sub>2</sub>O vol.%, and the speciation of solution is expected to change as it has been previously mentioned in this thesis.<sup>38</sup> In order to compare the behaviour of the DES acting as a pseudo-component to that of levulinic acid, the DES must be in the ionic mixture region, i.e. less than 40 H<sub>2</sub>O vol.%. Another reason

to work at low water content is to keep the selectivity towards HALO. Next, the kinetics of the extraction in both lixiviants using 30 vol.% H<sub>2</sub>O was investigated. The effect of the dissolution time on the extraction efficiency of YOX and HALO are shown in **Figure 5.9**. The dissolution process was found to be relatively slow, independent of the lixiviant used, as full dissolution of the YOX phosphor took 48 h. Although the dissolution times are very long, they are in accordance to what has been previously reported in the literature for the dissolution of YOX with mineral acids and ILs.<sup>21, 28</sup>

Last but not least, the effect of temperature on the extraction efficiency of YOX and HALO using levulinic acid or LevA:ChCl was also examined. The results are shown in **Figure 5.10**. For both lixiviants, increasing the temperature significantly increases the extraction efficiency of YOX, while that of HALO is almost unaffected.

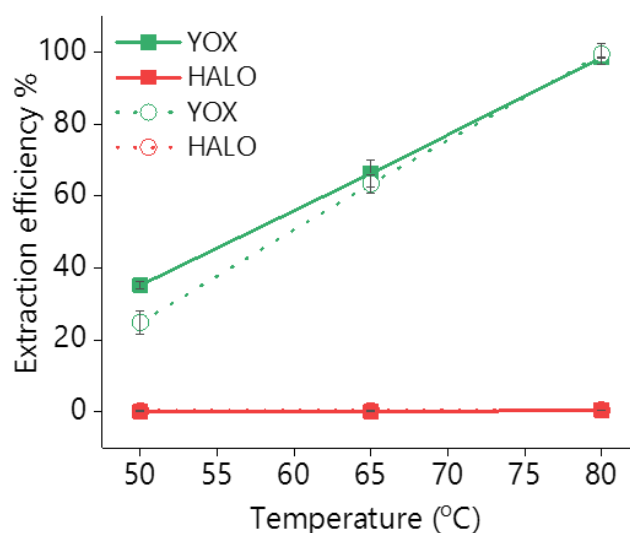


*Figure 5.10: Effect of the temperature on the extraction efficiency of YOX and HALO using levulinic acid (solid line) and LevA:ChCl (dotted line). Conditions: H<sub>2</sub>O vol.% = 30; t = 48h; L:S = 10; 500 rpm.*

Therefore, higher temperatures would be preferred for this dissolution process. A temperature of 80 °C seems appropriate since the thermal decomposition of LevA:ChCl is 159 °C,<sup>37, 39</sup> while that of levulinic acid is 134 °C.<sup>27</sup> Also, the decomposition temperature is higher than the maximum operational conditions (boiling point of water). Although the presence of water inhibits the esterification, high dissolution temperatures might reduce the extraction efficiency of the DES in the long term. As previously shown in the literature, the temperature has a large effect on the esterification degree of

carboxylic acid:ChCl DESs.<sup>37</sup> The esterification reaction between the levulinic acid and the ChCl will reduce the amount of available carboxyl groups for complexation, reducing the extraction efficiency.

### 5.2.3 Dissolution of synthetic mixture of phosphors

As a next step, the investigation of the dissolution behaviour of a synthetic mixture of HALO, YOX, LAP and BAM in both LevA:ChCl and levulinic acid was deemed necessary before the dissolution of a real residue. A real phosphor mixture, as mentioned before, consists of 40–50 wt.% HALO, 20 wt.% YOX, 5 wt.% BAM and 6–7wt.% LAP and the remaining amount is composed of SiO<sub>2</sub> as fine glass particles, and Al<sub>2</sub>O<sub>3</sub>.<sup>28</sup> For the synthetic mixture, the composition was chosen to mimic the composition of the real lamp phosphor waste and included: 58 wt.% HALO, 26 wt.% YOX, 9 wt.% LAP and 6 wt.% BAM, but without impurities such as SiO<sub>2</sub> or Al<sub>2</sub>O<sub>3</sub>. The extraction efficiency as a function of the dissolution time using LevA:ChCl and levulinic acid as lixiviants is shown in **Figure 5.11**.

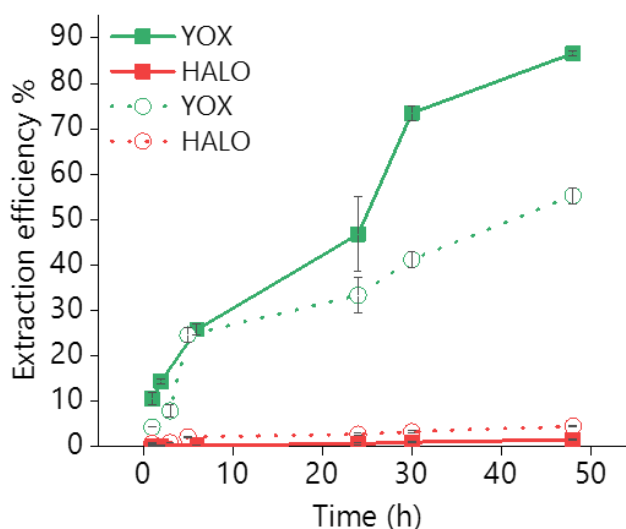


*Figure 5.11: Effect of the mixing time on the extraction efficiency of a synthetic lamp phosphor mixture using levulinic acid (solid line) and LevA:ChCl (dotted line). Conditions: H<sub>2</sub>O vol.% = 30; T = 80 °C; L:S = 10; 500 rpm.*

The dissolution of LAP and BAM was found to be below the detection limit of the ICP-OES; therefore, the results were not included in the graph and will not be discussed. The dissolution behaviour of the synthetic mixture is similar to that of the individual lamp phosphors: high extraction efficiency of YOX and low extraction efficiency of HALO. However, the extraction efficiency of YOX was found to be lower when leached in a

mixture of lamp phosphors than when leached individually. The decrease in the YOX solubility is much more noticeable for the LevA:ChCl than for the levulinic acid. Furthermore, the selectivity over HALO is lower when using LevA:ChCl (almost 5% of HALO is leached), which might explain the reduced extraction efficiency of YOX.

#### 5.2.4 Dissolution of real lamp phosphor waste

In order to validate the obtained results, the performance of LevA:ChCl and levulinic acid was tested on a real lamp phosphor waste. The real lamp phosphor waste was sieved, and only the fraction <125  $\mu\text{m}$  was used. This fraction was selected to ensure the homogeneity of the solid samples. In Appendix (**Figure 7.16**) the fractions of the phosphor powder that have a particle size >125 $\mu\text{m}$  include many contaminants like glass particles,  $\text{Al}_2\text{O}_3$  and possible other crushed parts of the lamps.

The composition of the waste was determined according to the procedure reported in the Chapter 2 and is presented in **Table 5.5**.

*Table 5.5: Composition of the lamp phosphor residue fraction <125  $\mu\text{m}$*

Element	Composition (wt.%)
<b>Y</b>	$10.1 \pm 0.7$
<b>Ca</b>	$7.9 \pm 0.7$
<b>Al</b>	$1.7 \pm 0.3$
<b>La</b>	$1.47 \pm 0.08$
<b>Ba</b>	$1.47 \pm 0.15$
<b>Ce</b>	$0.97 \pm 0.03$
<b>Eu</b>	$0.67 \pm 0.05$
<b>Tb</b>	$0.48 \pm 0.04$
<b>Sr</b>	$0.37 \pm 0.04$
<b>Mg</b>	$0.19 \pm 0.02$
<b>Mn</b>	$0.172 \pm 0.014$
<b>Sb</b>	$0.110 \pm 0.017$

The effect of the dissolution time on the extraction efficiency of the real lamp phosphor residue using LevA:ChCl and levulinic acid is shown in **Figure 5.12**. Once again, the concentration of metals present in LAP, BAM and CAT was found to be negligible. For both lixivants, the dissolution of YOX was lower than that obtained for the synthetic mixture while the co-dissolution of calcium (associated to the HALO phosphor) was found to be much higher. The higher calcium co-dissolution and its fast dissolution suggest that the calcium in the real waste is present in a more accessible form than in the synthetic mixture. Levulinic acid could leach more YOX in a more selective way than the DES LevA:ChCl. With the DES, the maximum extraction efficiency of YOX was already reached after 24 h, but for levulinic acid the maximum extraction efficiency was not reached even after 48 h, so longer times were tested. Longer dissolution times improve the extraction efficiency, but drastically decrease the selectivity against HALO.

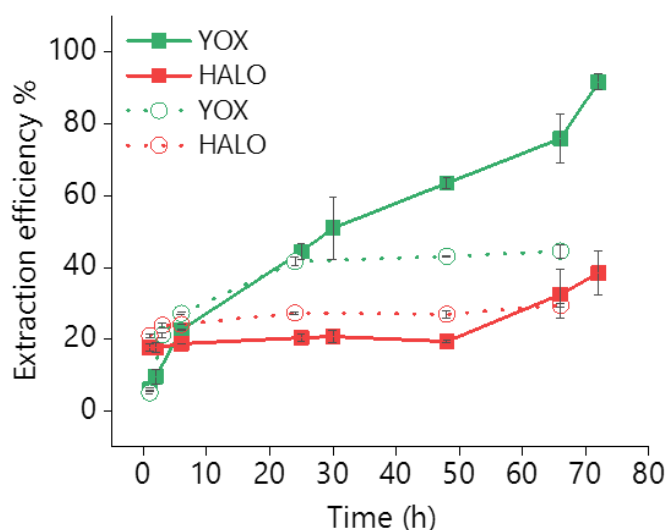


*Figure 5.12: Effect of the dissolution time on the extraction efficiency of a real lamp phosphor waste using levulinic acid (solid line) and LevA:ChCl (dotted line). Conditions:  $H_2O$  vol.% = 30;  $T = 80$  °C;  $L:S = 10$ ; and 500 rpm.*

The possible increase of the extraction efficiency of YOX was investigated by employing higher L:S ratios and their effect on the dissolution behaviour of the real residue is shown in **Figure 5.13**. For LevA:ChCl, the effect of the L:S on the extraction efficiency of YOX and HALO is quite small. For levulinic acid, increasing the L:S significantly increased the extraction efficiency of YOX, while the co-dissolution of HALO was almost unaffected. With L:S = 20, around 90% of the YOX could be leached in 48 h, while with L:S = 30, all the YOX was leached in 48 h.

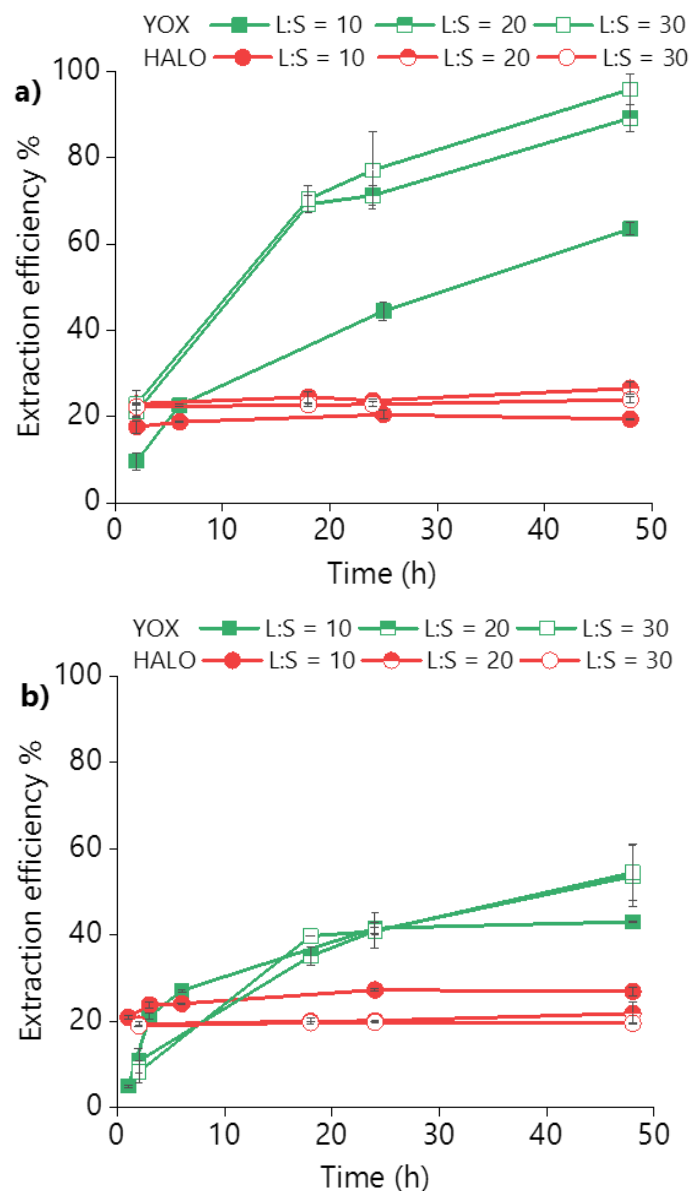


Figure 5.13: Effect of the L:S ratio and dissolution time on the extraction efficiency of a real lamp phosphor waste using (a) levulinic acid and (b) LevA:ChCl. Conditions:  $H_2O$  vol.% = 30;  $T = 80\text{ }^\circ\text{C}$ ; 500 rpm.

Based on the obtained results it became clear that the levulinic acid dissolution is preferred over the LevA:ChCl leaching. Apart from higher dissolution efficiencies, levulinic acid shows other benefits compared to the DES: (1) Levulinic acid can be directly used without need of diluting in another organic solvent, which is cheaper and greener. (2) Levulinic acid solution is less viscous than the corresponding DES, which implies faster mass transfer and lower energy consumption. (3) Contrarily to carboxylic acid-based DESs, levulinic acid is not decomposed by esterification. (4) Levulinic acid is less corrosive than levulinic acid:ChCl because of the absence of chloride ions.

Therefore, not only levulinic acid is greener, it also shows that the use of DESs over its individual components it is sometimes not justified.

### 5.2.5 Comparison with other hydrometallurgical and solvometallurgical processes

To critically assess the performance of these lixivants, the results were compared to other solvometallurgical and hydrometallurgical methods. First the comparison with one of the best behaving ILs in the literature was appropriate. It was reported that the dissolution with the IL [Hbet][NTf<sub>2</sub>], could dissolve 100% YOX with a negligible co-dissolution of HALO from a synthetic lamp phosphor mixture.<sup>28</sup> So, this experiment was repeated on the same sample of the real phosphor waste and the performance of the IL in its dissolution was measured as a function of the L:S ratio and dissolution time, the results of which are presented in **Figure 5.14**.

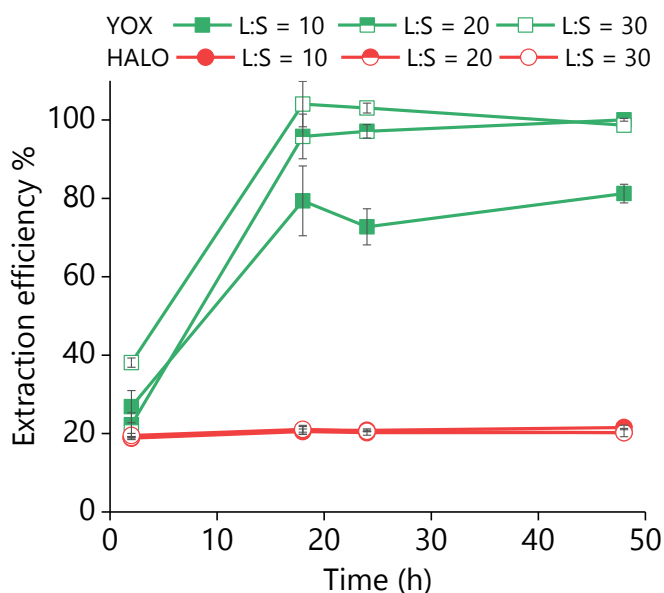


*Figure 5.14: Effect of the dissolution time and L:S ratio on the extraction efficiency of real lamp phosphor waste using the ionic liquid [Hbet] [NTf<sub>2</sub>]. Conditions: H<sub>2</sub>O vol% = 5; T = 80 °C; 500 rpm*

Similar to this investigation, the co-dissolution of calcium from the real waste is higher than what would be expected based on results of the synthetic phosphor mixture.

The calcium co-extraction was 20 %, which is exactly the same value as for the LevA:ChCl and for the pure levulinic acid. Full dissolution of YOX could be obtained after 24 h, at L:S ≥ 20. Similar results were obtained for [Hmim][HSO<sub>4</sub>]:H<sub>2</sub>O in which nearly full dissolution of YOX was achieved at 80 °C, L:S = 20 and 4 h. In this case the extraction of calcium accounted for 25 %.<sup>40</sup> In conclusion, the IL-based dissolution is faster than the levulinic acid leaching, but equally selective. However, ILs are much more

than 100 times more expensive than levulinic acid. In addition, less water can be used for the IL dissolution (due to its hydrophobicity), which translates into higher lixiviant requirements and more difficult liquid-solid separation.

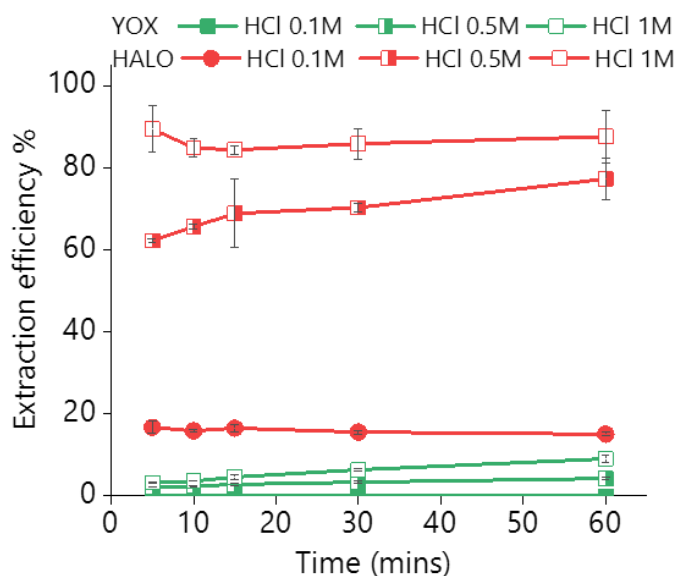


Figure 5.15: Effect of the dissolution time and HCl concentration on the extraction efficiency of real lamp phosphor waste using an aqueous solution of HCl. Conditions:  $T = 25\text{ }^{\circ}\text{C}$ ;  $L:S = 10$ ; 500 rpm.

Afterwards, in order to illustrate the advantages of the solvometallurgical approaches in terms of selectivity, the real lamp phosphor waste was leached with an aqueous solution of hydrochloric acid. The dissolution efficiencies are shown in **Figure 5.15**. Contrary to the levulinic acid-based lixiviants, the solubility of HALO is higher than that of YOX, which was expected based on the results previously reported in the literature.<sup>24, 41</sup> Increasing the acid concentration increases the leachability of HALO, and to a lower extent the leachability of YOX. Hydrometallurgy could be considered for the selective recovery of HALO. However, it has been reported that even with careful pH control the losses of Y and Eu were inevitable and accounted for 11% of the mass.<sup>41</sup> In addition, dissolution of HALO produces phosphoric acid that may react with Y and Eu to form insoluble phosphates.

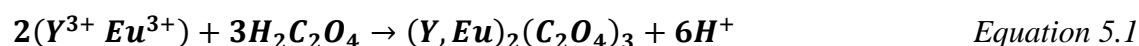
Therefore, even if hydrometallurgy is faster than solvometallurgy, it suffers from poor selectivity. Furthermore, solvometallurgy prevents the corrosive working environment caused by the evaporation of HCl from concentrated aqueous solutions because the DESs and its chloro species are not volatile.<sup>42</sup>

### 5.3 Recovery of REEs from lamp phosphor

After the investigation of the dissolution of YOX and HALO from both synthetic and the real phosphor waste, the recovery of Y and Eu was followed. For that reason, two different approaches were tested for the recovery of the metals from the pregnant leach solution, namely: precipitation with oxalic acid and solvent extraction.

#### 5.3.1 Recovery using precipitation with oxalic acid

Oxalic acid is widely used as a precipitant agent for REEs, because it forms insoluble oxalates with the REE ions (**Equation 5.1**), which can be calcined to produce REE oxides.<sup>43</sup> In previous works it has been reported that a stoichiometric amount of oxalic acid could recover 100% of the Y and Eu from an IL phase.<sup>28</sup>



The addition of oxalic acid to precipitate Y and Eu from a PLS obtained from the dissolution YOX using LevA:ChCl or levulinic acid with 30 vol.% H<sub>2</sub>O was studied and the results are shown in **Figure 5.16**.

For the levulinic acid-based system, a stoichiometric amount of oxalic acid was found to be sufficient for the full precipitation of the REEs if sufficient mixing time and temperature were applied, i.e. 20 min at 50 °C, or 15 min at 70 °C. For the LevA-ChCl system, a stoichiometric amount of oxalic acid was insufficient for the full precipitation of the REEs. Full recovery of REES was achieved only when 1.5 equivalents of oxalic acid were used, either after 5 min of mixing at 50°C or 70°C, or after 15 min of mixing at room temperature. Our first hypothesis was that, instead of forming oxalates with the REEs, some oxalic acid would become part of the DES structure (forming a ternary DES). However, in Appendix (**Figure 7.17**) the <sup>13</sup>C NMR of LevA:ChCl after the addition of the stoichiometric amount or 1.5 times the stoichiometric amount of oxalic acid are presented, and it is clear that no signs of oxalic acid were detected in either spectrum. This means that the oxalic acid had precipitated, but not in the form of a REE-oxalate.

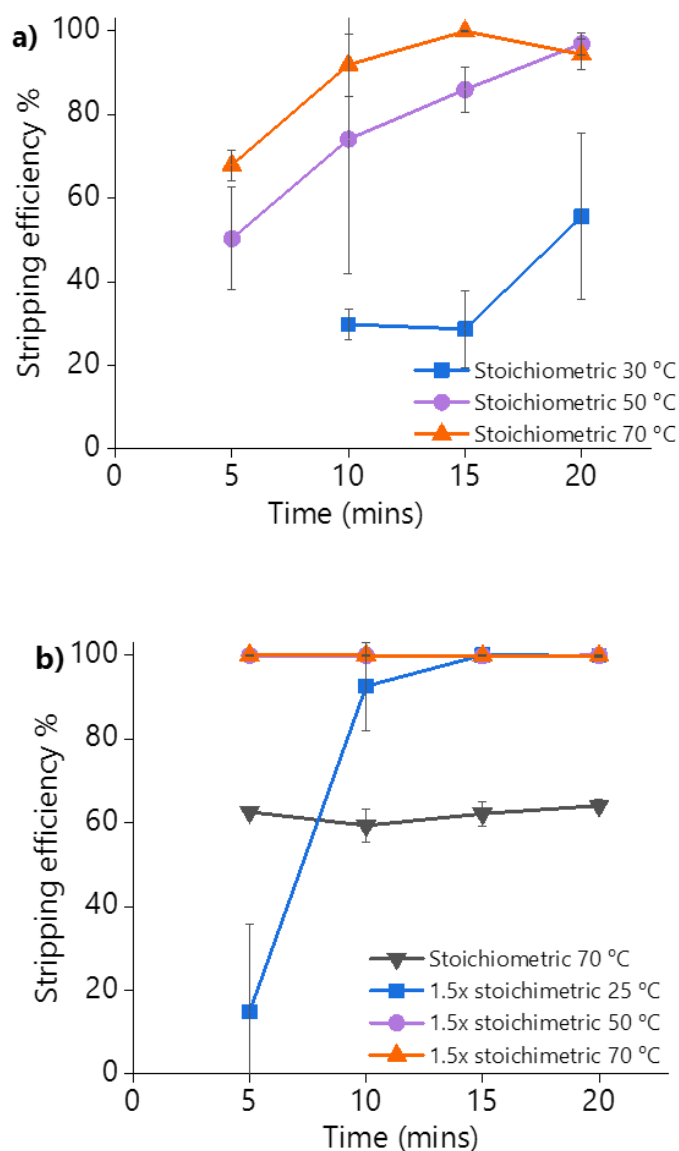


Figure 5.16: Stripping efficiency obtained by the addition of pure oxalic acid to (a) levulinic acid and (b) LevA:ChCl PLS, as a function of the amount of oxalic acid, mixing temperature and time. Conditions:  $H_2O$  vol.% = 30;  $T = 80$  °C;  $t = 48$  h;  $L:S = 10$ ; 500 rpm

The analysis of the  $^1H$  NMR, shown in Appendix (**Figure 7.18**) showed that the LevA:ChCl ratio changed after oxalic acid addition. Originally,  $x_{ChCl} = 0.33$ , after addition of stoichiometric amount of oxalic acid was  $x_{ChCl} = 0.3$  and after addition of 1.5 equivalents was  $x_{ChCl} = 0.27$  (i.e.,  $\approx 10$  and 20 mol% of ChCl losses, respectively). Those losses correspond to the formation (and precipitation) of oxalic acid:ChCl ( $x_{ChCl} = 0.3$ ) and oxalic acid:ChCl ( $x_{ChCl} = 0.4$ ), respectively. Those compositions are solids at the temperatures used for the precipitation experiments.<sup>44</sup>

Thus, it can be concluded that the recovery of REEs from DES-based PLSs using oxalic acid precipitation is not a suitable option due to the partial precipitation of the lixiviant and the contamination of the REE precipitate. Considering these results, levulinic acid would be preferred as lixiviant, reinforcing the conclusions of the dissolution section.

It can be noticed that experiments shown in **Figure 5.16** have much larger error bars compared to the rest of the experiments of this work. This is due to the very large concentration of REEs in the PLS when synthetic YOX is leached ( $Y = 74781$  ppm and  $Eu = 5867$  ppm), which leads to a very large volume of newly formed oxalates compared to the volume of the original liquid. Under those conditions, the mixing of the vial was not optimal. Furthermore, the precipitation of the oxalates is very fast, and it might continue to some extent during centrifugation.

The recovery of the REEs via oxalic acid precipitation from the PLS obtained from the levulinic acid dissolution of real lamp phosphor waste was also investigated and the stripping efficiency is shown in **Figure 5.17**.

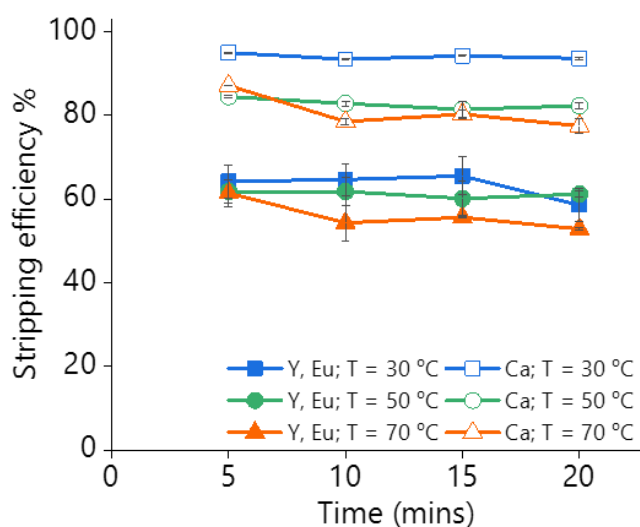


*Figure 5.17: Stripping efficiency via oxalic acid addition (stoichiometric amount) as a function of time and temperature of a levulinic acid PLS obtained from the dissolution of real lamp phosphor residue. Conditions:  $H_2O$  vol.% = 30;  $T = 80$  °C;  $t = 48$  h;  $L:S = 10$ ; and 500 rpm.*

The composition of the PLS was:  $Y = 8772$  ppm,  $Eu = 565$  ppm and  $Ca = 1579$  ppm. **Figure 5.17** shows that calcium is preferentially precipitated over yttrium and europium (which are equally extracted). This is why even if a stoichiometric amount of oxalic acid was added, not all the REEs were precipitated. Due to the calcium co-precipitation it is

not possible to obtain a clean REE-oxalate precipitate from a real levulinic acid-PLS. The precipitation from the PLS of the real waste is faster than from the PLS of the YOX dissolution (**Figure 5.16**), i.e. full precipitation in 5 min. The lower metal content of the real lamp phosphor residue PLS could explain this behaviour. **Figure 5.17** also shows that higher stripping efficiencies were obtained at lower temperatures (for both the calcium and the REEs). It has been previously reported that the co-precipitation of calcium can be reduced by low pH and/or high temperatures.<sup>45</sup> This method could be used for the full stripping of the levulinic acid, so it can be reused in subsequent dissolution steps. However, it is not suitable to produce a pure REEs oxalate residue.

### 5.3.2 Recovery using solvent extraction

Last but not least, the recovery of the metals from the PLS via solvent extraction was also investigated. In this work all the metals were extracted by the extractant bis(2-ethylhexyl)phosphoric acid (D2EHPA), which is a well-known extractant for REEs,<sup>46</sup> and stripped to an aqueous acidic solution. HCl has been selected in this work, but H<sub>2</sub>SO<sub>4</sub> and HNO<sub>3</sub> have also been reported as suitable options for stripping of REEs from a D2EHPA phase.<sup>45, 47</sup>

The extraction to a D2EHPA phase from a LevA:ChCl-based PLS and from a levulinic acid-based PLS were investigated. In both cases, a third liquid phase formation was observed if D2EHPA was used pure or diluted in aliphatic compounds, i.e. the aliphatic diluent GS190 or *n*-dodecane, even in presence of a modifier (1-decanol, 10-30 vol.%). When *p*-cymene was used as a diluent the third phase formation was noticeably reduced, and by using toluene could be totally avoided. The addition of a modifier (1-decanol) avoided the third phase formation of the *p*-cymene. The use of *p*-cymene is preferred over toluene for safety reasons, i.e. higher flash point. Furthermore, *p*-cymene can be considered as a green aromatic solvent according to different criteria.<sup>48</sup> Therefore, a mixture of D2EHPA, *p*-cymene and 1-decanol was selected as the organic phase. The effect of the D2EHPA concentration on the extraction efficiency was investigated for both PLSs. The concentration of D2EHPA was varied from 20-60 vol.% and that of 1-decanol was kept constant at 10 vol.%. Independently of the D2EHPA concentration, quantitative extraction of all the metals was obtained. The <sup>1</sup>H NMR spectra of both the D2EHPA phase and the depleted lixiviant phase were recorded and shown in Appendix (**Figure 7.19**). The absence of lixiviant in the organic phase, and the absence of extractant in the lixiviant phase were confirmed. The stripping of the metals to an aqueous HCl

solution was investigated as a function of the HCl concentration, and it was found that stripping with 6 mol L<sup>-1</sup> HCl (25 °C, 1 h mixing time, (aqueous / organic solution ratio= 1) was sufficient for the complete stripping of all the metals of the organic phase.

It should be mentioned that although a third phase formation was not observed when the extraction with D2EHPA was performed on a small scale (2 mL), a thin white layer at the interface was observed when the extraction was performed at a large scale (50 mL). This means that 100% of the metals were extracted from the PLS to the D2EHPA phase, which could be confirmed by ICP-OES measurement of the PLSs, but the concentration of metals in the D2EHPA phase did not correspond to 100% extraction efficiency. Stripping with 6 mol L<sup>-1</sup> HCl was quantitative. The third phase formation can be controlled by modifying the composition of the organic phase in terms of extractant concentration, and modifier type and composition. In this work, a proof-of-principle is provided on how all the metals can be recovered without contamination of the lixiviant, which can be reused in subsequent dissolution steps. Further optimisation of the extraction procedure will be done in a future work, including direct separation of the metals from the PLS, instead of transferring all the metals to an aqueous phase before separation.

## 5.4 Conclusions

For the first time DESs were employed for the extraction of REEs from spent fluorescent lamp phosphors. After a screening of different DESs on individual synthetic phosphors (YOX, HALO, LAP and BAM), the LevA:ChCl system showed the best dissolution behaviour as it dissolved more than 70% of YOX with very high selectivity towards the rest of the phosphors, especially HALO that is a contaminant. In order to confirm whether the levulinic acid or its combination and synergistic effect with the ChCl are the reason for this dissolution behaviour, both pure levulinic acid and LevA:ChCl were investigated. Both lixiviants showed high solubility of YOX while low solubility of the HALO phosphor. The similar results obtained for both lixiviants showed that the chloride coming from the choline chloride was not responsible for the high extraction efficiency of REEs. So, a first significant conclusion of this work is that if there is not critical point of view, then the unjustified use of DESs or other mixtures of components, in general, is possible.

Next the parameters of the dissolution were optimised and with these conditions, both a synthetic mixture and a real phosphor residue were leached in the selected lixiviants. When dissolution a synthetic mixture instead of the individual phosphors, lower YOX

dissolution efficiencies were obtained, but the dissolution was still selective. In the dissolution of real lamp phosphor waste, a further decrease of the dissolution of YOX and increase of co-dissolution of HALO was observed. This problem was overcome by increasing the L:S ratio, as it increased the YOX dissolution from real lamp phosphor waste. The obtained results were compared to that of the best-performing IL reported in the literature ([Hbet][NTf<sub>2</sub>]) and similar results in terms of extraction efficiency and selectivity were obtained, but both levulinic acid and LevA:ChCl are much cheaper alternatives. A simple hydrometallurgical approach was tested using different concentrations of HCl and full dissolution of HALO with a certain amount of YOX co-dissolution was obtained. This comparison emphasises the selectivity of solvometallurgical approaches.

Two recovery routes of REEs from the PLS were tested, the precipitation with oxalic acid and solvent extraction. The recovery of the REEs via oxalic acid addition is possible in the levulinic acid-PLS, but when performed on a LevA:ChCl-PLS some ChCl precipitated together with oxalic acid and the REEs. Furthermore, due to the co-precipitation of calcium, this is not a suitable method for the direct recovery of REEs from a real waste PLS. Thus, a second important conclusion for further research works in the field of DESs, is that oxalic acid precipitation from a DES based PLS is not a suitable method, due to the co precipitation of oxalic acid-ChCl.

The purification of the lixiviant could be achieved via solvent extraction, by extracting all the metals to a D2EHPA phase and stripping them to an aqueous HCl solution, from which they can be separated following existing methodologies. Throughout the entire work, levulinic acid was found to be as equally suitable for the recovery of REEs from lamp phosphor waste as the corresponding ChCl-based DES. However, levulinic acid can be directly used without need of diluting in another organic solvent, which is cheaper and greener. Moreover, levulinic acid is a green solvent that can be produced from renewable resources.<sup>49-52</sup>

Overall, through this investigation it was shown that a green and relatively cheap solvent such as levulinic acid can be utilised for the selective extraction of Y and Eu from spent fluorescent lamps. The recovery of the REEs is possible with solvent extraction and stripping in an aqueous acidic solution.

## 5.5 References

1. Jacques, L.; Lucas, P.; Le Mercier, T.; Rollat, A.; Davenport, W., *Rare earths : Science, Technology, Production and Use*. Elsevier: **2015**.
2. Jordens, A.; Cheng, Y. P.; Waters, K. E., A review of the beneficiation of rare earth element bearing minerals. *Minerals Engineering* **2013**, *41*, 97-114.
3. Binnemans, K.; Jones, P.; Acker, K.; Blanpain, B.; Mishra, B.; Apelian, D., Rare-Earth Economics: The Balance Problem. *JOM* **2013**, *65* (7), 846-848.
4. Van Gosen, B. S.; Verplanck, P. L.; Seal II, R. R.; Long, K. R.; Gambogi, J. *Rare-Earth Elements*; 1411339916; US Geological Survey: 2017.
5. Schüler, D.; Buchert, M.; Liu, R.; Dittrich, G. S.; Merz, C. *Study on Rare Earths and Their Recycling*; Öko-Institut e.V: Darmstadt, **2011**.
6. Commission, E., Tackling the Challenges in Commodity Markets and on Raw Materials. *Brussels: European Commission* **2011**.
7. Commission, E. *Report of the Ad-hoc Working Group on Defining Critical Raw Materials*; Brussels, **2010**.
8. Mathieux, F.; Ardente, F.; Bobba, S.; Nuss, P.; Blengini, G. A.; Dias, P. A.; Blagoeva, D.; de Matos, C. T.; Wittmer, D.; Pavel, C., Critical raw materials and the circular economy. *Publications Office of the European Union: Luxembourg* **2017**.
9. Bauer, D.; Diamond, D.; Li, J.; McKittrick, M.; Sandalow, M. D.; Telleen, P. *Critical materials strategy*; U.S. Department of Energy: Washington DC, **2011**.
10. Wübbeke, J., Rare earth elements in China: Policies and narratives of reinventing an industry. *Resources Policy* **2013**, *38* (3), 384-394.
11. Bernhardt, D.; Reilly, J. F. *Mineral Commodity Summaries 2020: U.S. Geological Survey*; **2020**.
12. Hatch, G. P., Dynamics in the global market for rare earths. *Elements* **2012**, *8* (5), 341-346.
13. Binnemans, K.; Pontikes, Y.; Jones, P.; Van Gerven, T.; Blanpain, B. In *Recovery of Rare Earths from Industrial Waste Residues: a Concise Review*, International Slag Valorisation Symposium, **2013**, 191-205.
14. Borra, C.; Blanpain, B.; Pontikes, Y.; Binnemans, K.; Gerven, T., Recovery of Rare Earths and Other Valuable Metals From Bauxite Residue (Red Mud): A Review. *Journal of Sustainable Metallurgy* **2016**, *2* (4), 365-386.

15. Venkatesan, P.; Vander Hoogerstraete, T.; Hennebel, T.; Binnemans, K.; Sietsma, J.; Yang, Y., Selective electrochemical extraction of REEs from NdFeB magnet waste at room temperature. *Green Chemistry* **2018**, *20* (5), 1065-1073.
16. Binnemans, K.; Jones, P. T.; Blanpain, B.; Van Gerven, T.; Yang, Y.; Walton, A.; Buchert, M., Recycling of rare earths: a critical review. *Journal of Cleaner Production* **2013**, *51*, 1-22.
17. <https://www.downtoearth.org.in/news/unpacking-europium-the-mainstay-of-the-lighting-industry-47080>. (accessed 19/03/2020).
18. Machacek, E.; Richter, J. L.; Habib, K.; Klossek, P., Recycling of rare earths from fluorescent lamps: Value analysis of closing-the-loop under demand and supply uncertainties. *Resources, Conservation and Recycling* **2015**, *104*, 76-93.
19. Lucas, A.; Emery, R., Assessing occupational mercury exposures during the on-site processing of spent fluorescent lamps. *Journal Of Environmental Health* **2006**, *68* (7), 30-34.
20. Binnemans, K.; Jones, P., Rare Earths and the Balance Problem. *Journal of Sustainable Metallurgy* **2015**, *1* (1), 29-38.
21. Tunsu, C.; Petranikova, M.; Ekberg, C.; Retegan, T., A hydrometallurgical process for the recovery of rare earth elements from fluorescent lamp waste fractions. *Separation and Purification Technology* **2016**, *161*, 172-186.
22. Binnemans, K.; Jones, P. T., Perspectives for the recovery of rare earths from end-of-life fluorescent lamps. *Journal of Rare Earths* **2014**, *32* (3), 195-200.
23. Chang, T.; You, S.; Yu, B.; Chen, C.; Chiu, Y., Treating high-mercury-containing lamps using full-scale thermal desorption technology. *Journal of hazardous materials* **2009**, *162* (2-3), 967-972.
24. Zhang, S.-G.; Yang, M.; Liu, H.; Pan, D.-A.; Tian, J.-J., Recovery of waste rare earth fluorescent powders by two steps acid leaching. *Rare Metals* **2013**, *32* (6), 609-615.
25. Otto, R.; Wojtalewicz-Kasprzak, A. Method for recovery of rare earths from fluorescent lamps, US7976798B2. **2011**.
26. Tunsu, C.; Ekberg, C.; Foreman, M.; Retegan, T., Studies on the Solvent Extraction of Rare Earth Metals from Fluorescent Lamp Waste Using Cyanex 923. *Solvent Extraction and Ion Exchange* **2014**, *32* (6), 650-668.
27. Shimizu, R.; Sawada, K.; Enokida, Y.; Yamamoto, I., Supercritical fluid extraction of rare earth elements from luminescent material in waste fluorescent lamps. *The Journal of Supercritical Fluids* **2005**, *33* (3), 235-241.

28. Dupont, D.; Binnemans, K., Rare-earth recycling using a functionalized ionic liquid for the selective dissolution and revalorization of  $\text{Y}_2\text{O}_3:\text{Eu}^{3+}$  from lamp phosphor waste. *Green Chemistry* **2015**, *17* (2), 856-868.
29. Gijsemans, L.; Forte, F.; Onghena, B.; Binnemans, K., Recovery of rare earths from the green lamp phosphor  $\text{LaPO}_4:\text{Ce}^{3+},\text{Tb}^{3+}$  (LAP) by dissolution in concentrated methanesulphonic acid. *RSC Advances* **2018**, *8* (46), 26349-26355.
30. Stodd, S. Lanthanide based deep eutectic solvents. PhD thesis, University of Leicester, 2018.
31. Tran, M. K.; Rodrigues, M.-T. F.; Kato, K.; Babu, G.; Ajayan, P. M., Deep eutectic solvents for cathode recycling of Li-ion batteries. *Nature Energy* **2019**, *4* (4), 339.
32. Ballantyne, A. D.; Hallett, J. P.; Riley, D. J.; Shah, N.; Payne, D. J., Lead acid battery recycling for the twenty-first century. *Royal Society Open Science* **2018**, *5* (5), 171368.
33. Riaño, S.; Petranikova, M.; Onghena, B.; Vander Hoogerstraete, T.; Banerjee, D.; Foreman, M. R. S.; Ekberg, C.; Binnemans, K., Separation of rare earths and other valuable metals from deep-eutectic solvents: a new alternative for the recycling of used NdFeB magnets. *RSC Advances* **2017**, *7* (51), 32100-32113.
34. Abbott, A. P.; Harris, R. C.; Holyoak, F.; Frisch, G.; Hartley, J.; Jenkin, G. R., Electrocatalytic recovery of elements from complex mixtures using deep eutectic solvents. *Green Chemistry* **2015**, *17* (4), 2172-2179.
35. Fan, F.-L.; Qin, Z.; Cao, S.-W.; Tan, C.-M.; Huang, Q.-G.; Chen, D.-S.; Wang, J.-R.; Yin, X.-J.; Xu, C.; Feng, X.-G., Highly Efficient and Selective Dissolution Separation of Fission Products by an Ionic Liquid [Hbet][Tf<sub>2</sub>N]: A New Approach to Spent Nuclear Fuel Recycling. *Inorganic Chemistry* **2018**, *58* (1), 603-609.
36. Nockemann, P.; Thijs, B.; Pittois, S.; Thoen, J.; Glorieux, C.; Van Hecke, K.; Van Meervelt, L.; Kirchner, B.; Binnemans, K., Task-specific ionic liquid for solubilizing metal oxides. *The Journal of Physical Chemistry B* **2006**, *110* (42), 20978-20992.
37. Rodriguez Rodriguez, N.; van den Bruinhorst, A.; Kollau, L. J.; Kroon, M. C.; Binnemans, K., Degradation of deep-eutectic solvents based on choline chloride and carboxylic acids. *ACS Sustainable Chemistry & Engineering* **2019**, *7* (13), 11521-11528.

38. Hammond, O. S.; Bowron, D. T.; Edler, K. J., The effect of water upon deep eutectic solvent nanostructure: An unusual transition from ionic mixture to aqueous solution. *Angewandte Chemie International Edition* **2017**, *56* (33), 9782-9785.
39. Delgado-Mellado, N.; Larriba, M.; Navarro, P.; Rigual, V.; Ayuso, M.; García, J.; Rodríguez, F., Thermal stability of choline chloride deep eutectic solvents by TGA/FTIR-ATR analysis. *Journal of Molecular Liquids* **2018**, *260*, 37-43.
40. Schaeffer, N.; Feng, X.; Grimes, S.; Cheeseman, C., Recovery of an yttrium europium oxide phosphor from waste fluorescent tubes using a Brønsted acidic ionic liquid, 1-methylimidazolium hydrogen sulfate. *Journal of Chemical Technology & Biotechnology* **2017**, *92* (10), 2731-2738.
41. Dupont, D.; Binnemans, K., Antimony recovery from the halophosphate fraction in lamp phosphor waste: a zero-waste approach. *Green Chemistry* **2016**, *18* (1), 176-185.
42. Foreman, M. R. S., Progress towards a process for the recycling of nickel metal hydride electric cells using a deep eutectic solvent. *Cogent Chemistry* **2016**, *2* (1), 1139289.
43. Brewer, J.; Winburn, R. S.; Beaudoin, J. Method for extraction and separation of rare earth elements, US10494694B2, **2017**.
44. Brown, C. G.; Sherrington, L. G., Solvent extraction used in industrial separation of rare earths. *Journal of Chemical Technology and Biotechnology* **1979**, *29* (4), 193-209.
45. Wu, D.; Wang, X.; Li, D., Extraction kinetics of Sc (III), Y (III), La (III) and Gd (III) from chloride medium by Cyanex 302 in heptane using the constant interfacial cell with laminar flow. *Chemical Engineering and Processing: Process Intensification* **2007**, *46* (1), 17-24.
46. Xie, F.; Zhang, T. A.; Dreisinger, D.; Doyle, F., A critical review on solvent extraction of rare earths from aqueous solutions. *Minerals Engineering* **2014**, *56*, 10-28.
47. Abreu, R. D.; Morais, C. A., Study on separation of heavy rare earth elements by solvent extraction with organophosphorus acids and amine reagents. *Minerals Engineering* **2014**, *61*, 82-87.
48. Alder, C. M.; Hayler, J. D.; Henderson, R. K.; Redman, A. M.; Shukla, L.; Shuster, L. E.; Sneddon, H. F., Updating and further expanding GSK's solvent sustainability guide. *Green Chemistry* **2016**, *18* (13), 3879-3890.
49. Bozell, J. J.; Moens, L.; Elliott, D.; Wang, Y.; Neuenschwander, G.; Fitzpatrick, S.; Bilski, R.; Jarnefeld, J., Production of levulinic acid and use as a platform chemical for derived products. *Resources, Conservation and Recycling* **2000**, *28* (3-4), 227-239.

50. Morone, A.; Apte, M.; Pandey, R., Levulinic acid production from renewable waste resources: Bottlenecks, potential remedies, advancements and applications. *Renewable and Sustainable Energy Reviews* **2015**, *51*, 548-565.
51. Yan, L.; Yao, Q.; Fu, Y., Conversion of levulinic acid and alkyl levulinate into biofuels and high-value chemicals. *Green Chemistry* **2017**, *19* (23), 5527-5547.
52. Yu, F.; Zhong, R.; Chong, H.; Smet, M.; Dehaen, W.; Sels, B. F., Fast catalytic conversion of recalcitrant cellulose into alkyl levulinate and levulinic acid in the presence of soluble and recoverable sulfonated hyperbranched poly (arylene oxindole)s. *Green Chemistry* **2017**, *19* (1), 153-163.

# Chapter 6: Conclusions and future work

6 Chapter.....	206
6.1 Conclusions.....	206
6.2 Suggestions for future work.....	210

## 6 Chapter

### 6.1 Conclusions

The aim of this study was to employ the relatively green media of DESs into the processing of MOs, either with the use of chemical or electrochemical dissolution. The importance of the MOs extraction is highlighted by the main years of research on this topic with the use of either pyrometallurgy or hydrometallurgy. Due to environmental issues of these former methods, alternatives such as DESs are important to be investigated. A very strong advantage of DESs, which was also an aim of this thesis to take advantage of, is their tuneability that can enhance the selectivity of processes.

Previous research on the processing of MOs in DESs had shown that DESs composed of acidic HBDs could dissolve higher amounts of metals, due to the existence of  $H^+$  in solution that can act as oxygen acceptor. However, no extensive investigation on the mechanism of MOs chemical dissolution was given. Hence, in Chapter 3 the chemical dissolution of MOs was investigated in different systems.

First the dissolution in EG:ChCl, a DES with neutral pH and poorly complexing HBD, as a baseline was investigated and it was observed that the solubilities of most MOs, with the exception of  $Cu_2O$ ,  $ZnO$  and  $PbO$  were generally low. For the MOs that were exceptions the  $Cl^-$  was the most important ligand. In general, the solubility of MOs in DESs showed a dependency on their lattice energies and enthalpies of formation, with higher lattice energies resulting in poorer MO solubility. The solubility products for these MOs were also calculated, and the values found to be in a similar range as for aqueous systems.

As a next system the addition of TFSA, a superacid with poor complexing abilities, in EG:ChCl was aimed to show the dependency of MOs on the acidity. As expected, the dissolution of MOs was highly dependent on the proton activity, with solutions of lower pH generally resulting in higher MO solubility. For most MOs the experimental solubilities were in accordance with the theoretically calculated for the amount of  $H^+$  in solution, with the exception of  $Cu_2O$ ,  $ZnO$  and  $PbO$  for which the solubilities were always above the theoretical line showing their higher affinity to dissolve in EG:ChCl due to the complexation with  $Cl^-$ .

The addition of lactic acid in EG:ChCl was shown to give much higher enhancement of solubilities for all MOs. This fact is justified by the surface complexation reaction. Once the oxide is protonated, intermediate species form that can act as active sites for ligand complexation, generally followed by ligand exchange for  $\text{Cl}^-$  in the bulk solution. Following this work, different HBDS were tested on the solubility of MOs and it was shown that the acidity of the HBD and its complexation abilities are very important for the dissolution of MOs, with the latter to have the highest influence. One major deviation from this trend was seen in OxA:ChCl, where precipitation of metal complexes resulted from the strong interaction of the metal with the oxalate anion. An interesting observation was the selectivity of OxA:ChCl towards Co and Mn over Ni, which could be beneficial in a process extracting metals from active materials of LIBs.

Dissolution rates were examined in four different systems and it was concluded that in the acidic and more complexing DESs the rates of dissolution are faster than in EG:ChCl alone. In the acidic EG:ChCl, dissolution was fast and stopped when all the  $\text{H}^+$  had been consumed. As longer times were required to reach the solubility levels in LevA:ChCl it was concluded that the rate of dissolution was more dependent on effective mass transport. For OxA:ChCl a more complex behaviour exists due to the precipitation of metals, with a relatively high initial rate of dissolution.

The very important advantage of DESs, in terms of the selectivity that they can provide into the system was validated on the extraction of metals from a synthetic powder LiNMC, widely used as an active material in LIBs, and from an industrially manufactured cathode. The dissolution of these materials in OxA:ChCl showed that Co and Mn can be dissolved fully from both materials, with negligible amount of Ni, so indeed selectivity can be obtained. The addition of water into the DES showed that can change the speciation in solution with Co to be precipitated, Mn to stay in solution together with Li and Ni to stay undissolved.

In Chapter 4, the electrochemical dissolution was investigated as a tool to enhance the rate of dissolution in poor lixiviants like EG:ChCl. First, the electrochemical properties of MOs were investigated by using the paint casting method. Cyclic voltammetry of the solid MOs showed that the redox couples of  $\text{Fe}_2\text{O}_3$ ,  $\text{Fe}_3\text{O}_4$ ,  $\text{CuO}$ ,  $\text{Cu}_2\text{O}$  and  $\text{PbO}$  can be observed. For the rest of MOs, whose reversibility and reactivity is poor no redox couple referring to the metal was observed, but instead another redox couple was present in all of the MOs CVs. This redox peak was assumed to be either from the oxidation of the

oxide part of the compound and the formation of a reactive specie of superoxide. Another explanation could also be the catalytic electrooxidation of ethylene glycol or other organic contaminants in EG:ChCl on the surface of the Pt WE with the presence of the transition MOs as well.

Chronopotentiometric measurements of the solid MOs was in total agreement with the results of the chemical dissolution, in the sense that the OCP of CuO, Cu<sub>2</sub>O, ZnO and PbO was decreasing over time and it was lower than the rest of MOs, while the OCP of Fe<sub>3</sub>O<sub>4</sub>, Co<sub>3</sub>O<sub>4</sub> and NiO were high and stable over time, showing their very low affinity to dissolve in EG:ChCl chemically.

Chronocoulometric studies were aimed to investigate the rate of electrochemical dissolution of MOs at a constant voltage of 1.2 V vs Ag/AgCl. It was observed that the band gap of MOs had an impact on their rate of dissolution, which is in agreement with previous results on the electrochemical dissolution of Cu and Fe sulfides. Thus Fe<sub>3</sub>O<sub>4</sub>, together with MnO<sub>2</sub> showed the higher rate of electrochemical dissolution due to their lower band gap.

The interesting result of Chapter 4 was the employment of the anodic dissolution of MOs in EG:ChCl. This method indeed enhanced the rate of dissolution, with the enhancement to be exceptional as in the case of Fe<sub>2</sub>O<sub>3</sub> and Fe<sub>3</sub>O<sub>4</sub> for which it provided more than 10000 times fold higher concentration of dissolved metals after electrochemical dissolution compared to just chemical and for other like Co<sub>3</sub>O<sub>4</sub> and NiO more than 100 times. Of course, during the oxidation of the MO the metal could not be further oxidised, since in most of them the metals were in their highest oxidation states. Hence, it is assumed that the driving force of this dissolution was the oxidation of oxide resulting in the formation of superoxide radical species that would be more reactive and could weaken the bond of the metal-oxide. Kinetic studies showed that the rate of the dissolution was diffusion limited. The anodic dissolution of MOs showed also that the level of dissolution was the same for all MOs and no selectivity could be achieved. This enhances further the assumption that the mechanism of anodic dissolution is not dependent upon the metal but instead from the oxide part. The enhancement of the electrochemical dissolution was at the same levels as the enhancement from the addition of 0.1 M TFSA, which was discussed in Chapter 3.

In Chapter 5, last but not least, the application of DESs on the extraction of REEs from spent fluorescent lamps was investigated for the first time. From all the DESs tested, LevA:ChCl showed the best potential as it could dissolve the higher amount of Y and Eu from their mixed oxide  $Y_2O_3:Eu^{2+}$  (YOX), with low co-dissolution of the contaminant HALO, showing again the levels of selectivity that can be obtained with the used of DESs. Very similar results were obtained if only the pure levulinic acid was employed, fact that led to the conclusion that the  $Cl^-$  from the choline chloride was not responsible for the high extraction efficiency of REEs. Both synthetic mixtures of phosphors and a real residue were dissolved in the pure levulinic acid and in the DES. When leaching a synthetic mixture instead of the individual phosphors, lower YOX extraction efficiencies were obtained, but the leaching was still selective. In the leaching of real lamp phosphor waste, a further decrease of the dissolution of YOX and increase of co-dissolution of HALO was observed. Increasing the L:S ratio could increase the YOX dissolution from real lamp phosphor waste. The obtained results were compared to that of the best-performing IL reported in the literature ([Hbet][NTf<sub>2</sub>]) and similar results in terms of leaching efficiency and selectivity were obtained, but both levulinic acid and LevA-ChCl are much cheaper alternatives. A simple hydrometallurgical approach was tested using different concentrations of HCl and full dissolution of HALO with certain YOX co-dissolution was obtained. This comparison emphasises the selectivity of solvometallurgical approaches.

The recovery of the REEs was also attempted, both with oxalic acid addition and solvent extraction. The recovery via oxalic acid addition is possible in the levulinic acid-PLS, but when performed on a LevA-ChCl-PLS some ChCl precipitated together with oxalic acid and the REEs. Furthermore, due to the co-precipitation of calcium, this is not a suitable method for the direct recovery of REEs from a real waste PLS. The purification of the lixiviant could be achieved via solvent extraction, by extracting all the metals to a D2EHPA phase and stripping them to an aqueous HCl solution, from which they can be separated following existing methodologies. Throughout the entire work of this Chapter, levulinic acid was found to be equally suitable for the recovery of REEs from lamp phosphor waste than the corresponding ChCl-based DES. However, levulinic acid can be directly used without need of diluting in another organic solvent, which is cheaper and greener. This work shows that pure levulinic acid is a promising solvent for use in solvometallurgy.

Overall, in this thesis the mechanism of MOs dissolution in DESs was explained. Two different EoL products were processed, a widely used cathode material of LIBs and spent fluorescent lamp phosphors and it was shown that for the first one the use of DESs helped the extraction of Co and Mn, that could not be extracted in aqueous oxalic acid solution. However, the process of the second material showed that the use of the pure levulinic acid and not the DES showed the same levels of extraction. Hence, a very important message of this thesis, apart from the importance of speciation on the development of selective processes, is that DESs should not be used recklessly and the simplest and cheapest alternatives should be first attempted.

## **6.2 Suggestions for future work**

The MOs dissolution in DESs, will be certainly an ongoing research due to the green character of DESs and the existence of MOs in high end materials and in minerals. The employment of different types of DESs or different HBAs and HBDs would be important, in order to investigate more couples of MOs that can be show selective dissolution, as in the case of  $\text{MnO}_2$  and  $\text{Co}_3\text{O}_4$  and NiO in OxA:ChCl.

Actually, for the recycling of the cathode materials of LIBs, a flowsheet is developed from the group for the selective extraction and then recovery of metals from the LiNMC powder coming from a real battery after its delamination. The optimization of the process, in terms of the purity of the products during the different streams of the flowsheet and the enhancement of the selectivity is going to be attempted. The use of a different HBA, other than choline chloride could also be beneficial, in order to eliminate any esterification reactions between the OH group of the choline chloride and the carboxylic acids serving as the HBDs.

The flowsheet of the extraction of Y and Eu using levulinic acid is also going to be attempted to be developed, with more optimised recovery process. The recyclability of the solvent is also crucial to be investigated, in order to eliminate the cost of the process.

Definitely future work is needed for the understanding of the mechanism of the anodic dissolution of MOs in DESs. The assumption that the oxidation of the oxide species to form a more reactive species that weakens the bond of the MO needs to be proven with the use of EPR, for example. This method of dissolution, which has been proven to work for sulfide minerals, is novel for MOs and more work is needed to investigate its potentials. The optimization of the cell is also a very crucial work, since the passivation

of the electrode stops the dissolution of MOs, so a different configuration with enhanced mass transport needs to be examined. Generally, due to the high cost, since electricity is also used, this method is going to be mostly exploited in the extraction of PGMs from their oxides or from mixtures of them. This method is definitely in its start and future work will be attempted on this field.

# Chapter 7: Appendix

7 Chapter.....	213
7.1 Supplementary Information for Chapter 3 .....	213
7.2 Supplementary information for Chapter 4 .....	224
7.3 Supplementary information for Chapter 5 .....	227

## 7 Chapter

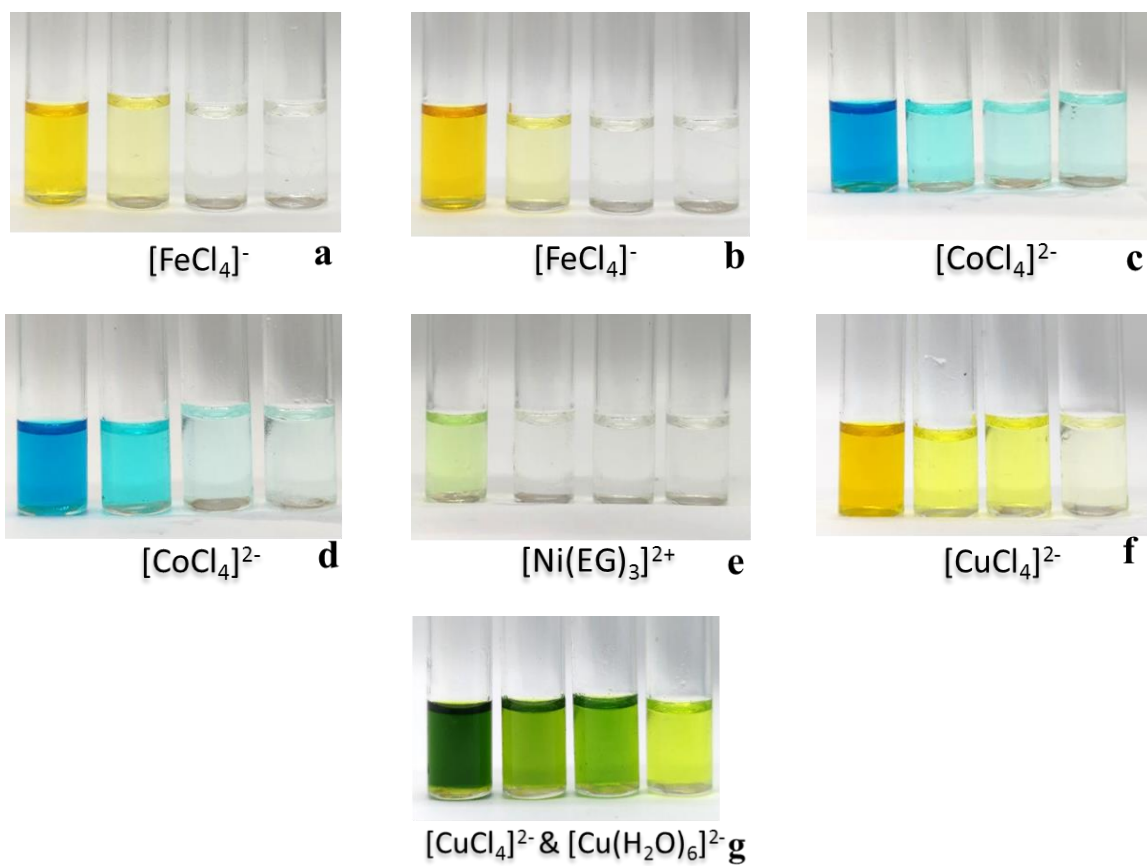
### 7.1 Supplementary Information for Chapter 3

Table 7.1: Calculation of solubility product constant  $K_{sp}$  for metal oxides in EG:ChCl at 50°C

Metal oxide	mg L <sup>-1</sup> of metal	Concentration of dissolved metal (mol L <sup>-1</sup> )	Concentration of dissolved O <sup>2-</sup> (mol L <sup>-1</sup> )	K <sub>sp</sub>
<b>MnO<sub>2</sub></b>	24	$4.3 \times 10^{-4}$	$8.7 \times 10^{-4}$	$1.63 \times 10^{-10}$
<b>MnO</b>	35	$6.5 \times 10^{-4}$	$6.5 \times 10^{-4}$	$4.17 \times 10^{-7}$
<b>Fe<sub>2</sub>O<sub>3</sub></b>	0.13	$2.4 \times 10^{-6}$	$3.7 \times 10^{-6}$	$3.01 \times 10^{-28}$
<b>Fe<sub>3</sub>O<sub>4</sub></b>	0.24	$4.5 \times 10^{-6}$	$5.9 \times 10^{-6}$	$3.5 \times 10^{-38}$
<b>Co<sub>3</sub>O<sub>4</sub></b>	3	$1.4 \times 10^{-4}$	$1.8 \times 10^{-4}$	$2.60 \times 10^{-27}$
<b>CoO</b>	75	$1.2 \times 10^{-3}$	$1.2 \times 10^{-3}$	$1.37 \times 10^{-6}$
<b>NiO</b>	13	$2.3 \times 10^{-4}$	$2.3 \times 10^{-4}$	$5.22 \times 10^{-8}$
<b>CuO</b>	251	$4 \times 10^{-3}$	$4 \times 10^{-3}$	$1.57 \times 10^{-5}$
<b>Cu<sub>2</sub>O</b>	1675	$2.5 \times 10^{-2}$	$1.2 \times 10^{-2}$	$7.61 \times 10^{-6}$
<b>ZnO</b>	578	$8.8 \times 10^{-3}$	$8.8 \times 10^{-3}$	$7.81 \times 10^{-5}$
<b>PbO</b>	1670	$8.1 \times 10^{-3}$	$8.1 \times 10^{-3}$	$6.5 \times 10^{-5}$

Table 7.2: Theoretical and experimental concentrations of dissolved metal oxides in the different solutions of EG:ChCl

Metal oxide	0.1 mol L <sup>-1</sup> TFSA		0.01 mol L <sup>-1</sup> TFSA		0.001 mol L <sup>-1</sup> TFSA		0.0001 mol L <sup>-1</sup> TFSA		
	Th	Exp	Th	Exp	Th	Exp	Th	Exp	
<b>MnO<sub>2</sub></b>	$2.5 \times 10^{-2}$	$3.8 \times 10^{-2}$	$2.5 \times 10^{-3}$	$8 \times 10^{-4}$	$2.5 \times 10^{-4}$	$8 \times 10^{-4}$	$2.5 \times 10^{-5}$	$1.9 \times 10^{-4}$	
<b>MnO</b>	$5 \times 10^{-2}$	$4.2 \times 10^{-2}$	$5 \times 10^{-3}$	$2 \times 10^{-3}$	$5 \times 10^{-4}$	$1.2 \times 10^{-3}$	$5 \times 10^{-5}$	$3.4 \times 10^{-4}$	
<b>Fe<sub>2</sub>O<sub>3</sub></b>	$1.6 \times 10^{-2}$	$3.5 \times 10^{-2}$	$1.6 \times 10^{-3}$	$7 \times 10^{-4}$	$1.6 \times 10^{-4}$	$3 \times 10^{-5}$	$1.6 \times 10^{-5}$	$3 \times 10^{-5}$	
<b>Fe<sub>3</sub>O<sub>4</sub></b>	$1.2 \times 10^{-2}$	$3.5 \times 10^{-2}$	$1.2 \times 10^{-3}$	$4 \times 10^{-4}$	$1.2 \times 10^{-4}$	$7 \times 10^{-5}$	$1.2 \times 10^{-5}$	$1 \times 10^{-5}$	
<b>Co<sub>3</sub>O<sub>4</sub></b>		$4.5 \times 10^{-2}$		$1.1 \times 10^{-3}$		$8 \times 10^{-5}$		$8 \times 10^{-5}$	
<b>CoO</b>	$5 \times 10^{-2}$	$5.1 \times 10^{-2}$	$5 \times 10^{-3}$	$1 \times 10^{-3}$	$5 \times 10^{-4}$	$6 \times 10^{-4}$	$5 \times 10^{-5}$	$4.2 \times 10^{-4}$	
<b>NiO</b>				$3 \times 10^{-4}$		$1 \times 10^{-4}$		$4 \times 10^{-6}$	
<b>CuO</b>				$4.9 \times 10^{-2}$		$9 \times 10^{-3}$		$3 \times 10^{-3}$	$7.7 \times 10^{-4}$
<b>Cu<sub>2</sub>O</b>				$9.2 \times 10^{-2}$		$2.1 \times 10^{-2}$		$1.7 \times 10^{-2}$	$5.2 \times 10^{-3}$
<b>ZnO</b>				$5.1 \times 10^{-2}$		$9 \times 10^{-3}$		$7.7 \times 10^{-3}$	$3.4 \times 10^{-3}$
<b>PbO</b>				$3.1 \times 10^{-2}$		$2 \times 10^{-2}$		$8 \times 10^{-3}$	$5.5 \times 10^{-3}$



*Figure 7.1: Difference in solutions colour of dissolved a)  $\text{Fe}_2\text{O}_3$ , b)  $\text{Fe}_3\text{O}_4$ , c)  $\text{Co}_3\text{O}_4$ , d)  $\text{CoO}$ , e)  $\text{NiO}$ , f)  $\text{CuO}$  and g)  $\text{Cu}_2\text{O}$  in different solutions of EG:ChCl with TFSA the proposed metal species. pH 1, 2, 3 and 4 from left to right.*



*Figure 7.2: Precipitates of a)MnO, b)CoO, c)CuO, d)ZnO and e)PbO in OxA:ChCl (left) and aqueous solution of 1.8M oxalic acid (right).*

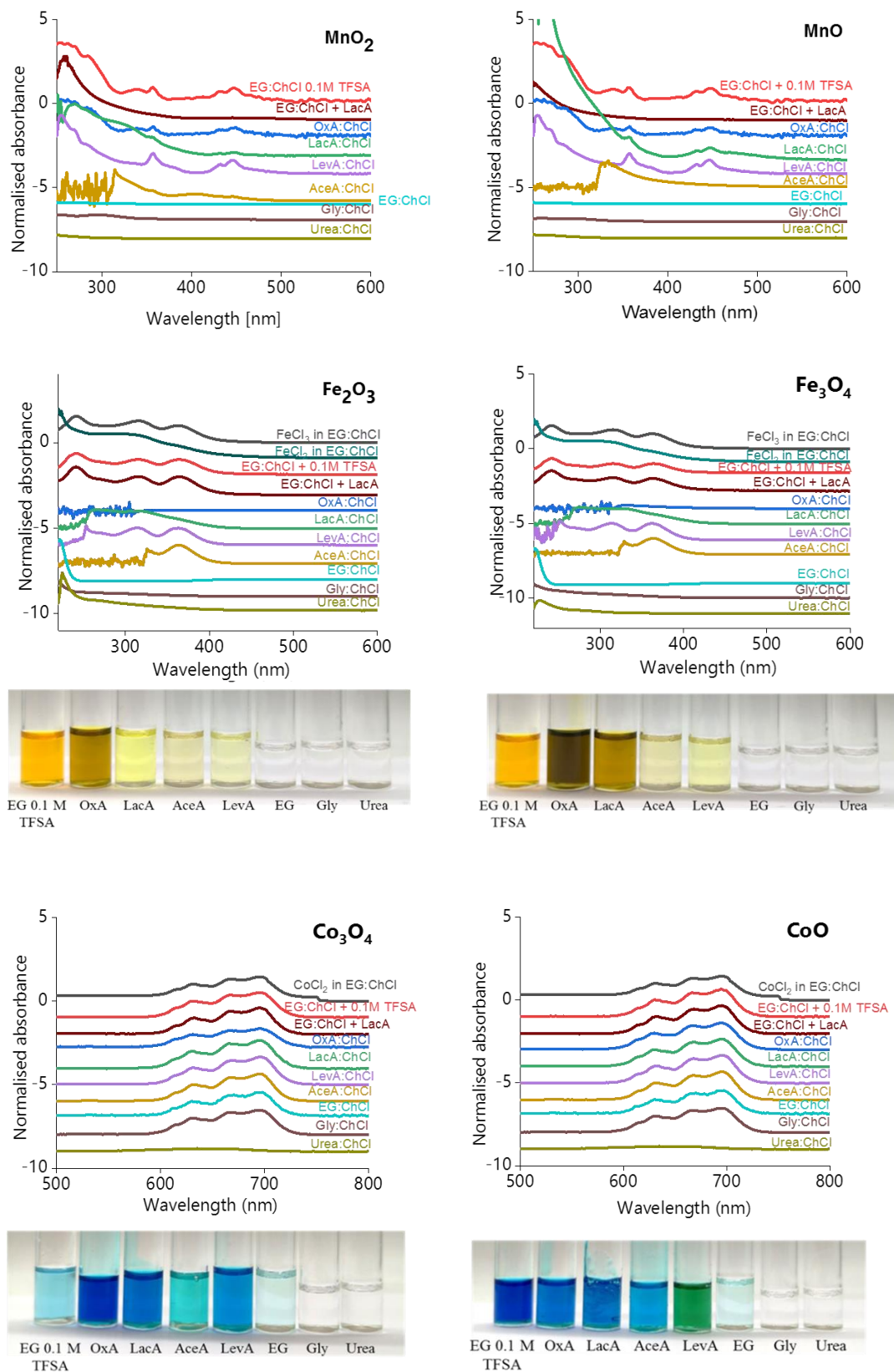


**Figure 7.3:** UV-Vis spectra of metal oxides and comparison of their coloured solutions upon dissolution in different DESs.

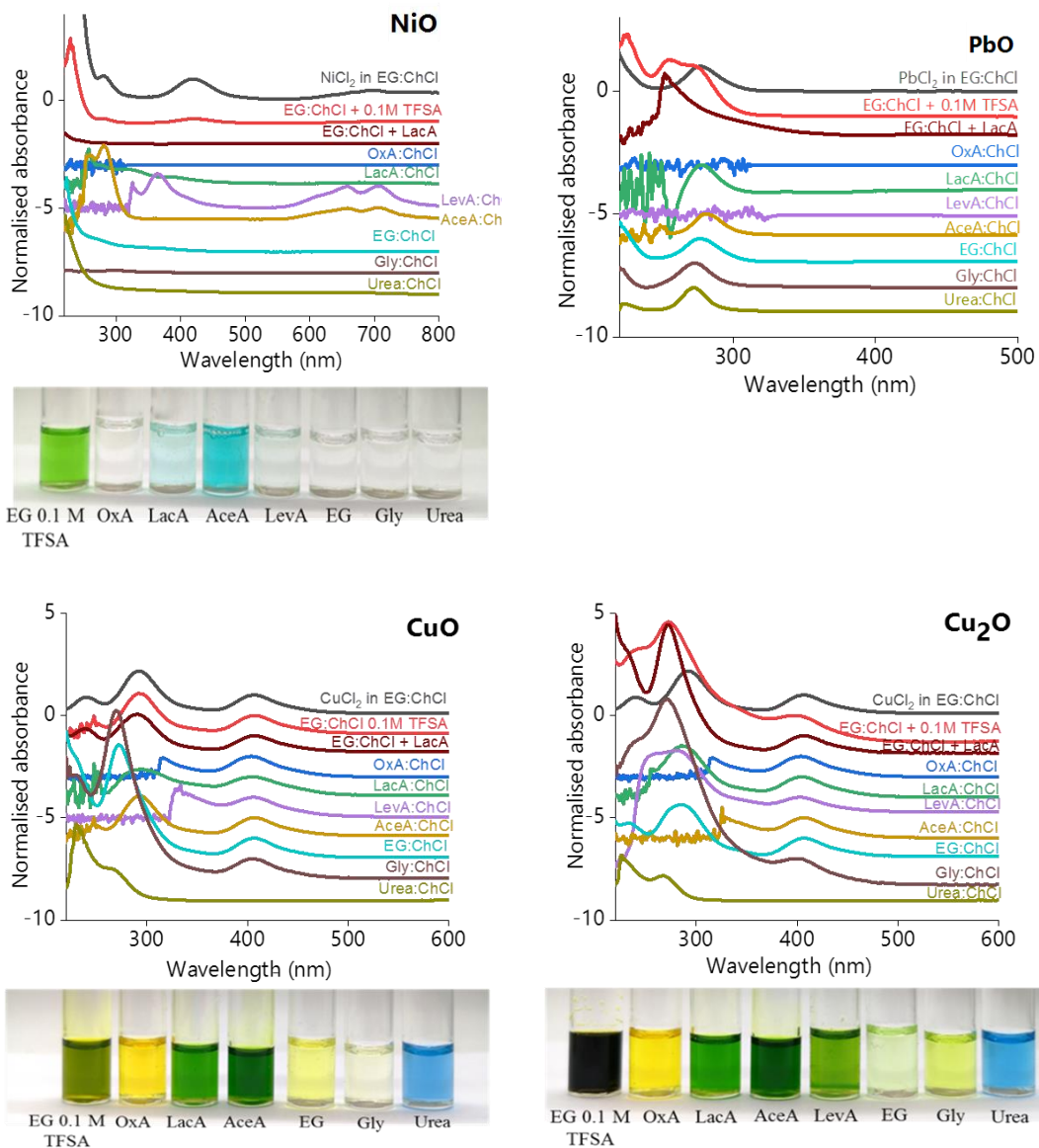


**Figure 7.4:** UV-Vis spectra of metal oxides and comparison of their coloured solutions upon dissolution in different DESs. (continued)

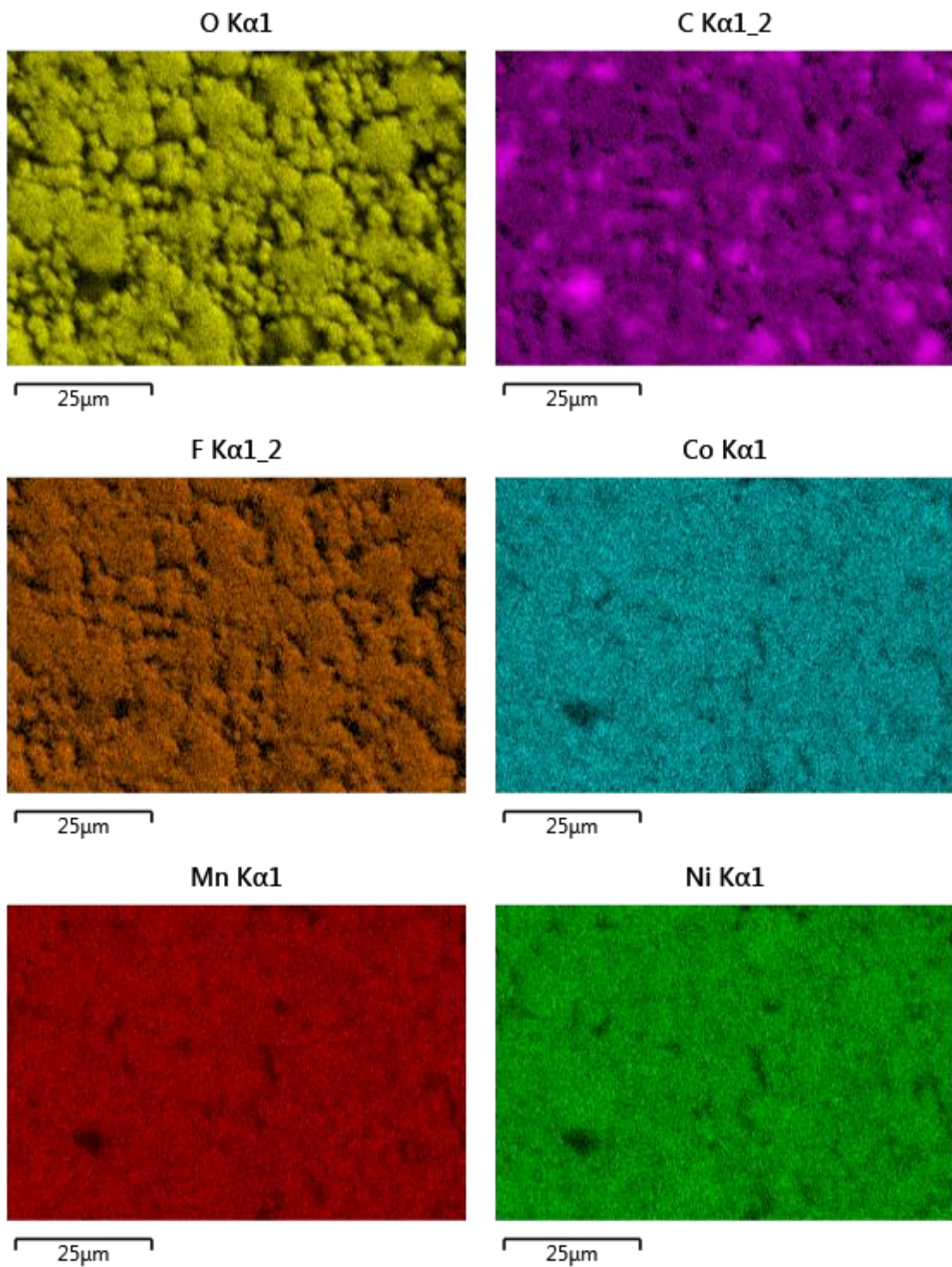


*Figure 7.5: Mapping of initial cathode material using scanning electron microscopy.*

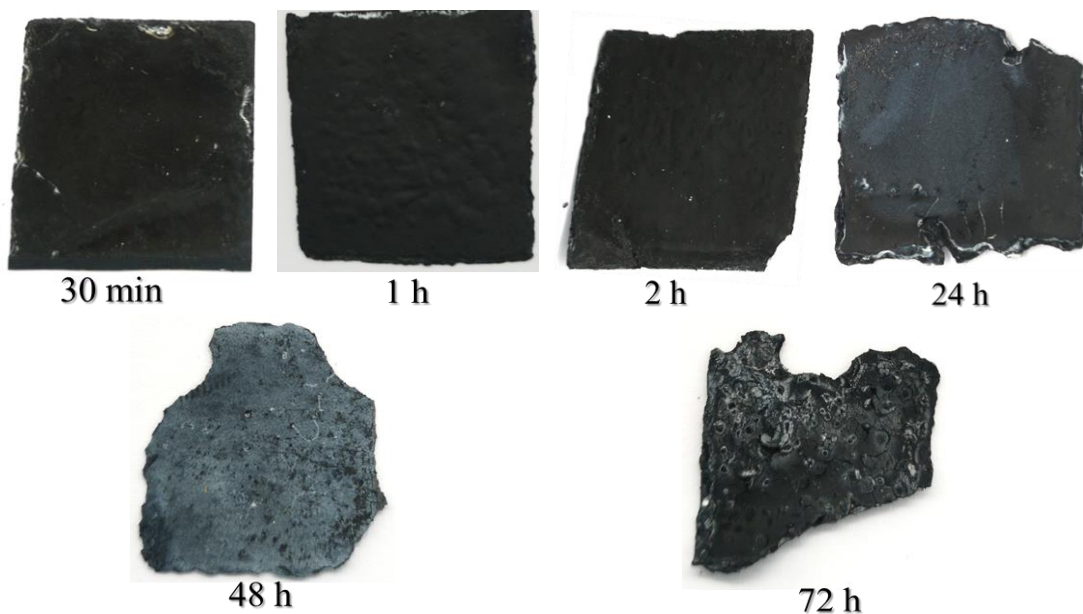


*Figure 7.6: Industrial cathodes after dissolution in OxA:ChCl. Conditions: Temperature=25 °C, L:S=30, no stirring*

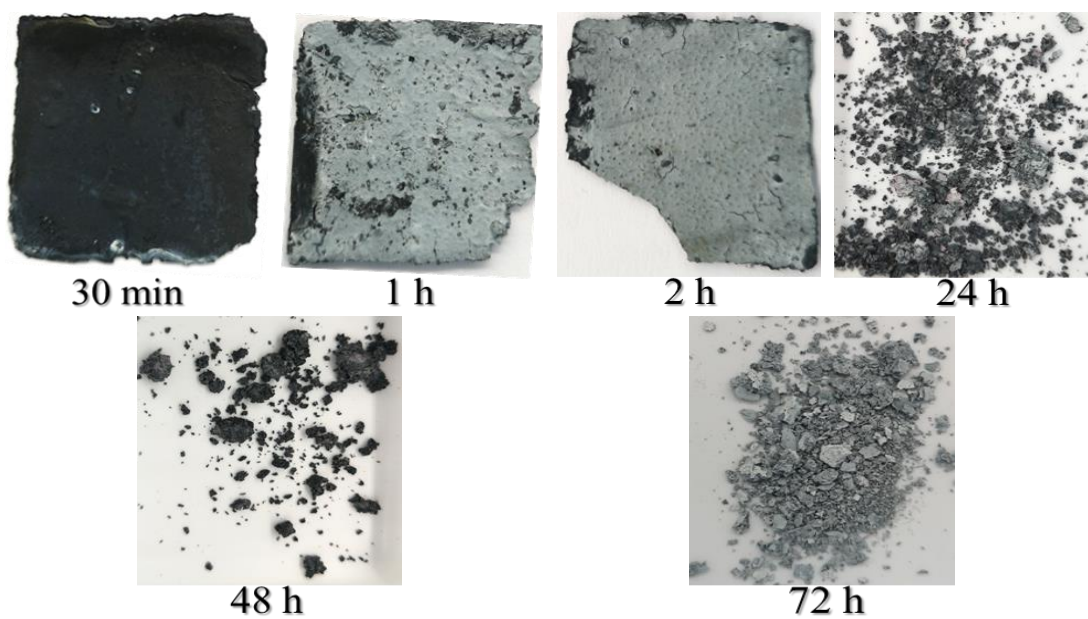
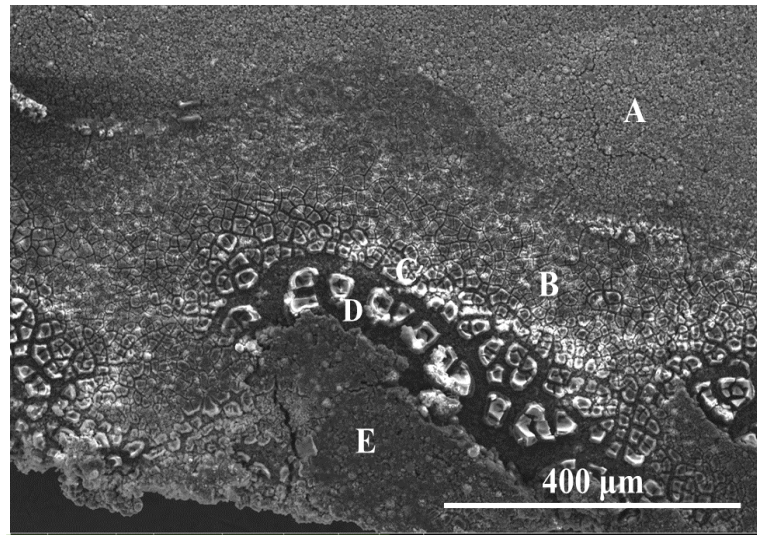


*Figure 7.7: Industrial cathodes after dissolution in OxA:ChCl. Conditions: Temperature=80 °C, L:S=30, no stirring*



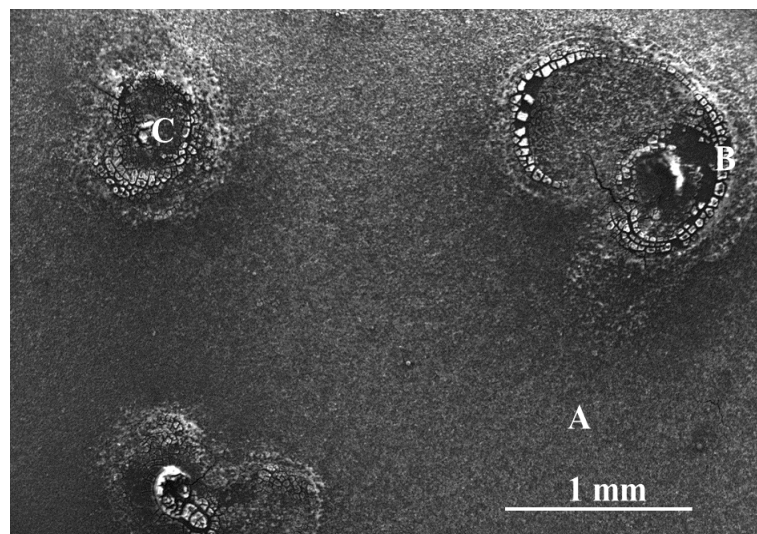
Area A			Area B		
Metal	Wt.%	$\sigma$	Metal	Wt.%	$\sigma$
Ni	18.7	0.2	Ni	11.9	0.1
Co	10.7	0.1	Co	6.9	0.1
Mn	16.2	0.1	Mn	8.0	0.1
Al	0.4	0.0	Al	9.7	0.1
O	23.6	0.1	O	34.6	0.1

#### Point C

Metal	Wt.%	$\sigma$
Ni	12.1	0.1
Co	6.9	0.1
Mn	6.5	0.1
Al	15.6	0.1
O	53.6	0.2

Point D			Area E		
Metal	Wt.%	$\sigma$	Metal	Wt.%	$\sigma$
Ni	16.9	0.1	Ni	16.7	0.2
Co	8.7	0.1	Co	8.6	0.1
Mn	9.4	0.1	Mn	8.5	0.1
Al	0.3	0.1	Al	4.1	0.0
O	2.1	0.0	O	21.8	0.0

Figure 7.8: SEM image of the cathode after dissolution in OxA:ChCl at 25 °C for 30 mins



Area A			Point B		
Metal	Wt%	$\sigma$	Metal	Wt%	$\sigma$
Ni	9.9	0.1	Ni	9.6	0.1
Co	5.7	0.1	Co	5.3	0.1
Mn	6.4	0.1	Mn	6.0	0.1
Al	0.2	0.0	Al	13.0	0.1
O	16.2	0.1	O	33.7	0.1

Point C		
Metal	Wt%	$\sigma$
Ni	8.6	0.1
Co	4.8	0.1
Mn	5.2	0.1
Al	1.8	0.0
O	7.4	0.1

Figure 7.9: SEM image of the cathode after dissolution in OxA:ChCl at 25 °C for 1 h

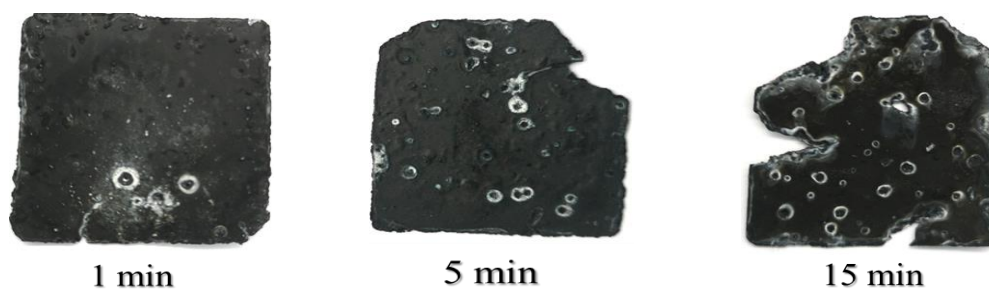
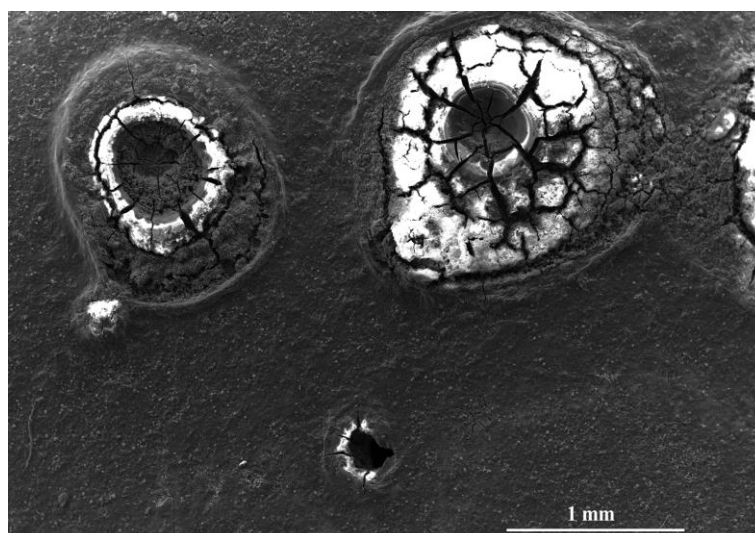
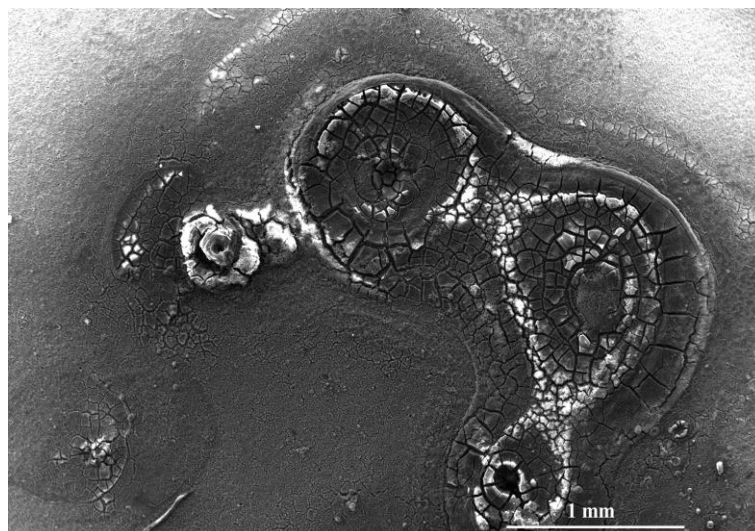


Figure 7.10: Industrial cathodes after ultrasound assisted dissolution in OxA:ChCl.



*Figure 7.11: SEM image of the cathode after ultrasound assisted dissolution in OxA:ChCl after 1 min and 10 mins.*

## 7.2 Supplementary information for Chapter 4

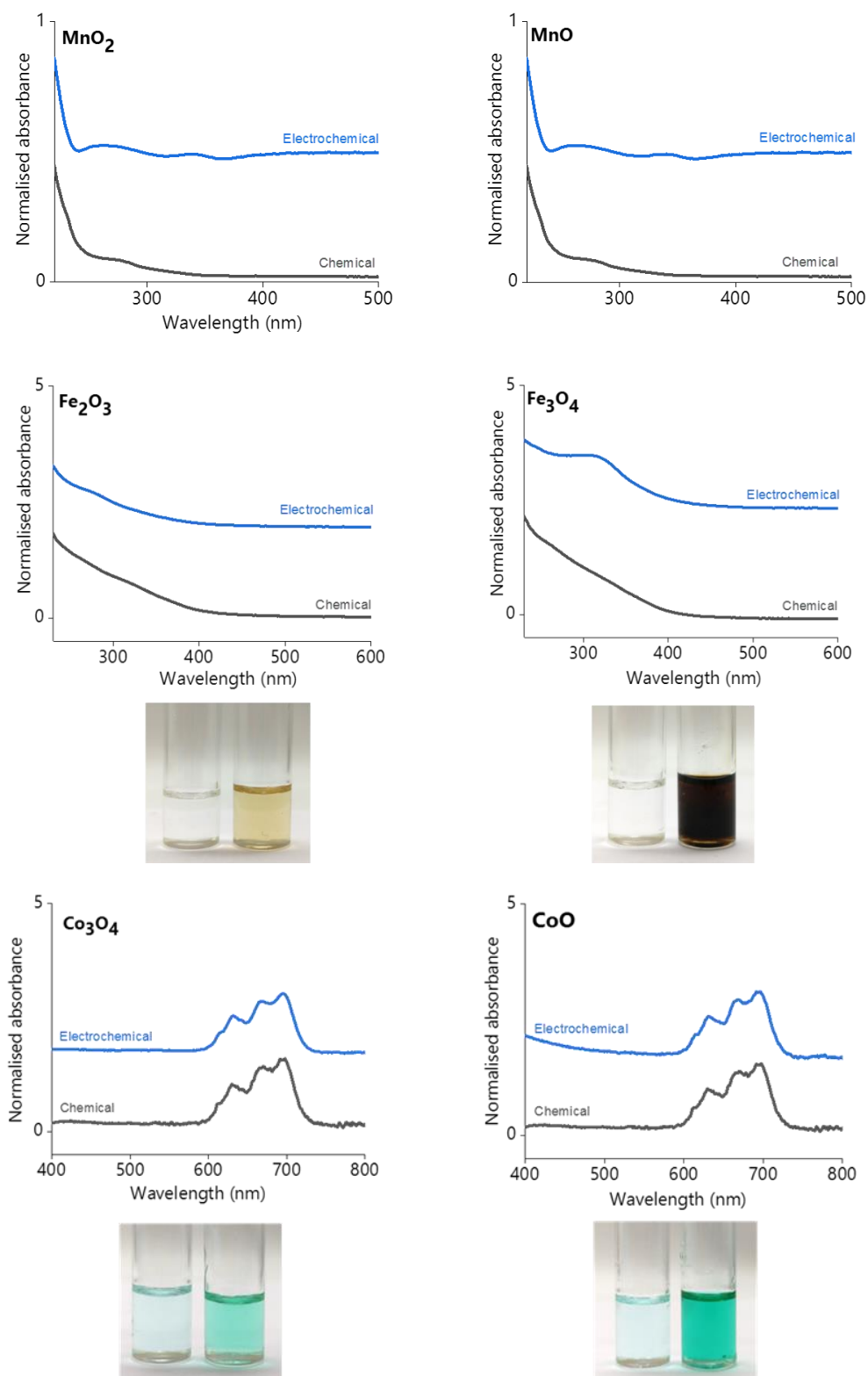


Figure 7.12 UV-Vis spectra of metal oxides in EG:ChCl after chemical and electrochemical dissolution and coloured solutions obtained after chemical( left) and electrochemical dissolution (right).

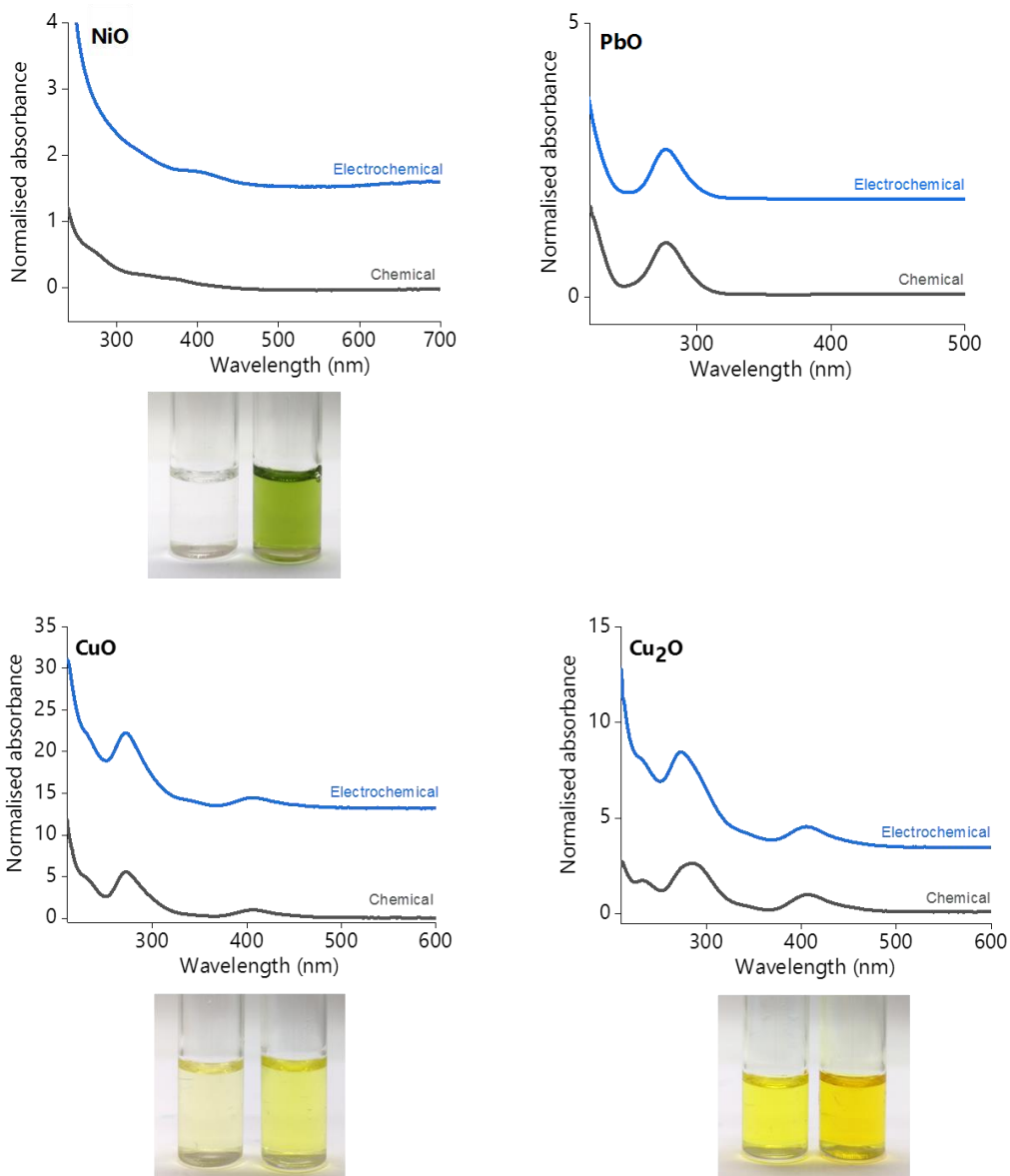


Figure 7.13: UV-Vis spectra of metal oxides in EG:ChCl after chemical and electrochemical dissolution and coloured solutions obtained after chemical( left) and electrochemical dissolution (right). (continued)



Figure 7.14: Deposits on WE after electrochemical dissolution of Cu<sub>2</sub>O (left) and PbO (right) in EG:ChCl.

Table 7.3: Deposits of metal oxides on Ni plate after bulk electrolysis in EG:ChCl



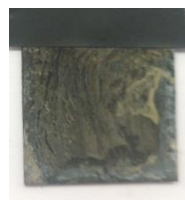
$\text{MnO}_2$



$\text{MnO}$



$\text{Fe}_2\text{O}_3$



$\text{Fe}_3\text{O}_4$



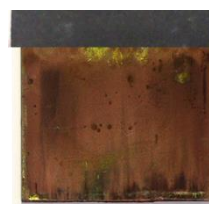
$\text{Co}_3\text{O}_4$



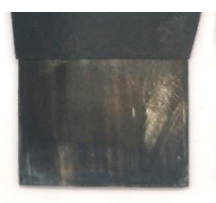
$\text{CoO}$



$\text{CuO}$



$\text{Cu}_2\text{O}$



$\text{ZnO}$



$\text{PbO}$

### 7.3 Supplementary information for Chapter 5

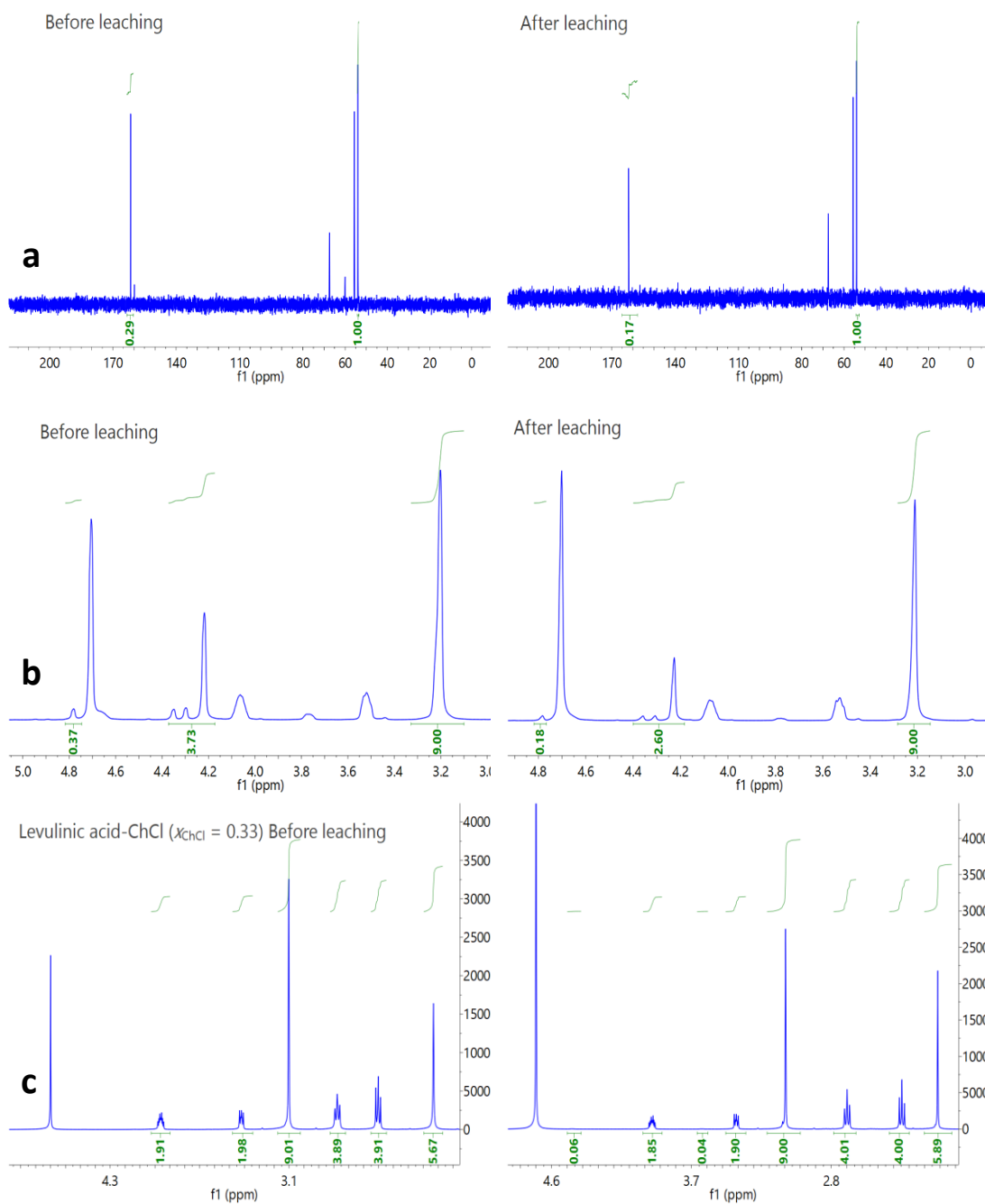


Figure 7.15: a)  $^{13}\text{C}$  NMR spectra of OxA:ChCl b)  $^1\text{H}$  NMR spectra of GlyA:ChCl and c)  $^1\text{H}$  NMR spectra of LevA:ChCl. Left-before dissolution, Right-after dissolution. Conditions:  $T = 80\text{ }^\circ\text{C}$ ;  $L:S = 10$ ;  $t = 48\text{ h}$ ;  $\text{H}_2\text{O vol.}\% = 30$ ; 500 rpm.

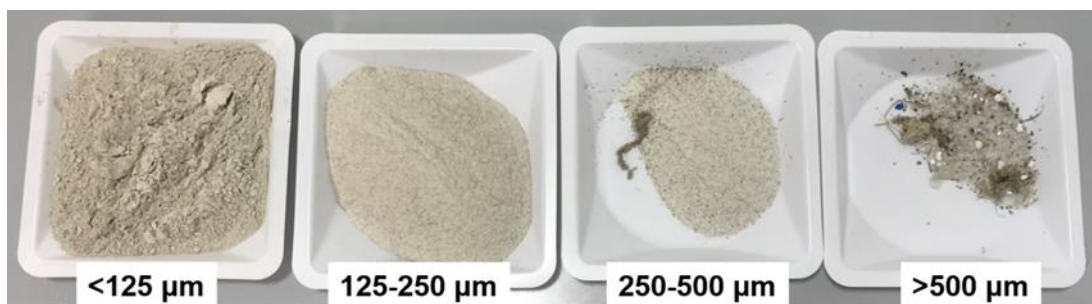


Figure 7.16: Fractions after sieving the phosphor waste.

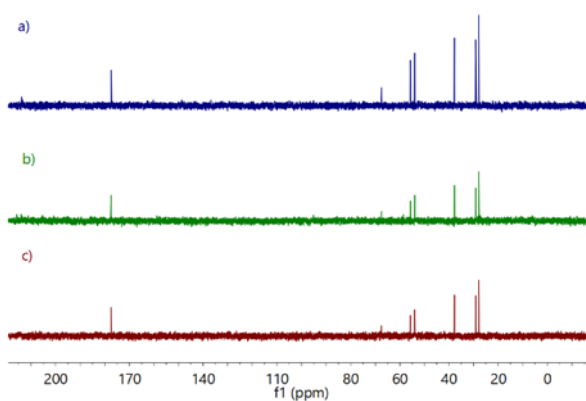


Figure 7.17:  $^{13}\text{C}$  NMR of (a) LevA:ChCl pregnant leach solution, (b) LevA:ChCl pregnant leach solution after addition of stoichiometric amount of oxalic acid and (c) LevA:ChCl pregnant leach solution after excess addition of oxalic acid.

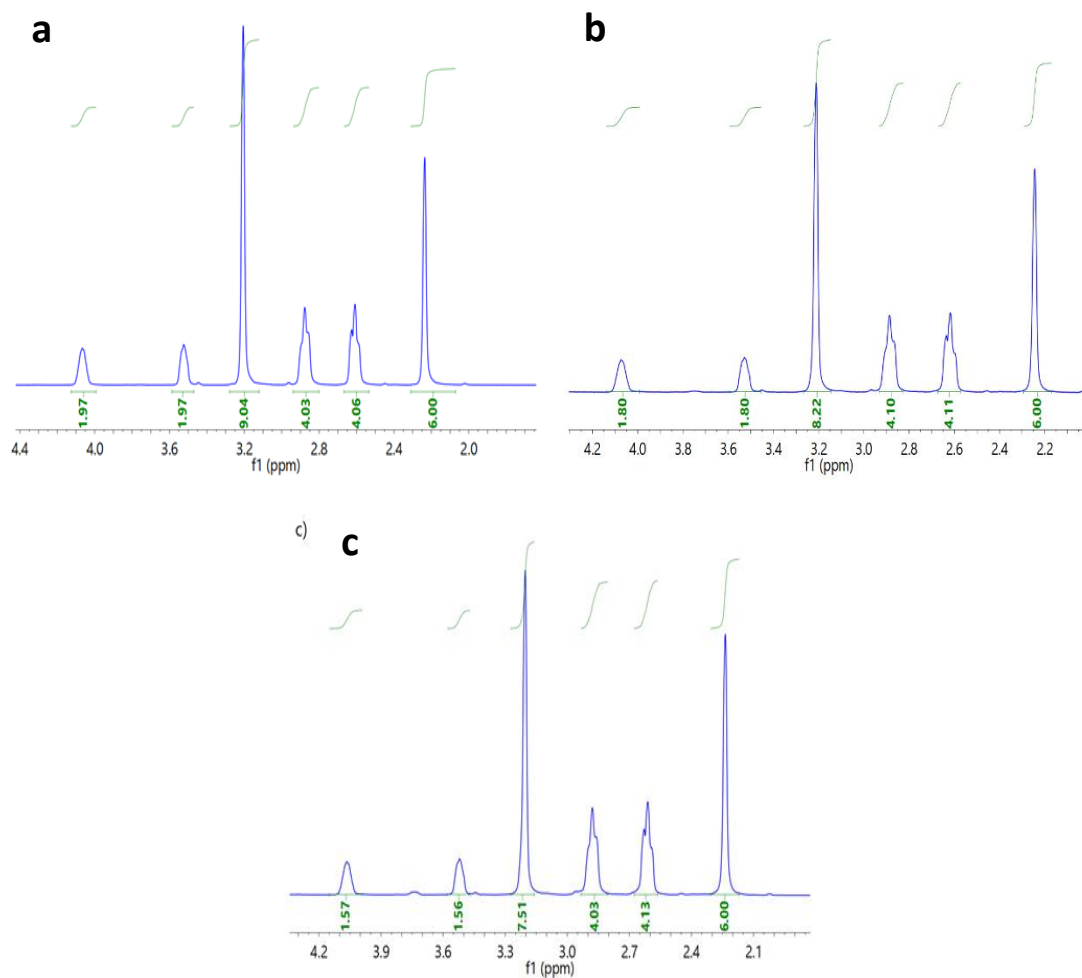


Figure 7.18:  $^1\text{H}$  NMR of (a) LevA:ChCl pregnant leach solution, (b) LevA:ChCl pregnant leach solution after addition of stoichiometric amount of oxalic acid and (c) LevA:ChCl pregnant leach solution after excess addition of oxalic acid.

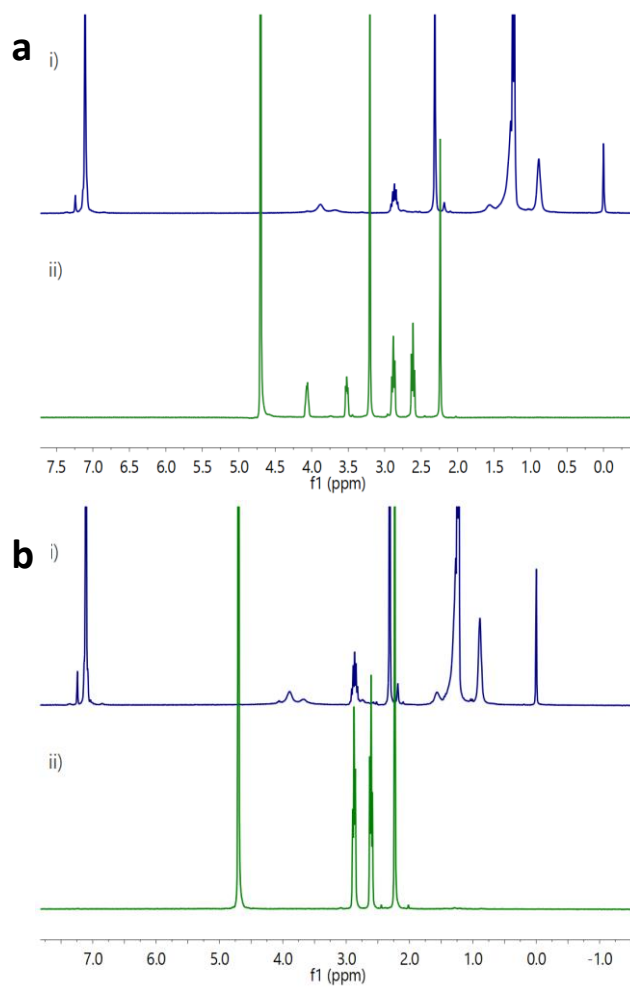


Figure 7.19:  $^1\text{H}$  NMR after (a) solvent extraction in LevA:ChCl (2:1) PLS of (i) DEHPA phase and (ii) LevA:ChCl (2:1) phase, and (b) solvent extraction in levulinic acid PLS of (i) DEHPA phase and (ii) levulinic acid phase.

The following published articles have been removed from the electronic version of this thesis due to copyright restrictions:

- The effect of pH and hydrogen bond donor on the dissolution of metal oxides in deep eutectic solvents, *Green Chem.*, 2020,22, 5476-5486, <https://doi.org/10.1039/D0GC02023K>
- Recovery of yttrium and europium from spent fluorescent lamps using pure levulinic acid and the deep eutectic solvent levulinic acid–choline chloride, *RSC Adv.*, 2020,10, 28879-28890, <https://doi.org/10.1039/D0RA05508E>

The unabridged version can be consulted at the University of Leicester Library.











































